



ISSN 1343-2230

CNS-REP-80
August, 2009

Annual Report 2007

Center for Nuclear Study,
Graduate School of Science, the University of Tokyo

Editors

Eiji Ideguchi

Center for Nuclear Study

CNS Reports are available from:

Wako-Branch at RIKEN

Center for Nuclear Study,

Graduate School of Science, the University of Tokyo

2-1 Hirosawa, Wako

351-0198, Japan

Tel: +81-48-464-4191

Fax: +81-48-464-4554

Annual Report 2007

Center for Nuclear Study,
Graduate School of Science, the University of Tokyo

Preface

This is the annual report of the Center for Nuclear Study (CNS), Graduate School of Science, the University of Tokyo, for the fiscal year 2007 (April 2007 through March 2008). In the CNS, during this period, a large number of scientific activities in various fields of nuclear physics have been carried out and a wide variety of fruitful results have been obtained. This report presents a report of such activities. Some highlights of the report are mentioned here.

The excitation energy and lifetime of the isomeric 0_2^+ state in ^{12}Be were determined by measuring decay spectra of delayed γ -rays from stopped ^{12}Be nuclei produced by the projectile fragmentation of ^{18}O at 100 A MeV. Using the branching ratios of the E2 and E0 decays, relatively large reduced transition strengths were deduced suggesting deformation of neutron-rich Be isotopes around $N = 8$. High-spin states in $^{49-51}\text{Ti}$ populated by fusion reactions of an RI beam were investigated, where high-resolution γ -ray spectroscopy with precise Doppler-shift corrections was achieved by using the position-sensitive Ge detector array, CNS GRAPE. To search for superdeformed rotational bands, high-spin states in $A \sim 100$ and $A \sim 30$ region were studied by in-beam γ -ray spectroscopy in the collaboration with Kyoto, Kyushu, Tohoku, Osaka, KEK, and JAEA group.

Research programs with CRIB continued in nuclear physics as well as nuclear astrophysics, together with the AVF upgrade project that enhances the capability of CRIB facility. A non-destructive beam monitor has been designed, and detailed simulations were made for the central region of the AVF cyclotron in order to derive the optimum design for high-transmission acceleration of heavy ions. Several new heavy ion beams of high-intensity and high charge states were developed with the Hyper ECR source. The first beam was successfully extracted from the super-conducting ECR source in collaboration with Tsukuba University.

The research programs of nuclear astrophysics include resonance search of light proton-rich nuclei with proton-rich RI beams from CRIB to investigate the solar model as well as the early stage of type II supernovae, and a direct measurement of the $^{18}\text{F}(p, \alpha)$ reaction for a nova problem. Elastic scattering and breakup of $^{17}\text{F}+^{12}\text{C}$ were measured for studying the reaction mechanism of a weakly bound nuclear system. Test producing RI beams of fp-shell nuclei is also in progress.

The CNS polarized proton target was applied to a measurement of spin-asymmetry in the p - ^8He elastic scattering. The analyzing power data, together with the p - ^6He data taken in 2005, will be essentially useful for understanding spin-orbit coupling in neutron-rich nuclei.

Considerable progress has been made in SHARAQ project. In summer 2007, all the magnets and rotating base were installed in E20 experimental area of RI beam factory. Equipped with electricity of 1 MVA and a cooling water of 1 m³, the SHARAQ magnets are ready to be excited. Detailed field-mapping measurement of dipole magnets will be started soon. Development of beam-line and focal plane detectors has advanced also. Low-pressure multiwire drift chambers developed for beam-line detectors were tested with an accelerated α -beam with an energy of 8.8 A MeV. They were found to work well with isobutane gas under as low pressure as several kPa. The design of cathode-readout drift chambers (CRDC) for the final focal plane detectors has been finalized. According to the design, two sets of CRDCs will be manufactured in collaboration with GANIL.

The experimental study in the PHENIX experiment at Relativistic Heavy Ion Collider (RHIC) at Brookhaven National Laboratory has made steady progress toward understanding of the properties of hot and dense nuclear matter created by colliding gold nuclei at relativistic energies. The CNS group has been concentrating on the physics analysis utilizing leptons and photons as probes which include determination of charm and bottom fraction in the non-photonic single electrons, systematics of J/ψ production in Cu+Cu and Au+Au collisions, deduction of photon yield at low transverse momentum in p+p and A+A collisions using the virtual-gamma method, and neutral pion production at high transverse momentum region as a function of azimuthal angle from the reaction plane in Au+Au collisions. The group has started active participation in the ALICE experiment at Large Hadron

Collider (LHC) at CERN. The group has been playing roles in the construction of the Transition Radiation Detector (TRD), which is the main device for electron identification. R & D of gas electron multiplier (GEM) and related techniques has been continuing. Development of an IC chip for 2D-imaging was made, and basic performance was tested.

Theoretical studies have been carried out by large-scale nuclear structure calculations in collaboration with RIKEN Nishina Center and the Department of Physics, University of Tokyo. Shell-model calculations, in particular, those by the Monte Carlo Shell Model, have produced crucial results to clarify the evolution of nuclear shells in exotic nuclei and the role of the tensor force on it. Many of such theoretical studies have been made in collaboration with various groups over the world. Properties of dilute neutron gas have been studied by lattice calculations. A preparation has been made for ab initio calculations by Monte Carlo Shell Model for medium-mass nuclei.

The 6th CNS International Summer School (CISS07) has been organized in August 2007 with many invited lecturers including three foreign distinguished physicists. There were 82 participants from 6 countries mainly from Asia.

Finally, I thank Ms. M. Hirano and other administrative staff members for their heartfelt contributions throughout the year.

Takaharu Otsuka
Director of CNS



Table of Contents

1a. Experimental Nuclear Physics: Low and Intermediate Energies

Searching for resonances in the ${}^6\text{Be}$	1
<i>R. Lichtenthaler, V. Guimarães, A. Lépine, K. C. C. Pires, M. Assunção, H. Yamaguchi, Y. Wakabayashi, S. Hayakawa, Y. Kurihara, S. Kubono, J.S. Yoo, S. Iwasa, S. Kato,</i>	
Elastic Scattering and Breakup of ${}^{17}\text{F}+{}^{12}\text{C}$ System at Low Energy	3
<i>C. J. Lin, H. Q. Zhang, H. M. Jia, X. X. Xu, Z. D. Wu, G. P. An, C. L. Zhang, F. Yang, S. Kubono, H. Yamaguchi, Y. Wakabayashi, S. Hayakawa, Y. Kurihara, D. N. Binh, N. Iwasa, Y. K. Kwon, C. Signorini, M. Mazzocco, M. Romoli and M. La Commara</i>	
Production of the spin-polarized ${}^{17}\text{N}$ beam via the inverse-kinematics transfer reaction	5
<i>K. Shimada, G. Amadio, T. Arai, Y. Hasama, N. Hatakeyama, S. Hayakawa, T. Inoue, S. Kagami, D. Kameda, H. Kawamura, Y. Kobayashi, S. Kubono, Y. Kurihara, J. Murata, D. Nagae, T. Nagatomo, C. Nakano, T. Sugimoto K. Suzuki, K. Takase, M. Takemura, T. Toyoda, H. Ueno, Y. Wakabayashi, H. Yamaguchi, A. Yoshimi and K. Asahi</i>	
The ${}^{18}\text{F}+p$ process and the Nova phenomenon	7
<i>S. Cherubini, C. Spitaleri, V. Crucillà, M. Gulino, M. La Cognata, L. Lamia, R.G. Pizzone, S. Puglia, G.G. Rapisarda, S. Romano, M.L. Sergi, A. Tumino, S. Kubono, H. Yamaguchi, Y. Wakabayashi, S. Hayakawa, N. Iwasa, S. Kato, H. Komatsubara, T. Teranishi, A. Coc, De Séreville</i>	
${}^{30}\text{S}$ Beam Production with CRIB: Analysis of 2006 Data and Preliminary Experimental Results from 2008	9
<i>D. Kahl, A. A. Chen, D. N. Binh, J. Chen, T. Hashimoto, S. Hayakawa, S. Kubono, Y. Kurihara, N. H. Lee, S. Michimasa, S. Nishimura, C. V. Ouellet, K. Setoodehnia, Y. Wakabayashi, and H. Yamaguchi</i>	
Development of ${}^{46}\text{Cr}$ secondary beam for β -decay measurement	11
<i>Y. Wakabayashi, H. Yamaguchi, S. Hayakawa, Y. Kurihara, D. N. Binh, S. Nishimura, Y. Gono, and S. Kubono</i>	
Low-lying s -wave resonance of ${}^8\text{B}$	13
<i>H. Yamaguchi, Y. Wakabayashi, S. Hayakawa, G. Amadio, S. Kubono, H. Fujikawa, A. Saito, J.J. He, T. Teranishi, Y.K. Kwon, S. Nishimura, Y. Togano, N. Iwasa, K. Inafuku, M. Niikura, and L.H. Khiem</i>	
Cluster states in ${}^{13}\text{C}$	15
<i>Y. Sasamoto, T. Kawabata, T. Uesaka, K. Suda, Y. Maeda, S. Sakaguchi, K. Itoh, K. Hatanaka, M. Fujiwara, A. Tamii, Y. Shimizu, K. Nakanishi, K. Kawase, H. Hashimoto, Y. Tameshige, H. Matsubara, M. Itoh, H. P. Yoshida and M. Uchida</i>	
Proton Inelastic Scattering Study on Very Neutron-rich Magnesium Isotopes	17
<i>S. Michimasa, Y. Yanagisawa, K. Inafuku, N. Aoi, Z. Elekes, Zs. Fülöp, Y. Ichikawa, N. Iwasa, K. Kurita, M. Kurokawa, T. Machida, T. Motobayashi, T. Nakamura, T. Nakabayashi, M. Notani, H. J. Ong, T. K. Onishi, H. Otsu, H. Sakurai, M. Shinohara, T. Sumikama, S. Takeuchi, K. Tanaka, Y. Togano, K. Yamada, M. Yamaguchi, and K. Yoneda</i>	
Study of Astrophysically Important States in ${}^{26}\text{Si}$ through Elastic Scattering with CRIB	19
<i>J. Chen, A. Chen, G. Amadio, S. Cherubini, M. La Cognata, H. Fujikawa, S. Hayakawa, N. Iwasa, J. J. He, D. Kahl, L. H. Khiem, S. Kubono, Y. Kurihara, Y. K. Kwon, J. Y. Moon, M. Niikura, S. Nishimura, A. Odahara, J. Pearson, R. Pizzone, A. Saito, C. Signorini, T. Teranishi, Y. Togano, Y. Wakabayashi, H. Yamaguchi</i>	
High-spin States in ${}^{51}\text{Ti}$	21
<i>M. Niikura, E. Ideguchi, N. Aoi, H. Baba, T. Fukuchi, Y. Ichikawa, H. Iwasaki, T. Kubo, M. Kurokawa, M. Liu, S. Michimasa, T. Ohnishi, T. K. Onishi, S. Ota, S. Shimoura, H. Suzuki, D. Suzuki, Y. Wakabayashi, K. Yoshida and Y. Zheng</i>	

Study of High-Spin States in A~30 Region	23
<i>E. Ideguchi, T. Morikawa, M.L. Liu, Y. Toh, M. Koizumi, A. Kimura, H. Kusakari, M. Oshima, B. Cederwall, K. Furutaka, Y. Hatsukawa, S. Mitarai, M. Sugawara and Y. Zheng</i>	
Search for Superdeformed Band in A~110 Region	25
<i>A. Yoshida, E. Ideguchi, S. Ota, T. Koike, K. Shirotori, H. Tamura, K. Hosomi, M. Mimori, K. Miwa, Y. Ma, T. Ohtomo, T. Yamamoto, M. Sato, T. Morikawa, T. Suzuki, T. Murakami, T. Kishida</i>	
Analyzing Power Measurement for the $\vec{p}+^8\text{He}$ Elastic Scattering at 71 MeV/u	27
<i>S. Sakaguchi, T. Uesaka, T. Wakui, T. Kawabata, N. Aoi, Y. Ichikawa, K. Itoh, M. Itoh, T. Kawahara, Y. Kondo, H. Kuboki, T. Nakamura, T. Nakao, Y. Nakayama, S. Noji, H. Sakai, Y. Sasamoto, M. Sasano, K. Sekiguchi, T. Shimamura and Y. Shimizu</i>	
$^{10}\text{B}+p$ Reaction at Astrophysical Energies	29
<i>S. Romano, S.M.R. Puglia, L. Lamia, C. Spitaleri, S. Cherubini, M. Gulino, M. La Cognata, R.G. Pizzone, G.G. Rapisarda, M.L. Sergi, S. Tudisco, A. Tumino, M.G. Del Santo, N. Carlin, F. Souza, A. Szanto de Toledo S. Kubono, H. Yamaguchi, Y. Wakabayashi, V. Kroha, C. Li, W. Qungang, E. Somorjai</i>	

1b. Experimental Nuclear Physics: PHENIX Experiment at BNL-RHIC

Progress of the PHENIX Experiment and Related Activities in 2007	31
<i>H. Hamagaki, T. Gunji, F. Kajihara, T. Isobe, S.X. Oda, Y. Morino, Y. Aramaki, Y.L. Yamaguchi, S. Sano, A. Takahara, J. Kikuchi, Y. Tanaka, and T. Fusayasu</i>	
Measurement of π^0 production with respect to the reaction plane in $\sqrt{s_{NN}} = 200$ GeV Au+Au collisions at RHIC-PHENIX	33
<i>Y. Aramaki, H. Hamagaki, T. Sakaguchi, and G. David, for the PHENIX Collaboration</i>	
J/ψ Production in Cu+Cu Collisions at $\sqrt{s_{NN}} = 200$ GeV at RHIC-PHENIX	35
<i>S.X. Oda, H. Hamagaki, T. Gunji, Y. Akiba, K. Das, A.D. Frawley, and W. Xie, for the PHENIX collaboration</i>	
χ_c Production in $p + p$ Collisions at $\sqrt{s} = 200$ GeV at RHIC-PHENIX	37
<i>S.X. Oda, H. Hamagaki, and K. Ozawa, for the PHENIX Collaboration</i>	
Acceptance Calculation of $J/\psi \rightarrow e^+e^-$ and $\Upsilon \rightarrow e^+e^-$ at LHC-ALICE	39
<i>T. Gunji, H. Hamagaki, S. Sano, A. Takahara</i>	
Development of the Detector Control System of the ALICE Transition Radiation Detector	41
<i>T. Gunji, H. Hamagaki, S. Sano, A. Takahara, T. Dietel, U. Westerhoff, K. Schweda, J. Mercado, K. Watanabe</i>	
Measurement of neutral pions at high transverse momentum and quantitative evaluation of medium transport coefficients in Au+Au collisions at $\sqrt{s_{NN}} = 200$ GeV with RHIC-PHENIX experiment	43
<i>T. Isobe, H. Hamagaki, T. Sakaguchi, G. David, B. Sahlmueller, J.L. Nagle, M.J. Tannenbaum, C. Klein-Boesing, and M.L. Putschke for the PHENIX Collaboration</i>	
Measurement of charm and bottom production in p+p collisions at $\sqrt{s} = 200$ GeV at RHIC-PHENIX	45
<i>Y. Morino for the PHENIX Collaboration</i>	
Evaluation of Electron Identification Capability of ALICE-TRD (Transition Radiation Detector) with Neural Network Method	47
<i>A. Takahara, H. Hamagaki, T. Gunji, Y. Morino, S. Sano, for the ALICE collaboration</i>	
Measurement of low p_T direct photon with virtual photon method in $\sqrt{s} = 200$ GeV p+p collisions at PHENIX	49
<i>Y.L. Yamaguchi, H. Hamagaki, T. Gunji, F. Kajihara, Y. Akiba, A. Toia, and T. Dahms, for the PHENIX collaboration</i>	

2. Accelerator and Instrumentation

Development of a readout circuit for 2D-imaging using GEM	51
<i>S. Sano, H. Hamagaki, Y. Tanaka, T. Fusayasu, F. Kajihara, and T. Gunji</i>	
SHARAQ Project – Progress in FY2007 –	53
<i>T. Uesaka, S. Shimoura, H. Sakai, K. Nakanishi, A. Saito, Y. Sasamoto, S. Michimasa, H. Kurei, T. Kawabata, N. Yamazaki, H. Miya, T. Kubo, Y. Yanagisawa, M. Fujinawa and G. P. Berg</i>	
Field Measurement System of the Superferric Quadrupole Magnets for SHARAQ Spectrometer	56
<i>Y. Sasamoto, K. Nakanishi, T. Uesaka, S. Shimoura, H. Sakai^a, T. Kubo^b, N. Yamazaki and R. Yoshino</i>	
Design of Focal-Plane Detector for SHARAQ Spectrometer	58
<i>S. Michimasa, S. Shimoura, T. Uesaka, H. Sakai, P. Roussel-Chomaz, J-F. Libin, P. Gangnant, and C. Spitaels</i>	
Performance of LP-MWDC for α beam at 35.2 MeV	60
<i>H. Miya, S. Shimoura, A. Saito, T. Kawabata, H. Kurei, S. Michimasa, K. Miki, K. Nakanishi, S. Ota, Y. Sasamoto, T. Uesaka and H. Sakai</i>	
Status of the polarized proton target	62
<i>Y. Shimizu, T. Kawahara, S. Sakaguchi, T. Uesaka, and T. Wakui</i>	
Current core monitor for E7 beam line	64
<i>S. Watanabe, Y. Ohshiro, H. Yamaguchi, R. Koyama, T. Watanabe, M. Kase, A. Goto, K. Hatanaka, and S. Kubono</i>	
First beam extraction from SC-ECR-IS at CNS	66
<i>Y. Ohshiro, S. Yamaka, S. Watanabe, T. Kageyama, T. Nakagawa, I. Arai, and S. Kubono</i>	
Optimization of the h=2 RF regime in the RIKEN AVF Cyclotron	68
<i>S.B.Vorozhtsov, A.S.Vorozhtsov, E.E.Perepelkin, S.Watanabe, S.Kubono, and A. Goto</i>	

3. Theoretical Nuclear Physics

Electromagnetic Transitions in Exotic Carbon Isotopes	71
<i>T. Suzuki and T. Otsuka</i>	
Lattice Calculation of Thermal Properties of Neutron Matter with NN Effective Field Theory	72
<i>T. Abe and R. Seki</i>	

4. Other Activities

The Sixth CNS International Summer School (CISS07)	75
<i>T. Kawabata, S. Kubono, S. Michimasa, T. Otsuka, H. Sakai, S. Shimoura, and T. Suzuki</i>	
Laboratory Exercise for Undergraduate Students	76
<i>T. Kawabata, K. Yako, S. Hayakawa, K. Miki, H. Sakai, and S. Shimoura</i>	

Appendices

Symposium, Workshop, Seminar, PAC and External Review	79
CNS Reports	81
Publication List	82
Talks and Presentations	88
Personnel	95

Experimental Nuclear Physics: Low and Intermediate Energies

Searching for resonances in the ${}^6\text{Be}$

R. Lichtenthaler^a, V. Guimarães^a, A. Lépine^a, K. C. C. Pires^a, M. Assunção^b, H. Yamaguchi^c,
Y. Wakabayashi^c, S. Hayakawa^c, Y. Kurihara^c, S. Kubono^c, J.S. Yoo^d, S. Iwasa^e, S. Kato^f

^a*Instituto de Física, Universidade de São Paulo*

^b*Center for Nuclear Study, Graduate School of Science, University of Tokyo*

^c*Korea*

The structure of the energy levels of light nuclei has still many states unknown. In particular in the mass $A=6$ triplet ${}^6\text{Li}$, ${}^6\text{He}$ ${}^6\text{Be}$, there are several excited states identified in the ${}^6\text{Li}$ and ${}^6\text{He}$ but only a few states in the isobar ${}^6\text{Be}$. Only the ground state $J^\pi = 0^+; \Gamma = 92\text{KeV}$, an excited state at $E = 1.67\text{MeV}$ with $J^\pi = 2^+; \Gamma = 1.16\text{KeV}$, and three broad states at high excitation energies at 23, 26, and 27MeV have been observed [1]. In addition to the interest in the nuclear structure of these states, the importance of the existence of excited states in the ${}^6\text{Be}$ below and above the ${}^3\text{He} - {}^3\text{He}$ threshold at 11.48MeV resides mainly in the astrophysics. The possible existence of resonances near to this threshold could have strong implications in the p-p burning since the ${}^3\text{He} + {}^3\text{He}$ capture is one the the most important captures in the p-p chain. In addition to that, possible resonances in this capture reaction at low energies would have consequences in the ${}^3\text{He}$ destruction and in the the Solar neutrino problem. The explanation for not observing such excited states in ${}^6\text{Be}$ until now could be in the nuclear reactions used to populate these states. In light nuclei, many excited states have are expected to have a pronounced cluster structure and a poor overlap between the projectile and the target could prevent the formation of states of a given structure. In [2] we have successfully used the ${}^3\text{He}({}^7\text{Li}, \alpha){}^6\text{Li}$ reaction to populate all the known excited states of ${}^6\text{Li}$ and, in addition, two new broad states at 12.45 and 15.31MeV excitation energies. The idea here is to use a similar reaction ${}^3\text{He}({}^7\text{Be}, \alpha){}^6\text{Be}$ to populate the ${}^6\text{Be}$. This reaction in fact involves two different mechanisms, a ${}^3\text{He}$ transfer or a neutron transfer from the projectile to the target, both leading to the same outgoing channel. By detecting the α particles emitted at forward angles, we would in principle select the ${}^3\text{He}$ transfer mechanism favoring the formation of an ${}^3\text{He} - {}^3\text{He}$ 'molecule' in the exit channel.

The experiment was performed at CRIB-RIKEN using a pure ${}^7\text{Be}$ beam and a ${}^3\text{He}$ gas target. The ${}^7\text{Be}$ beam of intensity of about $3 - 5 \times 10^5$ pps and $E_l = 53.4\text{MeV}$ was produced by the primary reaction ${}^7\text{Li}(p, n){}^7\text{Be}$ using the cryogenic H_2 target at CRIB. The system of two dipoles and a Wien Filter of CRIB makes the energy and mass selection of the the particles produced in the primary target. Two X-Y PPACs placed before the secondary target allow the measurement of the X-Y position of the beam particles and the reconstruction of their trajectory. The secondary gas cell target was made in São Paulo and has 1 inch diameter and 1.8cm length. Two ($6\mu\text{m}$) havar foils were used as windows. The pressure inside the gas target was of 1atm of ${}^3\text{He}$ at room temperature. A system of 2 E-DeltaE tele-

scopes (telescopes 1 and 2) was used to detect the particles scattered in the gas cell and a third E-DeltaE telescope (telescope 3) was mounted in the other sector to detect the recoil products in coincidence with the scattered particles. The DSSD DeltaE have thickness of $65\mu\text{m}$ for telescopes 1 and 2 and $20\mu\text{m}$ for telescope 3. The coincidence condition was necessary due to the enormous quantity of alpha and ${}^3\text{He}$ particles produced by the breakup of the ${}^7\text{Be}$ in the havar foils. Those particles produce a huge background that would completely mask the existence of any peak from the transfer reaction mainly in the high excitation energy range. By imposing the coincidence with protons or alphas on telescope 3 coming from the decay of the recoil ${}^6\text{Be}$ one is in principle able to select the alphas from the transfer reaction. The telescopes covered an angular range from $10 - 30$ deg for telescope 1 and $34 - 48$ deg for telescope 2 in the laboratory system. The coincidence telescope 3 was in the range -12 to -38 deg.

An E-DeltaE spectrum for telescope 1 is shown in Fig. 1 where one can see the lines corresponding to the ${}^3\text{He}$ and ${}^4\text{He}$ from the target. From the X-Y position of each scattered particle in the telescopes, the beam hit position and its incident angle in the target we are able calculate the scattering angle. A spectrum of the scattering angle versus the total energy for the alpha particles on telescope 1 in coincidence with telescope 3 is shown in Fig. 2. With the information of the alpha particle energy and angle emerging from the reaction we can calculate the excitation energy of the recoil particle ${}^6\text{Be}$. Then we constructed spectra of the excitation energy of ${}^6\text{Be}$ versus the scattering angle which is shown in Fig. 3. One can see that the maximum excitation energy of the experiment was of about 24.5MeV limited by the ${}^7\text{Be}$ beam energy. Due to the fact that the kinetic energy of the protons and alphas coming from the decay of the recoil become smaller as the excitation energy of ${}^6\text{Be}$ decreases, the havar exit window of the target imposes a lower limit in the energy of the decay particles that will punch through the foil and reach the telescope 3. This limit is around $E_{exc} = 10\text{MeV}$ so we don't expect to see states below this limit. The results are still preliminary but one can see that there are peaks in the energy range from $10 - 21\text{MeV}$ excitation energy which could correspond to new states of the ${}^6\text{Be}$ nucleus. However the analysis is still in progress and no conclusion can be drawn yet.

In Fig. 4 we show an spectrum of excitation energy in the low excitation energy range without the coincidence condition. We clearly see the existence of a peak at $E_{exc} = 1.5\text{MeV}$ with a width of about 1.165MeV that corresponds

to the first excited state of the ${}^3\text{He} - {}^3\text{He}$ molecule. The ground state of the ${}^6\text{Be}$ has a width of $\Gamma = 92\text{KeV}$ and would not be seen in this experiment due to the energy resolution.

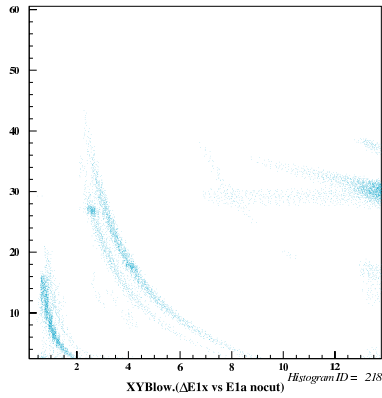


Figure 1. DeltaE-E spectrum for telescope 1. The lines correspond to ${}^3\text{He}$ and α particles.

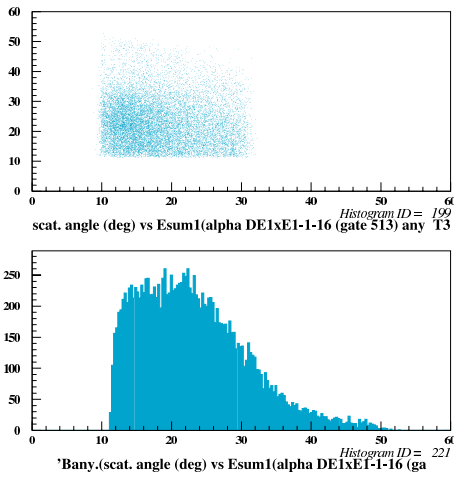


Figure 2. Alpha particle scattering angle versus E_{total} for telescope 1 (10 – 30 deg).

References

- [1] D.R. Tilley, C.M. Cheves, J.L. Goodwin, G.M. Hale H.M. Hofmann, J.H. Kelley, C.G. heu, H.R. Weller Nucl. Phys. **A708**(2002) 3 .
- [2] R. Kuramoto, R. Lichtenthaler *et al.*, Braz. Jou. of Phys. **34** (2004) 933.

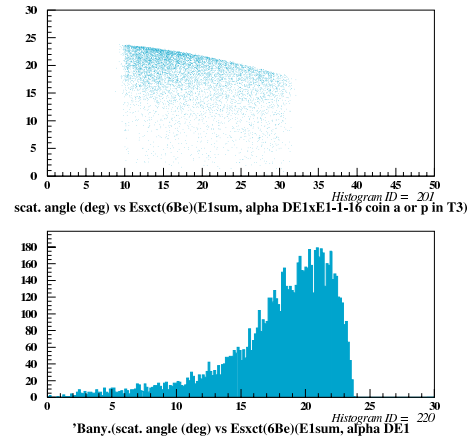


Figure 3. Alpha particle scattering angle versus $E_{exc}({}^6\text{Be})$ for telescope 1 and its projection on the $E_{exc}({}^6\text{Be})$ axis.

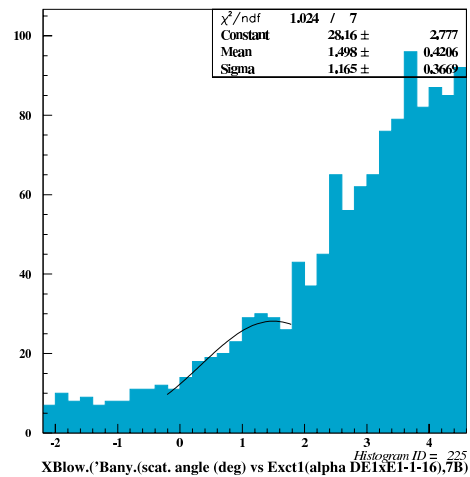


Figure 4. Excitation energy spectrum of ${}^6\text{Be}$ without the coincidence requirement. The first excited state of ${}^6\text{Be}$ is seen.

Elastic Scattering and Breakup of $^{17}\text{F}+^{12}\text{C}$ System at Low Energy

C. J. Lin^a, H. Q. Zhang^a, H. M. Jia^a, X. X. Xu^a, Z. D. Wu^a, G. P. An^a, C. L. Zhang^a, F. Yang^a, S. Kubono^b, H. Yamaguchi^b, Y. Wakabayashi^b, S. Hayakawa^b, Y. Kurihara^b, D. N. Binh^b, N. Iwasa^c, Y. K. Kwon^d, C. Signorini^e, M. Mazzocco^e, M. Romoli^f and M. La Commara^f

Center for Nuclear Study, Graduate School of Science, University of Tokyo

^a*China Institute of Atomic Energy, P. O. Box 275(10), Beijing 102413, P. R. China*

^b*Center for Nuclear Study, University of Tokyo, Hirosawa 2-1, 351-0198 Wako, Saitama, Japan*

^c*Department of Physics, Tohoku University, Miyagi, 980-8578, Japan*

^d*Department of Physics, Chung-Ang University, 156-756 Seoul, Korea*

^e*Dipartimento di Fisica and INFN, via Marzolo 8, I-35131 Padova, Italy*

^f*Dipartimento di Scienze Fisiche and INFN, via Cinthia, I-80125 Napoli, Italy*

Reaction mechanism induced by radioactive ion beam is a topic of current interest. ^{17}F nucleus is a typical single-proton halo/skin nucleus. Its binding energy is only 0.6 MeV, and its first excited state ($E_x = 0.495$ MeV, $2s_{1/2+}$) has a obvious halo structure. Recently, many experiments were performed by using ^{17}F beams [1, 2, 3, 4] for studying of the structure effects and the breakup effects. These experiments are mostly explored on the heavy target ^{208}Pb [1, 2, 3] except on the ^{12}C and ^{14}N [4] at energy of 170 MeV, which is far from the Coulomb barrier. The interaction between ^{17}F and ^{208}Pb is dominantly the Coulomb interaction, which plays an important role for breakup process. But for the light target nuclei, the nuclear interaction plays a dominating role.

We propose to measure the elastic scattering and breakup of $^{17}\text{F}+^{12}\text{C}$ system at low energy by means of the CNS radioactive ion beam (CRIB) separator. In order to identify the scattering ^{17}F and the breakup component ^{16}O , a large ionization chamber (IC) combined with three layers of silicon detector array were designed. Fig. 1 shows the schematic planform of the IC. The first layer of silicon detector array is six pieces of double-side silicon strip detectors (DSSD) with thickness of $64\ \mu\text{m}$ (each side has 16 strips and each strip has 3 mm in width with 0.1 mm interval), giving the ER signals of projectile-like particles (like ^{17}F , ^{16}O) and the ΔE signals of light particles (like breakup protons). The second and third layers are large area silicon detectors (LASD) with thickness of $300\ \mu\text{m}$, giving the ER signals of light particles. The experimental target was installed inside the IC, just after the entrance window.

The experiment was performed at CRIB during Oct. 27 C Nov. 6, 2007. A primary ^{16}O beam with energy of 101.21 MeV and intensity of 300 enA was accelerated by the AVF cyclotron, bombarding on the cooled D2 gas target with temperature of 90 K, pressure of 211.12 Torr and length of 8 cm. After the Wien filter, the typical intensity of secondary ^{17}F beam is about 5×10^5 pps, and the purity is about 92%. The main contaminator is the scattering of ^{16}O beam. Fig. 2 shows the status of the purity of ^{17}F beam. Before the IC, there are two PPACs for tracking the beam position and direction. After the entrance window ($1.5\ \mu\text{m}$ Mylar) of IC, the actual energy of ^{17}F beam bombarding on the target is 57.24 MeV. Before the formal ^{12}C

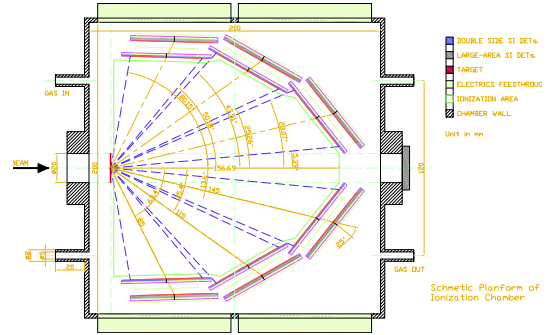


Figure 1. Schematic planform of ionization chamber and silicon detector array.

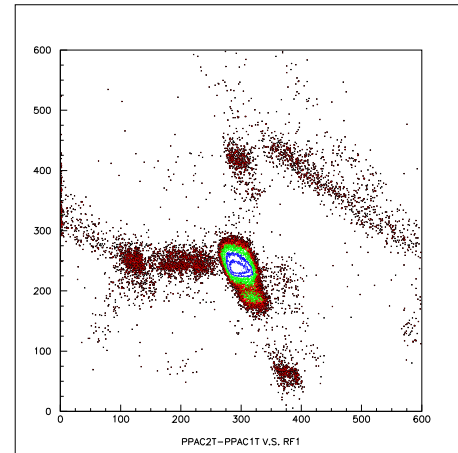


Figure 2. The purity of secondary ^{17}F beam.

($435\ \mu\text{g}/\text{cm}^2$) experiment, a ^{197}Au target with thickness of $2.49\ \text{mg}/\text{cm}^2$ was bombarded by the primary ^{16}O beam with intensity of 1×10^6 pps for calibrating the gain of amplifier, the solid angle of DSSD, etc., and for testing the resolution of IC. When the count rate was higher than 2×10^4 pps, IC lost the energy resolution due to the signal pileup in the preamplifier. In order to ensure the statistic precision, the IC was abandoned in the ^{12}C experiment. Only in a few experiment run, the IC was used at low beam intensity for test. The remained DSSDs and LASDs recorded the energies and positions of the projectile-like particles and breakup light particles. Fig. 3 shows the energy spectra of quasi-elastic particles deposited in the first, third, fifth, and

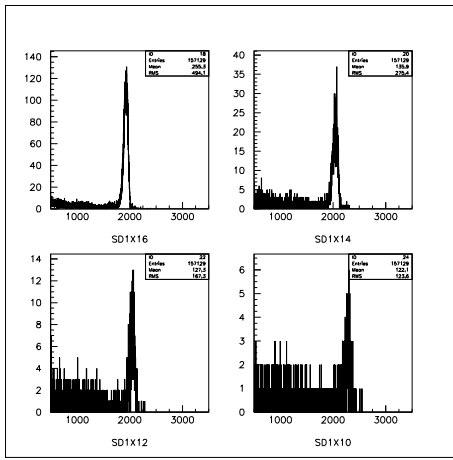


Figure 3. Energy peaks of quasi-elastic scatterings for some silicon strips at the forward angles.

seventh strips from the forward angle to the backward angle. It can be seen that the cross sections of quasi-elastic scatterings of $^{17}\text{F}+^{12}\text{C}$ systems decrease rapidly with the angle increasing.

Detail data analyses are still in progress. Good results are in expectation.

References

- [1] K. E. Rehm *et al.*, Phys. Rev. Lett **81** (1998) 3341.
- [2] J. F. Liang *et al.*, Phys. Rev. C **65** (2002) 051603; Phys. Rev. C **67** (2003) 044603.
- [3] M. Romoli *et al.*, Phys. Rev. C **69** (2004) 064614.
- [4] J. C. Blackmon *et al.*, Phys. Rev. C **72** (2005) 034606.

Production of the spin-polarized ^{17}N beam via the inverse-kinematics transfer reaction

K. Shimada^a, G. Amadio, T. Arai^b, Y. Hasama^b, N. Hatakeyama^b, S. Hayakawa, T. Inoue^b, S. Kagami^b, D. Kameda^c, H. Kawamura^d, Y. Kobayashi^c, S. Kubono, Y. Kurihara, J. Murata^d, D. Nagae^e, T. Nagatomo^c, C. Nakano^b, T. Sugimoto^f, K. Suzuki^b, K. Takase^b, M. Takemura^b, T. Toyoda^d, H. Ueno^c, Y. Wakabayashi, H. Yamaguchi, A. Yoshimi^c and K. Asahi^b

^a*Cyclotron and Radioisotope Center, Tohoku University
Center for Nuclear Study, Graduate School of Science, University of Tokyo*

^b*Department of Physics, Tokyo Institute of Technology*

^c*RIKEN Nishina Center*

^d*Department of Physics, Rikkyo University*

^e*Japan Synchrotron Radiation Research Institute*

^f*Japan Atomic Energy Agency*

Production of spin-polarized/aligned radioactive isotopes (RI) would provide useful tools for research fields. For example, the angular distribution of β or γ rays emitted from spin-polarized/aligned RI is utilized to extract decay properties [1], nuclear structure information [2] and hyperfine interactions between a nucleus and its environment [3]. In particular, the case of the spin-polarized RI in the form of a beam is exclusively useful not only because they can be immediately implanted in a sample material, but also because the sample position where the measurement is done can be separated spatially from the site of production from where normally huge interfering radiation comes. In addition, when the energy of the beam is conveniently low, the implantation in a thin sample material would be quite efficient, since their energy distribution becomes narrower as the energy decreases. One of the most appropriate methods to produce such a beam is that via an inverse-kinematics reaction. We have been developing a method to produce a beam of spin-polarized ^{17}N via a $^9\text{Be}(^{18}\text{O}, ^{17}\text{N})$ reaction [4, 5].

Previously we reported on the dependence of the produced polarization on the outgoing momentum [4]. The fact that the size of polarization observed there was not large may be attributed to the kinematic condition. In a normal-kinematics experiment such as that with a $^{11}\text{B}(d,p)^{12}\text{B}$ reaction [6] the obtained polarization shows an abrupt change including its sign. This suggests, by selecting suitable recoil angles and incident deuteron energy, ^{12}B polarization as large as 15 % should be obtained. Indeed, Yamamoto and Kubo [7] discusses a possibility of large spin polarization for the nuclei produced via an inverse-kinematics nucleon-transfer reaction using Brink's matching conditions [8]. According to them, the sign of polarization should depend on whether the reaction is near-side or far-side dominant. The kinematical matching conditions become different between the near-side and far-side trajectories, and consequently, the cross sections also become very different between them. This implies that even though the "averaged" polarization is small. A large spin polarization may be obtained when the near-side and far-side trajectories are distinguished, e.g. through the emission angle.

In the present report, we focus on the dependence of the spin polarization on the emission angle.

A beam of radioactive nuclei ^{17}N was produced with an in-flight isotope separator CRIB, and the spin polarization of ^{17}N was measured using the β -NMR technique. The incident energy of the primary ^{18}O beam was 126 MeV. The experimental details have been described in Refs. 4 and 5. Two major changes were made in the present experiment: (1) The region of the emission angle θ_L was varied by rotating the CRIB to sit at angles, 0.0° , 2.6° and 5.0° . Slits placed after the target in the F0 chamber were used to define the acceptance of particles by the CRIB. (2) The β -NMR apparatus was moved from the previous location F3 to a new location at the doubly achromatic plane F2, in order to accommodate with the rotation of the CRIB.

In order to select channels with small Q values, where the polarization is expected to increase [4, 9], the accepted momenta for the ^{17}N particles were limited to $(1.0045\text{--}1.0295)p_0$ using slits placed in the momentum-dispersive plane, where p_0 denotes the ^{17}N momentum corresponding to a peak in the momentum distribution of the ^{17}N beam.

The observed β -ray asymmetry AP as a function of the emission angle $\theta_{c.m.}$ in the center-of-mass system is shown in Fig. 1. Here P and $A = -0.57$ denote the polarization and the (averaged) asymmetry parameter for the $^{18}\text{O} \rightarrow ^{17}\text{N}$ β transition, respectively.

According to Brink [8], the kinematical matching condi-

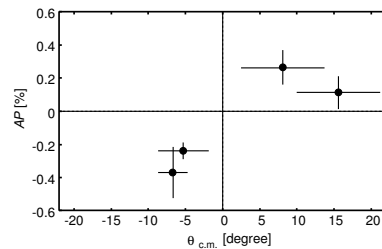


Figure 1. Observed β -ray asymmetry AP as a function of the emission angle $\theta_{c.m.}$ in the center-of-mass system. Vertical extension indicates the uncertainty in AP (one standard deviation), which was mainly due to the counting statistics.

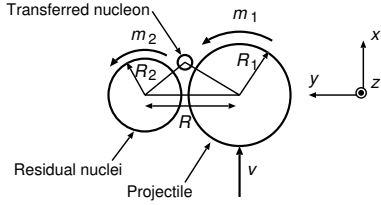


Figure 2. Diagram of the transfer process. Symbols are defined in the text.

tion for the probability of nucleon transfer to be large comprises two requirements, namely, the linear momentum of the transferred nucleon and the angular momentum of the reaction system have to be approximately conserved before and after the transfer process. The first is given by

$$\Delta k = k_0 - m_1/R_1 - m_2/R_2 \approx 0, \quad (1)$$

where k_0 is a wave number of the projectile per nucleon in the laboratory system, R_1 and R_2 the radii of the projectile and residual nucleus, respectively, and m_1 and m_2 the z -components of the orbital angular momenta l_1 and l_2 of the projectile and residual nucleus, respectively. They are illustrated in Fig. 2. Here the z axis is chosen parallel to a vector $\mathbf{k}_f \times \mathbf{k}_i$ where \mathbf{k}_i and \mathbf{k}_f are the incoming and outgoing wave vectors, respectively. The second requirement is written as

$$\Delta L = (m_2 - m_1) + \frac{1}{2}k_0(R_1 - R_2) + \frac{Q_{\text{eff}}R}{\hbar v} \approx 0, \quad (2)$$

where $R = R_1 + R_2$, Q_{eff} denotes the effective reaction Q value defined as $Q_{\text{eff}} = Q - \Delta V_C$ with ΔV_C being the difference in the Coulomb barrier between the initial and final channels, and v is the relative velocity of the projectile and residual nuclei. In addition, Brink defines the following third condition due to the parity restriction,

$$l_1 + m_1 : \text{even} \quad \text{and} \quad l_2 + m_2 : \text{even}. \quad (3)$$

They show that the cross section acquires a strong dependence on the z -component of nucleon orbital angular momenta before and after the transfer.

We evaluated values of $|\Delta k|$ and $|\Delta L|$ numerically as a function of the incident energy E_i of the ^{18}O beam according to Eqs. (1) and (2), and the result is shown in Fig. 3. In a simplest case of the $^9\text{Be}(^{18}\text{O}, ^{17}\text{N})^{10}\text{B}$ reaction with a ground state (g.s.) to g.s. transfer of proton, the proton is transferred from a $p_{1/2}$ state to a $p_{3/2}$ state, so that both l_1 and l_2 are 1. From Eq. (3) we obtain $m_1 = \pm 1$ and $m_2 = \pm 1$, which we used in the evaluation.

As seen in Fig. 3, at $E_i = 126$ MeV the condition (1) on Δk is mostly satisfied for the transfer from the $m_1 = +1$ to $m_2 = +1$ states. On the other hand, the condition (2) on ΔL are satisfied for the transfers except from $+1$ to -1 . The sign of m_1 plays an important role in a sign of the polarization of the ejectile, because the latter should be opposite to the former due to the angular-momentum conservation. The deflection angle of the ejectile is essentially governed by a balance between the attractive nuclear force and repulsive Coulomb force: The nuclear force should become dominant when the proton number Z of the target decreases, so

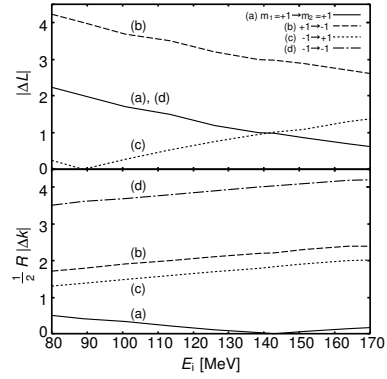


Figure 3. Dependence of $|\Delta k|$ and $|\Delta L|$ on the incident energy E_i of ^{18}O , evaluated according to Eqs. (1) and (2). The nuclear radius was evaluated assuming $1.4A^{1/3}$ fm and the Coulomb energy difference $\Delta V_c = -1.44(Z_1^f Z_2^f - Z_1^i Z_2^i)/R$ MeV, where Z_1^f, Z_2^f and Z_1^i, Z_2^i are the proton numbers for the nuclei in the final and initial states, and $R = R_1 + R_2$. (a) The transfer from $m_1 = +1$ to $m_2 = +1$, (b) from $+1$ to -1 , (c) from -1 to $+1$ and (d) from -1 to -1 .

that the dominating trajectory is considered to switch from the near-side to far-side trajectories [7, 9]. Thus, the transfers with $m_1 = +1$ contribute to negative polarization of ^{17}N , while $m_1 = -1$ to the positive. The sign of the polarization P observed for $\theta_{c.m.} > 0$ is negative (since $AP > 0$ whereas $A < 0$ for the ^{17}N β decay). This indicates that, in view of the hindrance of the $\pm 1 \rightarrow -1$ transfers due to large $|\Delta L|$ and $\frac{1}{2}R|k|$ values, respectively, the transfer from $+1$ to $+1$ should be dominant. The $|\Delta L|$ value for the transfer from $+1$ to $+1$ becomes smaller than that for the transfer from -1 to $+1$ for $E_i \geq 140$ MeV. Thus, the magnitude of the polarization of ^{17}N is expected to increase as E_i increase beyond 140 MeV.

We investigated the emission-angle dependence of the polarization of a radioactive beam of ^{17}N , produced via the inverse-kinematics low-energy transfer reaction. Although the maximum magnitude of the polarization obtained to date was not large, the sign of the ^{17}N polarization turned out to agree with that evaluated by considering the Brink's matching conditions.

References

- [1] Y. Hirayama *et al.*, Phys. Lett B **611** (2005) 239.
- [2] H. Ueno *et al.*, Phys. Lett. B **615** (2005) 186.
- [3] M. Mihara *et al.*, Physica B **376–377** (2006) 955.
- [4] K. Shimada *et al.*, CNS Ann. Rep. 2006 **31** (2007) 31.
- [5] K. Shimada *et al.*, RIKEN Accel. Prog. Rep. **41** (2008).
- [6] M. Tanaka *et al.*, Nucl. Phys. A **263** (1976) 1.
- [7] Y. Yamamoto and K. Kubo, Phys. Rev. C **49** (1994) 360.
- [8] D. M. Brink, Phys. Lett. B **40** (1972) 37; M. Ishihara *et al.*, Phys. Lett. B **73** (1978) 281.
- [9] K.H. Tanaka *et al.*, Phys. Rev. C **34** (1986) 580.

The $^{18}\text{F}+\text{p}$ process and the Nova phenomenon

S. Cherubini^a, C. Spitaleri^a, V. Crucillà^a, M. Gulino^a, M. La Cognata^a, L. Lamia^a,
 R.G. Pizzone^a, S. Puglia^a, G.G. Rapisarda^a, S. Romano^a, M.L. Sergi^a, A. Tumino^{a+}
 S. Kubono, H. Yamaguchi, Y. Wakabayashi, S. Hayakawa
 N. Iwasa^b, S. Kato^c, H. Komatsubara^d, T. Teranishi^e
 A. Coc^f, De Séreville^g

^aUniversità di Catania and INFN-LNS, Catania, Italy

Center for Nuclear Study, Graduate School of Science, University of Tokyo

^bDepartment of Physics, Tohoku University, Sendai, Japan

^cDepartment of Physics, Yamagata University, Yamagata, Japan

^dDepartment of Physics, Tsukuba University, Tsukuba, Japan

^eDepartment of Physics, Kyushu University, Fukuoka, Japan

^fCentre de Spectrométrie Nucléaire et de Spectrométrie de Masse, IN2P3, F-91405 Orsay, France,

^g Institut de Physique Nucléaire, IN2P3, F-91405 Orsay, France

⁺ Present address: Università KORE, Enna, Italy

From astrophysical considerations it is known that the reaction $^{18}\text{F}(\text{p},\alpha)^{15}\text{O}$ is of interest in the Novae phenomenon. The cross section of this reaction has to be studied in the energy range 100-500 keV (center of mass) roughly [1]. In particular, the contribution to the cross section of the resonance at 330 keV has to be investigated together with the interferences between several other levels occurring in the region of interest. In spite of several attempts to measure this cross section (see e.g. [2,3,4,5,6,7,8,9,10,11,12,13,14,15]) the situation is still not satisfactory.

We performed the first run of an experiment aiming at the measurement of the $^{18}\text{F}(\text{p},\alpha)^{15}\text{O}$ reaction using a ^{18}F beam produced at the CRIB set-up of the Center for Nuclear Study (CNS) of the University of Tokyo, based at the RIKEN campus in Wako, Japan.

In this first run, we used the thick target method in order to directly measure the cross section of the reaction at hand down to a cm energy of roughly 400 keV. As it is well known, this method allows for the investigation of a wide region of the excitation function using a single beam energy.

The experimental CRIB set-up is described in ref. [16] and it is displayed on figure 1. The beam was produced in-flight by the $^{18}\text{O}(\text{p},\text{n})^{18}\text{F}$ reaction. The energy of the ^{18}O primary beam was 72 MeV. This beam was used to bombard a primary target that was cooled using liquid nitrogen during the experiment.

The products coming from the production target were separated from the primary beam by the CRIB set-up. After the doubly achromatic separator a Wien filter was also used to further purify the ^{18}F beam. The final energy of the ^{18}F beam on a thick CH_2 target was roughly 13.5 MeV. The obtained ^{18}F beam was practically pure (purity > 99%) and with an intensity slightly more than 10^6 pps.

The detection setup is schematically shown in figure 2. The main parts of it are the doublet of parallel plate avalanche

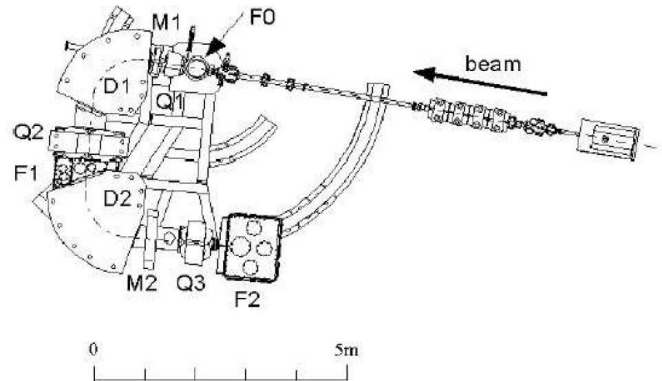


Figure 1. Schematic top view of the CRIB apparatus. The primary beam coming from the AVF cyclotron impinges on the primary target at F0 and the reaction products formed in the reactions are guided and separated by the doubly achromatic spectrometer.

counters (PPACs), eight bidimensional position sensitive silicon detectors (DPSSD) with a sensitive area of 45 by 45 mm each forming a 3 by 3 array with a central hole of roughly the dimensions of a single DPSSD and a pair of double sided multistrip silicon detectors (DSSSD).

The PPACs were used to reconstruct of the trajectory of each single incident particle so that the intrinsic beam divergence do not affects the angular resolution of the detection system. Also, these detectors were used as part of the time of flight measurement system. The DPSSD array and the DSSSD detected the outgoing particles over a wide portion of the solid angle.

Data analysis of the experiment is in a very initial state: in particular the PPACs calibration has been performed and the silicon detector calibration is presently carried on.

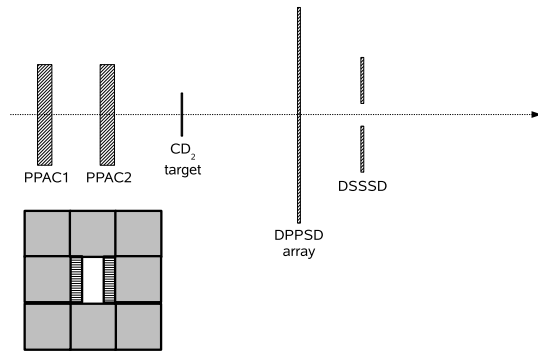


Figure 2. Schematic view of the experimental set-up. The DPSSD array and DSSSD are also shown in front view. The hatched items in this front view represent the two downstream DSSSD. The two PPACs serve as beam trackers allowing for the kinematical reconstruction of each single event.

References

- [1] A. Coc et al., *A.&A.*, 357 (2000) 561 and references therein.
- [2] M. Wiescher and K.U. Kettner, *Astrophys. J.* 263 (1982) 891.
- [3] K.E. Rehm, M. Paul, A.D. Roberts, et al., *Phys. Rev. C*52 (1995) R460.
- [4] R. Coszach, M. Cogneau, C.R. Bain, et al., *Phys. Lett. B*353 (1998) 184.
- [5] K.E. Rehm, M. Paul, A.D. Roberts, et al., *Phys. Rev. C*53 (1996) 1950.
- [6] K.E. Rehm, C.L. Jiang, M. Paul, et al., *Phys. Rev. C*55 (1997) R566.
- [7] J.S. Graulich, F. Binon, W. Bradfield-Smith, et al., *Nucl. Phys. A*626 (1997) 751.
- [8] S. Utku, J.G. Ross, N.P.T. Bateman, et al., *Phys. Rev. C*57 (1998) 2731 and *C*58 (1998) 1354.
- [9] Y.M. Butt, J.W. Hammer, M. Jaeger, et al., *Phys. Rev. C*58 (1998) R10.
- [10] J.-S. Graulich, S. Cherubini, R. Coszach, et al., *Phys. Rev. C*63 (2001) 011302 and references therein.
- [11] D.W. Bardayan, J.C. Blackmon, W. Bradfield-Smith, et al., *Phys. Rev. C*63 (2001) 065802.
- [12] D.W. Bardayan, J.C. Batchelder, J.C. Blackmon, et al., *Phys. Rev. Lett.* 89 (2002) 262501.
- [13] R.L. Kozub, D.W. Bardayan, J.C. Batchelder, et al., *Phys. Rev. C*71 (2005) 032801 (R).
- [14] R.L. Kozub, D.W. Bardayan, J.C. Batchelder, et al., *Nucl. Phys. A* 758 (2005) 753c-756c.
- [15] N. De Séreville, A. Coc, C. Angulo, et al., *Phys. Rev. C*67 (2003) 052801 (R) and references therein.
- [16] Y. Yanagisawa, S. Kubono, T. Teranishi, et al., *Nucl. Instr. Meth. A* 539 (2005) 74

³⁰S Beam Production with CRIB: Analysis of 2006 Data and Preliminary Experimental Results from 2008

D. Kahl, A. A. Chen, D. N. Binh^a, J. Chen, T. Hashimoto^a, S. Hayakawa^a, S. Kubono^a, Y. Kurihara^a, N. H. Lee^b, S. Michimasa^a, S. Nishimura^c, C. V. Ouellet, K. Setoodehnia, Y. Wakabayashi^a, and H. Yamaguchi^a

Department of Physics and Astronomy, McMaster University

^a*Center for Nuclear Study, Graduate School of Science, University of Tokyo*

^b*Department of Physics, Ewha Womans University*

^c*RIKEN (The Institute of Physical and Chemical Research)*

The $^{30}\text{S}(\alpha, p)^{33}\text{Cl}$ reaction is important to understanding the energy release in Type I X-Ray bursts (XRBs), as (α, p) reactions on $T_z = -1$, even-even nuclei may compete with the rp -process in the mass region $22 \leq A \leq 34$ [1]. In order to conduct the first direct experimental measurement of the $^4\text{He}(\alpha, p)^{33}\text{Cl}$ cross-section at astrophysical energies, the authors undertook a second ^{30}S radioactive beam production run in May 2008, as a follow-up to a December 2006 experiment [2].

In the future cross-section measurement, we plan to scan the Gamow window by bombarding a thick (windowed) ^4He gas target with a ^{30}S beam. To scan the center-of-mass energies corresponding to the XRB Gamow window ($0.4 \leq T_9 \leq 1.2$), $E_{\text{beam}} = 22.5$ MeV for $^4\text{He}(\alpha, p)^{33}\text{Cl}$. The $^{30}\text{S}(\alpha, p)$ Hauser-Feshbach cross-section at $T = 1.2$ GK is $16 \mu\text{b}$, whereas at $T = 2$ GK the theoretical cross-section jumps to 3 mb [3] [4]. To scan the 2 GK $^4\text{He}(\alpha, p)$ Gamow window, a ^{30}S beam with $E_{\text{beam}} = 32.3$ MeV is required on target. To get good reaction statistics over the course of one week, the ^{30}S beam intensity ought to be 1×10^5 pps.

This work is an on-going collaboration at the CNS radioactive ion beam separator (CRIB) facility [5] of the University of Tokyo at the Nishina Center of RIKEN. Analysis of the December 2006 data and preliminary results from the May 2008 experiment are reported below.

At the CRIB there are four focal planes of interest, denoted F0, F1, F2, and F3, respectively. The production target of the secondary beam is located at F0. After the first magnetic dipole is the momentum dispersive focal plane, F1, followed by a double achromatic focal plane, F2 [5]. Finally, a Wien filter is used before the scattering chamber F3. The ^{30}S beam is produced via $^3\text{He}(\alpha, n)^{30}\text{S}$ by impinging a ^{28}Si primary beam on a $2.5 \mu\text{m}$ Havar windowed gas cell of ^3He held at 400 Torr cooled to 80K with LN₂ located at F0. The primary beam is produced by the Hyper ECR ion source and accelerated by the RIKEN AVF Cyclotron. In December 2006 a $^{28}\text{Si}^{9+}$ primary beam of energy 6.9 MeV/u with intensity of 100 pA was tested, and in May 2008 a $^{28}\text{Si}^{10+}$ primary beam of energy 7.5 MeV/u with intensity of 10 pA was tested.

We developed a number of ^{30}S beams optimized to different parameters. In December 2006, we achieved ^{30}S beams on target at F3 with 3×10^3 pps per 100 pA, 14.1 ± 1.5 MeV, and 3.4% purity; a decimal was omitted in the Annual Report 2006 such that 0.56% purity mistakenly read

56% purity [2]. In May 2008, our results were notably improved, with ^{30}S beams at F2 attaining 6.2×10^3 pps per 10 pA, and at F3 attaining 30.5 ± 1.5 MeV and 30% purity. Beam data in the experimental scattering chamber F3 is obtained by two consecutive parallel plate avalanche counters (PPAC) and a ΔE -E silicon telescope as detailed in the Annual Report 2006 [2]. The flight time of particles from the F0 target to the F3 PPACa is denoted as the radio-frequency (RF) time, and will differ based on a particle's trajectory through the two magnetic dipoles. The particles' time of flight (ToF) is also recorded between the F3 PPACa and PPACb.

In December 2006, we experimented with two secondary beam charge states, $^{30}\text{S}^{15+}$ and $^{30}\text{S}^{16+}$. The $^{30}\text{S}^{15+}$ charge-state had significantly higher intensity on target, but offline analysis indicated the presence of the leaky-beam contaminant $^{28}\text{Si}^{14+}$ in the RF-ToF spectrum as shown in Fig. 1. Indeed, the $^{28}\text{Si}^{14+}$ primary beam particles had $E \approx 22$ MeV on target, and the $^4\text{He}(\alpha, p)$ cross-section will be much higher than $^4\text{He}(\alpha, p)$ with ^{30}S $E_{\text{beam}} = 11.3$ MeV [6]. The magnetic dipoles separate particles of the same energy by their charge-to-mass ratio ($\frac{m}{q}$). We determined that without use of a thin degrader (0.7 to $1.5 \mu\text{m}$ aluminized mylar) at F1, it was impossible to separate $^{30}\text{S}^{15+}$ ($\frac{m}{q} = 2$) from $^{28}\text{Si}^{14+}$ ($\frac{m}{q} = 2$) using the RF-ToF method at CRIB. Thus, a charge-state-booster increasing the yield of the fully-stripped ion $^{30}\text{S}^{16+}$ (unique $\frac{m}{q}$) was sought [7]. We tested a $508 \mu\text{g}/\text{cm}^2$ carbon foil after the production target at F0, but the preliminary results indicate under our conditions, carbon foil has the same charge-state equilibrium as the production target Havar foil exit window. Further data analysis and charge-state distribution measurements are planned. In order to increase the secondary beam energy and the total yield, we hypothesized that a higher energy primary beam would have a higher cross-section for the $^3\text{He}(\alpha, n)^{30}\text{S}$ production reaction. Although a $^{28}\text{Si}^{10+}$ primary beam may be accelerated by the RIKEN AVF Cyclotron 0.6 MeV/u faster than $^{28}\text{Si}^{9+}$, the intensity is one order of magnitude lower. Furthermore, during the May 2008 experiment, the $^{28}\text{Si}^{10+}$ primary beam intensity was quite unstable, and although up to 30 pA was achieved, the beam was only stable from 0.1 to 1.5 pA. Due to the primary beam current fluctuations, the May 2008 results must be interpreted with some uncertainty from possible errors in normalization.

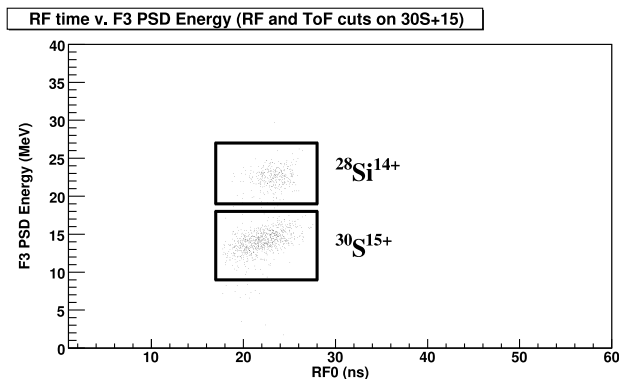


Figure 1. Particle RF time (ns) plotted against energy (MeV), gated on the particle group identified as $^{30}\text{S}^{15+}$ in the RF-ToF spectrum. In this December 2006 run the beam focus is at F3, and the Wien filter is set to 85 kV. A particle's radiofrequency (RF) time is the flight time from F0 to F3 PPACa, and the energy is measured by a $69\ \mu\text{m}$ thick silicon position sensitive detector (PSD). Two distinct energy groups emerge, indicating that the $^{30}\text{S}^{15+}$ beam (813 counts) is contaminated with $^{28}\text{Si}^{14+}$ leaky beam particles (335 counts).

In May 2008, the $^{30}\text{S}^{16+}$ beam had an energy of 30 ± 3 MeV on target, with nearly 80% transmission from F2 to F3. Activation of the Wien filter (WF) at 60 kV did not appear to reduce the $^{30}\text{S}^{16+}$ transmission from F2 to F3, but the Wien filter increased the $^{30}\text{S}^{16+}$ purity by nearly two orders of magnitude (from 0.55% to 30%). The Wien filter also surprisingly reduced the background of high energy particles (34 pps per 10 pA without WF versus less than 1 pps per 10 pA with WF). Previous results indicated that the WF reduced beam transmission from F2 to F3 while also increasing the background of high energy protons [8]. Opening the slits at F1 from 0 ± 5 mm to 0 ± 20 mm increased the $^{30}\text{S}^{16+}$ intensity from 140 pps per 10 pA to 500 pps per 10 pA, but the energy spread on target also increased from 3 MeV to 6 MeV (Full Width Half Maximum).

We also separated $^{30}\text{S}^{14+}$ in May 2008, with a maximum intensity of 1.2×10^4 pps per 10 pA and energy of 32 ± 5 MeV on target as shown in Fig. 2. We experimented with a $1.5\ \mu\text{m}$ aluminized mylar degrader at F1, but the transmission was reduced by 80%, and we clearly separated $^{30}\text{S}^{14+}$ from the leaky-beam contaminate $^{28}\text{Si}^{13+}$ without use of the degrader.

As we still wish to increase the ^{30}S beam intensity on target by one order of magnitude, we are considering the mean charge state distribution of ^{30}S in carbon foil to preferentially populate the charge state of interest. The secondary beam intensities reported for May 2008 are calculated for a primary beam of $^{28}\text{Si}^{10+}$ at 10 pA; improvements to the primary beam intensity correspond to equal improvements of secondary beam intensity. The AVF group has also reported the possibility to accelerate $^{28}\text{Si}^{10+}$ up to 8 MeV/u, but there may be $^{14}\text{N}^{5+}$ contamination arising from the Hyper ECR that would need to be removed. Our results from May 2008 compared with December 2006 indicate roughly

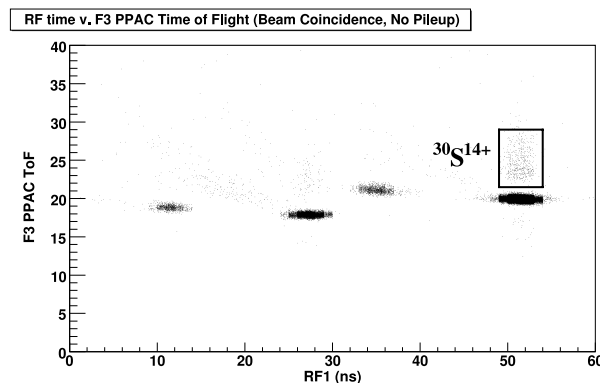


Figure 2. Particle radiofrequency (RF) time (ns) plotted against F3 Time of Flight (ToF) (ns). In this May 2008 run the beam focus is at F3, and the Wien filter is set to 60 kV. A particle's RF time is the flight time from F0 to F3 PPACa, and the ToF is the flight time between F3 PPACa and F3 PPACb. $^{30}\text{S}^{14+}$ comprises 0.8% of the data.

one order of magnitude ^{30}S intensity on target may be gained from a 0.5 MeV/u increase in primary beam energy. We plan to undertake the $^4\text{He}(^{30}\text{S},p)$ cross section measurement in 2009.

These experiments were made possible through the CNS and RIKEN collaboration. The McMaster University group is appreciative of funding from the National Science and Engineering Research Council of Canada.

References

- [1] J. Fisker, F. -K. Thielemann, and M. Wiescher, *Ap. J. Lett.* **608** (2004) 61.
- [2] D. Kahl *et al.*, CNS Annual Report 2006 **CNS-REP-76** (2007) 1.
- [3] T. Rauscher and F. -K. Thielemann, *Atomic Data Nuclear Data Tables* **75** (2000) 1.
- [4] T. Rauscher and F. -K. Thielemann, *Atomic Data Nuclear Data Tables* **79** (2001) 47.
- [5] S. Kubono *et al.*, *Eur. Phys. J. A* **13** (2002) 217.
- [6] M. A. Buckley and J. D. King, *Can J. Phys.* **62** (1984) 134.
- [7] C. Vockenhuber *et al.*, *Phys. Rev. C* **76** (2007) 035801.
- [8] S. Hayakawa *et al.*, CNS Annual Report 2006 **CNS-REP-76** (2007) 11.

Development of ^{46}Cr secondary beam for β -decay measurement

Y. Wakabayashi^a H. Yamaguchi^a S. Hayakawa^a Y. Kurihara^a D. N. Binh^{a,b}, S. Nishimura^c,
Y. Gono^c, and S. Kubono^a

^aCenter for Nuclear Study, Graduate School of Science, University of Tokyo

^bInstitute of Physics and Electronic, Vietnam Academy of Science and Technology

^cRIKEN (The Institute of Physical and Chemical Research)

1. Introduction

For the rapid proton capture process (*rp*-process) in X-ray burst and the core-collapse stage of supernova, weak interaction processes of proton-rich *pf*-shell nuclei far from stability play important roles [1]. Studies of the β and electron capture decays of these proton-rich *pf*-shell nuclei are of great astrophysical interest. These decays involved in the charged-current processes, e.g., $p \rightarrow n + e^+ + \nu$, are predominated by the Fermi and Gamow-Teller (GT) transitions. Thus, these experimental data are required to understand nuclear properties and astrophysical problems.

Information on the GT transitions can be derived directly from β -decay measurements. Recently, studies were performed for several proton-rich *pf*-shell nuclei [2, 3, 4, 5]. However, the GT transition strengths (B(GT)'s) of these proton-rich nuclei far from stability were measured for only a few low-lying states with large uncertainties due to the small production cross sections and short half lives. To determine the B(GT) accurately, it is important to know the feeding ratio and the half life of the β decay accurately.

For the β decay of ^{46}Cr , one of proton-rich *pf*-shell nuclei, the half life of 257(57) ms was measured with a large uncertainty, and only a gamma line of 993 keV was measured with β decay [2].

In this study, the final purpose of the experiment is to measure the properties of ^{46}Cr , namely, i) the total half life of the β decay with an accuracy better than 10 %, ii) the decay branching ratios to the ground state (Fermi transition) and GT states accurately, and iii) higher excited GT states if they exist.

2. Experimental procedure

Experimental runs to develop the ^{46}Cr secondary beam were performed using the low-energy RI beam separator (CRIB) [6, ?] of the Center for Nuclear Study (CNS), University of Tokyo. A primary beam of $^{36}\text{Ar}^{10+}$ at 3.6 MeV/nucleon bombarded a ^{12}C foil of 0.845 mg/cm². The primary beam was degraded to 3.0 MeV/u by a 2.2- μm -thick Havar foil placed in front of the primary target, in order to obtain the maximum production of ^{46}Cr .

A parallel-plate avalanche counter (PPAC) was set at a dispersive focal plane (F1) for beam monitoring. Another PPAC and a Si detector of 1.5 mm thickness were installed for particle identification (PI) at an achromatic focal plane (F2). To separate the contaminants in the secondary beam, the Wien Filter (W.F.) was used at the high voltage of ± 80 kV. A micro channel plate (MCP) [8, 9] was placed at the final focal plane (F3) to monitor the beam position. For the

window of MCP, we used a 0.7- μm -thick Mylar covered by thin aluminum and CsI. For particle identification (PI), a monolithic Si detector [10] was placed behind the MCP. This Si detector consists of 1.5- μm -thick and 500- μm -thick layers that are used as ΔE and E counters, respectively. A Ge detector was set at 260 mm from the ^{12}C primary target for measuring γ rays emitted from the fusion reaction products.

3. Experimental results

Figure 1 shows PI obtained by the monolithic Si detector from the experimental runs, where ΔE is the energy loss in the ΔE counter and Esum indicate the sum of ΔE and E counter. Here, the conditions of CRIB and W.F. were as follows; B ρ and F1 slit position were set to 0.4190 Tm and 0 ± 5 mm, respectively. These values correspond to the energy of $^{46}\text{Cr}^{17+}$ of 53 ± 1 MeV.

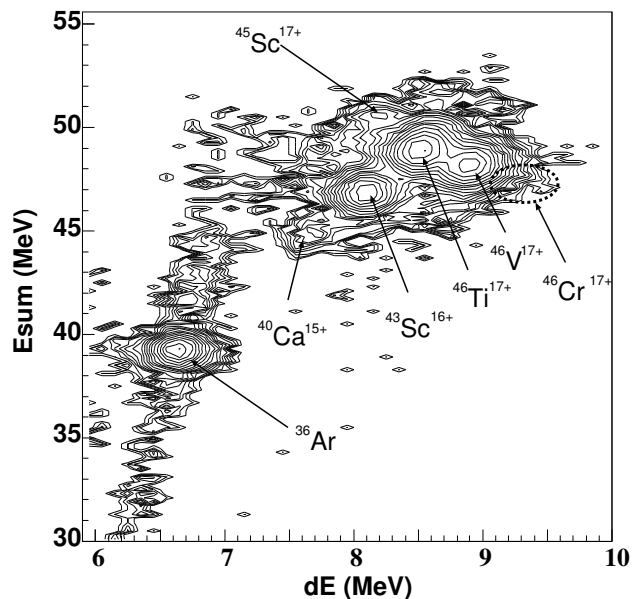


Figure 1. ΔE vs. E spectrum obtained by the monolithic Si detector placed at F3.

Several fusion products were observed together with $^{36}\text{Ar}^{13+}$ from the primary beam. To separate fusion products more clearly, a part of fusion products was selected in Fig. 1. Then the gated spectrum of RF- ΔE on fusion products was obtained, as shown in Fig. 2. From these spectra, it was found that the purity of $^{46}\text{Cr}^{17+}$ was 1.2 % and the

intensity was 2.4 particle per second (pps) with the primary beam of 20 particle nA. The purities and intensities of other nuclides in the secondary beam are also summarized in Table 1.

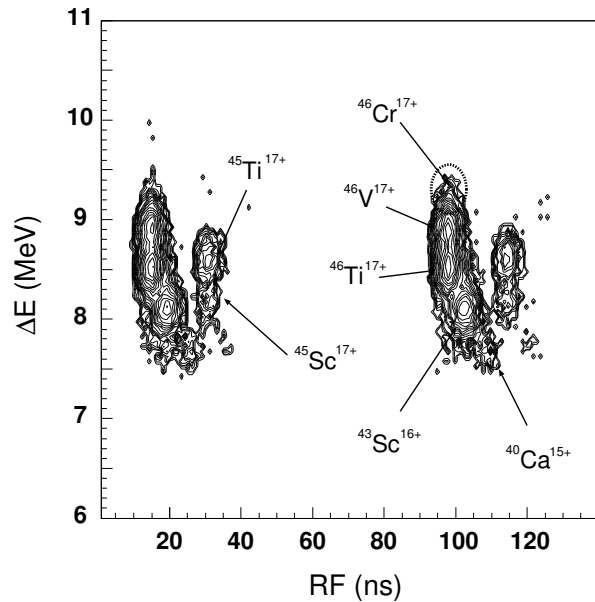


Figure 2. ΔE vs. RF spectrum gated on fusion products.

Based on the experimental result for ^{46}Cr , we may obtain the intensity of 24 pps and 5.2×10^6 particles in total for 6.5 days with the primary beam of 200 particle nA which is available from the AVF cyclotron.

Table 1. Purities and intensities of nuclides with the primary beam of 20 particle nA, where the purities and intensities are shown by the unit of % and pps, respectively. Half lives and branching ratios of each nuclide are also shown.

Nuclide	$^{46}\text{Cr}^{17+}$	$^{46}\text{V}^{17+}$	$^{45}\text{Ti}^{17+}$	$^{46}\text{Ti}^{17+}$
Purity (%)	1.2(2)	28.6(4)	3.0(1)	38.2(5)
Intensity (pps)	2.4	57.3	6.2	76.6
Half life	260 ms	422.4 ms	184.8 m	Stable
Branching ratio of γ ray (%)	21.6	0.01	0.315	Stable

Nuclide	$^{43}\text{Sc}^{16+}$	$^{45}\text{Sc}^{17+}$	$^{40}\text{Ca}^{15+}$	$^{36}\text{Ar}^{13+}$
Purity (%)	13.1(2)	0.9(1)	0.7(1)	15.4(1)
Intensity	26.4	1.8	1.4	33.2
Half life	3.891 h	Stable	Stable	Stable
Branching ratio of γ ray (%)	22.5	Stable	Stable	Stable

We may obtain a clean decay spectrum of ^{46}Cr by the β - γ coincidence method, because of the following reasons; i) ^{46}Ti , ^{45}Sc , ^{40}Ca , and ^{36}Ar are stable nuclei, ii) The decay rates of γ rays of ^{46}V and ^{45}Ti are very small due to these very low ratios involved in β decay, and iii) although ^{43}Sc has the ratio of γ ray of 22.5% emitted from β decay, the 373 keV γ ray with β decay of ^{43}Sc would not disturb

in a γ -ray spectrum because of the energy. Thus, we may have a good possibility to obtain an accurate half life and branching ratio of the β decay of ^{46}Cr .

This program has been approved by the RIKEN-CNS joint PAC for the final run.

References

- [1] K. Langanke and G. Martinez-Pinedo, Rev. Mod. Phys. **75**, 819 (2003).
- [2] T.K. Onishi et al., Phys. Rev. C **72**, 024308 (2005).
- [3] V.T. Koslowsky et al., Nucl. Phys. A **624**, 293 (1997).
- [4] I. Reusen et al., Phys. Rev. C **59**, 2416 (1999).
- [5] A. Jokinen et al., Eur. Phys. J. A **3**, 271 (1998).
- [6] S. Kubono et al., Eur. Phys. J. A **13**, 217 (2002).
- [7] Y. Yanagisawa et al., Nucl. Instrum. Methods Phys. Res. A **539**, 73 (2005).
- [8] J.L. Wiza, Nucl. Instrum. Methods **162**, 587 (1979).
- [9] D. Shapira et al., Nucl. Instrum. Methods Phys. Res. A **454**, 409 (2000).
- [10] A. Musumarra et al., Nucl. Instrum. Methods Phys. Res. B **409**, 414 (1998).

Low-lying s -wave resonance of ${}^8\text{B}$

H. Yamaguchi, Y. Wakabayashi, S. Hayakawa, G. Amadio, S. Kubono, H. Fujikawa, A. Saito^a,
J.J. He^b, T. Teranishi^c, Y.K. Kwon^d, S. Nishimura^e, Y. Togano^f, N. Iwasa^g, K. Inafuku^g,
M. Niikura, and L.H. Khiem^h

Center for Nuclear Study, Graduate School of Science, University of Tokyo

^a*Department of Physics, Graduate School of Science, University of Tokyo*

^b*Institute of Modern Physics, CAS*

^c*Department of Physics, Kyushu University*

^d*Department of Physics, Chung-Ang University*

^e*RIKEN (The Institute of Physical and Chemical Research)*

^f*Department of Physics, Rikkyo University*

^g*Department of Physics, Tohoku University*

^h*Institute of Physics and Electronics, Vietnam Academy of Science and Technology*

1. Introduction

The astrophysical S -factor $S_{17}(E)$ of the ${}^7\text{Be}(p,\gamma){}^8\text{B}$ reaction is one of the most important parameters in the standard solar model, because its value at the energy of the solar center is directly related to the flux of the ${}^8\text{B}$ neutrino, which is the dominant component of the solar neutrinos detected by many neutrino observatories on the earth. It is claimed that S_{17} should be determined with a precision better than about 5% in the energy region below 300 keV in order to test the solar model by comparing the theoretical prediction for the ${}^8\text{B}$ neutrino flux with the observations [1]. For that reason great efforts were spent by many experimental groups [2, 3, 4]. The precision of the existing data, however, is still limited because of the very small cross section of the ${}^7\text{Be}(p,\gamma){}^8\text{B}$ reaction in such a low energy region.

To evaluate S_{17} at low energies, one needs information about the nuclear structure of ${}^8\text{B}$ which, however, has been poorly known until recently. Only the lowest two excited states at 0.77 MeV and 2.32 MeV were clearly observed in the previous experiments [5]. It has been reported that a wide resonance is observed at around 3 MeV, and it was explained as a low-lying $2s$ state [6]. To investigate the reason why a $2s$ state appears at such a low energy is also an interesting subject [7, 8, 9]. This kind of wide states may affect the ${}^7\text{Be}(p,\gamma){}^8\text{B}$ reaction rate in the energy region far below 1 MeV. In another measurement [10], the wide state was not directly observed; nevertheless they concluded that their spectrum was consistent with the existence of the state, if it is located at 3.5 MeV with a width of 4 MeV or more. Thus we intended to study the resonance structure of ${}^8\text{B}$ to evidently observe the 3.5 MeV resonance reported in the previous measurements, and also to explore the unknown region $E > 3.5$ MeV.

2. Experimental result

The measurement was performed at CRIB [11, 12], and the experimental method is described in the previous report [13]. Excitation functions of ${}^7\text{Be}+p$ for three different ranges of the scattering angle were obtained as shown in Fig. 1, by calculating the center-of-mass energy from measured proton energy.

There were three major background proton sources which must be eliminated:

1) *Protons from the reaction with carbon contained in the target*

Since the data were measured with polyethylene (CH_2) target, there were proton events originated from carbon via processes such as fusion evaporation. Their contribution was measured using a carbon target of a similar thickness.

2) *Protons from inelastic scatterings*

The first excited state of ${}^7\text{Be}$ is located at 0.429 MeV, fairly close to the ground state. Therefore, innegligible numbers of protons from the inelastic scattering to the first excited state in ${}^7\text{Be}$ were detected. We used NaI detectors to detect de-excitation γ rays from inelastic events.

3) *Protons from 3-body (${}^7\text{Be}+p \rightarrow {}^4\text{He}+{}^3\text{He}+p$) events*

When a compound ${}^8\text{B}$ nucleus has an excited energy exceeding the threshold at 1.72 MeV, decay to the 3-body channel (${}^4\text{He}+{}^3\text{He}+p$) may occur. Protons from this 3-body channel are distributed over broad energy and angular ranges. At the forward-angle detector, ${}^4\text{He}$ or ${}^3\text{He}$ of the 3-body events are detected together with the proton with a high probability, and thus we can eliminate most of the background protons by selecting single hit events of protons. At larger angles, however, the ${}^4\text{He}$ or ${}^3\text{He}$ particles tend to miss the detector, and the background protons cannot be distinguished from the elastic-scattered protons. The amount of these background protons must be evaluated and subtracted from the spectrum. The energy and angular distribution of the background protons were estimated by a Monte Carlo simulation, and normalized by measured numbers of multiple hit (proton with ${}^4\text{He}$ and/or ${}^3\text{He}$) events.

The spectrum indicated as “total” in Fig. 1 includes all the proton events measured with the polyethylene target. The proton backgrounds described above were subtracted, and excitation functions for the elastic and inelastic scattering were obtained. The contributions by protons from 3-body events estimated by the simulation are also shown in the figure.

Because of the low statistics and limited energy range in the previous experiments [6, 10], the presence of the 2^- state at around 3.5 MeV had been questionable. We

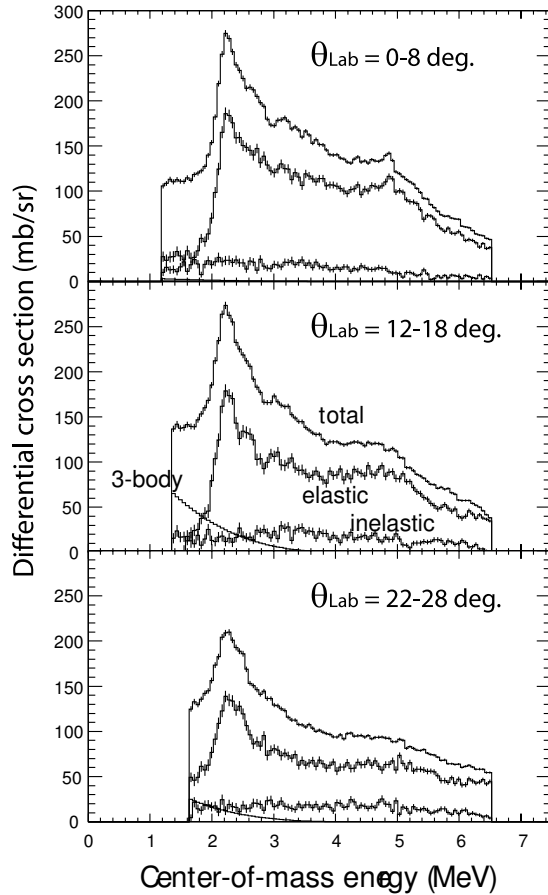


Figure 1. Excitation function of $p+{}^7\text{Be}$ scatterings measured at three different angular ranges. The excitation energy of ${}^8\text{B}$, E_{ex} equals to the center-of-mass energy $E_{\text{cm}}+0.1375$ MeV.

successfully performed measurements with more counting statistics and wider energy range, and the slowly varying excitation function beyond the peak around 2.3 MeV strongly suggests that the peak at 2.3 MeV is possibly enhanced by a broad state that locates at a higher energy. Following this assumption, which is virtually the same as the one taken in [10], we performed R-matrix analysis using SAMMY [14] code.

The R-matrix calculation provides a reliable determination of the resonance parameters (energy E , width Γ , spin J and parity π) even for such wide states. The best fit for $J^\pi = 2^-$ is shown in Fig. 2, where the energy and width are $E = 3.1$ MeV and $\Gamma = 3.8$ MeV. Although the 2^- resonance is broad and did not appeared as a distinct peak, the excitation function is sensitive to the variation of the energy and width. If we reduce the width by about half ($\Gamma=1.8$ MeV), the resulting excitation function, indicated as “narrow” in the figure, totally disagree with the original function, proving that the width of the 2^- resonance is truly affective to the calculated excitation function. We could not obtain satisfactory fits by introducing broad 1^- or any possible positive parity states (0^+ to 3^+), while a broad 2^+ state was introduced to explain the excitation function in a previous study [15].

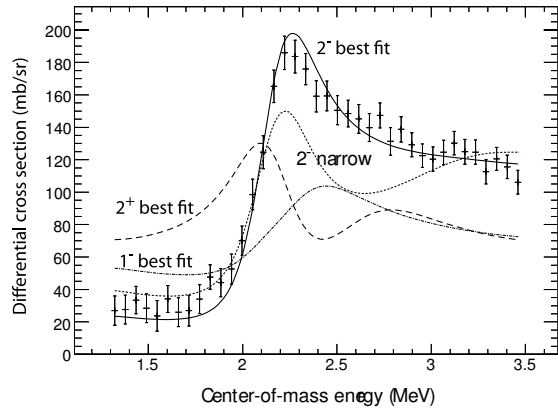


Figure 2. Preliminary analysis result on the proton excitation function of ${}^7\text{Be}$ below 3.5 MeV, measured at 0–8 degrees. R-matrix fit results with the known parameters for the 3^+ state at 2.3 MeV and various parameter sets (excitation energy E and width Γ) for a broad 2^- , 1^- or 2^+ state are illustrated.

In summary, our data supports the presence of a 2^- s -wave state in ${}^8\text{B}$ nucleus, and its energy and width were determined preliminarily as $E \sim 3.1$ MeV and $\Gamma \sim 3.8$ MeV.

3. Acknowledgements

We are grateful to RIKEN accelerator staff for their help. This work was supported by the Grant-in-Aid for Young Scientists (B) (Grant No. 17740135) of JSPS.

References

- [1] E.G. Adelberger *et al.*, *Rev. of Mod. Phys.* **70**, 1265–1291 (1998).
- [2] B. Filippone, A. Elwyn, C. Davids, and D. Koetke, *Phys. Rev. C* **28**, 2222 (1983).
- [3] F. Hammache *et al.*, *Phys. Rev. Lett.* **80**, 928 (1998).
- [4] A. Junghans *et al.*, *Phys. Rev. C* **68**, 065803 (2003).
- [5] D.R. Tilley *et al.*, *Nucl. Phys. A* **745**, (2004) 155.
- [6] V. Gol’dberg *et al.*, *JETP Lett.* **67**, (1998) 1013.
- [7] A. van Hees and P. Glaudemans, *Z. Phys. A* **314** (1983) 323.
- [8] A. van Hees and P. Glaudemans, *Z. Phys. A* **315** (1984) 223.
- [9] F. Barker, and A. Mukhamedzhanov, *Nucl. Phys. A* **673** (2000) 526.
- [10] G. Rogachev *et al.*, *Phys. Rev. C* **64** (2001) 061601(R).
- [11] S. Kubono *et al.*, *Eur. Phys. J. A* **13** (2002) 217.
- [12] Y. Yanagisawa *et al.*, *Nucl. Instrum. Methods Phys. Res., Sect. A* **539** (2005) 74.
- [13] H. Yamaguchi *et al.*, *CNS Annual Report 2005* (2006).
- [14] N. M. Larson, A Code System for Multilevel R-Matrix Fits to Neutron Data Using Bayes’ Equations, ORNL/TM-9179/R5 (2000) (unpublished).
- [15] D. Halderson *et al.*, *Phys. Rev. C* **69** (2004) 014609.

Cluster states in ^{13}C

Y. Sasamoto, T. Kawabata, T. Uesaka, K. Suda, Y. Maeda, S. Sakaguchi, K. Itoh^a, K. Hatanaka^b, M. Fujiwara^b, A. Tamii^b, Y. Shimizu^b, K. Nakanishi^b, K. Kawase^b, H. Hashimoto^b, Y. Tameshige^b, H. Matsubara^b, M. Itoh^c, H. P. Yoshida^d and M. Uchida^e

Center for Nuclear Study, Graduate School of Science, University of Tokyo

^aDepartment of Physics, Saitama University

^bResearch Center for Nuclear Physics (RCNP), Osaka University

^cCyclotron and Radioisotope Center (CYRIC), Tohoku University

^dDepartment of Physics, Kyusyu University

^eDepartment of Physics, Tokyo Institute of Technology

Alpha clustering is one of the important concepts in the nuclear structure. Alpha cluster states in self-conjugate $4N$ nuclei are expected to appear near α -decay thresholds as shown in the Ikeda diagram [1]. For example, it has been suggested that the 7.65-MeV 0_2^+ state in ^{12}C , which is strongly excited by the monopole transition, has a 3α configuration [2]. This state locates at 0.39 MeV above the 3α -decay threshold energy, and is not described by shell-model (SM) calculations. Recently, this state is theoretically considered to have the dilute-gas-like structure [3].

The next natural question is whether such a dilute state of clusters exists in the $A \neq 4N$ nuclei. Recently, it is proposed that the $3/2_3^-$ state in ^{11}B is a candidate for the dilute cluster state where a proton hole in the $p_{3/2}$ orbit couples to the 0_2^+ state in ^{12}C [4, 5]. The $3/2_3^-$ state in ^{11}B at $E_x = 8.56$ MeV, which is located just 100-keV below the α -decay threshold, is strongly excited by the monopole transition.

The large monopole strength for the $3/2_3^-$ state in ^{11}B , which is not explained by the SM calculations, is reasonably well described by the antisymmetrized molecular dynamics (AMD) calculation. According to the AMD calculation, the $3/2_3^-$ state has a loosely bound $2\alpha + t$ cluster structure with a dilute density. It is pointed out that the large monopole transition strength is one of the possible evidences for dilute cluster states.

Similar cluster states where a proton in the $p_{1/2}$ orbit instead of a proton hole in the $p_{3/2}$ orbit couples to the 0_2^+ state in ^{12}C are expected in ^{13}C . Such cluster states are considered to be excited by the monopole transitions similar to the $3/2_3^-$ state in ^{11}B . Therefore, it is important to measure the monopole transition strengths in ^{13}C for the clarification of the cluster structure. Since the spin-parity of the ground state in ^{13}C is $1/2^-$, the $1/2_2^-$ at $E_x = 8.86$ MeV and $1/2_3^-$ at $E_x = 11.08$ MeV states, which are allowed to be excited by the monopole transition, are candidates for such cluster states.

For the measurement of the monopole strengths, the inelastic alpha scattering is a good probe. Since only the isoscalar natural parity transitions are allowed in the (α, α') reaction, the reaction mechanism is expected to be simple. In the present work, we measured the inelastic alpha scattering at forward angles where the monopole transition is enhanced and searched for the cluster states in ^{13}C .

The experiment was performed by using a 400-MeV alpha beam at the Research Center for Nuclear Physics, Osaka University. The self-supporting ^{13}C and ^{nat}C targets with the thickness of 1.5 and 0.5 mg/cm² prepared by a thermal cracking method [6] were used. The alpha particles scattered from the target were momentum analyzed by the magnetic spectrometer Grand Raiden (GR). In order to obtain the isoscalar transition strengths, the cross sections for the $^{13}\text{C}(\alpha, \alpha')$ and $^{nat}\text{C}(\alpha, \alpha')$ reactions were measured at forward angles of $\theta = 0^\circ - 19.4^\circ$. Figure 1 shows the energy spectra for the $^{13}\text{C}(\alpha, \alpha')$ reaction at 0° and 2.5° .

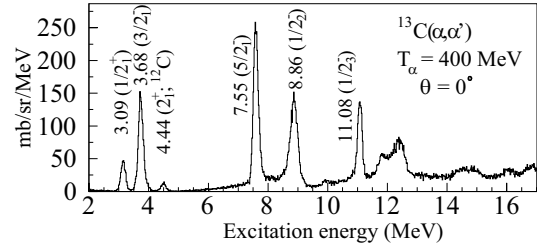


Figure 1. Energy spectra for the $^{13}\text{C}(\alpha, \alpha')$ reaction at 0° and 2.5° .

In order to deduce the transition strength from the measured cross section, the single folding distorted-wave Born approximation (DWBA) calculation was performed. In the single folding model, the optical potential is described as

$$U(r) = \int d\mathbf{r}' \rho_0(r') V(|\mathbf{r} - \mathbf{r}'|, \rho_0(r')) \quad (1)$$

where ρ_0 is the ground state density while $V(|\mathbf{r} - \mathbf{r}'|, \rho_0(r'))$ is the effective interaction. We used the effective α -nucleon interaction as follows,

$$V(|\mathbf{r} - \mathbf{r}'|, \rho_0(r')) = -V(1 + \beta_v \rho_0^{2/3}(r')) e^{-|\mathbf{r} - \mathbf{r}'|^2 / \alpha_v} - iW(1 + \beta_w \rho_0^{2/3}(r')) e^{-|\mathbf{r} - \mathbf{r}'|^2 / \alpha_w}. \quad (2)$$

Parameterizations for the interaction were $\alpha_v = \alpha_w = 4.383$ fm², $\beta_v = -1.9$ fm², $V = 16.943$ MeV and $W = 11.686$ MeV. The transition strengths obtained using this interaction are consistent with the strengths obtained from the electric scattering for the 2_1^+ and 0_2^+ states in ^{12}C . The density distribution of the ground state in ^{13}C is estimated from the charge-density-distribution of ^{13}C . Transition densities for each transition were calculated in the macroscopic description [9].

The measured cross sections for the discrete states are compared with the DWBA calculation in Fig. 2. Since only the natural-parity transitions are allowed in the inelastic alpha scattering, the one transferred spin-parity ΔJ^π are allowed for each state. Using the transition density with which the calculation represents the measured cross section, the isoscalar strength $B(E\lambda : IS)$ is obtained from the volume integrals of the transition density as follows,

$$B(E\lambda : IS) = \left| \int \delta\rho_L \hat{O}_L d\mathbf{r}^3 \right|^2 \quad (3)$$

where $\delta\rho_L$ and \hat{O}_L are the L -th order of the transition density and transition operator, respectively.

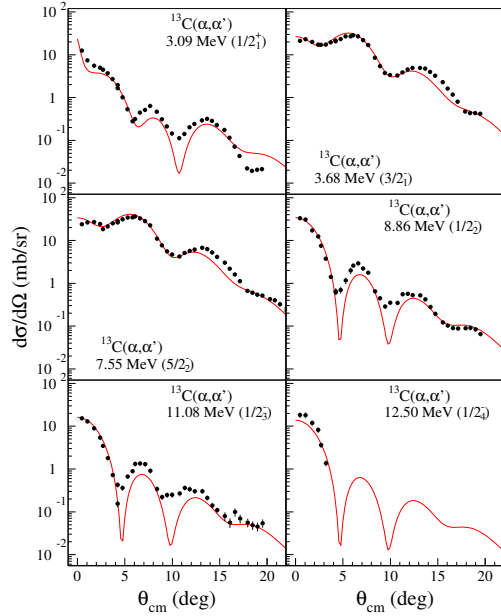


Figure 2. Cross sections for the $^{13}\text{C}(\alpha, \alpha')$ reaction at $E_\alpha = 400$ MeV. Solid-lines show the DWBA calculation.

The obtained isoscalar transition strengths in ^{13}C are tabulated in Table 1. Theoretical predictions by the SM calculation are also listed for comparison. The SM calculation was performed by using the SFO (Suzuki-Fujimoto-Otsuka) interactions within the $0-2\hbar\omega$ configuration space [11]. The theoretical level scheme for the negative-parity states are compared with the experiment in Fig. 3. The SM calculation reasonably explains the experimental level scheme below $E_x = 10$ MeV.

For the $5/2_1^-$ state, the predicted quadrupole strength is relatively smaller than the experimental value. The large monopole strengths were observed for the $1/2_2^-$ and $1/2_3^-$ states although the SM calculation gives the extremely small monopole strengths. The large monopole strengths for the $1/2_2^-$ and $1/2_3^-$ states are reflection of the exotic structure of these states which are not described by the SM calculation. Therefore, the $1/2_2^-$ and $1/2_3^-$ states are inferred to be cluster states.

Table 1. Measured transition strengths compared with the SM predictions.

		Experiment		Shell-model	
J^π	E_x (MeV)	$B(E2; IS)$ (fm^4)			
$3/2_1^-$	3.68	47 ± 5			
$5/2_1^-$	7.55	61 ± 6		44	
		Experiment		Shell-model	
J^π	E_x (MeV)	$B(E0; IS)$ (fm^4)			
$1/2_2^-$	8.86	37 ± 6		~ 0	
$1/2_3^-$	11.08	18 ± 3		~ 0	
$1/2_4^-$	12.5	24 ± 4		~ 0	

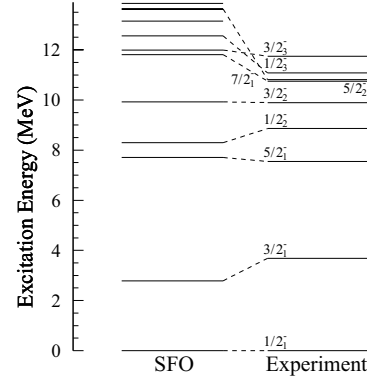


Figure 3. Experimental and theoretical energy level schemes for negative parity states in ^{13}C .

For further clarification, the present results should be compared with the cluster model calculations.

References

- [1] K. Ikeda *et al.* *Prog. Theor. Phys. Suppl. Extra Number* (1968) 464.
- [2] H. Morinaga, *Phys. Rev.* **101** (1956) 254.
- [3] A. Tohsaki *et al.*, *Phys. Rev. Lett.* **87** (2001) 192501.
- [4] T. Kawabata *et al.*, *Phys. Rev. C* **70** (2004) 034318.
- [5] T. Kawabata *et al.*, *Phys. Lett. B* **646** (2007) 6.
- [6] I. Sugai *et al.*, *Nucl. Instrum. Methods* **A521** (2004) 227.
- [7] F. Ajzenberg-Selove, *Nucl. Phys.* **A506** (1990) 1.
- [8] M. N. Harakeh *et al.*, *Giant Resonance* Clarendon Press, Oxford, (2001).
- [9] G. R. Satchler *Nucl. Phys. A* **472** (1987) 215.
- [10] S. Raman, *At. Data Nucl. Data Tables* **78** 1 (2001) 1.
- [11] T. Suzuki, *et al.*, *Phys. Rev. C* **67** (2003) 044302.

Proton Inelastic Scattering Study on Very Neutron-rich Magnesium Isotopes

S. Michimasa, Y. Yanagisawa^a, K. Inafuku^b, N. Aoi^a, Z. Elekes^c, Zs. Fülöp^c, Y. Ichikawa^d, N. Iwasa^b, K. Kurita^e, M. Kurokawa^a, T. Machida^e, T. Motobayashi^a, T. Nakamura^f, T. Nakabayashi^f, M. Notani^g, H. J. Ong^a, T. K. Onishi^d, H. Otsu^a, H. Sakurai^a, M. Shinohara^f, T. Sumikama^h, S. Takeuchi^a, K. Tanaka^a, Y. Togano^e, K. Yamada^a, M. Yamaguchiⁱ, and K. Yoneda^a

Center for Nuclear Study, Graduate School of Science, University of Tokyo

^aRIKEN (The Institute of Physical and Chemical Research)

^bDepartment of Physics, Tohoku University

^cATOMKI, Hungary

^dDepartment of Physics, University of Tokyo

^eDepartment of Physics, Rikkyo University

^fDepartment of Physics, Tokyo Institute of Technology

^gArgonne National Laboratory, USA

^hDepartment of Physics, Faculty of Science and Technology, Tokyo University of Science

ⁱNational Institute of Advanced Industrial Science and Technology

1. Introduction

We report here on the in-beam γ -ray spectroscopy using the very neutron-rich ^{36}Mg beam and a hydrogen target. The ^{36}Mg nucleus is located in the middle of the shell closures of $N = 20$ and 28 and is closer to the neutron drip line than nuclei belonging to the so-called ‘island of inversion’. In previous experimental studies on neutron-rich magnesium isotopes, ^{32}Mg was reported to be a well-deformed nucleus [1], and the disappearance of the magicity at $N = 20$ was indicated. The deformation of ^{34}Mg was reported to be larger than that of ^{32}Mg [2]. The present study is an experiment to search for the low-lying excited states in ^{36}Mg and to investigate evolution of nuclear deformations as a function of the neutron number.

2. Experiment

The experiment was performed at the unstable nuclear beam line in RIKEN. Ions of ^{48}Ca were accelerated up to 63 MeV/nucleon using the acceleration scheme of RFQ-RILAC-CSM-RRC and impinged on a $150\text{-}\mu\text{m}$ ^{181}Ta plate. A radioactive ^{36}Mg beam was isotopically separated by RIPS [3]. Particle identification of the secondary beam was performed by a standard method based on the energy loss, time of flight and magnetic rigidity. The secondary beam bombarded a liquid hydrogen target [4] of 105 mg/cm^2 .

To obtain a sufficient mass resolution for the reaction products, the TOF spectrometer [5] was placed downstream of the secondary target. The scattered particles were detected using a telescope placed at the end of the spectrometer. The telescope consisted of a silicon detector of $500\text{-}\mu\text{m}$ thick and two NaI(Tl) calorimeter. Almost the scattered particles passed through the silicon detector and stopped in the NaI(Tl) crystals. Scattered particles were identified based on TOF through the spectrometer, energy loss in the silicon detector and total energy measured using the calorimeter. Evaluated detection efficiency of the telescope for scattered particles was more than 90%.

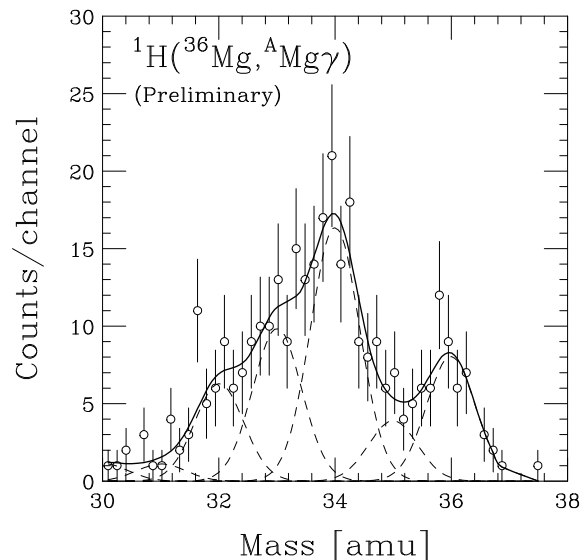


Figure 1. Particle identification of outgoing magnesium isotopes in coincidence with the ^{36}Mg beam.

The de-excitation γ ray from the inelastically scattered particle was detected using 160 NaI(Tl) scintillators (DALI2) [6] surrounding the secondary target. Further details on the experiment setup and on condition of the secondary beam were described in ref. [7].

3. Present Status of Analysis

The identification of outgoing magnesium isotopes in coincidence with an incident ^{36}Mg particle and γ rays is shown in Fig. 1. The ^{36}Mg particles scattered from the secondary target are identified with an accuracy of 0.4 amu (σ).

The three de-excitation γ -ray spectra in Fig. 2 are respectively obtained from the reaction channels of ($^{36}\text{Mg}, ^{34}\text{Mg}$), ($^{36}\text{Mg}, ^{35}\text{Mg}$) and ($^{36}\text{Mg}, ^{36}\text{Mg}$), which are assigned by the

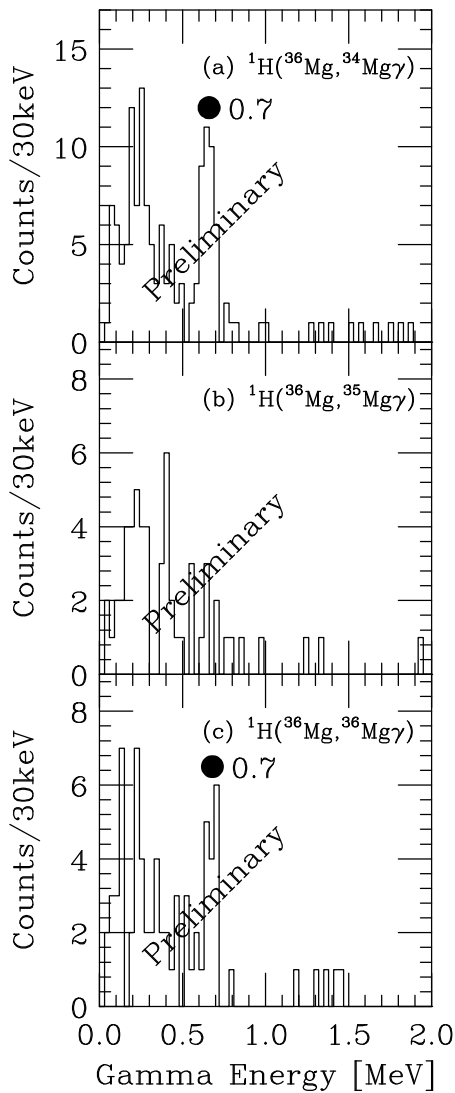


Figure 2. Gamma-ray spectra in (a) the (${}^{36}\text{Mg}, {}^{34}\text{Mg}$), (b) (${}^{36}\text{Mg}, {}^{35}\text{Mg}$) and (c) (${}^{36}\text{Mg}, {}^{36}\text{Mg}$) reactions, respectively.

identification of the incident particles and reaction products. In the two-neutron removal channel, a γ line at around 0.7 MeV is identified as shown in Fig. 2(a). This line is assigned to be the $2_1^+ \rightarrow 0_1^+$ transition in ${}^{34}\text{Mg}$, since its energy is consistent with that shown in the previous works [2]. In Fig. 2(b), no γ line originated from ${}^{35}\text{Mg}$ is identified significantly. In the inelastic channel, a γ line is identified at approximately 0.7 MeV as shown in Fig. 2(c). A de-excitation γ ray in ${}^{36}\text{Mg}$ was recently reported and its energy was at 660(6) keV [8]. The γ ray identified by the present experiment is consistent in energy with the reported γ line, and thus the 660-keV line have been confirmed. This line is assigned to be the $2_1^+ \rightarrow 0_1^+$ transition since no other peaks are found significantly in the spectrum.

Data analysis is now in progress to deduce the cross section of the proton inelastic scattering on ${}^{36}\text{Mg}$ and the deformation length of ${}^{36}\text{Mg}$.

References

- [1] T. Motobayashi *et al.*, Phys. Lett. B **346**, 9 (1995).
- [2] H. Iwasaki *et al.*, Phys. Lett. B **522**, 227 (2001).
- [3] T. Kubo *et al.*, Nucl. Instrum. Methods Phys. Res. B **70**, 309 (1992).
- [4] H. Ryuto *et al.*, Nucl. Instrum. Methods Phys. Res. A **555**, 1 (2005).
- [5] N. Aoi *et al.*, RIKEN Accel. Prog. Rep. **38**, 176 (2005).
- [6] S. Takeuchi *et al.*, RIKEN Accel. Prog. Rep. **36**, 148 (2003).
- [7] S. Michimasa *et al.*, CNS-REP-76, 15 (2007).
- [8] A. Gade *et al.*, Phys. Rev. Lett. **99**, 072502 (2007).

Study of Astrophysically Important States in ^{26}Si through Elastic Scattering with CRIB

J. Chen^a, A. Chen^a, G. Amadio^b, S. Cherubini^h, M. La .Cognata^h, H. Fujikawa^b, S. Hayakawa^b, N. Iwasa^j, J. J. He^{b1}, D. Kahl^a, L. H. Khiem^b, S. Kubono^b, Y. Kurihawa^b, Y. K. Kwon^c, J Y. Moon^c, M. Niikura^b, S. Nishimura^f, A. Odahara^e, J. Pearson^a, R. Pizzone^h, A. Saito^b, C. Signoriniⁱ, T. Teranishi^d, Y. Togano^g, Y. Wakabayashi^b, H. Yamaguchi^b

^a Department of Physics and Astronomy, McMaster University, Canada

^b Center for Nuclear Study, Graduate School of Science, University of Tokyo, Japan

^c Department of Physics, Chung-Ang University, South Korea

^d Department of Physics, Kyushu University, Japan

^e Department of Physics, Nishinippon Institute of Technology, Japan

^fRIKEN(The Institute of Physical and Chemical Research)

^g Department of Physics, Rikkyo University, Japan

^h Department of Physics, University of Catania and INFN, Italy

ⁱ Department of Physics, University of Padova and INFN, Italy

^j Department of Physics, Tohoku University, Japan

1. Introduction

This experiment is for data collection of the elastic scattering $^{25}\text{Al}+p$ following up the test experiment performed at CRIB before [1] and it aims to obtain structure information of the levels in ^{26}Si within the Gamow window at nova temperature to reduce the large uncertainty in the $^{25}\text{Al}(p,\gamma)^{26}\text{Si}$ reaction rate [2, 3, 4, 5]. A thick target method [6, 7] was used to scan the center-of-mass energy from 0 to 3.38 MeV with the secondary beam of 3.52 MeV/nucleon ^{25}Al impinging on the 6.58 mg/cm² CH₂ target, which corresponds to a range of excited states from 5.515 MeV ($^{25}\text{Al}+p$ threshold) to about 8.9 MeV.

The secondary ^{25}Al beam was produced by the reaction $^2\text{H}(^{24}\text{Mg},n)^{25}\text{Al}$, with the purity of about 50% and intensity of about 5×10^5 pps on target. The particle identification (PID) for the secondary beam was provided by two PPACs while PID for the scattered protons by ΔE -E telescopes as well as the TOF (time-of-flight) method.

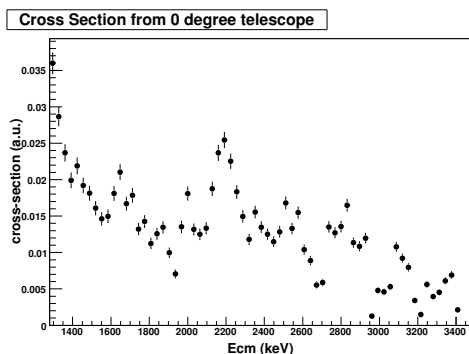


Figure 1. Proton spectrum at $\theta_{lab} = 0^\circ$ in the center of mass frame with energy loss corrected and background subtracted.

2. Data Analysis

When using the thick target method, the energy loss of the scattered proton traveling through the remaining part of the target must be taken into account. The total yields of background protons of different energies from a carbon target are normalized by the ratio of target thickness per energy bin and the ratio of the total number of beam events. Figure 1 shows a final proton spectrum after correcting the energy loss and subtracting the background protons.

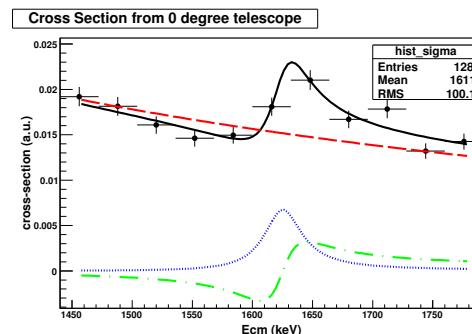


Figure 2. Breit-Wigner fit for the peak at $E_{cm} = 1697 \text{ keV}$, corresponding to the excited state $E_x = 7156 \text{ keV}$, $J^\pi = 2^+$. [5]

For preliminary purpose to find the resonant energies, a Breit-Wigner fit was applied for each single peak in the proton spectrum. Figure 2, 3, 4 are some sample fits. In the fit, the dash line represents the coulomb part, the dash-dot line coulomb-resonance interference and the dot line the pure resonant part.

An advanced R-Matrix [9] fit for the excitation function is being performed to extract physical parameters such as energy levels and proton widths. The analysis is still in progress.

¹ present address: School of Physics, University of Edinburgh, Mayfield Road, EH9 3JZ, Edinburgh, UK

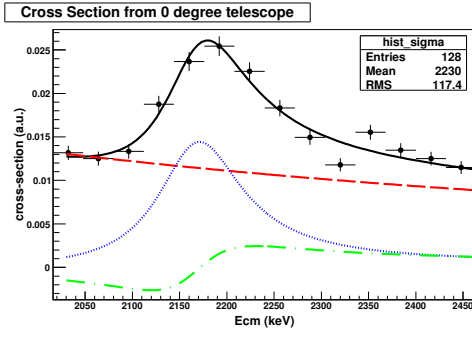


Figure 3. Breit-Wigner fit for the peak at $E_{cm}=2249\text{keV}$, corresponding to the excited state $E_x=7687\text{keV}$, $J^\pi=3^-$. [5]

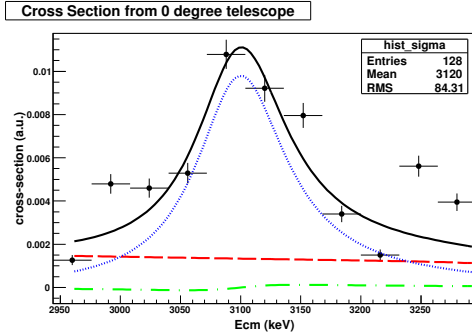


Figure 4. Breit-Wigner fit for the peak at $E_{cm}=3100\text{keV}$, corresponding to the excited state $E_x=8563\text{keV}$, $J^\pi=2^+$. [8]

References

- [1] J. Chen *et al.*, CNS Annual Reprot (2006) 5.
- [2] D. W. Bardayan *et al.*, Phys. Rev. C **65** (2002) 032801.
- [3] J. A. Caggiano *et al.*, Phys. Rev. C **65** (2002) 055801.
- [4] Y. Parpottas *et al.*, Phys. Rev. C **70** (2004) 065805.
- [5] D. W. Bardayan *et al.*, Phys. Rev. C **74** (2006) 045804.
- [6] S. Kubono, Nucl. Phys. A **693** (2001) 221-248.
- [7] A. H. Hernández *et al.*, NMB **143** (1998) 569-574
- [8] J. C. Thomas *et al.*, Eur. Phys. J.A **21** (2004) 419-435.
- [9] A. M. Lane, and R. G. Thomas, Rev. Mod. Phys. **30** (1958) 257

High-spin States in ^{51}Ti

M. Niikura, E. Ideguchi, N. Aoi^a, H. Baba^a, T. Fukuchi^a, Y. Ichikawa^a, H. Iwasaki^b, T. Kubo^a, M. Kurokawa^a, M. Liu^c, S. Michimasa, T. Ohnishi^a, T. K. Onishi^b, S. Ota, S. Shimoura, H. Suzuki^a, D. Suzuki^b, Y. Wakabayashi, K. Yoshida^a and Y. Zheng^c

Center for Nuclear Study, Graduate School of Science, University of Tokyo

^aRIKEN (The Institute of Physical and Chemical Research)

^bDepartment of Physics, Graduate School of Science, University of Tokyo

^cInstitute of Modern Physics, Chinese Academy of Sciences

Shell structure in the neutron-rich pf -shell nuclei has recently become the focus of much theoretical and experimental effort. As the neutron number increases, there may be rearrangements of the single-particle orbits and developments of new sub-shell closures. Emergence of a sub-shell gap at $N = 32$ reported in ^{52}Ca , ^{54}Ti and ^{56}Cr is one of the good examples [1, 2, 3]. Since nuclei with certain amount of spins need to promote nucleons across the major shell gap in order to gain the large angular momentum and single particle states could be appeared in those excited states, spectroscopic studies at high spin may serve as a sensitive probe of the location of single particle orbits. In this report, the in-beam γ -ray spectroscopy in ^{51}Ti via the secondary fusion reaction [4], $^{46}\text{Ar} + ^9\text{Be}$, are described.

The experiment was performed at the RIKEN Projectile-fragment Separator (RIPS) facility in RIKEN [5]. A secondary beam of ^{46}Ar was produced by projectile fragmentation of ^{48}Ca at the energy of 64 MeV/nucleon and its energy was lowered using aluminum energy degraders placed at the first and second focal planes (F1, F2) of RIPS. The intensity and energy of the low-energy radioactive isotope (RI) beam were 1×10^6 particle per second and about 4.0 MeV/nucleon, respectively. The secondary beam bombarded a 10- μm -thick ^9Be target placed at the final focal plane (F3) to induce secondary fusion reactions, $^9\text{Be} (^{46}\text{Ar}, xn) ^{55-x}\text{Ti}$.

Gamma rays emitted from evaporation residues were detected by the CNS Gamma-Ray detector Array with Position and Energy sensitivity (CNS-GRAPE) [6] together with two clover and one coaxial germanium detectors. These γ -ray detectors were placed around the secondary target to cover the angular range between 30° and 120° relative to the beam direction. In order to correct the Doppler shift of the γ rays emitted from moving particles ($\beta \sim 0.08$), pulse-shape analysis was performed for the output from CNS-GRAPE to determine the interaction points of the γ rays in the detector [7]. The energy resolution of 15 keV (FWHM) for 1.5-MeV γ rays was obtained after the Doppler correction.

Event identification was performed based on the velocity difference between the beam and the fusion products. The velocity of incident beam was deduced by time of flight (TOF) between plastic scintillator at F2 (F2pl) and parallel-plate avalanche counters at F3 (F3PPACs), and that of the outgoing particles was measured by TOF between the secondary target and PPAC placed downstream of the target.

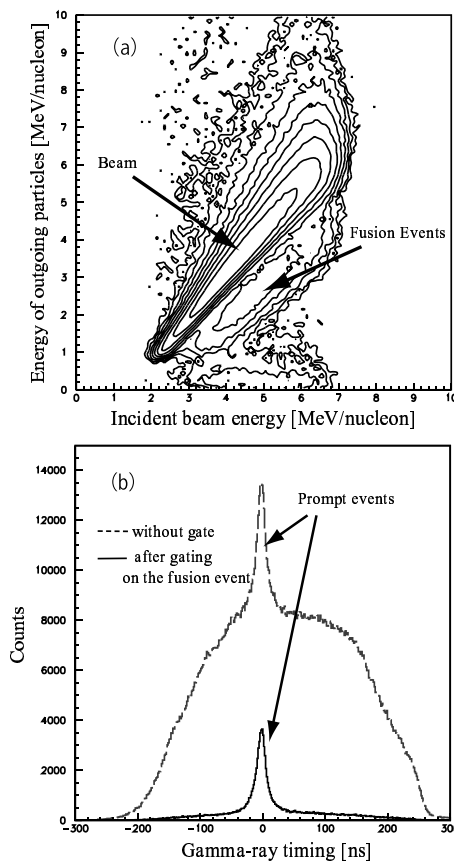


Figure 1. The energy of incident and outgoing particles (a) and timing spectrum of the germanium detectors (b).

The timing at the target was deduced by extrapolation from timing on F2pl and F3PPACs. Figure 1(a) shows the energy of the incident and outgoing particles. By gating on the fusion event region, backgrounds due to accidental coincidences are reduced as shown in Fig. 1(b) where timing spectra of the germanium detectors with and w/o the gate are presented.

In order to construct the level scheme, γ - γ coincidence analysis was carried out for ^{51}Ti . Prior to the present investigation, four γ transitions at 1437, 907, 410 and 892 keV corresponding to $7/2^- \rightarrow 3/2^-$, $11/2^- \rightarrow 7/2^-$, $15/2^- \rightarrow 11/2^-$ and $(13/2, 17/2) \rightarrow 15/2^-$, respectively, were reported by S. E. Arnell *et al.* [8]. Figure 2(a) shows summed γ -ray spectrum gated on the known 907- and 892-keV γ lines. Three new γ peaks at 667, 761 and 837 keV belonging to ^{51}Ti were observed and other peaks are mainly contami-

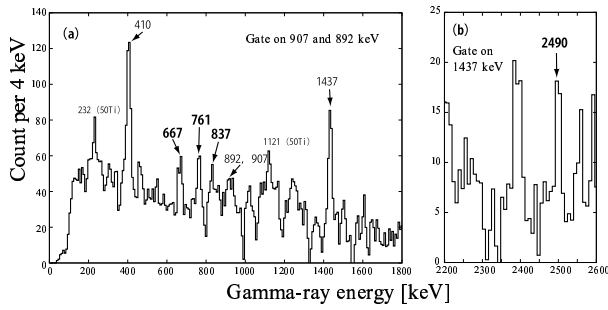


Figure 2. Parts of the coincidence spectra gated on 907 and 892 keV (a) and 1437 keV (b).

nants from ^{50}Ti . Based on the excitation function analysis [9] and on intensity arguments, 837-keV transition is placed above 761- and/or 667-keV transition. Additionally in a coincidence spectrum gated on 1437 keV (Fig. 2(b)), 2490-keV peak was observed as well, and this is tentatively placed in parallel with the 892-, 761- and 837-keV transitions. Because of low statistics, a placement of the 667-keV transition has uncertainty. The proposed level scheme of ^{51}Ti is given in the left-hand side of Fig. 3.

Multipolarity assignments for the observed γ transitions were made on the basis of the angular distribution analysis. The angular distributions of the 1437-, 907- and 410-keV lines are consistent with a transition of stretched- $E2$ character and those of the 892- and 761-keV transitions suggest an $M1/E2$ character. For the 837- and 2490-keV transitions, no angular distribution information is available due to the low statistics. Spin assignments above $15/2^-$ state are based on consideration of the decay branching from the 5244-keV state to the 4406- and 2754-keV states and on the close correspondence between the established and calculated states (see below).

The shell-model code ANTOINE [10] can be used for the energies and wavefunctions of the levels in ^{51}Ti within the full pf -shell model space. The calculation was carried out with GXPF1 effective interaction [11]. The calculated energy levels are shown in the right-hand side of Fig. 3. The calculation is generally in good agreement with the experiment and was used for spin assignments. The calculation indicates wavefunctions for the low-lying levels below 3646 keV ($13/2^-$) state being dominated (50–80%) by the $[\pi(f_{7/2})^2 \otimes \nu(f_{7/2})^8(p_{3/2})^1]$ configuration. The ($15/2^-$) state at 4406 keV, which corresponds to 4876 keV ($15/2^-$) state in the shell-model calculation, is dominated (72%) by $[\pi(f_{7/2})^2 \otimes \nu(f_{7/2})^7(p_{3/2})^2]$ configuration. The shell-model calculation gives two $17/2^-$ states correspond to the observed 5244 keV ($17/2^-$) state. Dominant shell-model components are and $[\nu(f_{7/2})^8(f_{5/2})^1]$ for 5645-keV state $[\nu(f_{7/2})^7(p_{3/2})^2]$ for 5865-keV state. From the systematics in the $^{49-51}\text{Ti}$, this ($17/2^-$) state might be dominated by $[\nu(f_{7/2})^7(p_{3/2})^2]$ configuration.

In summary, we have performed in-beam γ -ray spectroscopy in ^{51}Ti . By analysis of the excitation function, the γ - γ coincidence and the angular distribution, high-spin levels upto spin ($17/2$) state were identified. Further discussion on the deviation between data and shell-model calculations are now in progress.

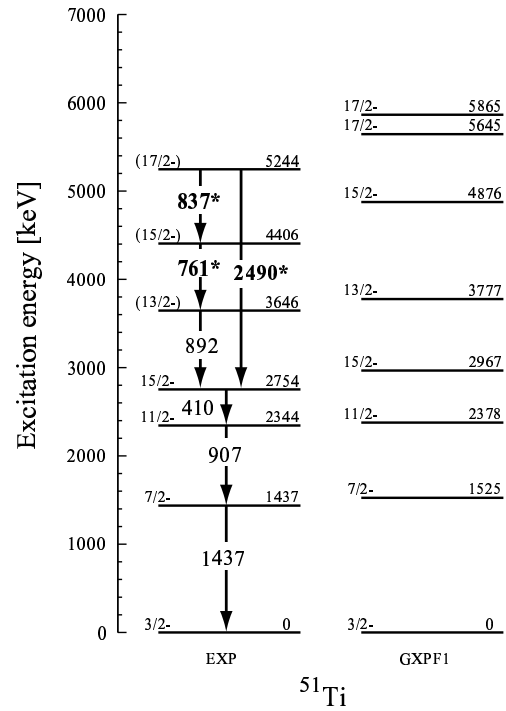


Figure 3. Comparison between proposed level scheme and shell-model calculation with the GXPF1 Hamiltonian for ^{51}Ti . Newly observed transitions are denoted by *.

References

- [1] A. Huck *et al.*, Phys. Rev. **C31** (1985) 2226.
- [2] R. V. F. Janssens *et al.*, Phys. Lett. **B546** (2002) 55.
- [3] J. I. Prisciandaro *et al.*, Phys. Lett. **B510** (2001) 17.
- [4] E. Ideguchi *et al.*, AIP Conf. Proc. **764** (2004) 136.
- [5] T. Kubo *et al.*, Nucl. Instrum. Methods **B70** (1992) 309.
- [6] S. Shimoura, Nucl. Instrum. Method **A525** (2004) 188.
- [7] M. Kurokawa *et al.*, IEEE Trans. Nucl. Sci. **50** (2003) 1309.
- [8] S. E. Arnell *et al.*, Phys. Scr. **6** (1972) 222.
- [9] M. Niikura *et al.*, CNS Ann. Rep. **2006** (2007) 23.
- [10] E. Caurier, IRES. Strasbourg 1989-2002
E. Caurier *et al.*, Acta Phys. Pol. **30** (1999) 705.
E. Caurier *et al.*, Rev. Mod. Phys. **77** (2005) 2.
- [11] M. Honma *et al.*, Phys. Rev. **C65** (2002) 061301.

Study of High-Spin States in A ~ 30 Region

E. Ideguchi, T. Morikawa^a, M.L. Liu, Y. Toh^b, M. Koizumi^b, A. Kimura^b, H. Kusakari^c,
M. Oshima^b, B. Cederwall^d, K. Furutaka^b, Y. Hatsukawa^b, S. Mitarai^a, M. Sugawara^e and
Y. Zheng

Center for Nuclear Study, Graduate School of Science, University of Tokyo

^aDepartment of Physics, Kyushu University

^bJapan Atomic Energy Agency

^cFaculty of Education, Chiba University

^dDepartment of Physics, Royal Institute of Technology

^eChiba Institute of Technology

High-spin level structures of A ~ 30 nuclei have been receiving increased attention in recent years [1, 2]. In this region several interesting phenomena have been investigated such as violation of mirror symmetry, cluster structure, shape coexistence, and the interplay between single-particle and collective motion [1, 2]. In ³²S and ³⁶S, presences of superdeformed structure were predicted [3, 4] but they were not experimentally confirmed. In order to investigate collective structures at high-spin, ³⁶S and its neighboring nuclei were studied, and current status is presented in this report.

In-beam γ -ray spectroscopy was employed to study high-spin states of ³⁶S and ³⁶Cl via the ¹⁸O + ²⁴Mg fusion-evaporation reaction. The ¹⁸O beam of 70 MeV was provided by the tandem accelerator of Japan Atomic Energy Agency. The targets used were an isotopically enriched ²⁴Mg foil of 1 mg/cm² thickness with 8 mg/cm² natPb backing and a 490 μ g/cm² thick self-supporting one. Fourteen HPGe detectors with BGO anti-Compton shields from the GEMINI-II array [5] were used to detect γ rays in coincidence with charged particles detected by a charged particle filter, Si-Ball [6]. The Si-Ball consists of 20 Δ E Si detectors mounted on the regular dodecahedron frame surrounding the target. Events were collected when at least two HPGe detectors and one Si detector were fired in coincidence. The data was analyzed by using RADWARE data analysis software package [7]. The multifold event data was sorted offline into a E γ -E γ correlation matrix. Figure 1 shows a total projection spectrum without charged-particle gate. Previously reported γ peaks are labeled with transition energies in keV. Gamma rays from ³⁸Ar, ^{35,36}Cl are clearly seen which are strong channels in the ¹⁸O + ²⁴Mg reaction at 70 MeV.

Since the HPGe detectors were placed at 6 different angles, namely 47° (4 Ge's), 72° (2 Ge's), 90° (2 Ge's), 105° (4 Ge's), 144° (1 Ge) and 147° (1 Ge) with respect to the beam direction, it is possible to perform angular distribution and the DCO (Directional Correlations from Oriented states) analysis of γ rays [8] in order to estimate multipolarities of them. Asymmetric angular correlation matrices were sorted in order to measure the DCO ratios. These matrices were sorted with γ rays detected in the two detectors at $\theta = 75^\circ$ or 90° on one axis and the coincident γ rays

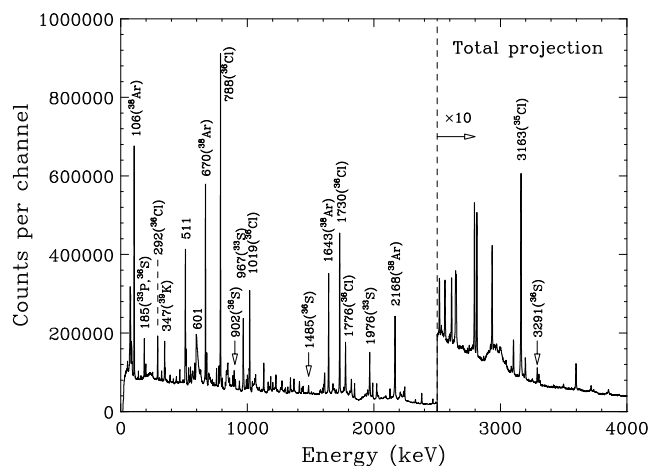


Figure 1. Total projection spectrum of E γ -E γ correlation matrix created without charged-particle gate. Previously reported γ peaks are labeled with transition energies in keV.

from the 47° on the other axis. The quantity

$$R_{DCO} = \frac{W_\gamma(47^\circ, 75^\circ \text{ or } 90^\circ)}{W_\gamma(75^\circ \text{ or } 90^\circ, 47^\circ)}$$

was measured for the transitions in ³⁶S and ³⁶Cl, where W γ (i,j) is the intensity of a transition on the i axis of the DCO matrix measured after gating on a transition on the j axis. In the present detector geometries, R_{DCO} will be ~1.5 for stretched quadrupole transitions and ~0.8 for pure dipole transitions. In Fig. 2 DCO ratios for γ rays in ³⁶S are shown.

High-spin levels in ³⁶S were previously reported up to the (6⁺) state at 6.69 MeV [9]. Spin and parity assignment of the (6⁺) state was based on the comparison with shell model calculation and it was not experimentally determined. Based on the γ - γ coincidence relations, γ -ray energy sum, and intensity balances of the transitions, previously reported level scheme for ³⁶S [9] was confirmed. In the present study, new γ -ray peaks at 1182, 1315 and 2218 keV were identified in coincidence with 3291 keV transition as shown in Fig. 3. Results of DCO analysis suggest stretched quadrupole character for 1182 and 2218 keV transitions and dipole character for 1315 keV transition. Further analyses to determine the spin and parity of the

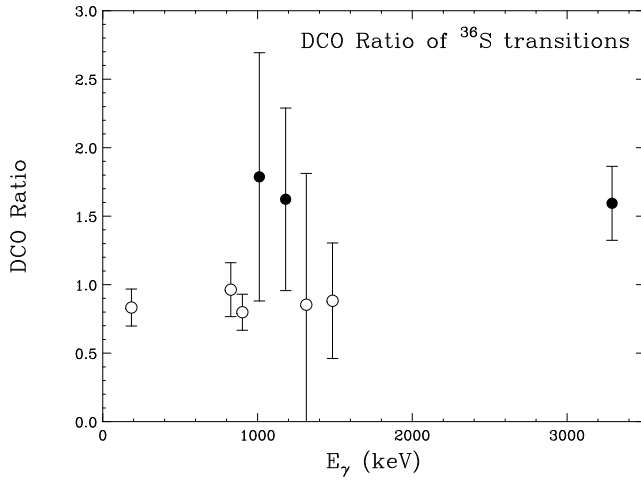


Figure 2. DCO ratios of γ transition in ^{36}S . Filled circles correspond to the γ rays estimated to have E2 multiplicities and open circles for M1.

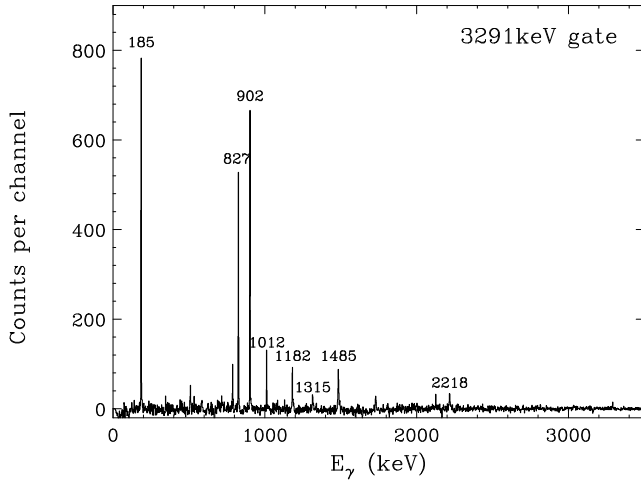


Figure 3. Gamma-ray energy spectrum obtained by gating on 3291 keV transition in ^{36}S .

6.69 MeV level, constructing level scheme and multiplicity assignments of the γ transitions between the levels are in progress.

In ^{36}Cl , high-spin levels up to $(7)^+$ state at 5.313 MeV were previously assigned [10]. On top of the $(7)^+$ state a 466 keV transition was tentatively placed and it was reported to be in coincidence with 1019 and 2795 keV transitions from $(7)^+$ to (6^+) and from $(7)^+$ to 5^- levels, respectively [8]. Figure 4 shows the γ -ray energy spectrum obtained by gating on 466 keV transition and it was found that 1019 and 2795 keV peaks did not appear in the spectrum. This indicates that the 466 keV transition de-excites from the $(7)^+$ state in parallel with 1019 and 2795 keV transitions. After the γ - γ coincidence analysis of ^{36}Cl data, 16 γ -ray peaks were newly identified. Data analysis is in progress.

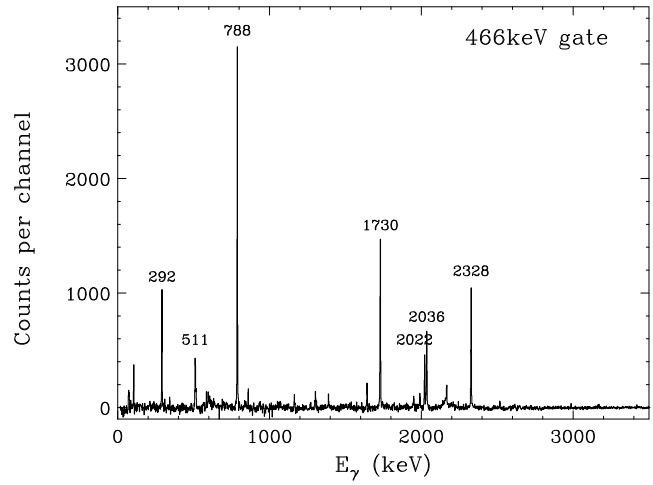


Figure 4. Gamma-ray energy spectrum obtained by gating on 466 keV transition in ^{36}Cl .

- [2] F. Della Vedova *et al.*, Phys. Rev. C **75** (2007) 034317.
- [3] H. Molique, J. Dobaczewski and J. Dudek, Phys. Rev. C **61** (2000) 044304.
- [4] T. Inakura, S. Mizutori, M. Yamagami and K. Matsuyani, Nucl. Phys. A **728** (2003) 52.
- [5] M. Oshima *et al.*, J. Radioanal. Nucl. Chem. (2008) to be published.
- [6] T. Kuroyanagi *et al.*, Nucl. Instrum. Methods Phys. Res. A **316** (1992) 289.
- [7] D.C. Radford, Nucl. Instrum. Methods Phys. Res. A **361** (1995) 297.
- [8] K.S. Krane, R.M. Steffen and R.M. Wheeler, Nuclear Data Tables **11** (1973) 351.
- [9] X. Liang *et al.*, Phys. Rev. C **66** (2002) 014302.
- [10] E.K. Warburton *et al.*, Phys. Rev. C **14** (1976) 996.

References

- [1] P. Mason *et al.*, Phys. Rev. C **71** (2005) 014316.

Search for Superdeformed Band in $A \sim 110$ Region

A. Yoshida^a, E. Ideguchi^b, S. Ota^b, T. Koike^c, K. Shirotori^c, H. Tamura^c, K. Hosomi^c,
M. Mimori^c, K. Miwa^c, Y. Ma^c, T. Ohtomo^c, T. Yamamoto^c, M. Sato^c, T. Morikawa^d, T. Suzuki^e,
T. Murakami^a, T. Kishida^f

^aDepartment of Physics, Kyoto University

^bCenter for Nuclear Study, Graduate School of Science, University of Tokyo

^cDepartment of Physics, Tohoku University

^dDepartment of Physics, Kyushu University

^eDepartment of Physics, Osaka University

^fRIKEN Nishina Center

Study of superdeformed (SD) states is an important tool for testing nuclear shell structure which stabilizes the nucleus at large deformation. Since the first observation of the superdeformed rotational band at high spin in ^{152}Dy [1], SD bands have been identified in many nuclei in the $A \sim 40, 60, 80, 130, 150,$ and 190 regions [2]. Observation of such SD nuclei in the specific mass regions with certain proton and neutron numbers supports the presence of the SD shell structures. Recent experimental work of Clark et al in ^{108}Cd [3] provides a new SD region in $A \sim 110$ nuclei. Theoretical calculations using a cranked Strutinsky method and a four-dimensional shape space representing quadrupole, octupole, hexadecapole, and necking degrees of freedom also predict that a new region of SD states in $A \sim 110$ nuclei with $45 < Z < 49$ and $57 < N < 65$ [4]. However, discovery of SD states was limited to ^{108}Cd so far.

In order to find new SD nuclei in $A \sim 110$ region with $45 < Z < 49$ and $57 < N < 65$ systematically, we have performed in-beam γ -ray measurements using a $^{20}\text{Ne} + ^{96}\text{Zr}$ reaction to investigate high-spin states of ^{107}Cd next to the ^{108}Cd , where a presence of SD structure is expected at high-spin levels. The experiment was performed at the Cyclotron and Radioisotope Center, Tohoku University. The ^{20}Ne ions, accelerated by the 930 cyclotron to an energy of 131 MeV, were used to bombard a stack of two self-supporting ^{96}Zr targets of 0.5 mg/cm^2 thickness. High-spin states in ^{107}Cd were populated by $^{96}\text{Zr}(^{20}\text{Ne}, 1\alpha 5n)^{107}\text{Cd}$ reaction.

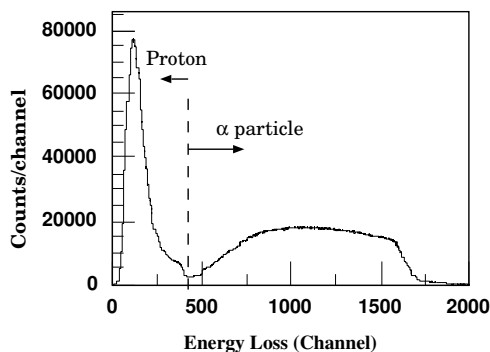


Figure 1. Energy spectrum of Si detector. Dashed line indicated in the spectrum is the energy threshold to identify protons and α particles.

Prompt γ rays were detected by Hyperball-2 array com-

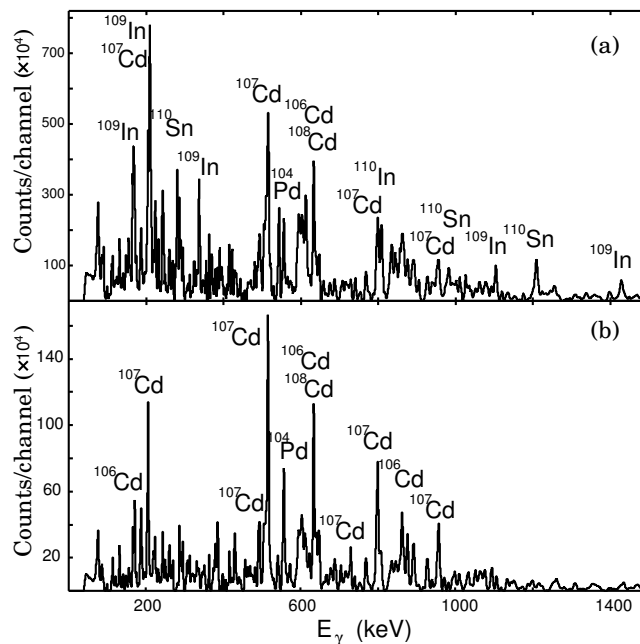


Figure 2. Gamma-ray energy spectrum without (a) and with (b) α -particle gate after Compton background subtraction. Previously reported γ peaks are labeled with isotopes.

posed of 12 coaxial Ge detectors and 6 Clover Ge detectors in this experiment. Clover detectors were placed at 90° and coaxial detectors were placed at $\sim 46^\circ$ and at $\sim 134^\circ$ (6 detectors each) relative to the beam direction. Each Ge detector was shielded with BGO counters for Compton background suppression. In order to pickup high-multiplicity γ -ray events, 2 sets of BGO multiplicity filters, each of which consists of 7 BGO crystals, were used. Evaporated charged particles in the reaction were detected by the Si-Ball charged particle filter [5] which consists of 30 Si detectors mounted on the truncated icosahedron shaped frame. Ten pentagonal and twenty hexagonal shaped Si ΔE detectors of $170 \mu\text{m}$ thickness were used. In front of each Si detector, thin Al absorber foil is mounted in order to prevent ^{20}Ne beam directly hitting the detector after scattering at the target. Detection efficiencies for protons and α particles were both $\sim 37\%$. With trigger condition of 4 Ge detectors firing in coincidence, 9.5×10^8 events were collected. The data was analyzed by using the RADWARE data anal-

ysis software package [6]. The multifold event data was sorted offline into a E_γ - E_γ correlation matrix and a E_γ - E_γ - E_γ cube.

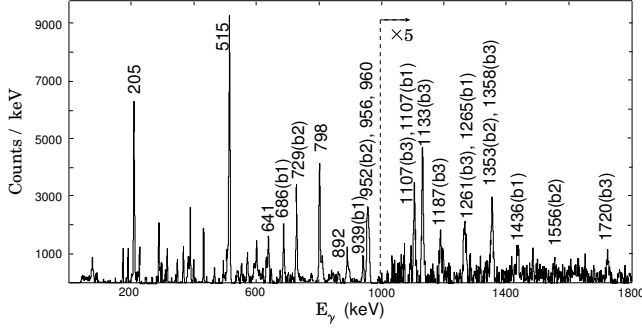


Figure 3. Gamma-ray energy spectrum gated by 1076 and 493 keV transitions. Assigned γ peaks are labeled with their transition energy in keV. In-band transitions of band 1, 2, 3 are also labeled with (b1), (b2), and (b3), respectively (see text).

Figure 1 shows an energy spectrum of charged particles obtained by the Si-Ball. Particle identification was performed by using the difference in energy loss of protons and α particles in the ΔE detector. As shown in the figure, peak around 150 channel and broad peak between 500 and 1800 channel corresponds to protons and α particles, respectively. Gamma-ray energy spectra without and with α particle gate were shown in Fig. 2(a) and (b), respectively. By the α -particle gate γ -ray peaks from Cd isotopes were enhanced.

High-spin states in ^{107}Cd were previously studied up to the $(51/2^+)$ state at 11.852 MeV via $^{94}\text{Zr}(^{17}\text{O},4n)$ reaction [7]. Several negative- and positive-parity bands were observed and two of positive-parity bands were interpreted as being signature partners of a three-quasiparticle $\nu g_{7/2} h_{11/2}^2$ configuration. Based on single and double gating on the matrix and cube, respectively, coincidence relations between observed γ rays were examined. Previously reported γ transitions up to the $47/2^+$ state were confirmed. Figure 3 shows γ -ray energy spectrum gated by 1076 and 493 keV peaks which correspond to $25/2^+ \rightarrow 23/2^-$ and $27/2^+ \rightarrow 23/2^+$ transitions, respectively. Previously reported and newly identified γ -ray peaks are labeled with their transition energies in keV, and in-band transitions of the signature partner bands are labeled with b1 (band 1) and b2 (band 2) for favored and unfavored bands, respectively.

In the present study, new γ -ray cascade transitions (band 3), which are labeled with b3 in Fig. 3, were identified. Multipolarities of the transitions were checked by the angular distribution analysis and it is consistent with the E2 character of the transitions. Based on the coincidence relations of γ rays, it was found that this band decays to both band 1 and band 2, but excitation energy and the spin are not determined since linking transitions were not observed.

In order to estimate the size of deformation of the band 3, dynamical moment of inertia ($J^{(2)} \equiv \hbar^2 \frac{dI}{d\omega}$) is compared with those of band 1 and 2 and with that of SD band in ^{108}Cd in Fig. 4. Although the number of transitions of

band 3 is not large, $J^{(2)}$ values of band 3 is larger than those of band 1 and 2 and comparable with those of SD band in ^{108}Cd . This may indicate the large deformation of the band 3. Data analysis to clarify the structure of band 3 is in progress

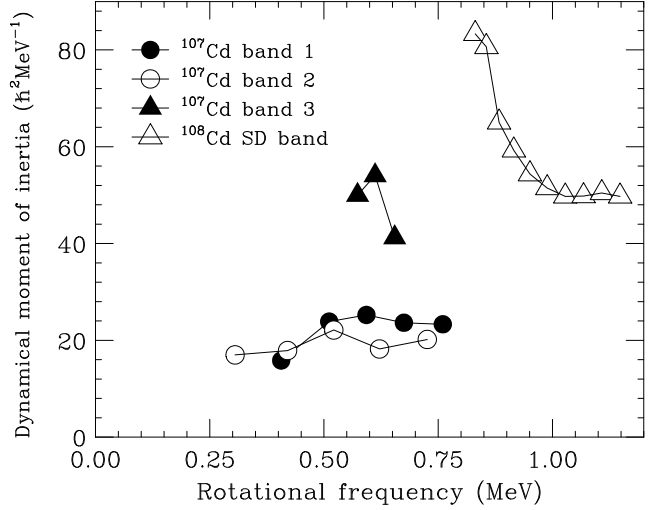


Figure 4. Dynamical moments of inertia for band 1,2,3 of ^{107}Cd and that of superdeformed band in ^{108}Cd .

References

- [1] P.J. Twin *et al.*, Phys. Rev. Lett. **57** (1986) 811.
- [2] B. Sing, R. Zysina, R.B. Firestone, Nucl. Data Sheet **97** (2002) 241.
- [3] R.M. Clark *et al.*, Phys. Rev. Lett. **87** (2001) 202502.
- [4] R.R. Chasman, Phys. Rev. **C64** (2001) 024311.
- [5] T. Kuroyanagi *et al.*, Nucl. Instrum. and Methods, A **316** (1992) 289.
- [6] D.C. Radford, Nucl. Instrum. Methods Phys. Res. **A361** (1995) 297.
- [7] D. Jerrestam *et al.*, Nucl. Phys. **A 545** (1992) 835.

Analyzing Power Measurement for the $\vec{p}+^8\text{He}$ Elastic Scattering at 71 MeV/u

S. Sakaguchi, T. Uesaka, T. Wakui^a, T. Kawabata, N. Aoi^b, Y. Ichikawa^c, K. Itoh^d, M. Itoh^a,
T. Kawahara^e, Y. Kondo^f, H. Kuboki^c, T. Nakamura^f, T. Nakao^c, Y. Nakayama^f, S. Noji^c,
H. Sakai^c, Y. Sasamoto, M. Sasano^c, K. Sekiguchi^b, T. Shimamura^f and Y. Shimizu

Center for Nuclear Study, Graduate School of Science, University of Tokyo

^a*Cyclotron and Radioisotope Center, Tohoku University*

^b*RIKEN (The Institute of Physical and Chemical Research)*

^c*Department of Physics, University of Tokyo*

^d*Department of Physics, Saitama University*

^e*Department of Physics, Toho University*

^f*Department of Physics, Tokyo Institute of Technology*

1. Introduction

Recently, much interest has been focused on the spin-dependent interaction in unstable nuclei. One of the most direct ways to study such interaction is to determine the spin-orbit part of the optical potential between protons and unstable nuclei. For this purpose, a polarized proton solid target which was specially designed for radioactive-beam experiments has been developed at CNS [1, 2]. Making use of this target, we measured the analyzing power of the proton elastic scattering on ^6He [3] and ^8He at 71 MeV/u in 2005 and 2007. The aim of the measurements is to deduce and compare the spin-orbit potentials between protons and $^4,6,8\text{He}$ particles. From the systematics of the potentials, the effects of excess neutrons on the spin-orbit interaction will be investigated. Details of the $\vec{p}+^8\text{He}$ elastic scattering measurement are reported.

2. Experiment

The experiment was carried out at the RIKEN Accelerator Research Facility (RARF) using the RIKEN Projectile-fragment Separator (RIPS). The ^8He beam was produced by a fragmentation reaction of an ^{18}O beam with an energy of 100 MeV/u bombarded onto a 13 mm^2 Be target. The energy and intensity of the beam was 71 MeV/u and 1.5×10^5 pps, respectively. Purity of the beam was 77%. As a secondary target, we used the polarized proton solid target. The target material was a single crystal of naphthalene with a thickness of 4.3×10^{21} protons/cm². Protons in the crystal were polarized by optical excitation of electrons and cross-polarization method under a low magnetic field of 0.09 T at high temperature of 100 K. Recoiled protons were detected using multiwire drift chambers (MWDCs) and CsI (TI) scintillators placed on the left and right sides of the beam line. Each MWDC was located 180 mm away from the target and covered a scattering angle of $50^\circ - 70^\circ$ in the laboratory system. A CsI scintillator with a sensitive area of $135\text{ mm}^H \times 60\text{ mm}^V$ was placed just behind the MWDC. Scattered particles were detected using another MWDC and $\Delta E - E$ plastic scintillator hodoscopes with thicknesses of 5 and 100 mm. The experimental setup is shown in Fig. 1.

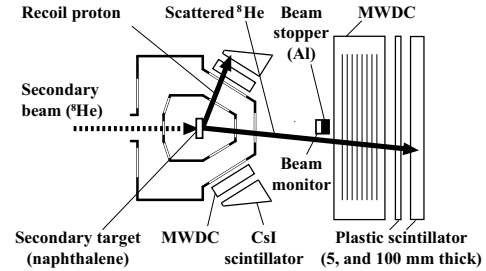


Figure 1. Experimental setup is shown.

3. Polarization measurement

The absolute value of the target polarization was determined by measuring the spin-dependent asymmetry ($P_y A_y$) of the $\vec{p}+^4\text{He}$ elastic scattering at 80 MeV/u. For the determination, the following relation between the analyzing power (A_y) and the target polarization (P_y) was used:

$$A_y = \frac{1}{P_y} \frac{\sqrt{N_L^\uparrow \cdot N_R^\downarrow} - \sqrt{N_R^\uparrow \cdot N_L^\downarrow}}{\sqrt{N_L^\uparrow \cdot N_R^\downarrow} + \sqrt{N_R^\uparrow \cdot N_L^\downarrow}} \quad (1)$$

Here, N_i^j denotes the yield, where i and j represent the scattering direction and polarizing direction, respectively. Figure 2 shows the analyzing power of the $\vec{p}+^4\text{He}$ scattering at 80 MeV/u. Open circles represent previously measured data [4]. Closed ones show the present data. The target polarization was determined to be $11.0 \pm 2.5\%$.

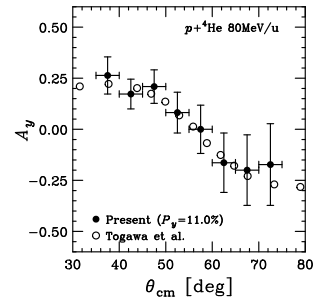


Figure 2. Analyzing power of the $\vec{p}+^4\text{He}$ elastic scattering at 80 MeV/u is shown. See text for detail.

Figure 3 shows the target polarization monitored by the

pulsed NMR method during the scattering experiment. Target polarization was developed for 90 hours before the beam irradiation. After ^8He beam irradiation, the beam was switched to ^4He for the determination of the target polarization. Polarizing direction was reversed three times during the experiment by 180° pulse NMR method [5] for the reduction of spurious asymmetry.

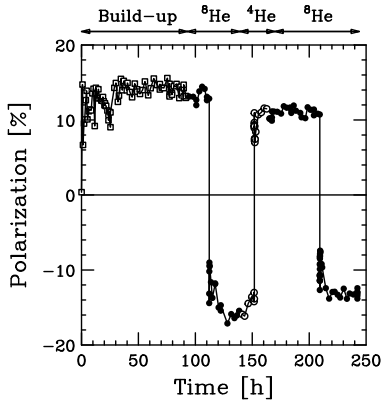


Figure 3. Target polarization monitored by the pulsed NMR method.

4. $\vec{p}+^8\text{He}$ elastic scattering measurement

The $\vec{p}+^8\text{He}$ measurement was carried out with the same experimental setup as the $\vec{p}+^4\text{He}$ measurement. In the $\vec{p}+^8\text{He}$ measurement, scattered particles were identified by the $\Delta E - E$ method to exclude the break-up events. Elastic scattering events were identified by the coincidence measurement of protons and ^8He particles, since ^8He does not have a bound excited state. One possible source of the background events is the quasi-free scattering of ^8He from protons in ^{12}C . However, contribution of this reaction is negligibly small since the energy of incident ^8He particle is as low as 71 MeV/u. Figure 4 shows scattering angle correlation of protons and ^8He particles. Clear loci lie on the solid curves which represent the kinematics calculation for the elastic scattering. In the case of quasi-free scattering, the scattering angles do not exhibit such strong correlation due to the fermi motion of protons in ^{12}C . By selecting the loci, the elastic scattering events are discriminated with good signal/background ratio.

Preliminary data of the differential cross section of $p+^8\text{He}$ elastic scattering at 71 MeV/u are shown in Fig. 5 by closed circles. Open circles represent the data previously obtained by A. Korshennikov *et al.* [6]. First data of the differential cross section in the backward angular region of $65 - 77.5^\circ$ were obtained with good statistics. The analyzing power will be deduced in the future analysis.

References

[1] T. Wakui, M. Hatano, H. Sakai, T. Uesaka and T. Tamii, Nuclear Instruments and Methods in Physics Research A **550** (2005) 521.

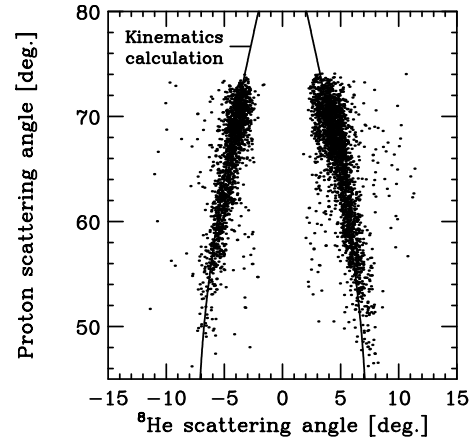


Figure 4. Scattering angle correlation of protons and ^8He particles. Elastic scattering events are clearly identified.

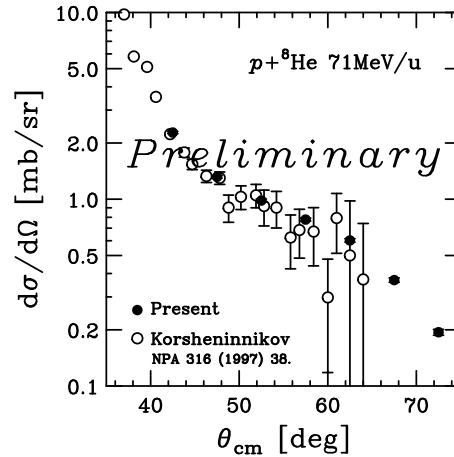


Figure 5. Preliminary results of the differential cross section of the $p+^8\text{He}$ elastic scattering at 71 MeV/u are shown by closed circles. Previous data [6] are also plotted by open circles.

- [2] T. Uesaka, M. Hatano, T. Wakui, H. Sakai and A. Tamii, Nuclear Instruments and Methods in Physics Research A **526** (2004) 186.
- [3] S. Sakaguchi *et al.*, Proc. International Nuclear Physics Conference (INPC2007), (Tokyo 2007) Volume 2, pp. 467.
- [4] H. Togawa *et al.*, RCNP Annual Report (1987) 1.
- [5] T. Kawahara, T. Wakui, T. Uesaka and S. Sakaguchi, CNS Annual Report 2005 (2006).
- [6] A. A. Korshennikov, K. Yoshida, D. V. Aleksandrov *et al.*, Nuclear Physics A **316** (1993) 38.

$^{10}\text{B}+\text{p}$ Reaction at Astrophysical Energies

S. Romano^a, S.M.R. Puglia^a, L. Lamia^a, C. Spitaleri^a, S. Cherubini^a, M. Gulino^a, M. La Cognata^a,
R.G. Pizzone^a, G.G. Rapisarda^a, M.L. Sergi^a, S. Tudisco^a, A. Tumino^{a+}

M.G. Del Santo^b, N. Carlin^b, F. Souza^b, A. Szanto de Toledo^b

S. Kubono, H. Yamaguchi, Y. Wakabayashi

V. Kroha^c, C. Li^d, W. Qungang^d, E. Somorjai^e

^aUniversità di Catania and INFN-LNS, Catania, Italy

^b Universidade de São Paulo - DFN, São Paulo, Brazil

Center for Nuclear Study, Graduate School of Science, University of Tokyo

^cInstitute for Nuclear Physics, Prague-Rez, Czech Republic

^dChina Institute of Atomic Energy, Beijing, China

^eAtomki - Debrecen - Hungary

⁺ Present address: Università KORE, Enna, Italy

The light elements, lithium beryllium and boron, play an important role in astrophysics. In the last years many efforts have been devoted to the study of their abundances. These are of importance both in the study of cosmology and of stellar structures and evolution. Actually hints on the primordial nucleosynthesis can be achieved from Li, Be and B primordial abundances. Moreover these studies can be a precious tool for testing and understanding the inner stellar structure, especially concerning the mixing processes in stellar envelopes [1]. These elements are mainly destroyed in the stellar interior by (p,α) reactions at temperature ranging from 2.5×10^6 K for lithium, 3.5×10^6 K for beryllium and 5×10^6 K for boron.

The simultaneous determination of the surface abundances can give additional information about the mixing mechanisms acting inside the stars [2]. The (p,α) reactions induced at a Gamow energy (E_G) of few keV are the main channel to destroy the light elements. Hence a precise cross-section measurement for such processes is needed. Owing to the difficulties encountered in charged-particle cross-section measurement at sub-Coulomb energies (e.g. coulomb barrier and electron screening effect), in the last years a number of indirect methods, such as the Coulomb Dissociation (CD) [3], the Asymptotic Normalization Coefficient (ANC) [4] and the Trojan Horse Method (THM) [5] were developed.

Among these methods the THM appears to be particularly suited to investigate low-energy charged-particle two-body reactions by selecting the quasi-free (QF) contribution to the cross section of an appropriate three-body process. This method allows to extract the information down to the astrophysical energies, overcoming the problem connected with Coulomb barrier and electron screening effects.

The $^{10}\text{B}(\text{p},\alpha)^7\text{Be}$ reaction has been extensively studied directly [6,7] as it is responsible for boron destruction in stellar environment and the bare S-factor has been extrapolated to the Gamow region from higher energy. Moreover, the study of this reaction is complicated by the presence of

the $E_x=8.701$ MeV ^{11}C resonant level ($J=5/2+$), very close to E_G .

The present paper reports on an indirect investigation of this reaction obtained by applying the THM to the $^2\text{H}(^{10}\text{B},\alpha)^7\text{Be}$ three-body process.

The first run of this experiment was performed at the Pelletron-Linac laboratory (Departamento de Física Nuclear (DFN) in Sao Paolo (Brazil)). The experiment was performed with a 27 MeV ^{10}B beam, with a spot size on target of 2 mm diameter and intensities up to 1 nA. The results of this experiment are discussed in [8].

In order to improve both angular and energy resolution, a new experiment was performed in Catania. In this paper we report on this new run and we will show some preliminary results.

The experiment was performed at the Laboratori Nazionali del Sud in Catania. The Tandem Van de Graaf accelerator provided at 24.4 MeV ^{10}B beam with a spot size on target of about 2 mm and intensities up to 1.5 nA. A deuterated polyethylene target (CD2) $\simeq 192 \mu\text{g}/\text{cm}^2$ thick was placed at 90° with respect to the beam direction. The experimental setup consisted of a pair of 1000 μm position sensitive detector (PSD), PSD-B and PSD-C, and one telescope ΔE -E with an ionization chamber as ΔE detector and a PSD (PSD-A) as E detector. This telescope was placed at the angle $6.9^\circ \pm 2.5^\circ$ and allowed for charge discrimination of the detected particles. PSD-B and PSD-C were placed on the opposite side of the beam and in coplanar geometry with the telescope and covered the laboratory angle ranges $8^\circ \pm 4^\circ$ (PSD-B) and $17.9^\circ \pm 4.5^\circ$ (PSD-C). The experimental setup was chosen in order to cover the whole phase space region where a QF contribution, known from a Monte Carlo simulation, was expected.

Standard electronics is used to filter and shape the signals and the trigger for the acquisition was made by selecting the coincidences between the PSD-A and one of the others

two PSDs.

The details of the application of the THM are presented elsewhere (see e.g. [5,8]). Here we just show the preliminary results obtained using this method.

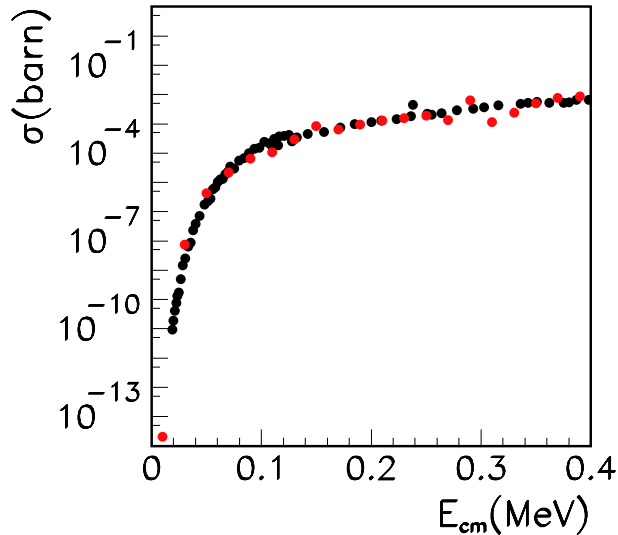


Figure 1. Comparison between directly measured cross section of the $^{10}\text{B}(p,\alpha)^7\text{Be}$ reaction [6,7], black dots, and that obtained in the present work with the THM, red points.

In the analysis only events with neutron momentum lower than 30 MeV/c (where the QF-mechanism is dominant) were selected. Using the PWIA approach it was possible to extract the nuclear part of the cross section of the $^{10}\text{B}(p,\alpha)^7\text{Be}$ reaction in the energy range $0 < E_{cm} < 400$ keV. Preliminary results are reported in Fig.1. This figure shows the comparison between the direct two body cross section [6,7] and the THM experimental data obtained in the present work. The energy dependence of the THM two-body cross section is in good agreement with the direct one and this will allow the extraction of the two-body "bare"-astrophysical $S(E)$ -factor [9]

References

- [1] Boesgaard A.M., "The light elements: lithium, beryllium and boron", Origin and Evolution of the Elements, Carnegie Observatories Astrophysics Series, Vol.4, 2004.
- [2] A.Stephens et al., APJ 491, 339 1997.
- [3] G.Baur et al., Nucl. Phys. A458, 188, 1986.
- [4] A.M.Mukhamedzhanov et al., Phys. Rev. C51, 3472 1995.
- [5] C.Spitaleri et al., Nucl.Phys. A719, 99c, 2003.
- [6] Angulo C. Et al., Z. Phys. A345, 231-242, 1993.
- [7] Youn et al., Nucl.Phys A533, 321,1991.
- [8] L.Lamia et al. Nucl.Phys. A787, 309-314, 2007, and references therein.
- [9] Rolfs C. and Rodney W.S. "Cauldrons in the cosmos", University of Chicago Press, Chicago, 1988.

**Experimental Nuclear Physics:
PHENIX Experiment at BNL-RHIC**

Progress of the PHENIX Experiment and Related Activities in 2007

H. Hamagaki, T. Gunji, F. Kajihara, T. Isobe, S.X. Oda, Y. Morino, Y. Aramaki, Y.L. Yamaguchi, S. Sano, A. Takahara, J. Kikuchi^a, Y. Tanaka^b, and T. Fusayasu^b

Center for Nuclear Study, Graduate School of Science, the University of Tokyo

^a *Advanced Research Institute for Science and Engineering, Waseda University*

^b *Nagasaki Institute of Advanced Science*

1. Introduction

It is intended in this article to make an overview of the activities of the group whose primary interest is in the study of basic properties of strongly interacting QCD matter.

Currently, the group has been actively involved in the PHENIX experiment at RHIC, Relativistic Heavy Ion Collider, of Brookhaven National Laboratory, USA. RHIC is the first collider ever built to find evidence of the phase transition from normal hadronic matter to deconfined quark matter, called quark-gluon plasma (QGP), and to study the properties of the hot QCD matter. Collisions between Au nuclei at cms energy of 200 GeV per nucleon are possible.

The group has also started participating in the ALICE experiment at LHC, Large Hadron Collider, which is currently under commissioning in CERN. At LHC, collisions between lead nuclei at cms energy of 5.5 TeV will be realized sometime in the year 2009.

R & D of a gaseous detector called GEM (Gas Electron Multiplier) has been continued.

2. PHENIX Experiment and RHIC Runs

The CNS group has been participating in the PHENIX experiment, whose activity is supported by the Japan-US cooperation in the field of high energy physics sponsored by MEXT. The PHENIX experiment is one of the major experiments at RHIC, which consists of two central arms (East and West), two muon arms (North and South) and inner detectors for event trigger and event characterization. The PHENIX experiment was designed so as to address as many signatures as possible for QGP formation by having a unique capability of measuring photons, electrons and muons as well as hadrons.

In JFY 2007, we have successfully completed RHIC Run 7 and Run 8. Run 7 started in March 27 2007 and ended in June 26 2007. It was devoted to Au+Au collisions, and 4.5×10^9 Au+Au collisions (integrated luminosity of $711 \mu\text{b}^{-1}$) were successfully recorded, which are three times larger than those so far accumulated.

Run 8 started in Nov. 26 2007 and ended in March 12 2008. The run consisted of the two parts; 200 GeV d+Au collisions and p+p collisions. Integrated luminosity of $\sim 80 \text{ nb}^{-1}$ was achieved, which corresponds to ~ 30 times of the luminosity so far accumulated.

For Run 7, two new detectors, HBD and RxNP, were added to the PHENIX experiment. HBD (Hadron Blind Detector) is expected to provide higher rejection power of Dalitz decay and γ external conversions, which is crucial to access low mass region in the lepton-pairs. RxNP, a new de-

tor for reaction-plane determination, is expected to provide higher accuracy for reaction plane determination.

The CNS group has been responsible for operation and calibration of the RICH (Ring Imaging Cherenkov) detector subsystem and ERT trigger system. RICH, a gaseous Cherenkov counter using CO₂ gas as a Cherenkov radiator, is a primary device for electron identification, and ERT is a 1st-level trigger system for electrons using RICH and EM-Cal.

3. Analysis of the PHENIX Experiment

Major analysis efforts have been placed on the physics with leptons and photons. Brief introduction to each topic is provided, and details will be described in the following separate articles.

One of the major discoveries at RHIC is strong suppression of hadron yield at high transverse momentum in central Au+Au collisions [1], which indicates a formation of high-density matter in the collisions. For Au+Au collisions at 200 GeV, neutral pion production was measured with good statistics for transverse momentum up to 20 GeV/c. By utilizing the results, an attempt has been made to constrain model-dependent parameterization for the transport coefficient of the medium, e.g. $\langle \hat{q} \rangle$ in the parton quenching model [2, 3]. The result is described in [4].

An effort has been made to understand more precisely the energy loss mechanism of light partons, by studying the path-length dependence of the energy loss. An idea behind this effort is that the collisional energy loss grows linearly with path-length while radiational energy loss grows as (path-length)². By measuring the azimuthal angle of jet fragments relative to the reaction plain, path length may be determined much more precisely compared to the case without reaction plain determination. Study is going on for π^0 in Au+Au collisions using dataset taken in Run 7. Current status is presented in [5].

Strong yield suppression found for ‘non-photonic’ electrons, comparable with the case for light partons, has been a recent hot topic [6]. Main ‘non-photonic’ sources at the RHIC energies are leptonic decay of charm and bottom mesons. In order to understand better the energy loss mechanism of heavy quarks, it is desirable to determine experimentally the fraction of contributions from charm and bottom quarks at each electron momentum bin. A new method utilizing electron-hadron correlation has been successfully applied to p+p collisions to determine the yield ratio between D (charm) and B (bottom) mesons. Analysis procedure and preliminary results are described in [7].

The J/ψ yield suppression has been considered to be a key signature of deconfinement of hadronic matter. The CNS group has been taking a leading role in the analysis of J/ψ productions. Final results for Cu + Cu collisions from the Run 5 are presented in [8]. Side-feed from excited states of charmonium may have significant effect on the J/ψ yield suppression, and a study was made to determine directly the side-feed fraction from measurement of J/ψ and gamma coincidence. Preliminary results are provided in [9].

Direct photon is a penetrating probe to provide direct information from interim of hot and dense matter. It is, however, extremely difficult to measure single photons from thermal sources, since they are mainly emitted with low energies where competing background primarily from hadron decays are overwhelming. Because of this difficulty, no positive results have been reported so far in case of the heavy ion collisions. A method of measuring low-mass high-pT electron pairs (virtual photons) and extrapolating to the real photon, was applied successfully to p+p and Au+Au collisions at RHIC, and positive results could be deduced. Current status is presented in [10].

4. ALICE Experiment at CERN LHC

The CNS group has started participating in the ALICE experiment at LHC. As a natural extension from the physics interest and achievements of our group at RHIC, main physics focus may be placed on the leptons and photons. We have joined to the TRD (Transition Radiation Detector) subgroup. TRD is the primary device for electron identification.

Measurement of quarkonia, that is, J/ψ and Υ , is considered to remain to be a key subject at LHC, and it is one of the apparent goals of the CNS group. In [11], brief introduction of the ALICE experiment is provided, and acceptance for J/ψ and Υ in the mid-rapidity region covered by the ALICE experimental setup was evaluated.

Performance test of a TRD sector (1/18 of the total) was performed using secondary beams obtained from CERN PS. The CNS group has participated in the test execution. Pion rejection factor has been evaluated using the neural network method, and the current status of the analysis is presented in [12].

Contribution to the TRD electronics development has also been made. Slow control system called DCS (Detector Control System) is to ensure correct and safe operation of TRD, which is capable of doing configuration, remote control and monitoring of low voltage (LV), high voltage (HV), front-end electronics (FEE), power control unit (PCU), cooling and gas system. Test bench of the TRD front-end electronics was built at CNS, and developing and debugging of the DCS system software have been made [13].

5. R & D efforts

Development and application of GEM (gas electron multiplier) has been a central R & D subject of our group in the last few years. GEM, originally developed at CERN [14], has very simple structure with regularly arrayed holes

pierced through a polyimide sheet with typical thickness of $50\mu\text{m}$ with both sides coated by copper foils with thickness of $\sim 5\mu\text{m}$ which serve as electrodes.

A new GEM was developed which uses a different method for making holes [15], and extensive study of basic performance has been performed.

As an application, GEM is considered to be very suited for two-dimensional imaging with X-rays or neutrons. Development of readout circuit with custom ASIC for integrated charge with fast repetition of up to 1 kHz has been anticipated. Last year, a prototype CMOS readout chip was designed and fabricated, which includes 64 channel charge integrators and fast sequential readout capability using two stages of 8 channel multiplexers; 8 of them in the first stage and one in the second stage. Design details of the CMOS chip and its test performance is described in [16].

6. Summary and Outlook

The major activities of the CNS group are presented, which includes PHENIX data analysis efforts, preparative works for the ALICE experiment at LHC, and R & D efforts on GEM.

In the coming year, PHENIX RUN execution and data analysis are expected to be continued. Meanwhile, strong commitment to the ALICE experiment is expected, and R & D efforts related to GEM will be continued.

References

- [1] K. Adcox, S.S. Adler, H. Hamagaki, T. Matsumoto, S. Nishimura, K. Oyama, T. Sakaguchi et al. (PHENIX Collaboration): Phys. Rev. Lett. **88**, 022301 (2002)
- [2] A. Dainese, C. Loizides, and G. Paic, Eur. Phys. J. C38, 461 (2005).
- [3] C. Loizides, Eur. Phys. J. C49, 339 (2007).
- [4] T. Isobe *et al.*, in this report.
- [5] Y. Aramaki *et al.*, in this report.
- [6] S. S. Adler, H. Hamagaki, S. Kametani, T. Matsumoto, K. Oyama, K. Ozawa, T. Sakaguchi et al. (PHENIX Collaboration): Phys.Rev.Lett.96 (2006) 032301.
- [7] Y. Morino *et al.*, in this report.
- [8] S.X. Oda *et al.*, in this report.
- [9] S.X. Oda *et al.*, in this report.
- [10] Y.L. Yamaguchi *et al.*, in this report.
- [11] T. Gunji *et al.*, in this report.
- [12] A. Takahara *et al.*, in this report.
- [13] T. Gunji *et al.*, in this report.
- [14] F. Sauli: Nucl. Instr. and Meth. A 386 (1997) 531.
- [15] M. Inuzuka et al.: Nucl. Instr. and Meth. A 525 (2004) 529 – 534.
- [16] S. Sano *et al.*, in this report.

Measurement of π^0 production with respect to the reaction plane in $\sqrt{s_{NN}} = 200$ GeV Au+Au collisions at RHIC-PHENIX

Y. Aramaki, H. Hamagaki, T. Sakaguchi^a, and G. David^a, for the PHENIX Collaboration

Center for Nuclear Study, Graduate School of Science, University of Tokyo

^aBrookhaven National Laboratory, New York, U.S.A

1. Introduction

It has been observed in central Au+Au collisions at $\sqrt{s_{NN}} = 200$ GeV at Relativistic Heavy Ion Collider (RHIC) that the neutral pion yield at high transverse momentum ($p_T > 5$ GeV/c) is strongly suppressed compared to the yield expected from p+p collisions. This suppression is considered due to an energy loss of hard scattered partons in the medium (jet quenching) [1].

Dependence of energy loss on path length should provide further insight of the energy loss mechanism. Some theoretical models suggest that LPM effect in QCD plays an important role in radiative energy loss process [2]. The magnitude of energy loss is proportional to the path length square. Detailed information on path length can be obtained by measuring the azimuthal angle of emitted particles relative to the reaction plane in non-central collisions. The impact parameter is not zero in non-central collisions and the medium has a spatial anisotropy as shown in figure. 1. The reaction plane is defined by the beam direction and the distance vector of the center of the two nuclei. The nuclear modification factor (R_{AA}) and its azimuthal angle dependence have been studied at RHIC. R_{AA} is generally expressed using centrality (cent) which is associated to impact parameter for collisions and p_T .

$$R_{AA}(p_T, cent) = \frac{\sigma_{pp}^{inel}}{\langle N_{coll}(p_T, cent) \rangle} \frac{d^2 N^{AA}(p_T, cent)/dp_T d\eta}{d^2 \sigma^{NN}/dp_T d\eta}, \quad (1)$$

where $N^{AA}(cent)$ is the number of neutral pions in a given centrality. σ_{pp}^{inel} is a cross section for inelastic nucleon-nucleon collisions. η is a pseudo-rapidity. If R_{AA} is equal to one, the particle production in Au+Au collisions can be expressed as a superposition of nucleon-nucleon collisions. The nuclear modification factor as a function of an azimuthal angles is expressed by the following equation.

$$R_{AA}(p_T, cent, \Delta\phi) = \frac{N^{AA}(p_T, cent, \Delta\phi)}{\int d\phi N^{AA}(p_T, cent, \Delta\phi)} \times R_{AA}(p_T, cent) \quad (2)$$

and $N^{AA}(p_T, cent, \Delta\phi)$ can be expressed in terms of a Fourier expansion with $\Delta\phi$.

$$N^{AA}(\Delta\phi) \propto 1 + 2 \sum_{n=1}^{\infty} (v_n^{raw} \cos(n\Delta\phi)), \quad (3)$$

where v_n^{raw} is the magnitude of the harmonics of n-th order. The second harmonics (v_2^{raw}) represents the strength of elliptic flow. The true azimuthal anisotropy v_2^{corr} is obtained

after making correction of the reaction plane resolution [3].

$$v_2^{raw} = v_2^{corr} \langle \cos(2\Delta\Psi) \rangle, \quad (4)$$

where $\Delta\Psi$ is a difference between the true azimuthal angle from reaction plane and the observed one.

The nuclear modification factor as a function of p_T and path length need to be measured in high p_T because the effect of the collective flow decreases in high p_T [4]. If the effect of the collective flow is negligible, we can extract the only information for the effect of energy loss from the R_{AA} for each path length. Since measurement of neutral pions up to $p_T \sim 20$ GeV/c is possible with the PHENIX electromagnetic calorimeters (EMCal), the probe for path length dependence of R_{AA} is used with high- p_T neutral pions ($\pi^0 \rightarrow 2\gamma$). The integrated luminosity in 2007 Au+Au run is $813 \mu\text{b}^{-1}$ which is 3.5 times larger than that in 2004 Au+Au runs.

2. Experimental Setup

A new reaction plane detector, called as RxNP, was installed in the PHENIX experiment in 2007 Au+Au run. Reaction plane is determined using Beam-Beam Counter (BBC) and RxNP. RxNP was designed to have a wider rapidity coverage ($1.0 < |\eta| < 1.5$ and $1.5 < |\eta| < 2.8$) compared with BBC ($3 < |\eta| < 4$) [5]. Better resolution for reaction plane determination is expected with RxNP.

PHENIX has two types of calorimeters in the central arm ($|\eta| < 0.35$). PbSc consists of the lead and scintillator plates and wavelength shifter fiber readout. The other is lead-glass calorimeter (PbGl). The PbSc has a nominal energy and position resolution of $8.1/\sqrt{E(\text{GeV})} \oplus 2.1$ [%] and $5.7/\sqrt{E(\text{GeV})} \oplus 21.55$ [mm], respectively. The PbGl has a nominal energy resolution of $5.9/\sqrt{E(\text{GeV})} \oplus 0.8$ [%] and $8.4/\sqrt{E(\text{GeV})} \oplus 0.2$ [mm], respectively.

3. Analysis

We selected events with a vertex position within ± 30 cm along beam direction. For each selected event, reaction plane was determined as a direction to which the largest number of particles are emitted.

The number of neutral pions was obtained by integrating the counts in a certain mass window (usually ± 2 sigma from the mass peak) of the 2-gamma invariant mass distribution, after subtracting the combinatorial background calculated using the mixed event technique. The number of neutral pions are counted for each of six $\Delta\phi$ bins in the interval from 0 to $\pi/2$ as shown in figure. 1.

The number of neutral pions as a function of azimuthal angle is shown in figure. 2. This fitting function includes up to the second term in Eq. (3).

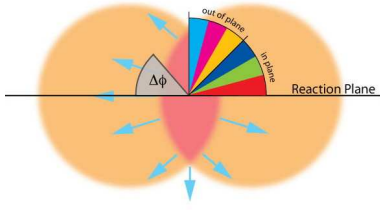


Figure 1. Schematics of the produced medium. In this analysis, azimuthal angles from reaction plane are divided into six azimuthal angular bins in the interval from 0 to $\pi/2$. The $\Delta\phi$ outside the interval is truncated into the interval, using the symmetrical relation.

Since we have two independent reaction plane from both of south and north for RxNP or BBC, we can evaluate the reaction plane resolution using the relative azimuthal angle ($\Delta\Psi \equiv \Psi^{SOUTH} - \Psi^{NORTH}$). The particles distribution for the relative azimuthal angles can be expressed by the following equation [6].

$$dN/d(\Delta\Psi) = \frac{e^{-\chi^2}}{2} \left(\frac{2}{\pi} (1 + \chi^2) + z [I_0(z) + L_0(z)] + \chi^2 [I_1(z) + L_1(z)] \right), \quad (5)$$

where $z = \chi^2 \cos(\Delta\Psi)$. I_k and L_k are a modified Bessel function and a modified Struve function of order k , respectively. The reaction plane resolution $\langle \cos(2\Delta\Psi) \rangle$ can be calculated using the following equation [7].

$$\langle \cos(2\Delta\Psi) \rangle = \frac{\sqrt{\pi}}{2} \chi e^{-\chi^2/2} \left[I_0\left(\frac{\chi^2}{2}\right) + I_1\left(\frac{\chi^2}{2}\right) \right] \quad (6)$$

Figure. 3 shows the reaction plane resolution for RxNP and BBC. The RxNP improved two times better reaction plane resolution than that with BBC for all centrality bins.

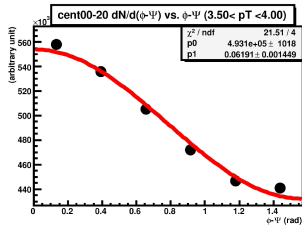


Figure 2. The neutral pion's distributions for each azimuthal angles in $3.5 < p_T < 4$ GeV/c (Centrality 0-20%). The solid line represents a fitting function which includes up to the second term in Eq. (3).

4. Result

Figure. 4 shows $v_2(\pi^0)$ as a function of p_T , where closed circles and open triangles represent results for RxNP and BBC, respectively. We have measured azimuthal anisotropy of neutral pions up to $p_T \sim 10$ GeV/c. The value of $v_2(\pi^0)$ with RxNP is consistent with that with BBC. Measurement of high- p_T $v_2(\pi^0)$ for 2007 is same as that for 2004 so far [8]. The results shown in Figure. 4 are so far analyzed

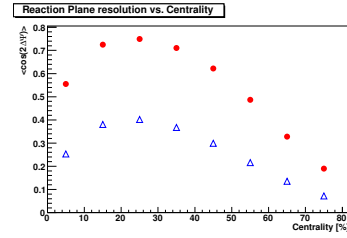


Figure 3. Reaction plane resolution for RxNP (closed circles) and BBC (open triangles) as a function of centrality.

with one-third of the data for measuring $v_2(\pi^0)$ with RxNP, and with full data set for measuring $v_2(\pi^0)$ with BBC. The $v_2(\pi^0)$ value with RxNP in 2007 will be expected to be measured up to higher p_T than that in 2004.

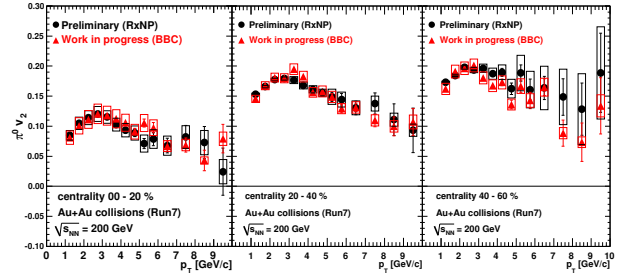


Figure 4. Circle solid points and triangular solid points show azimuthal anisotropy of neutral pion using the RxNP and the BBC, respectively. The black boxes mean systematic uncertainty for this analysis.

5. Summary

The new detector (RxNP) achieved two times better reaction plane resolution than with BBC. For studying the path length dependence of π^0 suppression systematically, we have started to measure the anisotropy of neutral pion up to $p_T \sim 10$ GeV/c. We will analyze the anisotropy of neutral pion with all the data. After finishing this measurement, we will measure the R_{AA} as a function of p_T and path length.

References

- [1] S.S. Adler *et al.*, Phys. Rev. Lett. **96** (2006) 202301.
- [2] X. Wang, M. Glulassy and M. plümer, Phys. Rev. D **51** (1995) 3436.
- [3] J. Barrette *et al.*, Phys. Rev. C **55** (1997) 1420.
- [4] S.S. Adler *et al.*, Phys. Rev. Lett. **96** (2006) 032302.
- [5] Letter of intent for PHENIX Reaction Plane Detector, 2006, PHENIX internal report
- [6] J.Y. Ollitrault, nucl-ex/9711003
- [7] A.M. Poskanzer and S. A.Voloshin Phys. Rev. C **58** (1998) 1679.
- [8] D.L. Winter for the PHENIX Collaboration, nucl-ex/0607009

J/ψ Production in Cu+Cu Collisions at $\sqrt{s_{NN}} = 200$ GeV at RHIC-PHENIX

S.X. Oda, H. Hamagaki, T. Gunji, Y. Akiba^a, K. Das^b, A.D. Frawley^b, and W. Xie^c, for the PHENIX collaboration

Center for Nuclear Study, Graduate School of Science, University of Tokyo

^aRIKEN(The Institute of Physics and Chemical Research)

^bFlorida State University

^cRIKEN BNL Research Center, Brookhaven National Laboratory

1. Introduction

The quarkonium yields are predicted to be suppressed in the quark gluon plasma (QGP) by the Debye color screening [1]. J/ψ is especially promising because of its large production cross section and di-lepton decay channels, which make it easily detected. The PHENIX experiment at RHIC measures J/ψ at midrapidity ($|y| < 0.35$) via its e^+e^- decay and at forward rapidity ($1.2 < |y| < 2.2$) via its $\mu^+\mu^-$ decay.

Models of J/ψ production in heavy ion collisions contain a number of competing effects, including destruction of J/ψ by thermal gluons in the QGP, modification of the J/ψ yield by the cold nuclear matter (CNM) effects, reduced feed-down from excited charmonium states that melt just above the QGP transition temperature, the bottom quark decay and enhancement of the J/ψ yield due to recombination of uncorrelated charm quark pairs [2].

The PHENIX Au+Au data at $\sqrt{s_{NN}} = 200$ GeV showed that J/ψ suppression at forward rapidity is larger than that at midrapidity and degree of the suppression at midrapidity is similar to that observed by the NA50 experiment at the SPS in Pb+Pb collisions at $\sqrt{s_{NN}} = 17.3$ GeV [3,4]. Since these results are not well understood theoretically, systematic study of J/ψ production in heavy ion collisions across the entire range of the number of participants (N_{part}) is required to disentangle the competing effects.

In 2005, PHENIX recorded Cu+Cu collisions at $\sqrt{s_{NN}} = 200$ GeV to obtain precise data in the range of $N_{part} \leq 126$, where Au+Au data is limited by statistics and systematic uncertainty and the CNM effects might be dominant. Accomplishments of the J/ψ measurement in the e^+e^- decay mode in Cu+Cu collisions by 2006 is described in Ref. [5]. In this report, the final analysis and results are described.

2. Analysis in 2007

The invariant yield of J/ψ is defined as follows,

$$\begin{aligned} & \frac{BR}{2\pi p_T} \frac{d^2 N}{dp_T dy} \\ &= \frac{1}{2\pi p_T} \frac{n(p_T, cent)}{N_{MB}(cent) \Delta p_T \Delta y \varepsilon(p_T, cent)}, \end{aligned} \quad (1)$$

where, $BR(= 5.94\%)$ is the branching ratio of J/ψ into an e^+e^- pair, n is the number of reconstructed J/ψ , ε is the overall efficiency, $\Delta y(= 1)$ is the rapidity bin width, Δp_T is the transverse momentum bin width and N_{MB} is

the number of minimum bias triggered events. The impact parameter decreases with the increase of the collision centrality, $cent$.

The analysis in 2007 was mainly concentrated on the evaluation of the overall efficiency. The overall efficiency is decomposed into three parts,

$$\begin{aligned} & \varepsilon(p_T, cent) \\ &= \varepsilon_{acc}(p_T) \times \varepsilon_{embed}(cent) \times \varepsilon_{L1}(p_T, cent), \end{aligned} \quad (2)$$

where ε_{acc} is the J/ψ reconstruction efficiency including acceptance in the e^+e^- decay mode, ε_{embed} is the embedding efficiency which represents the inefficiency by high particle multiplicity and ε_{L1} is the electron trigger efficiency for J/ψ .

The reconstruction efficiency ε_{acc} was evaluated with GEANT3 simulation. In Fig. 1, ε_{acc} is shown as a function of p_T of and is about 1%. Distributions of variables which were used to select electron candidates were examined by comparison between the real data and simulation. From the difference between the real data and simulation, the systematic error of ε_{acc} was deduced to be 6% (relative).

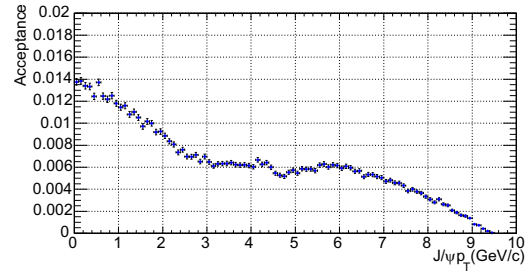


Figure 1. The J/ψ reconstruction efficiency including acceptance as a function of the transverse momentum of J/ψ . Only the statistical errors are shown.

The embedding efficiency ε_{embed} was estimated by embedding simulated single J/ψ events into the real data and reconstructing them. In the most central Cu+Cu collisions, ε_{embed} is $97 \pm 2(syst)\%$ and this means the inefficiency is only $3 \pm 2(syst)\%$.

The electron trigger efficiency for J/ψ (ε_{L1}) was determined for each centrality bin as a function of p_T of J/ψ from the measured single electron trigger efficiency with simulation samples of single J/ψ events. The determined ε_{L1} is larger than 70% for all p_T range and its systematic error was determined to be 4% (relative) by various param-

eterizations of the single electron trigger efficiency.

3. Results and discussion

To quantify the difference between a nucleus-nucleus collision and the superposition of nucleon-nucleon collisions, the nuclear modification factor, R_{AA} , is defined as follows,

$$R_{AA} = \frac{dN}{dy} \Big|_{AA} \Big/ \left(N_{coll} \cdot \frac{dN}{dy} \Big|_{pp} \right), \quad (3)$$

where $\frac{dN}{dy} \Big|_{AA}$ and $\frac{dN}{dy} \Big|_{pp}$ are the J/ψ yields in a nucleus-nucleus collision and in a $p + p$ collision, respectively, and N_{coll} is the number of collisions, estimated by the Glauber model. The $p + p$ collision data at the same energy taken in 2005 [6] is used as a reference. A calculation of the CNM effects estimated breakup cross sections, $\sigma_{breakup}$, with the d +Au collision data and EKS98 nuclear shadowing model [7]. Figure 2 shows R_{AA} in Cu+Cu and Au+Au collisions with predictions of the calculation (R_{AA}^{CNM}). Not only results of e^+e^- decay mode at midrapidity (a), but ones of $\mu^+\mu^-$ decay mode at forward rapidity (b) are shown.

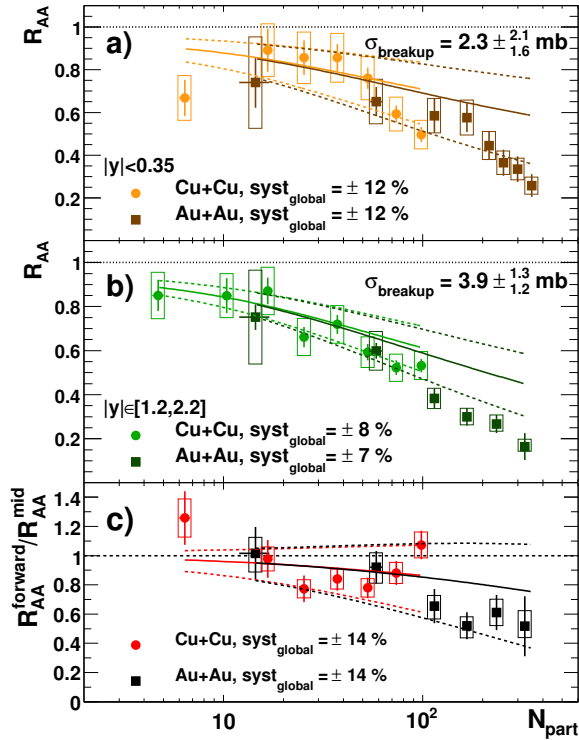


Figure 2. a) The nuclear modification factor R_{AA} of J/ψ as a function of the number of participants in Cu+Cu and Au+Au collisions at midrapidity with the prediction curves with the EKS98 nuclear shadowing model [7]. b) The same figure at forward rapidity. c) Forward/mid rapidity R_{AA} ratio.

Survival probability of J/ψ , $S^{J/\psi}$, can be defined as

$$S^{J/\psi} = R_{AA} / R_{AA}^{CNM}. \quad (4)$$

Bjorken energy density ε_{Bj} is an estimation of initial en-

ergy density using the transverse energy E_T in a collision,

$$\varepsilon_{Bj} = \frac{1}{A\tau_0} \frac{dE_T}{dy} \Big|_{y=0}, \quad (5)$$

where A is the transverse area of a collision and τ_0 is the thermalization time [8]. Figure 3 shows $S^{J/\psi}$ at RHIC and SPS as a function of ε_{Bj} with the assumption of $\tau_0 = 1$ fm/c [4, 9, 10]. The J/ψ suppression seems to start at $\varepsilon_{Bj} \sim 2.5$ GeV/fm³ regardless of rapidity and collision energy. This energy density corresponds to those in the most central S+U collisions at $\sqrt{s_{NN}} = 19.4$ GeV and the most central collisions at $\sqrt{s_{NN}} = 200$ GeV. If the QGP consists of gluons, up, down and strange quarks, $\varepsilon_{Bj} \sim 2.5$ GeV/fm³ corresponds to the temperature $T \sim 180$ MeV.

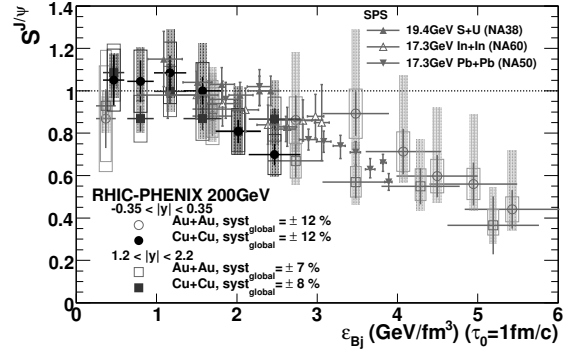


Figure 3. Survival probability of J/ψ ($S_{J/\psi}$) is shown as a function of the Bjorken energy density (ε_{Bj}). Results from SPS and RHIC are shown. For the SPS results, all errors are added in quadrature. For the RHIC results, the quadrature sum of statistical, uncorrelated and correlated systematic errors is represented by a bar, the global systematic error is represented by an open box, and the error of the breakup cross section is represented by a shaded box.

4. Summary

The analysis of J/ψ production in Cu+Cu collisions at $\sqrt{s_{NN}} = 200$ GeV has been completed. J/ψ suppression seems to be started in the most central Cu+Cu collisions. If the QGP which consists of gluons, up, down and strange quarks is assumed, the temperature in the most central Cu+Cu collisions is about 180 MeV.

References

- [1] T. Matsui and H. Satz, Phys. Lett **B178** (1986) 416.
- [2] H. Satz, J. Phys. **G32** (2006) R25.
- [3] A. Adare *et al.*, Phys. Rev. Lett. **98** (2007) 232301.
- [4] B. Alessandro *et al.*, Eur. Phys. J. **C39** (2005) 335.
- [5] S.X. Oda *et al.*, CNS Annual Report 2006 (2007) 43.
- [6] A. Adare *et al.*, Phys. Rev. Lett. **98** (2007) 232002.
- [7] A. Adare *et al.*, Phys. Rev. **C77** (2008) 024912.
- [8] J.D. Bjorken, Phys. Rev. **D27** (1983) 140.
- [9] R. Arnaldi *et al.*, Phys. Rev. Lett. **99** (2007) 132302.
- [10] S.S. Adler *et al.*, Phys. Rev. **C71** (2005) 034908.

χ_c Production in $p + p$ Collisions at $\sqrt{s} = 200$ GeV at RHIC-PHENIX

S.X. Oda, H. Hamagaki, and K. Ozawa^a, for the PHENIX Collaboration

Center for Nuclear Study, Graduate School of Science, University of Tokyo

^aDepartment of Physics, Graduate School of Science, University of Tokyo

1. Introduction

In quark gluon plasma (QGP), heavy quarkonia (J/ψ , ψ' , χ_c , Υ , etc.) are expected to dissociate at different temperatures depending on their binding energy and can be a Galileo thermometer [1]. While the heavy quarkonium data at RHIC so far is limited to measurements of J/ψ in $p + p$, $d+Au$, $Cu+Cu$ and $Au+Au$ collisions at $\sqrt{s_{NN}} = 200$ GeV [2], it is known by other experiments at different energy regions [3, 4, 5] that a significant fraction of J/ψ is produced by χ_c radiative decay. The feed-down fraction of J/ψ from χ_c , R_{χ_c} , is important to understand the behavior of J/ψ in QGP. The masses, widths and branching ratios (BR) of J/ψ and three states of χ_{cJ} ($J = 0, 1, 2$) are listed in Table 1. The definition of R_{χ_c} is as follows:

$$R_{\chi_c} = \frac{1}{\sigma_{J/\psi}} \sum_{J=0}^2 BR(\chi_{cJ} \rightarrow J/\psi\gamma) \sigma_{\chi_{cJ}}, \quad (1)$$

where σ is the inclusive production cross section. Since the branching ratio of χ_{c0} into J/ψ is much smaller than those of χ_{c1} and χ_{c2} , the contribution from χ_{c0} is usually neglected. In this report, measurement of R_{χ_c} in $p + p$ collisions at $\sqrt{s} = 200$ GeV at midrapidity ($|y| < 0.5$) by the PHENIX experiment at RHIC is described.

Particle	Mass (MeV/c ²)	Width (MeV/c ²)	BR ($\chi_c \rightarrow J/\psi\gamma$)
$J/\psi(1S)$	3096.92 ± 0.01	0.093 ± 0.002	-
$\chi_{c0}(1P)$	3414.75 ± 0.35	10.4 ± 0.7	$1.32 \pm 0.11\%$
$\chi_{c1}(1P)$	3510.66 ± 0.07	0.89 ± 0.05	$35.9 \pm 1.9\%$
$\chi_{c2}(1P)$	3556.20 ± 0.09	2.05 ± 0.12	$20.3 \pm 1.0\%$

Table 1. Masses, widths and radiative decay branching ratios of J/ψ and three χ_c states from PDG2007 [6]

2. Signal Reconstruction

To measure R_{χ_c} , firstly, the $J/\psi \rightarrow e^+e^-$ decay ($BR = (5.94 \pm 0.06)\%$ [6]) is detected with the pair mass range of $2.9 < M_{ee} < 3.3$ GeV/c². Secondly, the mass of $e^+e^- \gamma$ is reconstructed and the mass difference, $\Delta M = M_{ee\gamma} - M_{ee}$, is calculated. The χ_c mass peak locates at $\Delta M \sim 0.44$ GeV/c². Thirdly, the acceptance of the $\chi_c \rightarrow J/\psi\gamma$ decay is corrected event by event.

$$R_{\chi_c} = \frac{1}{N_{J/\psi}} \left\langle \frac{1}{\varepsilon_{acc,J/\psi}} \right\rangle^{-1} \frac{\Delta y_{J/\psi}}{\Delta y_{\chi_c}} \times \sum_{i=1}^{N_{\chi_c}} \frac{1}{\varepsilon_{acc,\chi_c}^{J/\psi \text{ det}}(p_{T,\chi_c})} \frac{1}{\varepsilon_{acc,J/\psi}(p_{T,J/\psi})}, \quad (2)$$

where N_C is the number of detected charmonia C , $\varepsilon_{acc,J/\psi}(p_{T,J/\psi})$ is the J/ψ acceptance including reconstruction and trigger efficiency as a function of the trans-

verse momentum p_T of J/ψ , $\varepsilon_{acc,\chi_c}^{J/\psi \text{ det}}(p_{T,\chi_c})$ is the conditional efficiency of χ_c if J/ψ is detected as a function of p_T of χ_c , Δy_C is the rapidity gap used in the acceptance calculation, and $\langle \dots \rangle$ means the average over detected J/ψ .

3. Simulation

The acceptance of J/ψ and the conditional efficiency of χ_c were evaluated using PISA which is a GEANT3 simulator [7] for PHENIX. The conditional efficiency of χ_c is shown in Fig. 1 as a function of p_T of χ_c and is about 10% at $p_T = 0$ GeV/c.

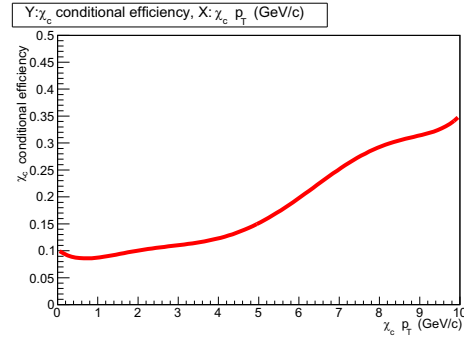


Figure 1. The χ_c conditional efficiency if J/ψ is detected, $\varepsilon_{acc,\chi_c}^{J/\psi \text{ det}}$, as a function of p_T of χ_c .

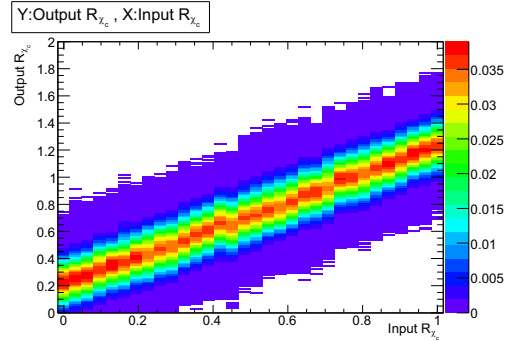


Figure 2. The relation between the input (true) R_{χ_c} and output (measured) R_{χ_c} obtained with the fit function of a Gaussian and a third order polynomial.

One of the difficulties of this analysis is background photons and the effect was estimated using an event generator, PYTHIA [8]. The parameters of PYTHIA were tuned to reproduce the observed p_T spectrum of J/ψ and photon multiplicity. Generated χ_c events by PYTHIA were simulated by PISA and reconstructed. The number of reconstructed J/ψ was kept to be 4.1×10^3 which is the number of reconstructed J/ψ in the real data. The combined function of a Gaussian (signal) and a third order polynomial (back-

ground) was fitted to the reconstructed χ_c peak. The output (measured) R_{χ_c} was obtained varying the input (true) R_{χ_c} . The relation between the input and output R_{χ_c} is shown in Fig. 2. The offset of output R_{χ_c} of about 0.2 is due to the background and limited statistics.

4. Data Analysis

The analysed $p + p$ collision data was taken in 2005 and 2006, and the integrated luminosity is 14.5 pb^{-1} . The number of reconstructed J/ψ with the like-sign pair (e^+e^+ and e^-e^-) subtraction for the accidental coincidence is 4.1×10^3 . The raw spectrum of the mass difference ΔM is shown in Fig. 3. The possible peak was fitted with the combined function of a Gaussian and a third order polynomial and the output R_{χ_c} was found to be 0.39 ± 0.10 . From the output R_{χ_c} with the evaluated systematic error of 0.16 and the relation in Fig. 2, the probability density function of the input R_{χ_c} was obtained and is shown in Fig. 4.

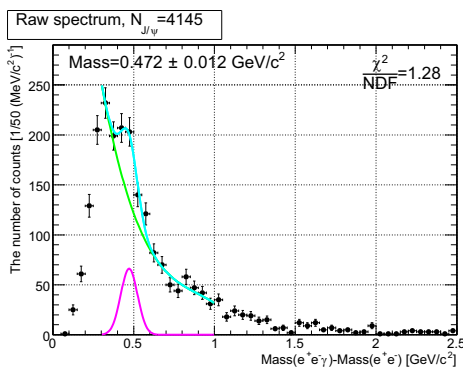


Figure 3. The raw spectrum of the mass difference. The fitted combined function of a Gaussian and a third order polynomial, and both components are shown.

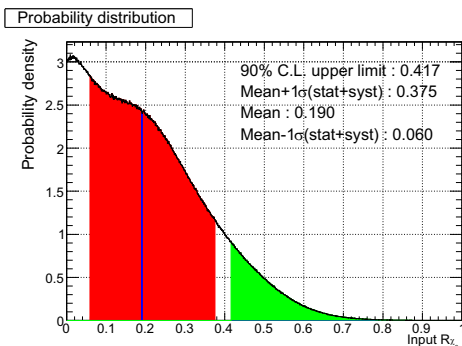


Figure 4. Probability density function of the input R_{χ_c} . The 90% confidence level upper limit of the input R_{χ_c} is 0.42.

5. Result

Figure 5 shows the obtained upper limit of $R_{\chi_c} < 0.42$ (90% C.L.) in $p + p$ collisions at $\sqrt{s} = 200 \text{ GeV}$ with results of other experiments. There is no strong energy dependence of R_{χ_c} . The color evaporation model predicts that no energy dependence of R_{χ_c} and $R_{\chi_c} = 0.24\text{--}0.3$ [9, 10]. This prediction agrees with the observed constant trend of R_{χ_c} . PHENIX has interpreted the obtained J/ψ data with calcu-

lations of Ref. [11]. The assumption in the calculations is $R_{\chi_c} = 0.3$ [12] and is consistent with the obtained upper limit.

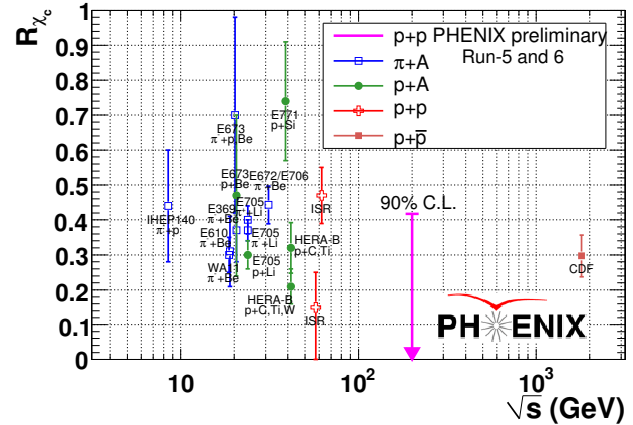


Figure 5. The 90% confidence level upper limit of R_{χ_c} in $p + p$ collisions at $\sqrt{s} = 200 \text{ GeV}$ is 0.42. The R_{χ_c} values obtained from other experiments are also shown as a function of center of mass energy \sqrt{s} .

6. Summary

The feed-down fraction of J/ψ from χ_c , R_{χ_c} , has been measured in $p + p$ collisions at $\sqrt{s} = 200 \text{ GeV}$ via the decay chain of $\chi_c \rightarrow J/\psi\gamma \rightarrow e^+e^-\gamma$. The 90% confidence level upper limit is $R_{\chi_c} < 0.42$ and no strong \sqrt{s} dependence was found. This observed trend of R_{χ_c} agrees with the color evaporation model.

References

- [1] H. Satz, J. Phys. **G 32**, R25 (2006).
- [2] A. Adare *et al.* (PHENIX Collaboration), arXiv:0801.0220 [nucl-ex], and references are therein.
- [3] F. Abe *et al.* (CDF Collaboration), Phys. Rev. Lett. **79**, 578 (1997).
- [4] I. Abt *et al.* (HERA-B Collaboration), Phys. Lett. **B 561**, 61 (2003).
- [5] N. Brambilla *et al.*, CERN Yellow Report 2005-005, arXiv:hep-ph/0412158.
- [6] W.-M. Yao *et al.* (Particle Data Group), J. Phys. **G 33**, 1 (2006) and 2007 partial update for the 2008 edition.
- [7] GEANT Detector description and simulation tool, CERN Program Library Long Write-up W5013.
- [8] T. Sjostrand *et al.*, arXiv:hep-ph/0603175.
- [9] J.F. Amundson *et al.*, Phys. Lett. **B 372**, 127 (1996).
- [10] M.L. Mangano, AIP Conf. Proc. **357**, 120 (1996).
- [11] R. Vogt, Acta. Phys. Hung. **A 25**, 97 (2006).
- [12] R. Vogt, Nucl. Phys. **A 700**, 539 (2002).

Acceptance Calculation of $J/\psi \rightarrow e^+e^-$ and $\Upsilon \rightarrow e^+e^-$ at LHC-ALICE

T. Gunji, H. Hamagaki, S. Sano, A. Takahara

Center for Nuclear Study, Graduate School of Science, University of Tokyo, Japan

1. Introduction

High energy heavy ion collision provides powerful tool to realize the QCD phase transition from hadronic matter to the hot and dense QCD matter composed of de-confined quarks and gluons, called Quark-Gluon-Plasma (QGP).

Large Hadron Collider (LHC) at European Organization for Nuclear Research (CERN) will start its operation in 2008 and first Pb+Pb collisions at $\sqrt{s_{NN}} = 5.5$ TeV is scheduled in 2009. Heavy ion program at LHC will give more fruitful understanding of the hot and dense QCD medium at higher temperature regime as well as the nuclear structure at small x regime, which may be the key to understand the dynamics of the QCD phase transition.

2. LHC-ALICE Experiment

The ALICE experiment is one of the experiments performed at LHC and only the experiment dedicated for heavy ion collisions [1]. Figure 1 is the detector setup for the ALICE experiment. ALICE detectors are designed to have the

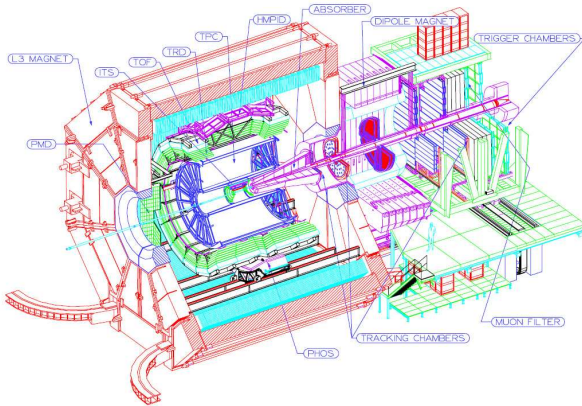


Figure 1. Layout of the ALICE detectors

capability to measure hadrons, leptons and photons over a wide kinematic range (transverse momentum, rapidity and azimuth). The main component of the ALICE detectors is the central barrel, where hadrons, electrons and photons are measured at central rapidity region ($|\eta| < 0.9$). The ALICE central detectors are located inside the L3 magnet, which gives a solenoidal magnetic field ($B \leq 0.5$ T). The central barrel detector consists of two main tracking detectors, which are Inner Tracking System (ITS) and Time Projection Chamber (TPC), and two main particle identification detectors, which are Transition Radiation Detector (TRD) and Time Of Flight detector (TOF) [1]. TRD plays the main role in providing electron identification [5]. Transition Radiation (TR) is generated when a relativistic charged particle with $\gamma \geq 1000$ passes through the boundaries between

two media with different dielectric constants. TRD consists of the radiator which generates TR and the drift chamber behind the radiator to detect TR and measure dE/dx of charged particles. Since typical energy of emitted TR is 10 keV, Xe (85%) gas is used in drift chamber. Test experiment was performed in 2007 at CERN PS beamline and the performance of the electron identification capability is reported in Ref. [3].

3. Quarkonia Measurement at ALICE

Heavy quarkonia (J/ψ , ψ' , χ_c , Υ) have long been considered as one of the most promising probes for the de-confinement of QGP [4]. In QGP, the production of heavy quarkonia could be suppressed due to the color Debye screening effect and the magnitude of suppression depends on the temperature of the medium and the radius of $q\bar{q}$ pairs [4]. Recent lattice QCD calculations suggest that the dissociation temperature of J/ψ is $\sim 2 T_c$ and that of Υ is $4 T_c$, while that of χ_c and ψ' is just above T_c , where T_c is the critical temperature (~ 170 MeV) [5]. Therefore the heavy quarkonia serve as the thermometer in QGP. J/ψ and Υ measurements can be performed in central rapidity region via their e^+e^- decay channel. The ITS and TPC provide the tracking and momentum of charged particles and the TPC and TRD provide the electron identification. Acceptance and efficiency calculations for $J/\psi \rightarrow e^+e^-$ and $\Upsilon \rightarrow e^+e^-$ are performed based on the Monte Carlo simulation and their results are described in this article.

4. Simulation Study for Acceptance Calculation

AliRoot [6], the ALICE software package, which provides an object-oriented framework for the generation, detector response simulation and analysis of the simulated data, was used for this study. Most of the software is written in C++ and based on the ROOT packages [7], although for the tracking of Monte Carlo generated particles routines from GEANT3 [8] are used.

J/ψ and Υ are generated with flat rapidity $-1 \leq y \leq 1$ and with flat transverse momentum distribution up to 15 GeV/c. The number of events generated for J/ψ and Υ is approximately 170,000 events for each. Magnetic field was set to be 0.5 T. Acceptance of J/ψ and Υ , ϵ_{acc} , is defined as follows:

$$\epsilon_{acc}^{J/\psi, \Upsilon}(p_T, y) = \frac{N_{acc}^{J/\psi, \Upsilon}(p_T, y)}{N_{gen}^{J/\psi, \Upsilon}(p_T, y)}, \quad (1)$$

where $N_{gen}^{J/\psi, \Upsilon}$ and $N_{acc}^{J/\psi, \Upsilon}$ are the number of J/ψ and Υ accepted and generated, respectively. Momentum is extracted with the TPC and electron identification is performed with the TPC and the TRD using dE/dx and TR measurement. A Bayesian approach is used for the parti-

cle identification. Conditional probability for the track to be e, π, μ, K, p is calculated with the TPC and TRD, separately. Then conditional probabilities are combined as follows:

$$P(i) = \frac{\prod_{j=\text{TPC,TRD}} P(i|j)}{\sum_{k=e,\pi,\mu,K,p} \prod_{j=\text{TPC,TRD}} P(k|j)}. \quad (2)$$

In the TRD, electron identification is performed using two dimensional likelihood method, where the correlation of the energy deposit and the drift time of secondary electrons are used to define the probability for electrons and pions. Left of Fig. 2 shows electron probability distribution defined by Eq. (2) for the daughter e^+e^- from J/ψ and Υ and right of Fig. 2 shows the electron identification efficiency for $p(e) \geq 0.5$. TRD improves the efficiency above 1 GeV/c. Since π rejection is worse for higher momentum due to relativistic rise of dE/dx for π and constant for e , the efficiency decreases for higher momentum [5].

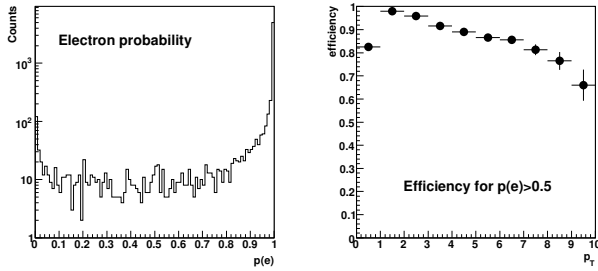


Figure 2. Left: electron probability distribution for daughter e^+e^- from J/ψ and Υ . Right: efficiency for $p(e) \geq 0.5$ with TPC+TRD as a function of p_T

5. Simulation Results

Figure 3 shows the invariant mass spectra for J/ψ (left) and Υ (right), where electron probability $P(e) \geq 0.5$ cut is applied and ghost pairs, which share the same hits in TPC, are rejected. The mass resolution for J/ψ and Υ is 30 MeV and 90 MeV, respectively.

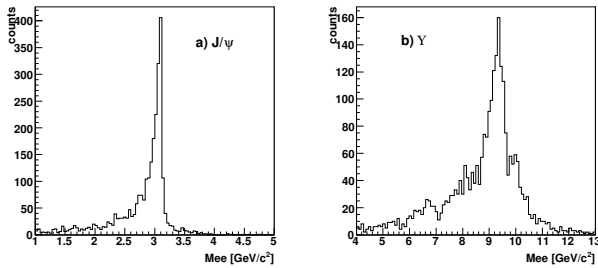


Figure 3. Invariant Mass spectra for J/ψ and Υ with 5.0k statistics

Figure 4 shows the acceptance defined as Eq. (1) as a function of p_T for J/ψ (left) and Υ .

Acceptance of J/ψ for $|y| < 1$ is 30% in low p_T and increases for higher p_T , while that of Υ is 30% for all p_T . Rapidity dependence of the acceptance shows that the accep-

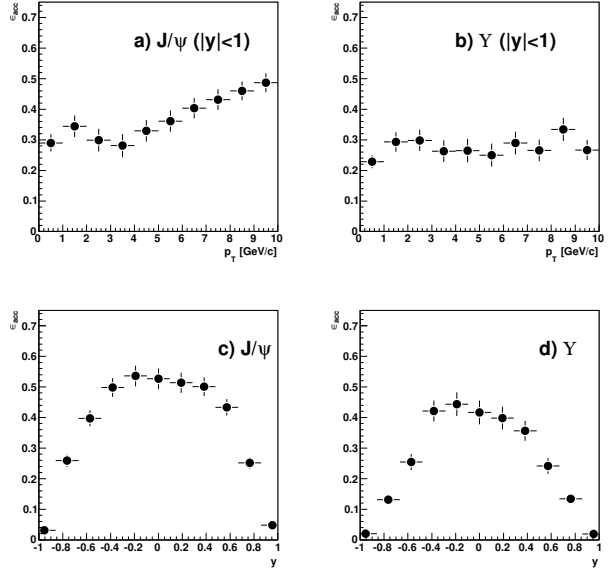


Figure 4. Acceptance of J/ψ and Υ via di-electron decay as a function of p_T and y .

tance increases by a factor of ~ 1.3 for $|y| \leq 0.5$ compared to that for $|y| \leq 1$. Taken into account this acceptance, production cross section of J/ψ and Υ at $\sqrt{s_{NN}}=5.5$ TeV, and the beam luminosity of $5 \times 10^{26} \text{ cm}^{-2} \text{ sec}^{-1}$, the number of J/ψ and Υ are expected to be $\sim 10^4$ and $\sim 10^3$, respectively during the scheduled heavy ion running (10^6 sec).

6. Summary and Outlook

First quantitative analysis of J/ψ and Υ at LHC-ALICE started and acceptance for J/ψ and Υ detection is calculated using AliRoot. Acceptance of J/ψ and Υ as functions of p_T and y is calculated and further analysis on the efficiency calculation such as the multiplicity dependence and feasibility study for the heavy quarkonia measurement in Pb+Pb collisions will be done.

References

- [1] ALICE Collaboration, Physics Performance Report Vol. 1 J. Phys. **G 30** (2003) 1517.
- [2] ALICE Collaboration, "ALICE TRD Technical Design Report", CERN/LHCC 2001-021, ALICE TDR 9, 3 Oct. 2001.
- [3] A. Takahara *et al.* in this report
- [4] T. Matsui and H. Satz, Phys. Lett. **B 178**, (1986) 416.
- [5] M. Asakawa and T. Hatsuda, Phys. Rev. Lett. **92**, (2004) 012001.
- [6] AliRoot and ALICE Offline Project, <http://aliceinfo.cern.ch/Offline>
- [7] Root, <http://root.cern.ch/>
- [8] GEANT3.21 Package, CERN Program Library W5013

Development of the Detector Control System of the ALICE Transition Radiation Detector

T. Gunji, H. Hamagaki, S. Sano, A. Takahara, T. Dietel^a, U. Westerhoff^a,
K. Schweda^b, J. Mercado^b, K. Watanabe^c

Center for Nuclear Study, Graduate School of Science, University of Tokyo, Japan

^a *Institut für Kernphysik, University of Muenster, Germany*

^b *Physics Institute des University Heiderberg, Germany*

^c *Institute of Physics, University of Tsukuba, Japan*

1. Introduction

The ALICE experiment at Large Hadron Collider (LHC) in European Organization for Nuclear Research (CERN) will start its operation in 2008. The main purpose of the ALICE experiment is to study the characteristics of hot and dense QCD matter, composed of quarks and gluons, created by ultra-relativistic heavy ion collisions [1].

We started to participate in the ALICE Transition Radiation Detector (TRD) Project in 2002, where the performance evaluation of the prototype TRD and the real size TRD were conducted [2, 3, 4]. We also started to develop the control softwares for the TRD and activity in 2007 is reported in this article.

2. ALICE Transition Radiation Detector

The ALICE TRD will cover the wide kinematic region of $|\eta| < 0.9$ in pseudorapidity and 2π in azimuthal angle. The ALICE TRD is divided into 18 azimuthal sectors, where one sector has 5 longitudinal sections and 6 TRD layers in radial direction [5].

Each detector consists of a radiator composed of polypropylene fiber mats of 48 mm thickness and a readout chamber behind the radiator with a 30 mm drift region, a 7mm amplification region and a segmented cathode readout pad plane [5]. The readout electronics is mounted behind the chamber as shown in Fig. 1. The chambers are operated with Xe/CO₂ (85/15%) gas mixture to achieve a higher detection efficiency for transition radiation photons [5].

Figure 2 shows the overall TRD electronics chain. Signals induced on the cathode pads is fed into a Multi-Chip-Module (MCM), which is composed of a charge-sensitive preamplifier and shaper (PASA), a custom 10 bit 10MHz ADC and digital circuitry called TRAP chips (digital filter, tracklet preprocessor, and tracklet processor). Digital filters perform the required nonlinearity, baseline and gain corrections and crosstalk suppression. The Tracklet Preprocessor contains hit detection and hit selection, calculates the position using pad response function, and detects clusters. Tracklet processor identifies high- p_T track candidates for further processing such as trigger generation [5, 6].

The readout electronics on one TRD chamber is controlled by Detector Control System Board (DCSB), which contains an FPGA and an ARM core running the Linux operating system. It controls the voltage regulator shutdown on the Readout Boards (ROB), configures all of the MCM chips including TRAP chips on the chamber and distributes

clock and trigger signals [5].

Each MCM processes 18-21 channels and about 120 MCM chips are mounted on one chamber. About 34 MCM chips are connected in groups on two ROB in redundant daisy chained network, the slow control serial network (SCSN), where there are two traffic links [5].

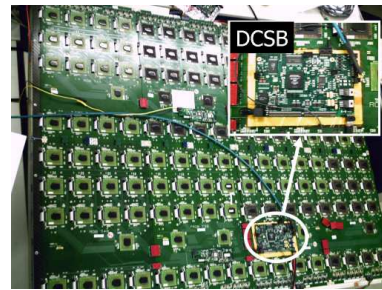


Figure 1. Readout electronics mounted on one TRD chamber

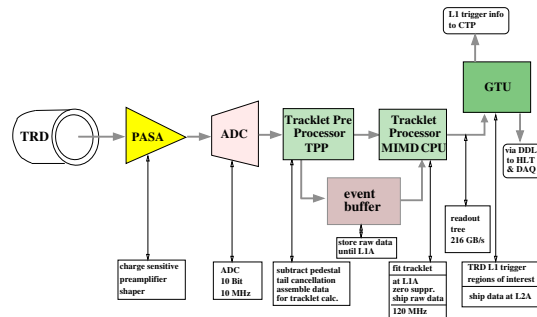


Figure 2. Overall TRD electronics chain

3. Detector Control System

The main task of the Detector Control System (DCS) is to ensure correct and safe operation of the TRD. It enables to do configuration of the MCMs, remote control and monitoring of the states for low voltage (LV), high voltage (HV), front-end electronics (FEE), power control unit (PCU), cooling and gas system.

Figure 3 shows TRD front-end communication chain. In the lowest level, the Control Engine (CE) is running on DCS boards to communicate with the underlying hardware via the SCSN, to process the received commands from upper layer and to provide values or acknowledgement to the FeeServer. FeeServer takes care of the communication path, updates published values from CE and returns the values to

upper layer to monitor the state of DSC board. The supervisory layer uses PVSS, which is the SCADA (Supervisory Control And Data Acquisition) system [7]. A middle layer between PVSS and DCS is called InterComLayer, which receives the command from PVSS, contacts to the data base, decodes the command data, and sends data to the FeeServer.

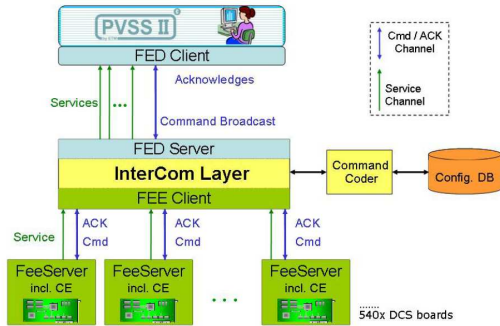


Figure 3. TRD front-end communication chain

There are two ROB's with 34 MCM chips and one DCS board in CNS. Setup for the tests is completed in 2007 including the configuration database and all needed softwares such as InterComLayer, CE, FeeServer and PVSS. Noise level and its fluctuation are checked first for all MCM chips, where the results are shown in Fig. 4. RMS of 1 ch corresponds to 1000 electrons, which is the requirement of the electronics. Noise level varies strongly channel by channel. A recursive digital filter of first order has been implemented to determine the pedestal, subtract it and add well defined baseline values [6].

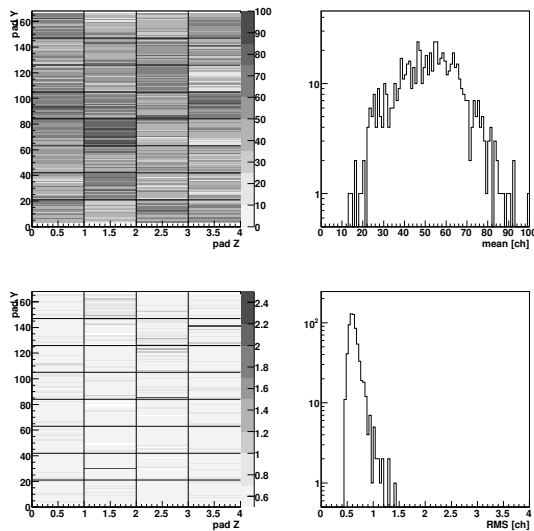


Figure 4. Noise distributions from all channels in 34 MCM chips. Upper and lower left are mean and RMS of noise for each channel, respectively. Upper right is mean and lower right is RMS distribution summed up all channels.

One of the main tasks is to debug and develop the control softwares for CE, FeeServer, and InterComLayer. One of the works is already done, which is to mask some of dead

MCM chips in daisy chained network and re-define the suitable network architecture not to use those chips [6], where the algorithm is implemented in CE and firmware of DCS board. Another work is to prepare the control panel using PVSS to check the state of all MCM chips and to check the response after receiving the trigger signal. Figure 5 shows the control panel for this test prepared using PVSS. This panel will be checked at CERN and will be installed in the future.

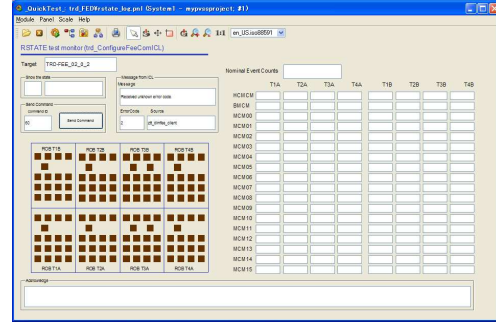


Figure 5. Control panel to check the MCM status and response to the pretrigger.

4. Summary and Outlook

Test system of the ALICE-TRD front-end electronics and control softwares is built in 2007 and debugging and development of the control softwares have been started. Softwares in CE and firmware of DCS board are developed to adapt to the situation where some of the MCM chips are broken and for the SCSN to be re-configured according to them. PVSS control panel is prepared to check the state of all MCM chips. These softwares will be tested using the TRD supermodule at CERN and will be installed.

Another interesting topic, which will be done in the future, is to study the trigger algorithm in tracklet processor and preprocessor since TRD can provide high p_T and/or electron trigger to ALICE, where the evaluation has not been started yet by the collaborators.

References

- [1] ALICE Collaboration, Physics Performance Report Vol. 1 J. Phys. **G 30** (2003) 1517.
- [2] T. Gunji *et al.* CNS Annual Report 2002.
- [3] T. Gunji *et al.* CNS Annual Report 2003.
- [4] Y. Morino *et al.* CNS Annual Report 2004.
- [5] ALICE Collaboration, "ALICE TRD Technical Design Report", CERN/LHCC 2001-021, ALICE TDR 9, 3 Oct. 2001.
- [6] ASICCC: ALICE TRAP User Manual (Darmstadt, Heiderberg, Mannheim, Kaiserslautern) <http://www.kip.uni-heidelberg.de/ti/TRD/doc/trap>
- [7] PVSS <http://itcobe.web.cern.ch/itcobe/Services/Pvss>

Measurement of neutral pions at high transverse momentum and quantitative evaluation of medium transport coefficients in Au+Au collisions at $\sqrt{s_{NN}} = 200$ GeV with RHIC-PHENIX experiment

T. Isobe, H. Hamagaki, T. Sakaguchi^a, G. David^a, B. Sahlmueller^b, J.L. Nagle^c, M.J. Tannenbaum^a, C. Klein-Boesing^b, and M.L. Porschke^a for the PHENIX Collaboration

Center for Nuclear Study, Graduate School of Science, University of Tokyo

^a*Brookhaven National Laboratory, USA*

^b*University of Muenster, German*

^c*University of Colorado, USA*

1. Introduction

As the temperature or density of many-body system of hadrons are increased, a normal nuclear state is expected to transit into a new state of matter where quarks and gluons become color de-confined. The new state of matter is called ‘‘Quark Gluon Plasma’’ (QGP).

Such an extreme state of matter is expected to be formed in ultra-relativistic heavy ion collisions. At Relativistic Heavy Ion Collider (RHIC) in Brookhaven National Laboratory (BNL), USA, Au+Au collisions whose center of mass energy per nucleon ($\sqrt{s_{NN}}$) is 200 GeV have been performed.

One of the most intriguing observations at RHIC is that the yield of π^0 at high transverse momentum (p_T) in the central $\sqrt{s_{NN}}=200$ GeV Au+Au collisions is suppressed compared with the yield of p+p collision scaled by the number of underlying nucleon-nucleon collisions [1]. The direct photon yield is not suppressed in the Au+Au collisions [2], implying that the initial hard scattering yield in Au+Au is well reproduced as the N_{coll} scaled yield in p+p. The observed suppression is interpreted as a consequence of the jet-quenching effect, that is, hard-scattered partons produced in the initial stage suffer a large energy loss while traversing the hot and dense matter.

Measurement of identified particle up to the highest possible p_T is crucial to constrain the theoretical models and separate contributions of initial and final state effects from the energy loss mechanism. The suppression of π^0 provides important constraints on calculations of the energy loss, as neutral pions can be identified up to very high p_T .

2. Measurement of neutral pions

The PHENIX experiment [3] is capable of measuring photons with two types of highly segmented electromagnetic calorimeters (EMCal) [4]. One is a lead scintillator sampling calorimeter (PbSc), and the other is a lead glass Cherenkov calorimeter (PbGl). Using the EMCal, π^0 s can be detected via the two-photon decay mode ($\pi^0 \rightarrow 2\gamma$). The combinatorial back ground is estimated with an event mixing method. The corrections for geometrical acceptance, particle identification efficiency, and overlapping effect in high multiplicity are also estimated with GEANT simulation.

In RHIC Year-4 run, PHENIX recorded the integrated luminosity of 0.24 nb^{-1} in the $\sqrt{s_{NN}}=200$ GeV Au+Au collisions.

Figure 1 shows the fully corrected π^0 invariant yield as a function of p_T for each centrality of collision [5].

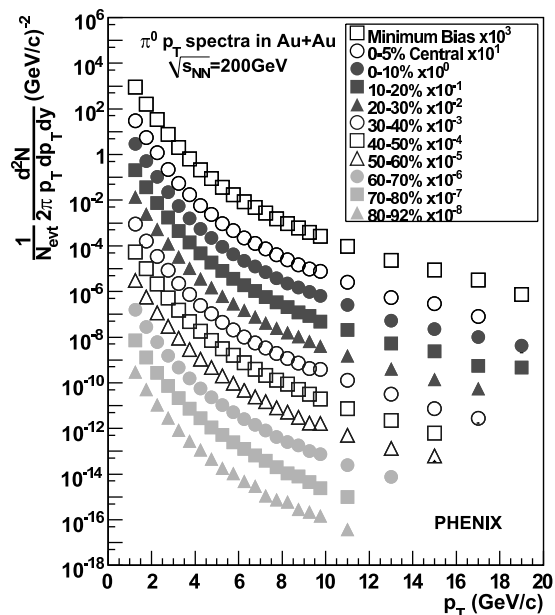


Figure 1. Neutral pion invariant yields as a function of p_T for ten centrality selections and minimum bias Au+Au collisions at $\sqrt{s_{NN}} = 200$ GeV. (PbSc and PbGl combined)

3. Neutral pions R_{AA} and constraint of medium transport coefficients

From the comparison with the p+p data measured at the same experiment, the nuclear modifications on the neutral pion production in Au+Au collisions are studied. The amount of nuclear effect for π^0 production can be quantified using a nuclear modification factor (R_{AA}). R_{AA} is the ratio between the measured yield and the expected yield from the p+p result, and is defined as

$$R_{AA}(p_T) = \frac{d^2 N_{AA} / dp_T d\eta}{T_{AA}(b) d^2 \sigma_{NN} / dp_T d\eta}, \quad (1)$$

where the numerator is the invariant π^0 yield in unit rapidity and the denominator is the expected yield in the p+p collisions scaled with the number of underlying nucleon-nucleon collisions ($T_{AA}(b)$) in Au+Au. $T_{AA}(b)$ is defined

as

$$T_{AA}(b) = N_{\text{coll}}(b)/\sigma_{NN}, \quad (2)$$

where $N_{\text{coll}}(b)$ is the average number of binary nucleon-nucleon collisions at an impact parameter b with an inelastic cross section σ_{NN} .

Figure 2 shows the R_{AA} of π^0 for most central events (0-5%) together with a theoretical prediction which employs the GLV model [6]. The suppression is very strong by a factor of ~ 5 , and is almost constant from $p_T \sim 4$ GeV/ c up to $p_T \sim 20$ GeV/ c .

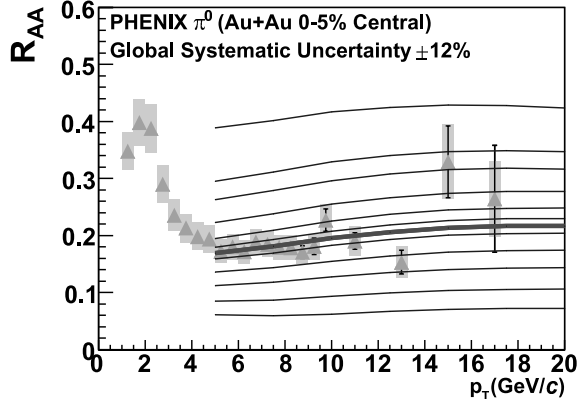


Figure 2. Neutral pion R_{AA} measured as a function of p_T in the most central (0-5 %) collisions. In addition to the statistical and p_T -uncorrelated errors, p_T -correlated errors are shown on the data points as boxes. Also shown are predictions from the GLV [6] model with different dN_{eff}^g/dy values. The theoretical curves shown correspond to dN_{eff}^g/dy values of 600, 800, 900, 1050, 1175, 1300, 1400, 1500, 1800, 2100, 3000, 4000 (from top to bottom). The bold line indicates the best fit case (1400).

Based on the comparison of π^0 suppression pattern with a theoretical calculation by I. Vitev who employs GLV energy loss formalism, the effective gluon density (dN_{eff}^g/dy) of the dense matter produced in $\sqrt{s_{NN}} = 200$ GeV Au+Au collisions are estimated quantitatively. The probable parameter is extracted using the likelihood function. The definition of the function is given in [7], and the likelihood function ratio, the ratio of each likelihood in minimum likelihood (i.e. best value), is calculated for the estimation of the standard deviation from the best value. Figure 3 shows the number of standard deviation away from the best fit parameter value. Based upon the π^0 data, the dN_{eff}^g/dy performed at RHIC is estimated to be about 1400^{+300}_{-100} . On the assumption of the formation of gluon dominated plasma with the formation time of 0.6 fm, it corresponds to the energy density of 17 GeV/ fm^3 , which is much larger than the expected critical density of ~ 1 GeV/ fm^3 .

4. Summary

π^0 is measured in $\sqrt{s_{NN}} = 200$ GeV Au+Au collisions in RHIC Year-4, and it is compared with GLV calculation. A strong π^0 suppression by a factor of ~ 5 is observed, and stays almost constant up to 20 GeV/ c . It supports a presence of the dense matter with the high energy density,

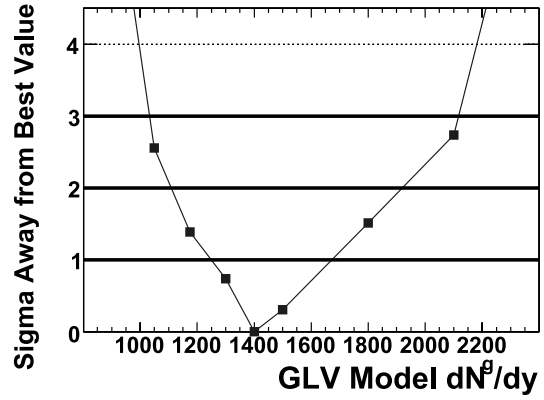


Figure 3. the number of standard deviations away from the minimum (best) dN_{eff}^g/dy parameter value for the GLV model calculations.

which is much larger than the expected critical density of ~ 1 GeV/ fm^3 .

References

- [1] S.S. Adler *et al.*, Phys. Rev. Lett. **91** (2003) 072301
- [2] S.S. Adler *et al.*, Phys. Rev. Lett. **94** (2005) 232301
- [3] K. Adcox *et al.*, Nucl. Instr. and Meth. A **499** (2003) 469
- [4] L. Aphecetche *et al.*, Nucl. Instr. and Meth. A **499** (2003) 521.
- [5] S.S. Adler *et al.*, arXiv:0801.4020
- [6] I. Vitev *et al.*, Phys. Rev. Lett. **89** (2002) 252301
- [7] S.S. Adler *et al.*, arXiv:0801.1665

Measurement of charm and bottom production in p+p collisions at $\sqrt{s} = 200$ GeV at RHIC-PHENIX

Y. Morino for the PHENIX Collaboration

Center for Nuclear Study, Graduate School of Science, University of Tokyo

1. Introduction

Heavy-flavors (charm and bottom) are good probes to study the medium created with $Au + Au$ collisions at RHIC, since heavy-flavors are primarily produced in initial collisions. Heavy-flavor production in $p + p$ collisions serves as a testing ground of perturbative QCD (pQCD) and an important reference to $Au + Au$ collisions. RHIC-PHENIX has measured single electrons from heavy-flavor decays for $0.3 < p_T < 9.0$ GeV/c at mid-rapidity ($|\eta| < 0.35$) in $p + p$ and $Au + Au$ collisions at $\sqrt{s_{NN}} = 200$ GeV [1, 2]. Measurement of single electrons has the advantage of the good ratio of signal to background and a large branching ratio at PHENIX, while charm and bottom components are not separated. The yield ratio of the number of electrons from charm over that from bottom is one of the most important parameters to interpret the results in $Au + Au$ collisions of heavy quarks in the medium. A fixed-order-plus-next-to-leading-log (FONLL) pQCD calculation predicts the contribution from bottom becomes dominant above 4 GeV/c [3]. However, there is a large uncertainty about cross section of heavy flavor at even with FONLL. Thus, experimental determination of this ratio is a key issue.

2. Partial reconstruction of D^0

PHENIX has determined the ratio of the number of electrons from charm over that from bottom via partial reconstruction of $D^0 \rightarrow e^+ K^- \nu_e$ decay in $p + p$ collisions at $\sqrt{s} = 200$ GeV. Unlike charge sign pairs of electrons for $2.0 < p_T < 7.0$ GeV/c and hadrons for $0.4 < p_T < 5.0$ GeV/c were reconstructed. Kaon identification was not made for hadrons and hadrons were assigned to mass of kaon (~ 494 MeV). Like-sign charge pairs of electrons and hadrons were used for background subtraction. Since charge asymmetry of electrons and hadrons was only produced by weak decay, combinatorial background and contributions from photonic electrons were canceled out completely. Most of contribution from jet was also canceled out, since jet was basically charge independent.

Figure 2 shows a raw invariant mass distribution of electrons and hadrons. N_{tag} was defined as the number of unlike sign pair (N_{unlike}) minus the number of like sign pair (N_{like}) in the mass range from 0.4 to 1.9 GeV/c². Tagging efficiency (ϵ_{data}) was defined as follows, by using the number of non-photonic electrons (N_e).

$$\epsilon_{data} \equiv \frac{N_{tag}}{N_e} = \frac{N_{c \rightarrow tag} + N_{b \rightarrow tag}}{N_{c \rightarrow e} + N_{b \rightarrow e}}$$

Here, c (b) means charm (bottom). As a next step, the tagging efficiency for charm and bottom was defined as follows. Here, ϵ_c (ϵ_b) is a tagging efficiency in the case of charm (bottom) production. ϵ_c (ϵ_b) was obtained from us-

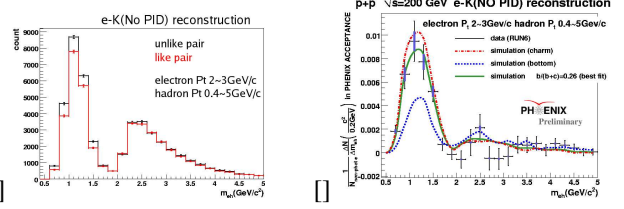


Figure 1. (a) Raw invariant mass distribution of electrons and hadrons. (b) Reconstruction signals with the mass distributions of charm and bottom from PYTHIA and the mass distribution when charm and bottom components are mixed at the obtained ratio.

ing PYTHIA and EvtGen simulation. Then, the fraction of bottom contribution to the single electrons can be obtained as,

$$\frac{b \rightarrow e}{c \rightarrow e + b \rightarrow e} = \frac{\epsilon_c - \epsilon_{data}}{\epsilon_c - \epsilon_b}$$

Extracted signals (N_{tag}) contain not only signals from daughters of semi-leptonic decay of D^0 , but also those from daughters of semi-leptonic decay of other heavy flavored hadrons and jet contributions which were not canceled completely. These contributions were also estimated using PYTHIA. However, since such contribution for ϵ_c (ϵ_b) is not dominant ($\sim 15\%$) the uncertainty of ϵ_c (ϵ_b) from PYTHIA becomes rather small.

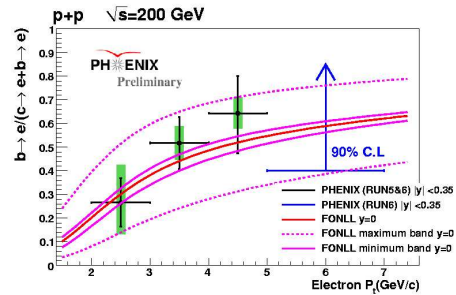


Figure 2. Ratios of the number of electrons from charm over that from bottom as a function of electron p_T with FONLL prediction

Figure 2 shows reconstruction signals with the mass distributions of charm and bottom from PYTHIA and the mass distribution when charm and bottom components are mixed at the obtained ratio. Figure 2 shows the obtained ratios of the number of electrons from charm over that from bottom as a function of electron p_T with FONLL prediction. The measured ratio is consistent with FONLL predictions. Bottom contribution becomes dominant above electron $p_T \sim 3$ GeV/c.

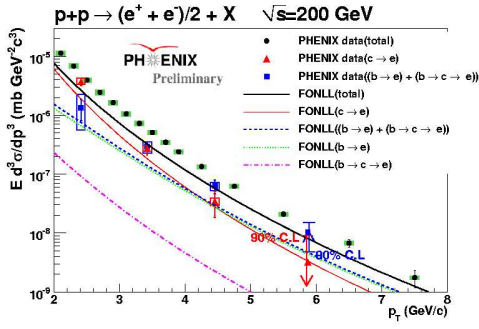


Figure 3. Electron spectra from charm and bottom with FONLL predictions.

Electron spectra from charm and bottom were obtained from the ratio of the number of electrons from charm over that from bottom and the spectrum of non-photonic electrons [2]. Figure 3 shows obtained electron spectra from charm and bottom with FONLL predictions. The ratio of bottom cross section at PHENIX over predicted value at FONLL is about 2, which is almost same as HERA-B and CDF [4, 5]. Electron spectrum from bottom was extrapolated to $p_T = 0$ by using the spectrum shape predicted by FONLL [6]. The bottom cross section at mid-rapidity was $d\sigma_{b\bar{b}}/dy|_{y=0} = 1.34 \pm 0.38(stat)_{-0.64}^{+0.74}(sys)\mu b$, by using a $b \rightarrow e$ total branching ratio of $10 \pm 1\%$. Total bottom cross section was obtained as $\sigma_{b\bar{b}} = 4.61 \pm 1.31(stat)_{-2.22}^{+2.57}(sys)\mu b$, by using rapidity distribution from NLO pQCD calculation [7].

3. Di-electron continuum

PHENIX has measured the electron-positron pairs mass spectrum in $p + p$ and $Au + Au$ collisions at $\sqrt{s} = 200$ GeV [8, 9]. A cocktail of known sources accounts for the continuum in the mass region below ~ 1 GeV/ c^2 in $p+p$ collisions. Except for the vector meson peaks, the e^-e^+ pairs in the mass range above 1.1 GeV/ c^2 is dominated by heavy quarks correlated through flavor conservation. Figure 4 shows the e^-e^+ pair yield remaining after subtracting the contribution of the cocktail in $p + p$ collisions. The remaining components are $c\bar{c}$, $b\bar{b}$ and Drell-Yan process. To extract signals from $c\bar{c}$, the e^-e^+ pair yield in the range from 1.1 to 2.5 GeV/ c^2 was integrated. Integrated yield was extrapolated to zero e^-e^+ pair mass according to the spectral shape of mass distribution given by the PYTHIA simulation and converted cross section of charm. Contributions from $b\bar{b}$ and Drell-Yan process were estimated and subtracted. Total cross section of charm was obtained as $\sigma_{c\bar{c}} = 544 \pm 39(stat) \pm 142(sys) \pm 200(model)\mu b$, by using rapidity distribution from NLO pQCD calculation [7]. This result is compatible with PHENIX previous result of non-photonic electron which gave $\sigma_{c\bar{c}} = 567 \pm 57(stat) \pm 224(sys)\mu b$ [2].

Alternative method was used to extract signals from $b\bar{b}$. The e^-e^+ pair distribution after subtraction of Drell-Yan was fitted by the e^-e^+ pair distributions from charm and bottom which were produced by PYTHIA. The obtained total cross

section of bottom is $\sigma_{b\bar{b}} = 3.9 \pm 2.5(stat)_{-2}^{+3}(sys)\mu b$. This result is also compatible with the result of non-photonic electron in Section 2.

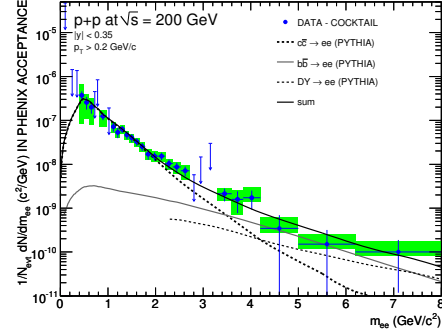


Figure 4. The e^-e^+ pair yield remaining after subtraction of the cocktail.

4. Summary and Outlook

The ratio of the electron yield from charm over that from bottom was measured via partial reconstruction of $D^0 \rightarrow e^+ K^- \nu_e$ decay in $p+p$ collisions at $\sqrt{s} = 200$ GeV. Bottom contribution becomes dominant above electron $p_T \sim 3.5$ GeV/ c . This suggests not only charm but also bottom may lose large energy in the hot and dense medium. Total cross section of bottom was obtained from the ratio and non-photonic electron spectrum.

Total cross sections of charm and bottom were also measured via di-electron continuum. The result from di-electron continuum are consistent with that from non-photonic electron spectra.

Direct reconstruction of D^0 meson has been tried at PHENIX. Clear peaks has been observed in $D^0 \rightarrow K^- \pi^+ \pi^0$ and $D^0 \rightarrow K^- \pi^+$ channels in $p+p$ collisions at $\sqrt{s} = 200$ GeV. Cross check of charm production will be performed by direct reconstruction.

References

- [1] A. Adare *et al.* *Phys. Rev. Lett.* **98**, 172301 (2007)
- [2] A. Adare *et al.* *Phys. Rev. Lett.* **97**, 252002 (2006)
- [3] M. Cacciari *et al.* *Phys. Rev. Lett.* **95**, 122001 (2005)
- [4] D. Acosta *et al.* *Phys. Rev. Lett.* **91**, 241804 (2003)
- [5] S. Chekanov *et al.* *Eur. Phys. J C* **50**, 299 (2007)
- [6] M. Cacciari, private communication.
- [7] M. L. Mangano, P. Nason and G. Ridolfi *Nucl. Phys B* **405**, 507 (1993)
- [8] A. Adare *et al.* arXiv:0706.3034
- [9] A. Adare *et al.* arXiv:0802.0050

Evaluation of Electron Identification Capability of ALICE-TRD (Transition Radiation Detector) with Neural Network Method

A. Takahara, H. Hamagaki, T. Gunji, Y. Morino, S. Sano, for the ALICE collaboration

Center for Nuclear Study, Graduate School of Science, University of Tokyo, Japan

1. Introduction

Lattice QCD calculations predict the phase transition at high temperature (170 MeV)[1]. The new phase is called Quark Gluon Plasma (QGP), deconfined state of quarks and gluons. The ALICE experiment is one of the experiments at CERN LHC to realize such a phase transition and to study QGP property with heavy ion collision at $\sqrt{s_{NN}} = 5.5$ TeV. Suppression of $J/\psi (= c\bar{c})$ and $\Upsilon (= b\bar{b})$ yield is expected when QGP occurs by color debye screening [2]. Color screening is one of the QGP effects that resolves hadrons when debye Length is shorter than its diameter. Debye length is proportional to T^{-1} . The melting temperature of J/ψ and Υ are twice and four times as large as T_c respectability that is the critical temperature of QGP [3]. Then, the temperature of QGP is measured by J/ψ and Υ yield. J/ψ and Υ have a decay mode to e^+e^- and, their yield will be measured by e^+e^- in ALICE experiment. The TRD Super Module will be used to identify electron in ALICE experiment. The ALICE experiment requires pion rejection factor > 100 at electron efficiency = 90%, which is defined as a number of all pions per that of miss identified pions. We tested an electron identification capability of ALICE TRD Super Module in 11/2007 at CERN with PS beam line.

2. TRD

Transition radiation is emitted when a charged particle crosses the boundary between two materials. In single interface, the probability rises with Lorentz factor γ of the particle. One TRD Super Module has 30 TRDs. The layout is 6 layers and 5 stacks. In real experiment, direction of stacks corresponds to beam axis and direction of layers corresponds to direction of radius. The typical area of one TRD is 120 cm \times 159 cm. One TRD is composed of 42mm Radiator for transition radiation, 30mm drift region and 144 \times 16 read out pads[4]. The drift region employs a scheme of two plane of wires, both running azimuthal direction. The read out pad is typically 0.7cm \times 9cm. TRDs radiator consist of polypropylene fiber mats, sandwiched between two Rohacell HF71 sheets. When a charged particle comes into the radiator, it radiates one soft Xray (2-20 keV) with $\gamma > 1000$. Therefore, TRD Super Module provides electron/pion separation for 0.5 - 100 GeV/c, because in this momentum region, γ of pions doesn't reach 1000. The baseline gas mixture for the ALICE TRD is 85% Xe and 15% CO₂. Absorption length of Xe for 2 keV and 20 keV are 1 mm and 20mm, respectively. Therefore, TR photon is absorbed near the entrance of drift chamber. As a result, As shown in Fig. 1, when an electron comes into the TRD, pulse shape vs. time has double peaks while pulse

shape of pion has one peak.

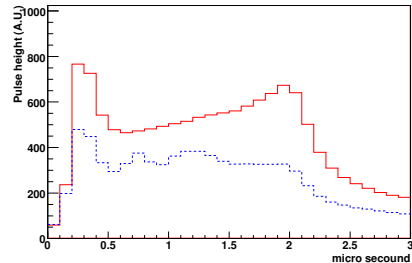


Figure 1. time vs. pulse height. line is electron, dashed line is pion

Electrons were identified by the shape of pulse height vs. time. The test beam data was analyzed with Neural Network Method.

3. Experiment

The TRD was tested at 1, 2, 3, 4, 5, 6, and 7 GeV/c beams. The test beam was a mixture of electrons and pions. Fig. 2 shows the setup. Size of two silicon strip detectors Si1 and

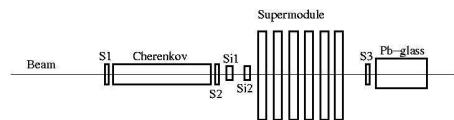


Figure 2. A schematic view of the beam test set up. Si1 is not used. We used Si2 and Si3 to make trigger.

Si2 are 32 mm \times 32 mm. their strip size is 50 μ m \times 50 μ m. They are used for tracking. We used Cherenkov counter and Pb-glass to identify electrons. The size of Pb-glass is 6cm \times 6cm \times 25 cm. We set two scintillators Si2 and Si3 to make trigger. Their size is 5cm \times 5cm. Figure 3 shows a scatter plot between ADC ch distribution of Cherenkov counter (x axis) and Pb-glass (y axis). Electron is defined ADC ch of cherenkov counter > 900 and ADC ch of Pb-glass > 1000 . Pion is defined in ADC ch of cherenkov counter < 400 and ADC ch of Pb-glass < 600 .

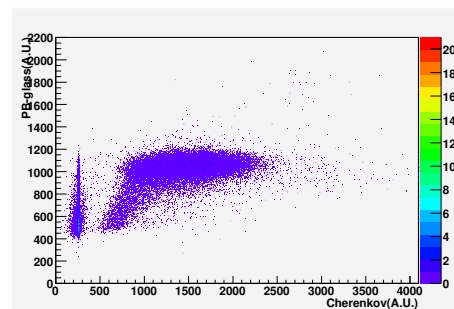


Figure 3. cherenkov vs Pb-glass in a.u..

4. Analysis

Test beam data was analyzed to get the pion rejection factor with Neural Network (NN) Method. NN is a computational emulating on biological Neural Network. Figure 4 shows the network to be used in this analysis. There are an input layer, a hidden layer and an output layer. Each layer has its own neurons. All neurons in hidden layer connect to all the neurons in input and out put layers. The number of input neurons corresponds to the number of TRD layers (6) times the number of time bins used for value of pulse height to be fed into neurons. Each connection has random weight at first time. Each value of neurons in hidden (output) layer is decided by $\frac{1}{exp(-X)}$, and X is defined by summation of each value of neurons in input (hidden) layer times each weight between them. Back propagation method is one of the NN teaching method.

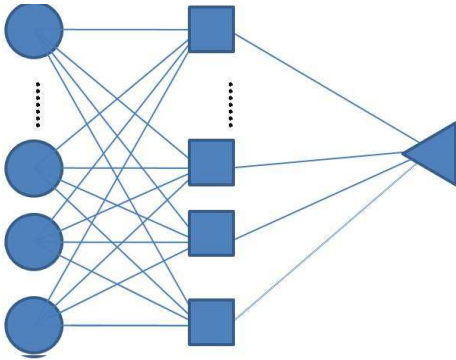


Figure 4. structure of the neural network used in this analysis. Circle neurons are input layer, square neurons are hidden layer, and triangle neuron is output layer.

The test beam data was divided into two groups. One is for teaching, another is for test. The data has the information on pulse height of each time bin where bin size is $0.1 \mu s$ and total number of time bins is 30 on the incident particle, which is electron or pion judged from Cherenkov and Pb-glass. In teaching cycle, all the weight between neurons in each two layers are updates and adjusted to much the output from network to the required output, which is defined as teach signal (1 for electron and 0 for pion). The process was repeated, until the error between output value of network and teach signal become stable.

The dependence of the pion rejection factor on number of neurons was checked. Firstly, Fig. 5 shows the dependence of pion rejection factor on number of input neurons, where the number of neurons in hidden layer is set to be 2 times as large as that of neurons in input layer. When number of input neuron is 90, summation of pulse height in 2 time bins is fed into the input neurons. The pion rejection factor is obvious rising with number of input neurons until 30 input neurons, and finely rising until 180. The pion rejection factor 52 is achieved. Therefore, number of input neurons was fixed to 30 in next Fig. 6.

Fig.6 shows the dependence of pion rejection factor on number of hidden neurons. The pion rejection factor rises until 20, and is stable over 20.

Fig.7 shows the pulse shape of events that were identified

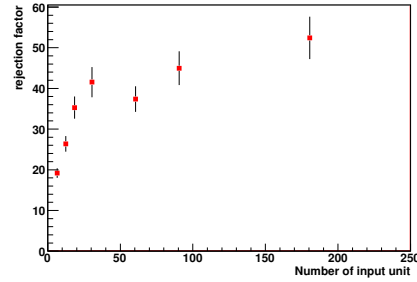


Figure 5. number of input neurons vs pion rejection factor

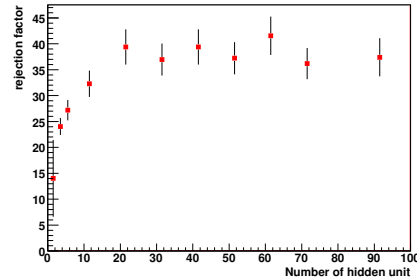


Figure 6. number of hidden unit vs pion rejection factor

pion by Pb-glass and Cherenkov detector but were identified electron by NN. They don't have two peaks, but their pulse height as high as that of electrons.

5. Summary and Outlook

The pion rejection factor rises with number of input neurons until 180, and is stable for more than 30. Hidden neuron was required as equal number of input neurons. The best pion rejection factor is 52. It is close to the requirement, but does not reach that.

In the next step, large pulse height in pion event will be investigated in detail.

References

- [1] J.F.Gunion,R. Vogt,Nucl.Phys B 492(1997)301-307
- [2] T.Matsui,H.Satz,J.Phys.G 32,R25(2006)
- [3] F.Karsch,Nucl.Phys A 590(1995)367c
- [4] ALICE TRD Technical Design Report

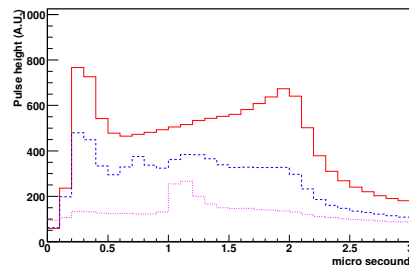


Figure 7. the short dashed line is pulse shape of miss identify event

Measurement of low p_T direct photon with virtual photon method in $\sqrt{s} = 200$ GeV p+p collisions at PHENIX

Y.L. Yamaguchi, H. Hamagaki, T. Gunji, F. Kajihara, Y. Akiba^a, A. Toia^b and T. Dahms^b,
for the PHENIX collaboration

Center for Nuclear Study, Graduate School of Science, University of Tokyo

^a RIKEN (The Institute of Physical and Chemical Research)

^b Department of Physics and Astronomy, Stony Brook University, SUNY

1. Introduction

Direct photon is a powerful probe to investigate properties of Quark Gluon Plasma (QGP) since photons penetrate a dense and hot partonic matter created by heavy ion collisions. Special interest is in thermal photons from QGP, since they carry the thermodynamic information of the matter such as the temperature of the matter, degree of freedom and so on. Thermal photons are considered to be a primary contributor in the low p_T region of the inclusive photon spectrum [1],

A measurement of ‘real’ direct photon using an electromagnetic calorimeter is notoriously difficult in the energy region below 4 GeV since the systematic errors cannot be reduced due to a large hadron background, particularly π^0 . Recently, an alternative method using a ‘virtual’ direct photon measurement, i.e. a measurement of e^+e^- pairs from ‘virtual’ direct photon decays was demonstrated to provide the photon yield with less systematic error in Au+Au collisions [2]. It is primarily because the e^+e^- pair mass can be reconstructed with high resolution using the hit information from the drift chamber and components from hadron decays in the e^+e^- pair mass distribution can be estimated reliably using a hadronic cocktail calculation which incorporated the measured yields of the mesons at PHENIX. The same method is applicable to the direct photon yield in p+p collisions, which serves as a reference to the direct photon yield in Au+Au collisions. The first result of the direct photon measurement with the virtual photon method in $\sqrt{s} = 200$ GeV p+p collisions at RHIC-PHENIX is presented and the comparison of the direct photon yields in p+p and Au+Au collisions is also shown in this report.

2. Analysis

For real events, the correlated pair mass distribution is obtained after combinatorial background subtraction using an event mixing method. However the cross pairs from decays with 4 electrons in the final state such as $\pi^0, \eta \rightarrow \gamma e^+e^- \rightarrow e^+e^-e^+e^-$ and from two independent decays in the same jet or the back-to-back jets still remain in the correlated pair mass distribution. The contribution of the cross pairs are evaluated using like-sign pair distributions and a Monte Carlo simulation since these pairs are clearly visible in like-sign pair distributions. Their contributions are about 20% in $100 < m_{ee} < 300$ MeV. After these background pairs are subtracted, remaining pairs are composed of the pairs from hadron decays and virtual photon decays.

The relation between the photon production and the asso-

ciated e^+e^- pair production is expressed by the Kroll-Wada formula, Eq. 1 in ref. [3].

$$\frac{d^2 n_{ee}}{dm_{ee}} = \frac{2\alpha}{3\pi} \frac{1}{m_{ee}} \sqrt{1 - \frac{4m_e^2}{m_{ee}^2}} \left(1 + \frac{2m_e^2}{m_{ee}^2}\right) S dn_\gamma, \quad (1)$$

where α is the fine structure constant, m_e and m_{ee} are the masses of the electron and the e^+e^- pair, respectively, and S is a process dependent factor. In the case of hadrons such as π^0 and η Dalitz decays, S is given as $S = |F(m_{ee}^2)|^2 \left(1 - \frac{m_{ee}^2}{M_{hadron}^2}\right)^3$, where F denotes the form factor and M_{hadron} is the mass of the parent hadron. The S factor is zero for $m_{ee} > M_{hadron}$. On the other hand, the S factor becomes unity for $m_{ee} \ll p_T$ in the case of virtual direct photon. It will be possible to extract the virtual direct photon component from the e^+e^- pair mass spectra by utilizing the difference in e^+e^- pair mass dependence of the S factor. Therefore the e^+e^- pair mass distribution for $m_{ee} < 300$ MeV and $p_T > 1.0$ GeV/c is focused on.

3. Result

Figure 1 show the e^+e^- pair mass distributions in p+p and

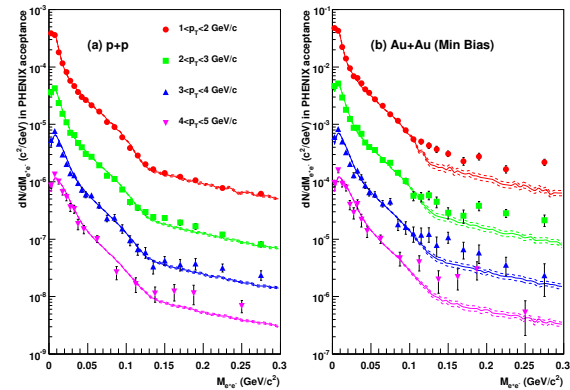


Figure 1. The e^+e^- pair mass distributions in p+p (left) and Au+Au (right) collisions for several p_T regions compared to the hadronic cocktail calculation.

Au+Au collisions for several p_T regions. The symbols and lines show the real data and hadronic cocktail calculation, respectively. Enhancement of the e^+e^- pair yield is clearly seen for $m_{ee} > 100$ MeV in Au+Au collisions. It is noted here that a small excess over the cocktail is also observed for p+p collisions in the high p_T region.

The following function is used for fitting the data to determine the fraction of the virtual direct photon component in the e^+e^- pair mass distribution.

$$f(m_{ee}) = (1-r) \cdot f_{cocktail}(m_{ee}) + r \cdot f_{direct}(m_{ee}), \quad (2)$$

where $f_{cocktail}$ is the mass distribution from the decay of neutral hadrons estimated using the cocktail calculation and f_{direct} is that from the virtual direct photon decays, and r is the virtual direct photon fraction. The fit result in p+p

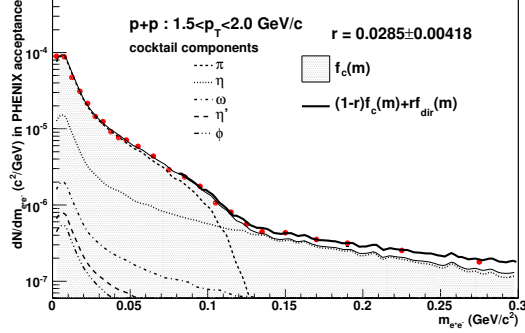


Figure 2. The e^+e^- pair mass distribution in p+p collisions for $1.5 < p_T < 2.0$ GeV/c together with the fit result by Eq. 2.

collisions for $1.5 < p_T < 2.0$ GeV/c is shown as a thick line in Fig. 2. Figure 3 shows the obtained fractions of the virtual direct photon component as a function of p_T in p+p and Au+Au collisions. The symbols show the result and the lines are the expectations from next-to-leading-order perturbative QCD (NLO pQCD) calculations [4] with different theoretical scales. A clear excess above the NLO pQCD calculation is seen in Au+Au collisions while the result in p+p collisions is consistent with the NLO pQCD calculation.

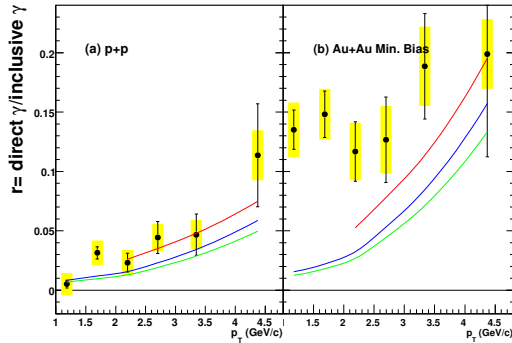


Figure 3. The obtained fractions of the virtual direct photon component as a function of p_T in p+p (left) and Au+Au (right) collisions.

Finally, the real direct photon yield is obtained by multiplying the inclusive photon yield to the virtual direct photon fraction. Figure 4 shows the direct photon spectra in p+p and Au+Au collisions as a function of p_T . The close and open symbols show the result from 'virtual' and 'real' photon analyses, respectively. The star symbol shows the p+p result and the triangle, circle and box symbols show the Au+Au results for minimum bias, centrality of 0-20% and 20-40%, respectively. This is the first time that the direct photon production in p+p collisions has been measured in $1.0 < p_T < 4.0$ GeV/c. The p+p result is well described

by a modified power law function as shown by the dashed curve. The obtained yield in Au+Au collisions show an excess over the N_{coll} -scaled p+p fitted curve in the low p_T region, where N_{coll} is the number of nucleon-nucleon collisions. Fitting the result for Au+Au central collision with an exponential plus the N_{coll} -scaled p+p fitted curve provides the inverse slope parameter of $221 \pm 23 \pm 18$ MeV.

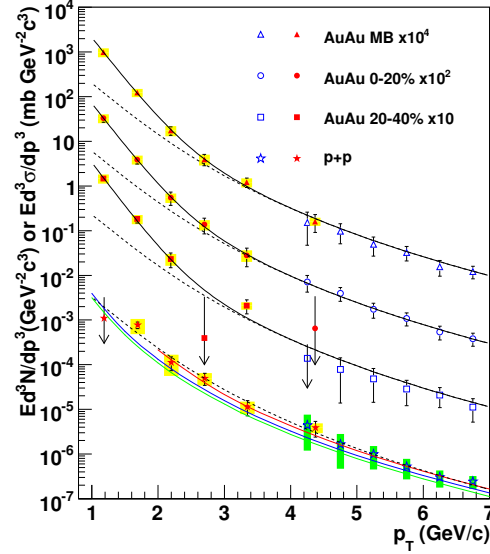


Figure 4. The direct photon spectra in p+p and Au+Au collisions as a function of p_T .

4. Summary and Outlooks

The direct photon measurements with a virtual photon method has been performed for p+p and Au+Au collisions at RHIC-PHENIX. An excess of the direct photon yield above a binary-scaled p+p result has been observed in Au+Au collisions. The excess is fitted with an exponential function with an inverse slope parameter of $221 \pm 23 \pm 18$ MeV. This result was submitted to Phys. Rev. Lett. [5]. Implications of the results are under various investigations.

The contribution from nuclear effects to the direct photon yield in the low p_T region will be estimated using the data for Run-8 d+Au collisions and the analysis of the p+p data set with more statistics is now on going.

References

- [1] S. Turbide *et al.*, Phys. Rev. C **69** 014903 (2004).
- [2] Y. Akiba for the PHENIX collaboration, RIKEN Accel. Prog. Rep. **39**, 190 (2006).
- [3] N.M. Kroll and W. Wada, Phys. Rev. **98** 1355 (1955).
- [4] L.E. Gordon and W. Vogelsang, Phys. Rev. D **48** 3136 (1993) and W. Vogelsang, private communication.
- [5] A. Adare *et al.*, for the PHENIX collaboration, arXiv:0804.4168[nucl-ex].

Accelerator and Instrumentation

Development of a readout circuit for 2D-imaging using GEM

S. Sano, H. Hamagaki, Y. Tanaka^a, T. Fusayasu^a, F. Kajihara, and T. Gunji

Center for Nuclear Study, Graduate School of Science, University of Tokyo
^aNagasaki Institute of Applied Science

1. Introduction

Gas Electron Multiplier (GEM) is a Micro Pattern Gas Detector (MPGD), which has been developed recently [1]. While GEM is utilized in physics experiments as HBD (Hadron Blind Detector) or TPC (Time Projection Chamber) [2,3], GEM will have various applications as a 2D-imaging detector of X-rays or neutrons. A motivation to develop 2D-imaging using Gas Electron Multiplier (GEM) is to visualize a motion of the car engines by using neutron.

Thermal neutrons (~ 25 meV) have a large attenuation coefficient (~ 3 cm²/g) for water because of hydrogen atom, but a small attenuation coefficient (~ 0.1 cm²/g) for metals. Therefore the motion of the liquid inside the engines of cars can be seen by using thermal neutrons. Thermal neutrons can be caught with boron evaporated on the surface of GEM.

This imaging needs the fast frame-readout rate of 1000 fps, because the maximum rotational speed of the engine is in the order of thousands rpm. The number of channel is determined from the position resolution and the imaging area as follows.

- ~ 1 mm position resolution
- above 10 cm*10 cm imaging area
- 10000 \sim 100000 channel
- 1000 fps frame-readout rate
- 0.3% linearity

In order to realize these requirements, custom electronics with high density and high speed are needed. As the first step to establish such a readout system for 2D-imaging, a prototype of an LSI (Large Scale Integrated circuit) chip which includes 64-channel readout circuit was designed and fabricated. The performance test was also executed.

2. Design and fabrication of LSI chip

The readout electronics implemented in the LSI chip is a simple Q/V conversion circuit with charge sensitive amplifiers (integrators) whose conversion gain is 1 V/pC. The outputs of 64 integrators are connected to a multiplexer and extracted to the outside of the LSI chip serially.

The schematic view of the designed circuit implemented in the LSI chip is shown in Fig. 1. The detail of Amplifier is described in [5]. The analog output 'Vout' puts the signal of the output of an integrator before (pre) and after (post) discharge (correlated double sampling), where pre-post can reject the effect of base line shift. As a prototype, a readout rate of 512 kHz are required to readout 256 channel of four LSI chips with the rate of 1000 fps. The 8-ch multiplexer units consists of the CMOS switches, and are arranged to two layers, MUX1 and MUX2, in order to reduce the total parasitic capacitance arising at CMOS switches connected with the output signal line. This circuit is designed with 0.25 μ m CMOS technology.

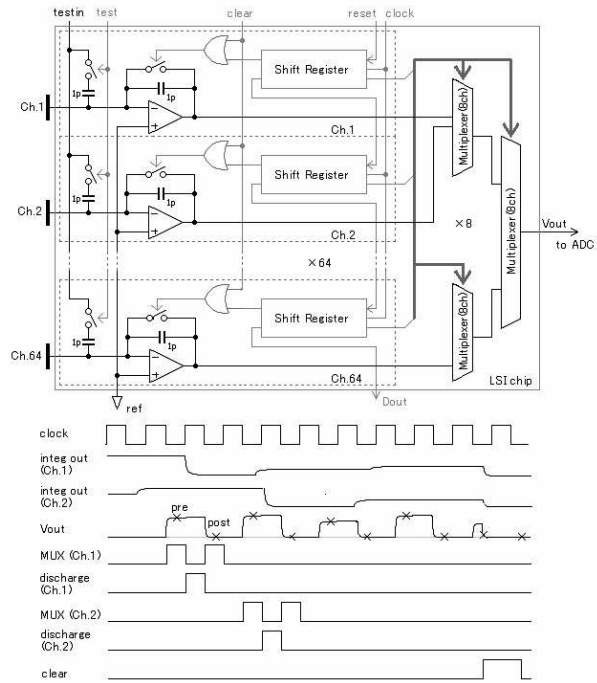


Figure 1. Schematic overview of readout circuit set in LSI chip and timing diagram of analog and digital signals for two channels.

Figure 2 (left) shows the layout of the whole chip, and (right) one cell which includes an integrator, a multiplexer, and a shift register for one channel. The simulation with layout parameters (post layout simulation) was done. Layout parameters mean the wire resistance and the parasitic capacitance between elements which were extracted from the designed layout by using a layout verification tool (ASSURA [6]). The result of the post layout simulation has no problem in the performance.

3. Performance test

Performance test was made for ten LSI chips, using a custom-made simple test circuit with analog readout via an 8-bit ADC.

3.1. Channel dependence of conversion gain

Figure 3 shows the chip and channel dependence of the conversion gain (pre-post[V])/1[pC] for the 0.75 pC charge input. Systematic gain variation common to all chips is seen. The channel dependence of the gain such as the gains of Ch1 and Ch64 are higher than one of Ch32 appeared. The dispersion between each channels is 3.3%.

3.2. Linearity check

Linearity check was done for ten LSI chips. Figure 4 shows the relation between input charge and the output of integrator (left), and the residual distribution for the left panel (right) for Ch1 of LSI01. Dispersion of performance

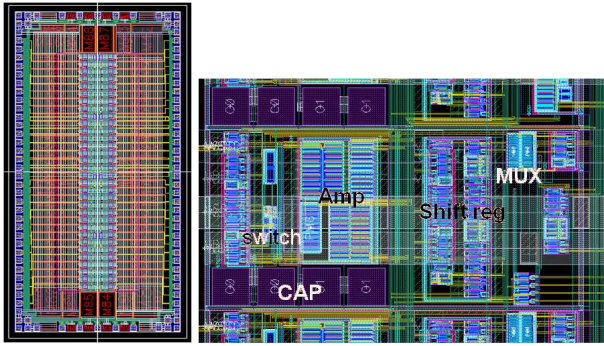


Figure 2. Layout of over LSI chip (left) and of one-channel (right). The size of the bare chip is 5 mm*2.5 mm.

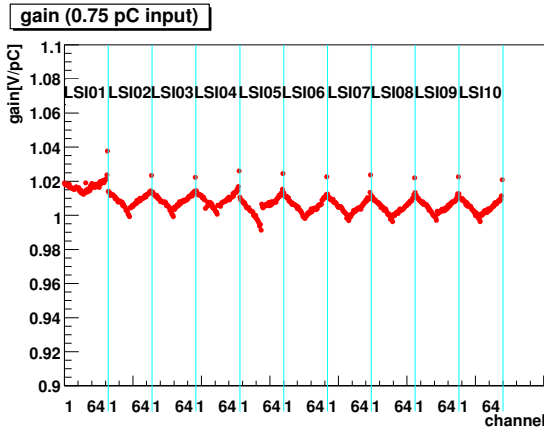


Figure 3. The chip and channel dependence of the gain at the 0.75 pC input charge.

between each channels is small such that the residual distribution shown in Fig. 4 (left) was obtained for all channels and all ten chips. Bars are the rms values of about 1000 events, which are within one LSB (4mV) for all range.

3.3. Rising of Analog output

Figure 5 shows the shape of signals taken with an oscilloscope, where Ch1 is 'Vout', the clock width is 1 μ s. To obtain the readout rate of 512 kHz, clock width should be 1 μ s and the sampling timing is 0.5 μ s after the start of rising of 'Vout'. 'Vout' is still transient and does not reach the plateau in 1 μ s.

Possible causes for this problem of slow rising of 'Vout' are as follows.

- The small size of switches of MUX2 ($W/L = 10 \mu\text{m}/0.25 \mu\text{m}$.) would make the large on-resistance.
- Parasitic capacitance between 'Vout' line and power supply lines.
- Small number of VIAs on the lines of 'Vout' would make the large resistance.

Improvement of rising of 'Vout' is the most important task for the fast frame-readout.

3.4. Other results

The other results of the performance test were summarized in Table 1.

4. Summary and outlook

An LSI chip for 2D-imaging using GEM was designed and fabricated for the first step. The performance test of

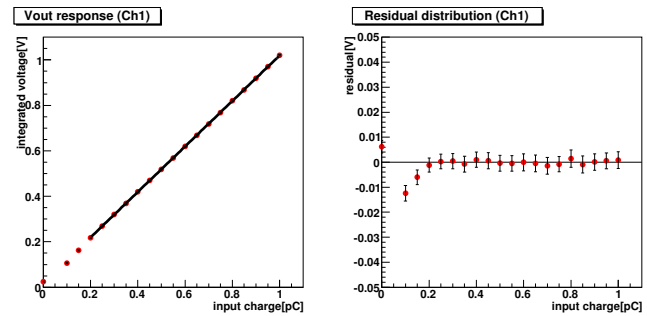


Figure 4. Linearity (left) and residual distribution (right).

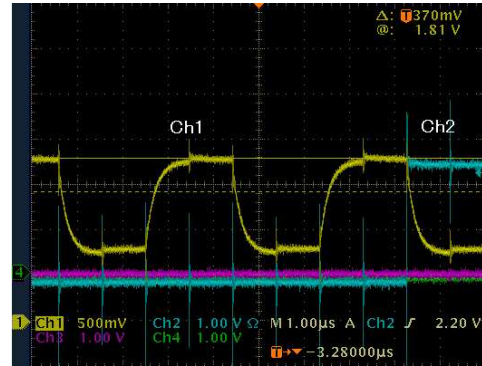


Figure 5. Ch1 and Ch2 are 'Vout' and 'Dout', respectively.

the fabricated LSI chips was also executed. Good linearity and some stable results were obtained, and dispersion of the performance between each channels is small. One remaining and crucial problem is that the rising of analog output 'Vout' is slow, which needs to be cured for the fast frame readout.

References

- [1] F. Sauli, Nucl. Instrum. and Method. A 386 (1997) 531.
- [2] Z. Frankel, *et al.*, Nucl. instrum. and Method. A 546 (2005) 466.
- [3] S.X. Oda, *et al.*, Nucl. instrum. and Method. A 566 (2006) 312.
- [4] S. Sano, *et al.*, CNS Annual Report 2006 (2007) 83.
- [5] ASSURA (Cadence Design Systems) <http://www.cadence.com/>

parameter	result
channel switching	normal
leak current of analog signal	<0.1pA
noise	<4mV
	~4mV (20ms freq)
base line shift	<4mV
cross talk	<0.5%

Table 1. The other results obtained from the performance test.

SHARAQ Project – Progress in FY2007 –

T. Uesaka, S. Shimoura, H. Sakai^a, K. Nakanishi, A. Saito^a, Y. Sasamoto, S. Michimasa, H. Kurei, T. Kawabata, N. Yamazaki, H. Miya^d, T. Kubo^b, Y. Yanagisawa^b, M. Fujinawa^b and G. P. Berg^c

Center for Nuclear Study, Graduate School of Science, University of Tokyo

^a *Department of Physics, Graduate School of Science, University of Tokyo*

^b *RIKEN Nishina Center*

^c *Department of Physics, Notre Dame University*

^d *Department of Physics, Rikkyo University*

SHARAQ [1] has started taking a concrete shape in FY2007. In this report, progress in FY2007 is summarized.

1. Spectrometer

In summer 2007, the high-resolution SHARAQ spectrometer was assembled in E20 experimental area of the RIBF building. A newly fabricated dipole magnet D2 and superconducting doublet quadrupole magnets (SDQ), together with recycled D1 and Q3 magnets, were installed on a rotating base. Figure 1 shows a snapshot of the assembling, where yokes of the D2 magnets are stacked one by one.



Figure 1. A snapshot of the SHARAQ spectrometer assembling

Prior to the assembling, measurement of magnetic field distribution in Q1000 and Q500 magnets, which comprise SDQ, was made. In high-resolution ion-optical analysis in RI beam experiments, accurate and precise knowledge of magnetic field is essentially important. The measurement, details of which are described in Ref. [2], was carried out from June to August of 2007. A device designed for measurement of axial symmetric field [3] was used to determine dominating quadrupole and other multi-pole components reliably. From the measurement, it is found that (1) produced quadrupole field strength is compatible with the designed value, while multi-pole strengths are at least two order of magnitude smaller than the quadrupole; (2) effective lengths of Q1000 and Q500 decrease by $\sim 2\%$ at around 50% of the maximum excitation, where saturation of iron begins to occur; (3) cross talk, i.e. change of Q500 magnetic field due to Q1000 excitation, or vice versa, is as small as

10^{-3} in the region between the magnets, as shown in Fig. 2, and makes a negligible effect on the effective length.

We also started preparation of field measurement for dipoles, D2 and D1. A search coil method, which was used in S800 [4], will be adopted. A cart carrying search coils and a rail on which the cart traverses were completed in FY2007. The measurement will be carried out after fine-tuning of the devices.

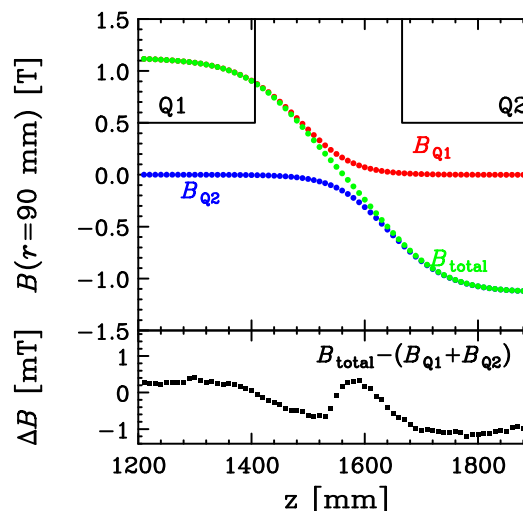


Figure 2. Quadrupole field distribution in SDQ

2. High-resolution Beamline

Based on the detailed design made in the last fiscal year [5], we have fixed specifications of beamline devices, including two normal conducting dipole magnets with a 30° bending angle, vacuum chambers for beamline detectors, vacuum pumps, and DC power supplies. Four normal conducting quadrupole magnets and one superconducting triplet quadrupole magnets (STQ) are recycled. One of the normal conducting quadrupole was renovated to enlarge a bore radius from 150 mm to 180 mm so that it can accept large-emittance secondary beams from BigRIPS.

Construction of the beamline will be completed by the end of February, 2009.

3. Detector R&D

Design of cathode-readout drift chambers (CRDC) for the final focal plane detectors has been finalized [6]. It has an effective area of 550 mm (H) \times 300 mm (V) to cover the focal plane of the spectrometer. To minimize multiple

scattering effects, operation at as low pressure as $P_{\text{gas}} \sim 3\text{--}5$ kPa was studied through simulations with GARFIELD. Based on the results, expected performance of the CRDC was examined and the requirements on drift voltage, pad pattern, and readout electronics were specified. Detailed design and fabrication of the CRDC are in progress in collaboration with GANIL group. The CRDC will be installed to SHARAQ in fall of 2008.

Low-pressure multiwire drift chambers (LP-MWDC) developed as beam-line detectors started to work in FY2007 [7]. It is a key in high-resolution experiments with SHARAQ to establish thin tracking detectors working under beam intensity of higher than 1 MHz. We have started with a test with α -rays from a source, and then applied the detector to a beam-irradiation test by an accelerated α -beam with an energy of 8.8 MeV/A [8]. The results clearly demonstrated that LP-MWDC with an isobutane gas should work under as low pressure as several kPa, while it was found that further improvements in the electronics are required for better determination of energy loss of particles.

4. Experimental Area

Electricity and cooling water for normal conducting magnets in SHARAQ and in the high-resolution beamline have been arranged in FY2007. Specifications of the magnets together with required electricity and cooling water flow are shown in Table 1. To cover the total electrical power consumption of 985 kVA, 1 MVA AC power supply was installed in E20 experimental area. It supplies 415 V AC output to six DC power supplies for the normal conducting magnets. A cooling water system providing a total flow of 1060 ℓ/min with a cooling power of 880 kW was also installed.

Table 1. Normal conducting magnets in SHARAQ and the high-resolution beamline

	SHARAQ			beamline			total
	D1	Q3	D2	Q-H16	Q-H17	Q-H18	
Max. field [T] ^a <i>radient</i> [T/m]	1.55	7.7	1.55	3.3	4.0	11	—
Max. current [A]	1070	480	1000	330	550	95	—
Max. voltage [V]	190.5	158.4	282.3	86	130.4	300	—
Power consumption [kW]	220	76.1	268	28.4	107.8	28.5	743.1
Cooling water [ℓ/min]	99.4	65.6	290	31	119	29.5	634.5
Pressure loss (design) [atm]	3.5	3.5	5	3.5	3.5	5	—
Temperature increase [°C]	22	25	13	20	20	11	—
Electrical Capacity of PS [kVA]	267	58	420	44	158	38	985
Cooling water for PS [ℓ/min]	30	12	30	8	11	15	104

5. Towards commissioning

Figure 3 shows a view of SHARAQ as of March 2008. As shown in the figure and described above, all the elements constituting SHARAQ (Fig.3) and the high-resolution beamline are taking shapes. The SHARAQ spectrometer will be completed by fall of 2008 with vacuum chambers, pumping systems, and the focal plane CRDC. Construction of the high-resolution beamline will be con-

tinued to the very end of February 2009. We hope all these efforts will bear fruit in the commissioning run scheduled in March 2008 and in the following physics runs in FY2009. In the commissioning run, detector performances and basic ion-optical properties of the magnet system will be evaluated.

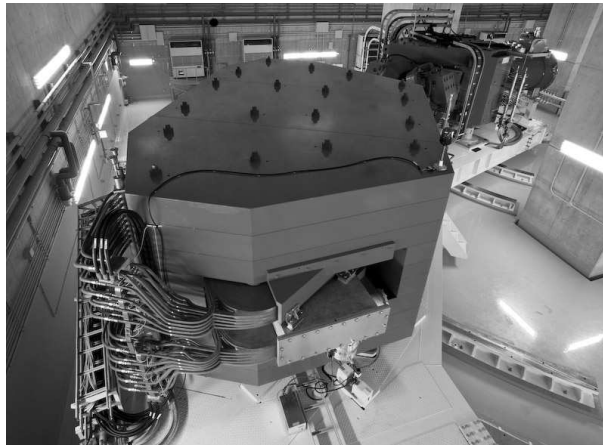


Figure 3. Photograph of SHARAQ spectrometer as of March 2008.

Acknowledgements

The authors thank Al. Zeller in Michigan State University for providing us search coils for dipole field measurements. They also express their gratitude to members of BigRIPS group for valuable suggestions and helps on all occasions.

References

- [1] T. Uesaka et al., Nucl. Instr. Meth. B, in print.
- [2] K. Nakanishi et al., CNS Annual Report 2006 (2007).
- [3] Y. Yanagisawa, private communication.
- [4] , D. Bazin et al., Nucl. Instr. Meth. B 204 (2003) 629.
- [5] T. Kawabata et al., Nucl. Instr. Meth. B, in print.
- [6] S. Michimasa et al., CNS Annual Report 2006 (2007).
- [7] A. Saito et al., CNS Annual Report 2006 (2007).
- [8] H. Miya et al., CNS Annual Report 2006 (2007).

Field Measurement System of the Superferric Quadrupole Magnets for SHARAQ Spectrometer

Y. Sasamoto, K. Nakanishi, T. Uesaka, S. Shimoura, H. Sakai^a, T. Kubo^b, N. Yamazaki and R. Yoshino

Center for Nuclear Study, Graduate School of Science, University of Tokyo

^a*Department of Physics, University of Tokyo*

^b*RIKEN (The institute of Physical and Chemical Research)*

New missing mass spectroscopy with an RI-beam is planned to be conducted at RIBF with the SHARAQ spectrometer [1, 3]. The SHARAQ spectrometer is designed to achieve a resolving power of $p/\delta p = 1.5 \times 10^4$ and a high angular resolution of $\delta\theta \sim 1$ mrad for particles with a maximum magnetic rigidity of $B\rho = 6.8$ Tm.

The SHARAQ spectrometer consists of three quadrupoles and two dipole magnets. The first doublet quadrupoles (SDQ) are superconducting magnets to provide a large field gradient of 14.1 T/m. The nominal effective lengths of the quadrupoles are 500 mm (Q500) and 1000 mm (Q1000), respectively. The design of SDQ is similar to that of the BigRIPS triplet quadrupole magnets (STQ) [2].



Figure 1. Photograph of SDQ magnet.

To achieve the designed performance, the field mapping is important because the ion-optics calculations show that the major aberrations originate from the inhomogeneous field distribution of SDQ in the region of $r > 12$ cm [3]. We have plan to correct the higher order aberration by the precise ion optical calculation using the measured magnetic field maps. In this report, the field measurement system for SDQ magnet is described.

In this system we measured a voltage in hall probes together with the following parameters,

- temperature of the room and around the hall probe,
- electric current provided to the hall elements,
- current and voltage of the DC power supplies, and
- miscellaneous data to monitor the status of the cryostat.

The diagram of the system is shown in Fig. 2. In order to measure the magnetic field, the 3-axis hall probes (Arepoc co.ltd. AXIS-3) were used. The temperature was measured using the platinum resistance thermometer. The electric current from the current source was monitored from the voltage of a resistor placed in series between the source and the hall probe.

The data acquisition was controlled by a Linux-based PC. The data were registered in the digital multimeter (keithley 2701) which was linked to the PC via the Ethernet network communication. The hall probe mount was swept over the measured volume by a pulse motor operated via the GPIB devices.

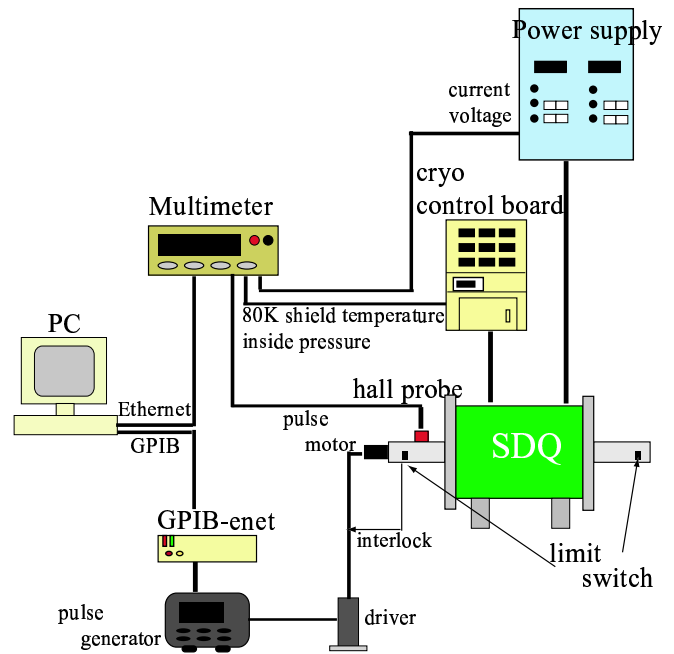


Figure 2. Diagram for the measurement system.

Whole system including the DC power supplies is required to be stable enough to measure the magnetic field with precision of $\Delta B/B \sim 10^{-4}$. Prior to the measurement, the stability of the system was examined.

Figure 3 shows the typical time variation of current and voltage of the power supplies in a half day. The currents did not exhibit significant variation, while the voltage gradually changed. The variation of the voltage was found to depend on the room temperature. It was found that the DC power

supplies were sufficiently stable to keep the magnetic field of $\Delta B/B \sim 10^{-4}$ for a few tens of hours.

Figure 4 shows a typical variation of temperature around the hall probe. In most cases, the variation was $0.1 \sim 0.5 \text{ }^\circ\text{C}$ in a day. This variation results in the fluctuations of about 10^{-4} for the hall probe voltage since the temperature coefficient of the hall probe is $2 \times 10^{-4}/\text{K}$.

Major variation in the hall voltage was found to be due to the variation of current from the source. As is expected, the stability of the current source was consistent with the designed value of 0.01% per day, however, the current from the source has sometimes varied more than two figures of the designed variation. After the large variation for the current source was corrected, the stability of $< 10^{-4}$ was obtained in the whole system including SDQ as shown in Fig. 5.

In summary, it was found that the field measurement is able to be performed with the required accuracy using this system. More details of the method and results for the field measurement will be reported in [4].

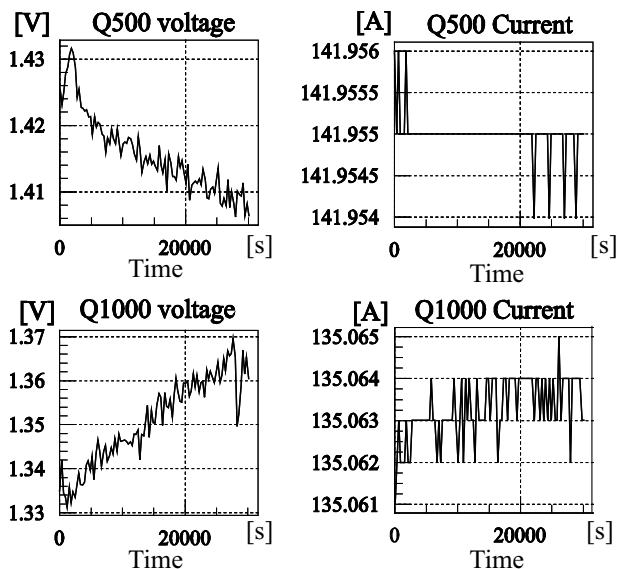


Figure 3. Typical output of the power supply in a half day.

References

- [1] T. Uesaka et al.: CNS Ann. Rep. 2005 (2006) 61.
- [2] K. Kusaka et al.: IEEE Trans. Appl. Supercond., vol 14, no. 2, pp 310-315, (2004).
- [3] T. Uesaka et al.: RIKEN Accel. Prog. Rep. 40 (2007) 155.
- [4] K. Nakanishi et al.: in this report.

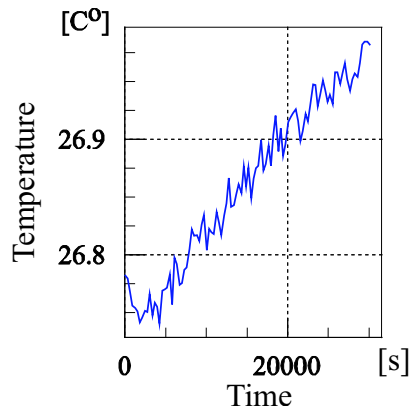


Figure 4. Temperature around the hall probe measured by the platinum resistance thermometer.

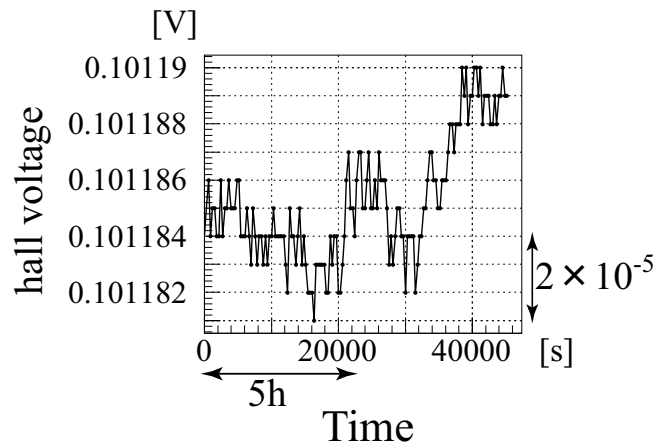


Figure 5. Output voltage of the hall probe.

Design of Focal-Plane Detector for SHARAQ Spectrometer

S. Michimasa, S. Shimoura, T. Uesaka, H. Sakai^a, P. Roussel-Chomaz^b, J-F. Libin^b, P. Gangnant^b,
and C. Spitaels^b

Center for Nuclear Study, Graduate School of Science, University of Tokyo

^aDepartment of Physics, University of Tokyo

^bGANIL, France

The construction of the SHARAQ spectrometer [1] and dispersion-matching beam line [2] were started in the RI Beam Factory (RIBF) at RIKEN. In order to realize high-resolution nuclear spectroscopy utilizing radioactive-ion probes, one of key devices is tracking detectors located at the dispersive focal plane of SHARAQ, which are used to measure Q values of induced reactions. Figure 1 shows a typical detector setup installed in the final focal plane of the SHARAQ spectrometer. The focal plane is located at

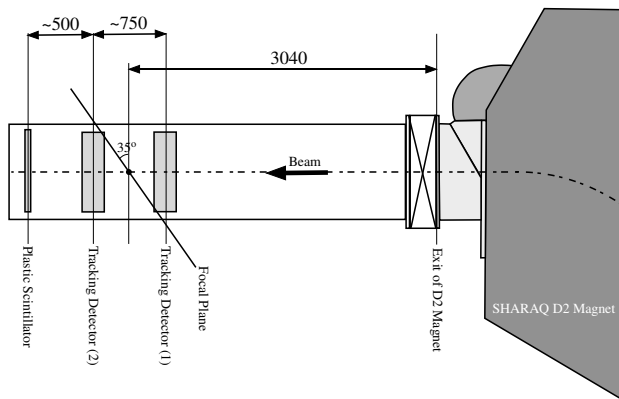


Figure 1. Typical detector setup for the dispersive focal plane of SHARAQ. The final focal plane of SHARAQ is inclined at 35 degrees relative to the central orbit.

3.04-meter downstream from the exit of the SHARAQ D2 magnet and inclined at 35 degrees relative to the central orbit. Focal-plane detectors consist of two tracking detectors and a plastic scintillator. By a combination of these detectors both a track and a timing of particles passing through the focal plane are measured. We have designed a tracking detector for SHARAQ in this fiscal year collaborating with an experimental group of GANIL.

In order to achieve high-resolution measurements using the SHARAQ spectrometer, the tracking detectors should fulfill the requirements as summarized in Table 1. As a tracking detector fitting all the conditions, we have adopted Cathode-Readout Drift Chamber (CRDC) [3] operated in low gas pressure. Although similar types of tracking detec-

Effective area	> 500 mm (H) × 300 mm (V)
Multiple scattering	≪ 1 mrad (σ)
Detection counting Rate	~ 10 ⁴ particles/sec
Position resolution	300 μ m (FWHM)
Detection efficiency	≈ 100%

Table 1. Required performance of the focal-plane detectors.

tors were used as focal-plane detectors of several magnetic spectrometers [4], we have to achieve smaller multiple scattering and higher position resolution.

Figure 2 shows the front view and cross section of CRDC designed for the SHARAQ spectrometer, and its specification is listed in Table. 2. The effective area of the CRDC

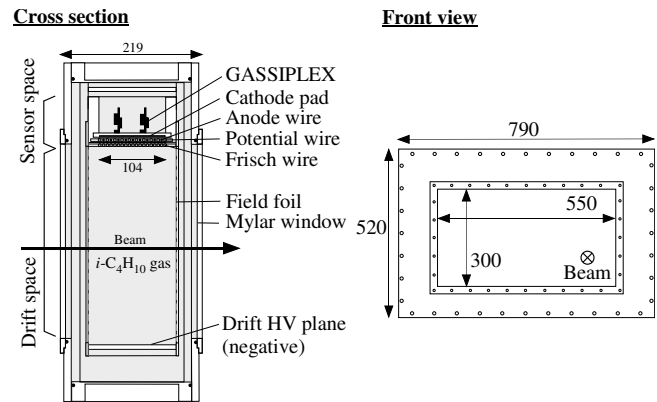


Figure 2. Cross section and front view of SHARAQ CRDC. The front view is shown in a half scale of the cross section.

Effective area	550 mm (H) × 300 mm (V)
Anode wire (A)	10 wires, 20 μ m ϕ
Potential wire (P)	11 wires, 100 μ m ϕ
Frisch grid wire (F)	21 wires, 100 μ m ϕ
Cathode pad (C)	2 mm (H) × 50 mm (T), 2 rows × 256 pads
Pitch of A-P and F-F	5 mm
Distance of A-C and A-F	2,3 or 5 mm (Adjustable)
Mylar window	10 μ m
Foil used for field cage	1.5 μ m
Detector gas	Isobutane, 15–50 torr

Table 2. Specification of the CRDC for SHARAQ.

is 550 mm horizontally and 300 mm vertically. Secondary electrons produced by energy loss of heavy ions move vertically in electric field made by the drift HV plane and field cage made by thin foils, and finally cause avalanches around the anode wires. The vertical hit position of the heavy ion is deduced by drift time of secondary electrons and the horizontal hit position is deduced by charge distributions induced on the cathode pads. In the sensor part of the CRDC, 10 anode wires are placed between 11 potential wires. The potential wires and Frisch grid are arranged to make axially-

symmetric electric fields in the vicinity of anode wires and to minimize position dependence in avalanche gains. The CRDC has two rows of the cathode pads perpendicular to the beam axis, and each row consists of 256 cathode pads arranged by the 2.2-mm pitch. The thickness of the sensor space is 104 mm and total thickness of the CRDC is 219 mm.

The CRDC was designed for uses in vacuum and for low-pressure operations at 15–50 torr. The low-pressure operation is effective not only for reduction of gas thickness itself but also for reduction of Mylar windows' thickness sealing the detector gas. Since the material thickness of the CRDC is totally 10^{-4} of radiation length, the effect of multiple scattering is evaluated to be approximately 0.1 mrad (σ) for ^{12}C at 200 A MeV.

In the drift space, high negative voltage is supplied to form an electric field for electron drift. The field cage is made by thin Mylar foils evaporated aluminum strips where appropriate voltages are provided to make a parallel and constant electric field. The maximum high voltage in the drift space is designed to be more than 5 kV. When electrons move in 30-cm-thick isobutane gas at 15 torr, the drift time is estimated to be approximately 6 μs by simulations using the GARFIELD code [5].

The CRDC has 2 signals from the anode wires and 2 multiplexed signals from the cathode pads. The charge signals from the cathode pads are read out by using GASSIPLEX chips [6], which developed at CERN for multiplexed readouts of pad chambers. The GASSIPLEX is mounted close to cathode pads inside the detector as shown in Fig. 2. Its highly multiplexed performance allows us to transmit charge signals from 128 cathode pads by a cable and to read out all the information with a CAEN sequencer with a CRAM module [7]. The readout process needs totally $\sim 25 \mu\text{s}$. Since the counting rate capability of the detector is almost determined by this readout time, CRDC operation at the event rate of 10^4 Hz is estimated to be available.

The position resolution of CRDC is roughly estimated as following relation:

$$R_{H(V)} \approx 2.35\sigma_{T(L)}\sqrt{L/N},$$

where R_H and R_V are for horizontal and vertical position resolutions in FWHM, respectively. The σ_T and σ_L respectively means the transverse and longitudinal diffusions per a unit-length drift. The L means a drift length of secondary electrons and N means the number of secondary electrons produced by the energy loss of heavy ions in the detector gas. When we consider the case of 5-kV drift HV and isobutane at 15 torr, σ_T and σ_L are estimated to be ~ 840 and $\sim 520 \mu\text{m/cm}$ by using the GARFIELD code, respectively. Since the average energy required to produce an ion-electron pair in pure isobutane is 23 eV [8], a 250 A-MeV ^{12}C particle produces about 1600 ion-electron pairs in 5-cm isobutane gas at 15 torr. Position resolution in the 30-cm electron drift is estimated to be $R_{H(V)} \approx 270$ (170) μm . However, this values fulfills the above-mentioned requirement.

In the operation of low-pressure gas chamber, one must consider about a sufficient avalanche amplification of secondary electrons because the energy deposit of heavy ions is relatively small. The quantity of induced charge Q can be estimated as

$$Q = (-1.60 \times 10^{-4}) \times \varepsilon GN \quad [\text{fC}],$$

where G is an avalanche gain around anode wires, N is the number of produced secondary electron, and ε means a ratio between mirror charge induced on a cathode pad and total charge produced by avalanche processes. The value of ε is determined by geometrical condition between anode wires and cathode pads, and ε of the nearest cathode pad from an avalanche point is estimated to be 0.03. The avalanche gain of isobutane gas at low pressure was reported in ref. [9]. The avalanche gain of $20\text{-}\mu\text{m}$ anode wires in pure isobutane at 32 torr is $\sim 2 \times 10^4$ when 1-kV voltage is provided on the anode wires. In the 250 A-MeV ^{12}C case, mirror charge of ~ -150 fC is estimated to be yielded on the cathode pad. Since the designed dynamic range of the GASSIPLEX chip is up to -300 fC, this condition is acceptable.

In the summary, we examined the setup configuration of the focal plane detectors that utilize high-resolution features of the SHARAQ spectrometer. As tracking chamber used in SHARAQ a large-area CRDC operated with low-pressure pure isobutane was adopted to reduce the effects of multiple scattering. The manufacturing of the CRDC just started in GANIL and this detector system will be used at the first experiment of the SHARAQ spectrometer in FY2008.

References

- [1] T. Uesaka *et al.*, CNS-REP-76, (2007) 63.
- [2] T. Kawabata *et al.*, CNS-REP-76, (2007) 65.
- [3] M.H. Tanaka *et al.*, Nucl. Instrum. Methods Phys. Res. A **362** (1995) 521.
- [4] J. Yurkon *et al.*, Nucl. Instrum. Methods Phys. Res. A **422** (1999) 291.
- [5] R. Veenhof, GARFIELD, CERN Program Library W5050.
- [6] The GASSIPLEX is a re-designed chip of the AMPLEX by J.C. -Santiard of CERN. The AMPLEX is described in E. Beuville *et al.*, Nucl. Instrum. Methods Phys. Res. A **288** (1990) 157.
- [7] V551 C.A.E.N sequencer User Guide, V550 C.A.E.N CRAM User Guide.
- [8] F. Sauli, CERN 77-09, 1997.
- [9] Yu.I. Devydov *et al.*, Nucl. Instrum. Methods Phys. Res. A **545** (2005) 194.

Performance of LP-MWDC for α beam at 35.2 MeV

H. Miya^a, S. Shimoura^b, A. Saito^c, T. Kawabata^b, H. Kurei^b, S. Michimasa^b, K. Miki^c,
K. Nakanishi^b, S. Ota^b, Y. Sasamoto^b, T. Uesaka^b and H. Sakai^c

^aDepartment of Physics, Rikkyo University

^bCenter for Nuclear Study, Graduate School of Science, University of Tokyo

^cDepartment of Physics, University of Tokyo

1. Introduction

We are developing Low-Pressure Multi-Wire Drift Chambers with stripped cathodes and delay-line readouts (LP-MWDCs) as tracking detectors [1], which will be used in the SHARAQ beam line under construction at RIBF [2, 3]. The LP-MWDC has characteristics that positions of beam particles are determined with signals from anode wires and cathodes, and the chamber gas is operated at the low pressure of less than 20 kPa to reduce the effect of the multiple scattering. Figure 1 shows a schematic structure of the LP-MWDC. The strips of the cathode (CX, CY) are connected to delay lines [4]. The anode plane (AX, AY) consists of 16 anode wires and 17 potential wires. The LP-MWDC has outputs of 2 cathodes and 32 anode wires.

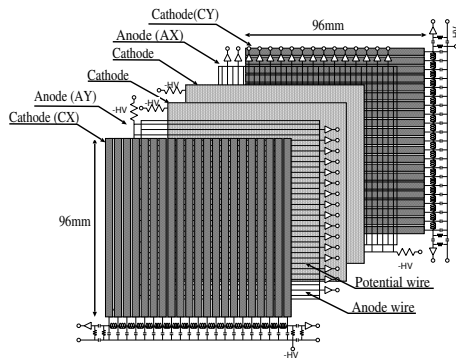


Figure 1. A schematic structure of the LP-MWDC with stripped cathodes and delay-line readouts.

In March 2008, we performed a test experiment to study performances of the LP-MWDC for an α beam at 35.2 MeV. Here, we report basic characteristics of the LP-MWDC, derived from on-line analysis.

2. Experiment

The test experiment was performed at E7B course in RIKEN RIBF operated by RIKEN Nishina Center and CNS, University of Tokyo. An α beam at 35.2 MeV was supplied by the AVF cyclotron accelerator. The energy deposition of the α beam in the LP-MWDC is comparable to a ^{12}N beam at 200A MeV, which is a candidate for the first experiment to be performed with the SHARAQ. Figure 2 shows a schematic view of the experimental setup. A plastic scintillator with the size of $50 \times 50 \text{ mm}^2$ and the thickness of 5 mm was used as a trigger counter. The LP-MWDC was operated using an isobutane gas ($i\text{-C}_4\text{H}_{10}$) at 4, 5, 10, 15 and 20 kPa. The timings from the anodes and the cathodes, and the pulse heights from the cathodes were measured.

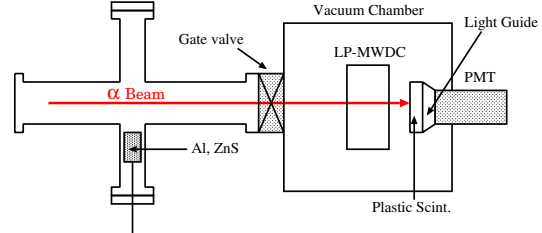


Figure 2. A schematic view of the experimental setup.

The data of these timings and pulse heights were taken with CAEN V1190A multi-hit TDC and CAEN V792N QDC, respectively.

3. Results

Figures 3 (a) and (b) show the detection efficiencies of the cathodes and the anodes for the gas pressure of 20 kPa (open triangle), 15 kPa (closed square) 10 kPa (open square), 5 kPa (closed circle), and 4 kPa (open circle) as a function of the applied voltage of the cathodes and the potential wires. The efficiencies are defined as the ratio of the counted number of the cathodes and the anodes to the counted number of the plastic scintillator. Since the threshold levels for the cathodes and the anodes are different due to electric noise levels, the efficiency of the cathodes is less than that of the anodes. The threshold levels of the cathodes and the anodes were evaluated to be 100 fC and 40 fC, respectively, based on the energy deposition of the α -particle and the gas multiplication factor [1].

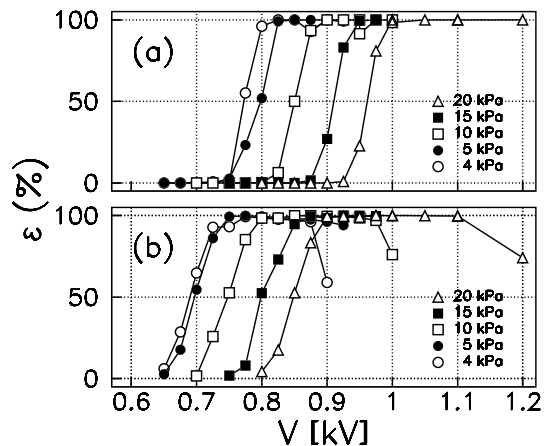


Figure 3. The efficiencies of (a) the cathodes and (b) the anodes for gas pressures as a function of the applied voltage .

A position measurement via the delay-line readout of the cathodes was demonstrated by using a mask with 2 mm

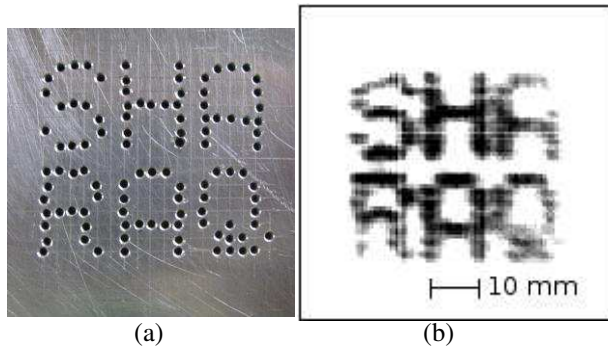


Figure 4. (a) The photo of the mask with 2 mm pitch holes shaped “SHARAKU” and (b) the position image of the beam by the cathode readouts (CX, CY).

pitch holes shaped “SHARAKU” in front of the LP-MWDC. Figure 4 (a) and (b) show the photo of the mask and the beam position image determined by the cathode signals.

4. Summary

We performed a test experiment for the LP-MWDC with stripped cathodes and delay-line readouts to study the performance using the α beam at 35.2 MeV. We obtained the detection efficiencies of the cathodes and the anodes as functions of the gas pressure and the applied voltage. Further quantitative off-line analysis to obtain the detection efficiencies and the position resolution is in progress.

References

- [1] A. Saito *et al.*: CNS Ann. Rep. 2007 (2008);
A. Saito *et al.*: CNS Ann. Rep. 2006 (2007).
- [2] T.Kawabata *et al.*: CNS Ann. Rep. 2006 (2007).
- [3] T. Uesaka *et al.*: CNS Ann. Rep. 2007 (2008).
- [4] H. Kumagai *et al.*: Nucl. Instrum. and Meth. in Phys. Res. A470 (2001) 562.

Status of the polarized proton target

Y. Shimizu, T. Kawahara^a, S. Sakaguchi, T. Uesaka, and T. Wakui^b

Center for Nuclear Study, Graduate School of Science, University of Tokyo

^aDepartment of Physics, Toho University

^bCyclotron and Radioisotope Center, Tohoku University

1. Introduction

A polarized proton target has been developed for \vec{p} -RI scattering experiments at CNS [1]. The target is operated in a low magnetic field of 0.1 T and a high temperature of 100 K. This feature enables the target to be used in \vec{p} -RI scattering experiments under the inverse kinematic condition.

The polarized proton target was used to measure the vector analyzing power of $\vec{p}+^8\text{He}$ elastic scattering in May 2007 at the RIKEN projectile fragment separator (RIPS) [3]. In this report, we describe the developments of the polarized proton target system and the performance of the polarized proton target during the scattering experiment in 2007.

2. Developments of the polarized proton target

2.1. Upgrade of control system

Protons in the crystal of aromatic molecules are polarized by combining methods called “microwave-induced optical nuclear polarization” and “integrated solid effect” [2]. This method requires for the target system to have a magnet for a polarization holding field, a laser for optical excitation, a microwave system and a field sweep system for polarization transfer, and an NMR system for measuring relative value of proton polarization.

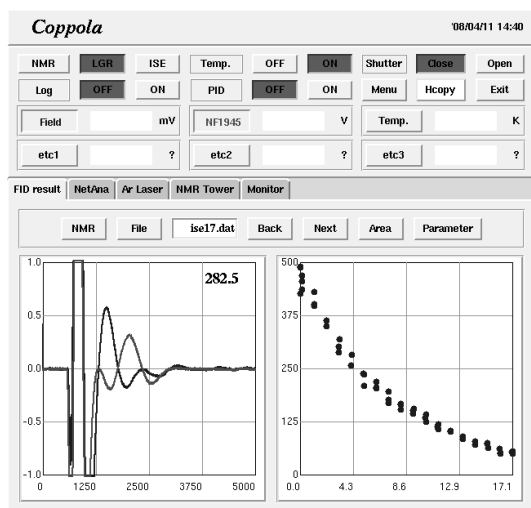


Figure 1. A view of the GUI for controlling the polarized proton target system.

Almost all devices of the polarized proton target system were connected to a General Purpose Interface Bus (GPIB) for remote control purpose. The GPIB controllers, National Instruments GPIB-Enet/100 and PCI-GPIB board were used. The software for controlling the polarized pro-

ton target system was developed by using a programming language C with standard C libraries. In order to allow us to easily operate the polarized proton target system, a Graphical User Interface (GUI) program written in Perl/Tk was developed in 2007. Figure 1 shows the GUI named as *Coppola* (Control Of Proton POLARization).

2.2. Enhancement of optical power

The polarizing process have been obtained that the laser irradiation and the sweep of magnetic field during the irradiated microwave. This processes was repeated at 2 kHz in the previous studies. The repetition rate had been limited by the magnetic field sweeping system.

In the magnetic field sweeping system, current was supplied to a coil by a voltage-current (VI) converter circuit. The circuit in the previous studies included an element called Q-snabber to prevent unwanted oscillation. Since increase in frequency caused damage of the circuit due to heating on the Q-snabber, the repetition rate was limited about 2 kHz in the previous studies. In order to use higher frequency beyond this limitation, we have reconfigured the VI converter circuit. The new VI converter circuit without the Q-snabber could steadily work at the repetition rate of up to several kHz. The whole system could be operated with a repetition rate of 2.6 kHz. In the present system, the repetition rate was limited by the optical chopper used to chop the light of constant-wave laser. The repetition rate will be increased by another optical chopper.

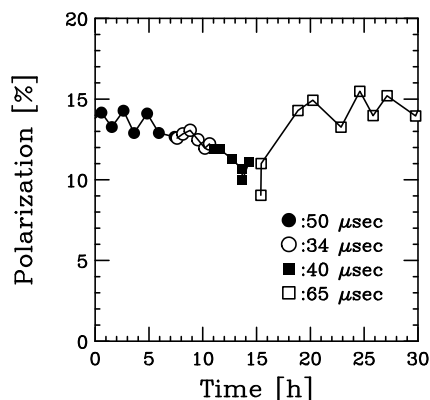


Figure 2. The proton polarization with four different pulse widths.

The pulse width of laser was 20 μsec in the previous studies. From the evolution of the optimum pulse width in Ref [1], it is expected that longer pulse width leads to result in higher proton polarization. Figure 2 shows the proton polarization with four different pulse widths (34, 40, 50, and 65 μsec). Longer pulse width was not tried to avoid the depolarization effect by laser damage. From this result, we adopted the pulse width of 65 μsec in $\vec{p}+^8\text{He}$ scattering

experiment.

3. Performance of the polarized proton target

During the $\vec{p}+^8\text{He}$ scattering experiment, the proton polarization was measured by the pulsed NMR method and its direction was reversed by the 180° NMR pulse method [4]. The experiment of the $\vec{p}+^4\text{He}$ reaction was performed to calibrate the proton polarization. The average values of the proton polarization was approximately 11.1 %. Figure 3 shows the proton polarization measured throughout the experiment. The open square shows the proton polarization in the optimization of the laser pulse width and the beam turning. The open and closed circles show the proton polarization in the $\vec{p}+^4\text{He}$ and the $\vec{p}+^8\text{He}$ scattering experiments, respectively.

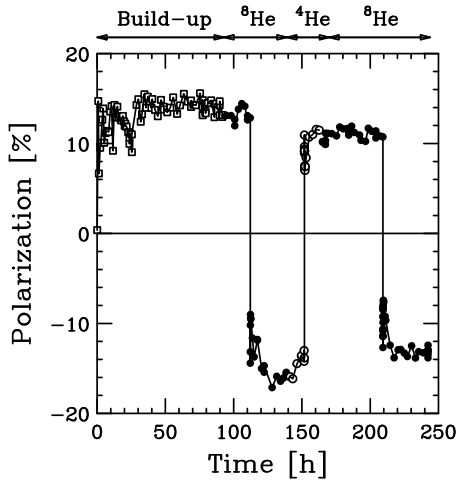


Figure 3. The time development of polarization during $\vec{p}+^8\text{He}$ scattering experiment.

We compare the optical parameters and the average values of the proton polarization in the previous experiment and those in the $\vec{p}+^8\text{He}$ scattering experiment as shown in Table 1. In the previous experiment, two Ar-ion lasers were used. Since one of the Ar-ion lasers was broken, we use the one Ar-ion laser in the $\vec{p}+^8\text{He}$ scattering experiment. Although the laser power was reduced, the comparable polarization was obtained due to the higher repetition rate of 2.6 kHz and the longer pulse width of 65 μsec .

Table 1. Comparison of the optical parameters and polarization at $\vec{p}+^6\text{He}$ scattering experiment in 2005 and $\vec{p}+^8\text{He}$ scattering experiment in 2007.

	$\vec{p}+^6\text{He}$	$\vec{p}+^8\text{He}$
Laser power	22 W	18 W
Repetition rate	2.0 kHz	2.6 kHz
Pulse width	20 μsec	65 μsec
Average pol.	$11.5 \pm 2.5 \%$	$11.1 \pm 2.5 \%$

4. Summary

A optimized control system has been designed and constructed for the polarized proton target system. The control is performed through the GPIB and a user-friendly GUI pro-

gram written in Perl/Tk is provided.

We have succeeded in increasing the repetition rate of the polarization process up to 2.6 kHz by improving a VI converter circuit. Laser pulse width was extended to 65 μsec for higher polarization. These improvements were applied to $\vec{p}+^8\text{He}$ scattering experiment in 2007. The average values of the proton polarization was approximately 11.1 %. The repetition rate can be increased at least by a factor of two by introduction of a high-speed optical chopper.

References

- [1] T. Wakui *et al.*, Nucl. Instrum. Methods Phys. Res. A **550**, 521 (2005).
- [2] A.Henstra *et al.*, Chem. Phys. Lett. **165**, 6 (1990).
- [3] S. Sakaguchi *et al.*, RIKEN Accelerator Progress Report vol. 41 (2007).
- [4] T. Kawahara *et al.*, CNS Annual Report 2005, 81 (2006).

Current core monitor for E7 beam line

S. Watanabe, Y. Ohshiro, H. Yamaguchi, R. Koyama^{a,c}, T. Watanabe^a, M. Kase^a, A. Goto^a,
K. Hatanaka^b, and S. Kubono

Center for Nuclear Study, Graduate School of Science, University of Tokyo

^a*RIKEN (The Institute of Physical and Chemical Research)*

^b*Research Center for Nuclear Physics (RCNP), Osaka University*

^c*Sumitomo Heavy Industries, Ltd. (SHI)*

Basically there are 2 types of beam current monitors: a dc current monitor with a beam destructive electrode to collect ion charges precisely, and a pulsed current monitor with a nondestructive electromagnetic coupler to measure induced electromagnetic field by moving charged particles. Usually the latter has lower sensitivity than the former. A nondestructive beam current monitor with high sensitivity, like Faraday cup, is needed in the beam transport line. A wide band core monitor has been developed to measure Fourier components in a detected pulsed beam signal [1]. A measurement of Fourier component is effective to eliminate an RF noise comprising first, third, fifth or higher odd harmonics influenced from the operating AVF cyclotron Dee voltages. Because of a flat top acceleration regime, 3rd order harmonics will appear strongly in the detected pulsed beam signal because of an electromagnetic coupling between the associate beam monitor and a high power RF equipment. On the other hand, the second, fourth, or higher even harmonics components of the pulsed beam signal can be used to measure beam current amplitude. A lock-in amplifier with 200 MHz measurement range, can eliminate unnecessary rf noise and selectively amplified the Fourier component of the beam signal [2]. Recently, a DC current monitor with a metal alloy core with a high permeability in the highest frequency range has been developed [6]. These technologies stimulate the development of core monitor for E7 beam line because of CRIB experiments needs nondestructive current monitor. Required sensitivity in the dc current measurement is estimated to be in the order of 10 nA, while its accuracy should be as good as that of Faraday cup system used in the F0 target chamber.

The developed core monitor is shown in Fig. 1. Specifications of core monitor are listed in Table 1. An offline test by using beam simulator for a repetitive pulsed beam has been done. A schematic of beam simulator is shown in Fig. 2. The gain of the pick up core in frequency domain of interest has been measured as shown in Fig. 3. The pulsed beam test, called online test, at CBECR beam line with a metal alloy RF buncher [4] has been done. The mass analyzed dc beam from a volume type ion source [3] had received velocity modulation at the metal alloy RF buncher to produce the pulsed beam. The bunching frequency is chosen to simulate AVF RF acceleration frequency ranging from 12 to 24 MHz. A pulsed 10keV H⁺ beam, for example, is measured by a 100MHz Faraday cup [5]. Amplitude gain of the core monitor is calibrated with the 100MHz Faraday cup. The results of both measurements, offline and online beam test, had compared. In Fig. 3, differ-

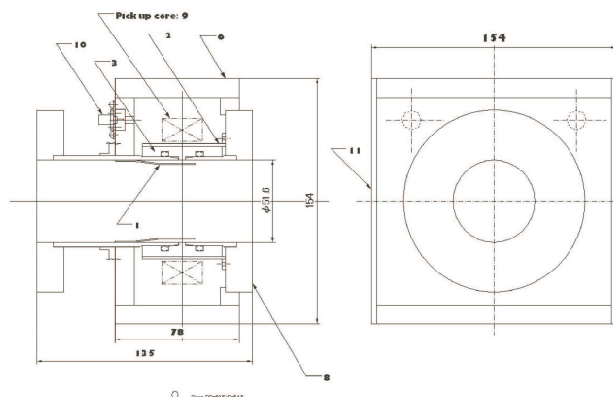


Figure 1. Cross section of core monitor; 1=beam shield, 2=hoop, 3=insulator, 6=shield yoke, 8=vacuum flange(ICF114), 9=pick up core, 10=signal connector, 11= side panel.

ence between input signal (diamond) and detected signal (square) in correspondence frequency is equivalent to core loss. This result shows that the good agreement between both the tests was found.

References

- [1] M. Wada *et al.*, RIKEN Accel. Prog. Rep. 38 (2005).
- [2] R. Koyama, *et al.*, Proc. 4th Annual Meeting of Particle Accelerator Society of Japan and the 32nd Linear Accelerator Meeting in Japan, p. 318 (2007).
- [3] S. Watanabe, CNS Annual report 2006, pp. 53-54.
- [4] T. Koseki *et al.*, JJAP Vol. 45, No. 5A, 2006, pp. 4227-4231.
- [5] S. Watanabe, CNS Annual report 2004, pp. 63-64
- [6] S. Ninomiya *et al.*, Proc. of EPAC2006, Edinburgh, Scotland. pp. 1145-1147.

Table 1. Specifications of core monitor

Length of vacuum chamber	135 mm
Inner diameter of vacuum chamber	51.6 mm
Inner diameter of beam shield	45.4 mm
Gap length of vacuum pipe	4 mm
Number of coil turns	5 turns for signal pick up, 1 turn for test signal
Signal connector	SMA
Vacuum flange	ICF114 (SUS304)
Pick up core	Hitachi FT-3KM ($S=138.8 \text{ mm}^2$, $L_m=285.1 \text{ mm}$)
Insulator	Polypenco PEEK PK-450

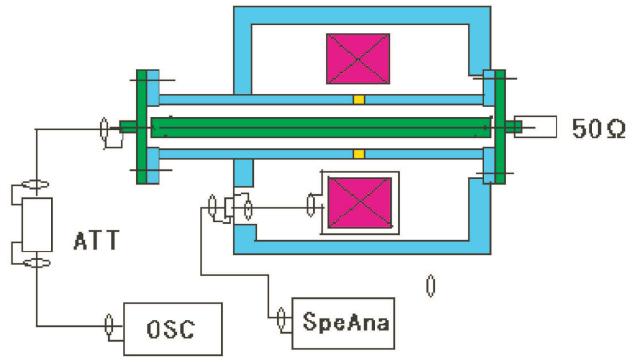


Figure 2. Schematic of beam simulator. Signal from OSC (signal generator) is passed through beam pipe with inner conductor. Induced magnetic flux in the ring core is detected by winding coil and detected signal is passed to SpeAna (spectrum analyzer).

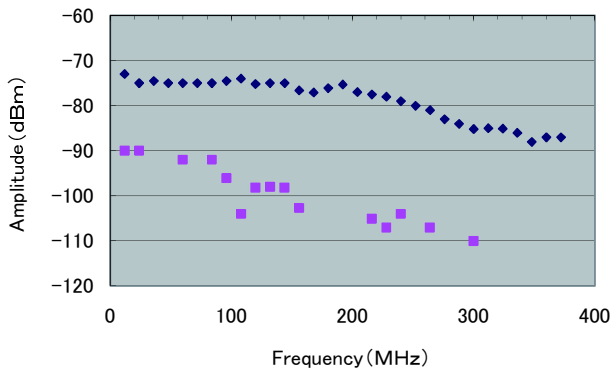


Figure 3. Gain-frequency characteristics of core monitor measured by beam simulator. Difference between input signal (diamond) and detected signal (square) in correspondence frequency is equivalent to core loss.

First beam extraction from SC-ECR-IS at CNS

Y. Ohshiro, S. Yamaka, S. Watanabe, T. Kageyama^a, T. Nakagawa^a, I. Arai^b and S. Kubono *Center for*

Nuclear Study, Graduate School of Science, University of Tokyo

^a *RIKEN (The Institute of Physical and Chemical Research)*

^b *Graduate School of Pure and Applied Sciences, University of Tsukuba*

1. Introduction

A nuclear astrophysics program of CNS has been promoted in RIKEN AVF Cyclotron facilities. For the experiments using a CRIB [1], a variety of high charge state ions of gas or metal have extracted from a Hyper ECR ion source [2] and injected to the AVF cyclotron. To increase the higher charge state ion, a superconducting ECR ion source (called SC-ECR-IS) [3] has been moved from University of Tsukuba. It was reassembled by CNS-RIKEN group at RIBF-E21 room in March 2007. This report describes the build up the superconducting magnets, design of beam analyzing system, production of ion beams, and newly tested metallic ions.

2. Start-up of SC-ECR-IS

A photograph of the SC-ECR-IS installed in the RIBF-E21 room is shown in Fig. 1. Superconducting solenoid coils (NbTi wire) are cooled by two liquid helium free compact cryostats. For keeping stably the coil temperature, a housing room of the coils was evacuated up to vacuum pressure of 3×10^{-5} Torr. And, two refrigerators were overhauled. Then, the coil temperature of 5.5 K was stably obtained by operating the refrigerators for ten days.

However, the coil temperature increased to quenching one (7 K) in less than 3 minutes after the refrigerator stop. So, we equipped a coil power supply with some anti-quenching systems: urgent power shutdown, step by step control of setting current and limitation of coil voltage. And, a magnetic mirror field was generated in safety by three superconducting coils (C1, C2 and C3).

A measured magnetic mirror field along an axis of the ion source was shown in Fig. 2. The peaks of the mirror field strength were consistent with a data of Tsukuba group by 1.85 T, 0.4 T and 1.24 T. Running current of 30 A, 20 A and 30 A for the coils of C1, C2, and C3, respectively, was used for producing $10 \text{ e}\mu\text{A}$ of $^{132}\text{Xe}^{30+}$ ions in Tsukuba.

3. Beam analyzing system

A photograph of a beam analyzer following the ECR ion source is also shown in Fig. 1. An analyzer magnet was converted from CNS-SF-ECR at Tanashi and designed by drift space of 67.5 cm. It was too short for the SC-ECR-IS because distance between a plasma electrode position and a return yoke edge of the ion source already had over 31 cm mechanically. So, the magnet entrance edge was put to distant of 123 cm from the plasma electrode position.

Good solution of the beam analyzing system calculated by using a Winagile code [4] was shown in Fig. 3. Transmission efficiency by the beam simulation was over 95%. From the result of calculation, the image slit was set to the

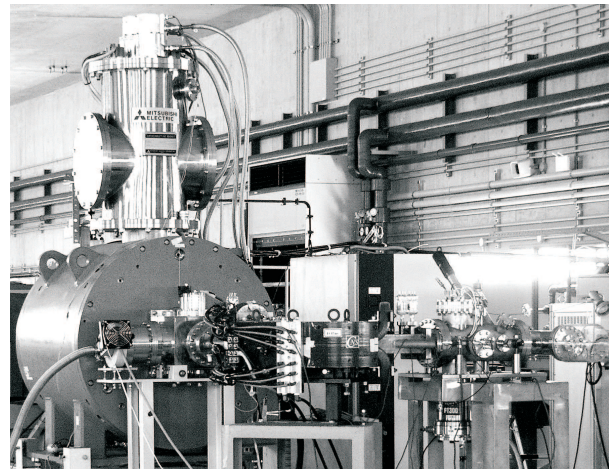


Figure 1. Photograph of a superconducting ECR ion source and a beam analyzing system.

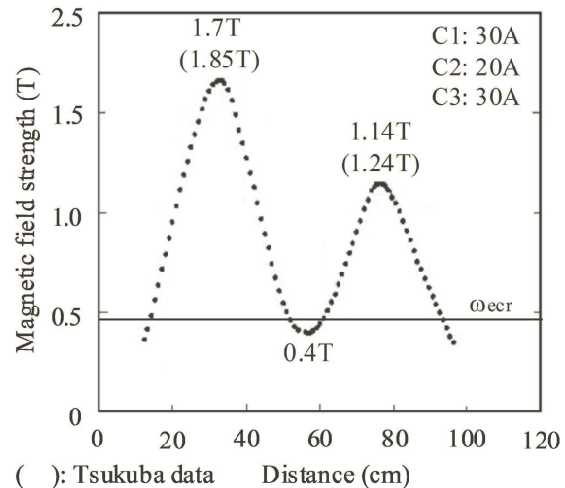


Figure 2. A magnetic mirror field of the ion source measured.

place of distance of 51 cm from the magnet exit edge (see Fig. 3). Then, we succeeded in obtaining the good mass resolution like the spectrum shown in Fig. 4.

4. Production of ions

Charge state distribution of Ar ions was shown in Fig. 4. The ion source was tuned for the production of Ar^{11+} ions. The ions up to Ar^{16+} are observed in the distribution. The typical beam intensity of Ar^{11+} from the ion source is approximately $100 \text{ e}\mu\text{A}$. Moreover, by supplying the supporting gas of oxygen into a plasma chamber, the intensity of this ion was increased up to $130 \text{ e}\mu\text{A}$. Operating conditions of the ion tuning were as follows: Electric currents of the three coils of C1, C2, and C3 were 23.3 A, 25.2 A and 58.7 A, respectively. The injected RF power of 14 GHz was 730 W. And, Gas pressure of the extraction stage was 4×10^{-7}

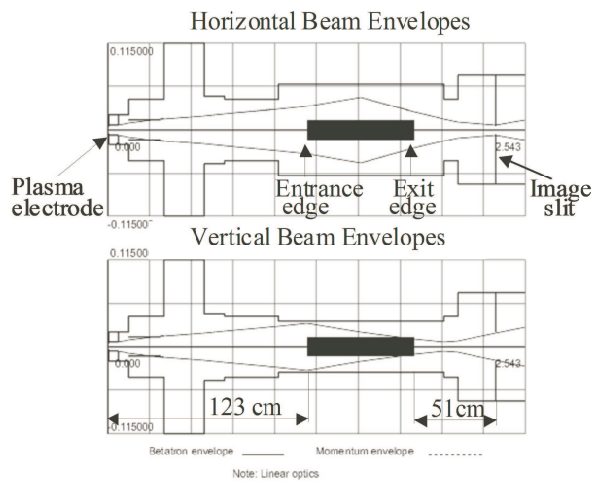


Figure 3. Beam envelope of the analyzing system calculated by a Winagile code.

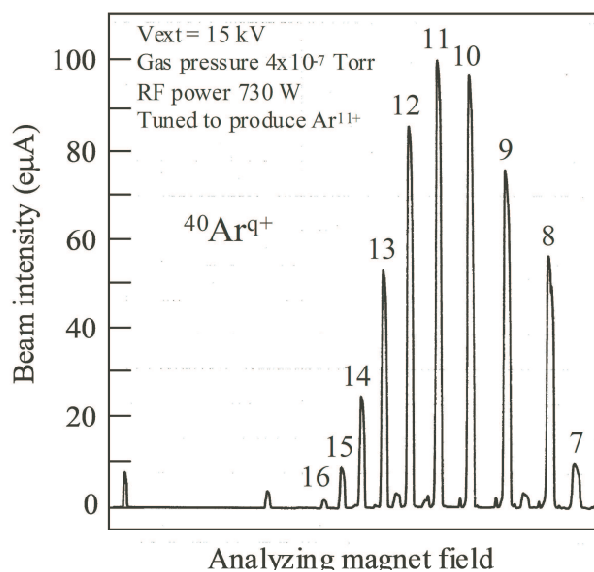


Figure 4. Charge state distribution of Ar ions. The ion source was tuned for the production of Ar^{11+} ions.

Torr. The extraction voltage was 15 kV.

After that, metallic ions like boron or iron were produced in the ECR ion source by a MIVOC method. As materials charged in a small container, a volatile substance like o-Carborane, $\text{C}_2\text{H}_{12}\text{B}_{10}$ or Ferrocene, $\text{Fe}(\text{C}_5\text{H}_5)_2$ was used for the ions of boron or iron, respectively. Such materials have vapor pressure 4.5×10^{-2} Torr or less in normal temperature. The metallic vapor was adjusted by a gas controller and introduced into the plasma chamber.

The beam intensities of metallic ions obtained by the ion source were shown in Table 1. The ion beams were extracted by the higher intensity. Especially, a beam of $^{11}\text{B}^{4+}$ ions was 3.4 times the intensity of the Hyper ECR ion source. And, the higher charge state ion beams were also extracted with high intensity. For example, a beam of $^{11}\text{B}^{5+}$ ions was obtained by $47 \text{ e}\mu\text{A}$, which was 8.5 times the intensity of the Hyper ECR source.

Ion	Beam intensity ($\text{e}\mu\text{A}$)	
	SC-ECR-IS	Hyper ECR-IS
$^{11}\text{B}^{4+}$	160	47.5
$^{11}\text{B}^{5+}$	47	5.5
$^{56}\text{Fe}^{13+}$	23	9
$^{56}\text{Fe}^{15+}$	7	3

Table 1. Metallic ion intensities obtained.

5. Conclusion

The Superconducting ECR ion source was installed and tested in the RIBF room. The gaseous or metallic multiplied ions were obtained successfully with high intensity. The new ECR ion source will be an extremely effective machine for high beam intensity extraction from the AVF Cyclotron. We are now preparing for installation of the ion source to the AVF cyclotron.

References

- [1] Y. Yanagisawa et al., Nucl. Instrum. Methods Phys. Res. A 539, 74 (2005).
- [2] Y. Ohshiro et al., CNS. Annual Report 2005 (2006) 59.
- [3] T. Kurita, A dissertation submitted to the Doctoral Program in Physics, the University of Tsukuba.
- [4] P. J. Bryant, Proc. of EPAC 2000, Vienna, Austria, pp1357-1359.

Optimization of the $h=2$ RF regime in the RIKEN AVF Cyclotron

S.B.Vorozhtsov^a, A.S.Vorozhtsov^a, E.E.Perepelkin^a, S.Watanabe, S.Kubono, and A. Goto^b *Center for*

Nuclear Study, Graduate School of Science, University of Tokyo

^a *JINR (Joint Institute for Nuclear Research), Dubna, Russia*

^b *RIKEN (The Institute of Physical and Chemical Research)*

1. Introduction

A central region of RIKEN AVF cyclotron was designed to accelerate a beam with harmonic number of 2. In order to boost the utilization of the machine, optimization study of the regime is being preceded. The results of the previous investigations are described in Refs. [1] and [2]. The present work focuses on: a) continuation of the cyclotron electromagnetic field model construction; b) realistic injection line simulation; c) modification of the electrode structure.

2. Computer model of electromagnetic field

The computer model of the electromagnetic fields of the AVF cyclotron was prepared and successfully checked against the measurements. The following structure elements comprise the computer model: magnet yoke, spiral sectors and center plugs, trim and harmonic coils, inflector, RF shield, RF Dee electrodes, deflector (ESD) and magnetic channel (Fig. 1). Electric and magnetic field distributions and mechanical structures were transmitted to the beam dynamics code for simulations, and particle losses on the surface of the system elements were estimated.

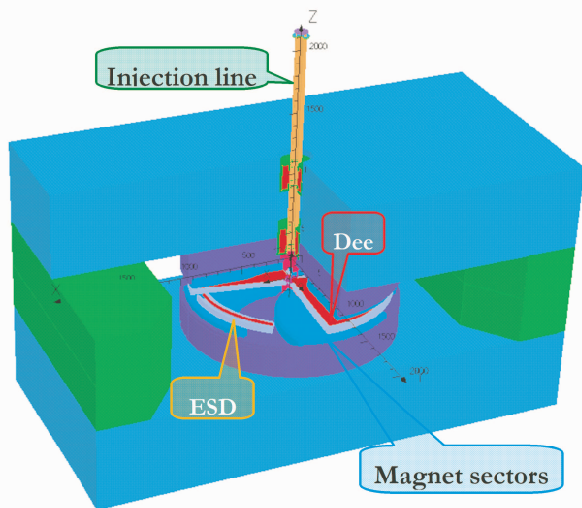


Figure 1. General view of the cyclotron computer model.

3. Beam simulation

An improvement of the transmission efficiency and the beam quality of the existing regime was considered for previous investigation. The parameters of the regime are as follows: accelerated particle $^{14}\text{N}^{5+}$, final energy =7 MeV/A, beam intensity 1 μA , bending factor $K=70\text{MeV}$, the 2nd RF harmonics acceleration and RF frequency of 16.3 MHz. Dee voltage of 46.7 kV. No flat-top harmonics was used in the simulations.

The easiest way to increase the transmission is to find

out better operational parameters instead of changing the present geometry of the central region. A preliminary calculation showed that the broadening of the beam could be controlled and the beam transmission could be improved by changing the injection energy of the beam and the RF Dee voltage. In the simulation the extraction voltage of the ECR ion source was decreased from 10.4 kV to 9 kV and the RF Dee voltage from 46.7 kV to 40 kV. These values were adopted in order to obtain a sufficiently small vertical angles of particle trajectory at the exit of the inflector as well as to ensure the beam passage through the puller. The reason to ensure the beam passage through the puller is that the beam crossing the first acceleration gap at the positive RF phase that gives the electric focusing there. It is noted that the phase at this gap was adopted to be negative (defocusing) in order to avoid over-focusing. The magnetic field amplitude of the first trim coil was also changed by approximately 50 % to ensure the beam sitting on 0° RF phase in the isochronous field region.

The cyclotron injection line [3] is shown in Fig. 2. From point of view of the state of art the Low Energy Beam Transport (LEBT) in the present system probably requires re-designing to show better functionality. The improvement of the LEBT plays a key role in the cyclotron upgrade program, which implies the final beam intensity increase: if there is low beam intensity at injection, then no way to get higher beam intensity at extraction.

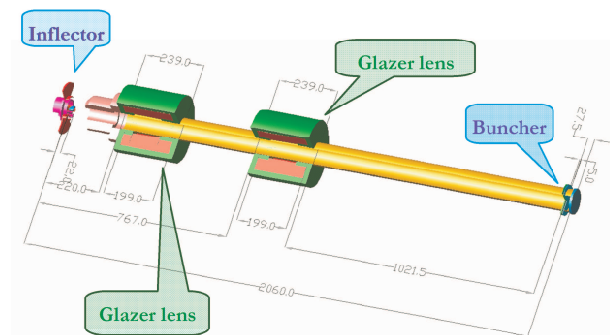


Figure 2. LEBT layout.

The TRACE2D [4] calculations of the LEBT functionality demonstrate that the beam space charge effects are not negligible and should be taken into account. The obtained results serve as a guiding line for the following 3D CBDA [5] simulation described below.

The bunching effect is shown in Fig. 3. The reference bunch in the middle of a set of 12 bunches comprising so called gsuper-bunchh to simulate CW beam from the ion source was selected for simulation of the acceleration process in the cyclotron itself.

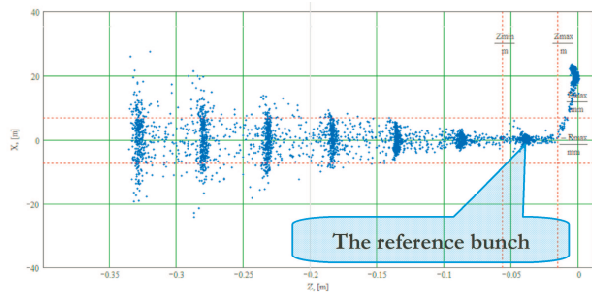


Figure 3. Bunching effect near the cyclotron midplane ($Z=0$).

The resulting RF phase range after the buncher was within $\pm 10^\circ$ RF ($2\sigma=2$ standard deviations) at the entrance of the inflector.

The result obtained in calculations was that the beam transmission in the range from the inflector entrance to the electro-static deflector was improved from 40 % to 65 %.

Further increase of the beam transmission through the central region electrode structure leads to some geometrical modifications. The changes concerned widening of the channel aperture between the 1st and the 2nd accelerating gap and removal of the post near the 2nd acceleration gap.

References

- [1] S. B. Vorozhtsov, A. S. Vorozhtsov, E. E. Perepelkin, S. Watanabe, S. Kubono, Y. Ohshiro, T. Mitsumoto, and A. Goto. h Beam Simulation of RIKEN K78 AVF Cyclotronh. CNS ANNUAL REPORT 2006, CNS-REP-76, December, 2007, p.57-58.
- [2] S. B. Vorozhtsov, A. S. Vorozhtsov, E. E. Perepelkin, S. Watanabe, S. Kubono, T. Mitsumoto, and A. Goto. gCalculations of the beam transmission and quality in the RIKEN AVF Cyclotronh: RIKEN Accel. Prog. Rep. 40 (2007).
- [3] A. Goto. Beam injection and extraction of RIKEN AVF cyclotron. CNS-RIKEN Workshop on Upgrade of AVF Cyclotron, CNS Wako Campus, 3-4 March 2008.
- [4] http://laacg1.lanl.gov/laacg/services/download_trace.phtml
- [5] E.E. Perepelkin and S.B. Vorozhtsov. eCBDA - Cyclotron Beam Dynamics Analysis code. User's Guidef. JINR, Dubna, July 31, 2006.

Theoretical Nuclear Physics

Electromagnetic Transitions in Exotic Carbon Isotopes

Toshio Suzuki^{a,b}, and Takaharu Otsuka^{b,c,d}

^a*Department of Physics, College of Humanities and Sciences, Nihon University*

^b*Center for Nuclear Study, University of Tokyo*

^c*Department of Physics, Graduate School of Science, University of Tokyo*

^d*RIKEN (The Institute of Physical and Chemical Research)*

Recently, neutron-rich carbon isotopes have been studied experimentally and their interesting exotic nature of structures have been revealed. Structure and electromagnetic properties of exotic neutron-rich carbon isotopes are investigated by shell model calculations. A recent shell model Hamiltonian for the p -shell, SFO [1], which properly takes into account important roles of spin-isospin interactions, is used for the study as a starting point. The Hamiltonian can describe magnetic and spin properties of p -shell nuclei quite well; agreements of calculated magnetic moments of p -shell nuclei with the observation have been systematically improved, and Gamow-Teller transition strengths in ^{12}C and ^{14}N are rather well reproduced. The Hamiltonian explains the change of magic numbers as well as shell evolutions near drip-lines [2]. This is due to the roles of the tensor force embedded in the Hamiltonian though its strength is not as strong as that of meson exchange interaction.

Here, the Hamiltonian is modified to enhance the effects of the tensor force in the $p - sd$ cross matrix elements by replacing the tensor components by $\pi + \rho$ meson exchange interactions. Corrections in $T=1$ monopole terms are also made. Behavior of neutron effective single-particle energies for the modified Hamiltonian is studied. The $1s_{1/2}$ and $0d_{5/2}$ orbits become almost degenerate at $N = 10$, and the $0d_{5/2}$ orbit gets to become gradually lower than the $1s_{1/2}$ orbit for $N > 10$ (see Fig. 1).

Topics on (1) electric quadrupole (E2) transitions in ^{16}C and ^{18}C , and (2) magnetic dipole (M1) transitions in ^{17}C , which show exotic nature of the carbon isotopes most prominently, are investigated. The E2 transition strengths are calculated with the use of neutron-number dependent effective charges [3] to take account of the decoupling of neutron and proton degrees of freedom. The anomalous hindrance of the transitions from the first 2^+ states observed [4] is rather well reproduced.

Exotic properties of two M1 transitions in ^{17}C , $1/2_1^+ \rightarrow 3/2_{g.s.}^+$ and $5/2_1^+ \rightarrow 3/2_{g.s.}^+$, are investigated. Conventional shell model Hamiltonians give similar transition rates for the two transitions while an anomalous asymmetry in the transition strength is observed [5]. We show that this asymmetry of the transition rates between the two M1 transitions [5] can be explained by our new modified Hamiltonian. Considerable suppression of the transition from the $1/2_1^+$ state is also obtained [6]. An important role of the tensor force as well as the shell evolution toward the neutron drip-line region is pointed out.

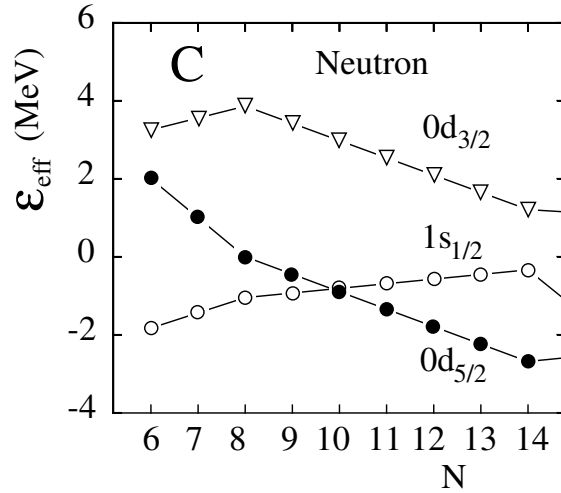


Figure 1. Neutron effective single particle energies for carbon isotopes obtained by the present Hamiltonian. N denotes number of neutrons.

References

- [1] T. Suzuki, R. Fujimoto and T. Otsuka, *Phys. Rev. C* **67**, 044302 (2003).
- [2] T. Otsuka, T. Suzuki, R. Fujimoto, H. Grawe and Y. Akaishi, *Phys. Rev. Lett.* **95**, 232502 (2005).
- [3] H. Sagawa and K. Asahi, *Phys. Rev. C* **63**, 064310 (2001); H. Sagawa, X. R. Zhou, X. Z. Zhang and T. Suzuki, *Phys. Rev. C* **70**, 054316
- [4] H. J. Ong et al, submitted to *Phys. Rev. C*.
- [5] D. Suzuki et al., submitted to *Phys. Lett. B*.
- [6] T. Suzuki and T. Otsuka, to be submitted.

Lattice Calculation of Thermal Properties of Neutron Matter with NN Effective Field Theory

T. Abe and R. Seki^a

Center for Nuclear Study, Graduate School of Science, University of Tokyo, Japan

^a*Department of Physics and Astronomy, California State University, Northridge, USA*

Neutron matter is of great interest in nuclear physics as a quantum many-body system [1]. The 1S_0 nucleon-nucleon (NN) interaction is strongly attractive, dominating the physics of neutron matter. The interaction yields the unnaturally large, negative scattering length a_0 with a moderate (natural) size of the effective range r_0 . The large value of a_0 corresponds to the strongly attractive interaction, and the NN pairing forms nearly a bound state. Owing to this interaction, neutron matter is a strongly interacting many-body system, exhibiting superfluidity, and must be treated nonperturbatively. Superfluidity in neutron matter is of astronomical interest because of the close relation to the internal structure and thermal evolution of neutron stars. Strong neutron-neutron correlations generated by the interaction are important for understanding the structure of neutron-rich unstable nuclei, especially of the weakly-bound, surface structure near the neutron drip line.

Investigations over many years have much clarified thermodynamical properties of neutron matter, but their reliable quantitative information is not yet fully available [1]. For example, the 1S_0 pairing gap at zero temperature Δ is firmly established in the *BCS approximation*, because various conventional NN potentials give nearly the same Δ_{BCS} as a function of the neutron matter density [1]. But several many-body calculations have shown that additional medium polarization effects drastically reduce the Δ to a fraction of Δ_{BCS} [1], while a recent work [2] does so only by about ten percent. Similar to this work, the quantum Monte Carlo calculations (using realistic NN interactions) recently reported yield Δ close to Δ_{BCS} : In the low density region of our interest (less than $k_F \approx 0.6 \text{ fm}^{-1}$), Δ by an auxiliary field diffusion Monte Carlo (AFDMC) calculation is nearly the same as Δ_{BCS} [3], and that by a Green's function Monte Carlo (GFMC) calculation [4] is smaller, approximately by 1/3.

We report a determinantal quantum Monte Carlo lattice calculation with NN effective field theory (EFT) with the objective of a reliable determination of Δ and the thermal properties of low-density neutron matter. As an extension of Ref. [5], our lattice Monte Carlo calculation is based on the Hamiltonian formulation [6], different from the Lagrangian formulation [7]. Note that EFT is also being applied to nuclear structure problems [8, 9, 10].

Our pionless neutron-neutron EFT interaction consists of the leading order (LO) and the next-to-leading order (NLO), and is determined from a_0 and r_0 on finite-spacing lattices [11]. The lattice Hamiltonian corresponds to the attractive Hubbard model in the LO and to the extended, attractive Hubbard model in the NLO [12]. The LO EFT description of low-density neutron matter is close to the unitary limit

($1/(k_F a_0) \rightarrow 0$) [13], to which much attention has been paid in the field of condensed matter and atomic physics.

In this work, we calculate Δ , the critical temperature T_c , and the pairing temperature scale T^* . These quantities are determined from correlation functions: 1) Δ is computed directly from the off-diagonal long-range order of the spin pair-pair correlation function. 2) T_c is extracted from the inflexion point of the spin pair-pair correlation sum. 3) T^* is determined from the temperature dependence of the Pauli spin susceptibility (the spin-spin correlation function).

The calculation is performed in two steps: First, we compute Δ , T_c , and T^* at the lattice-filling of $n = 1/4$ (one-eighth filling of the lattice). Second, we take the thermodynamic and continuum limits. The thermodynamical limit is taken using the finite-size scaling method with the $n = 1/4$ data of various lattice sizes; $N_s = 4^3, 6^3, 8^3$, and 10^3 . The continuum limit is taken as the $n \rightarrow 0$ limit, using the data of $n = 1/16, 1/8, 3/16, 1/4, 3/8$, and $1/2$. Here, we perform the continuum-limit computation using the data of $k_F = 60 \text{ MeV}$ and $N_s = 6^3$, as we expect the k_F and N_s dependence is weak in the n variation.

Figure 1 displays the density-dependence of our EFT Monte Carlo Δ in the thermodynamical and continuum limits, in comparison to the representative Δ_{BCS} [14] and to a higher-order RPA calculation including polarization effects [15]. As noted above, most of the RPA results are far smaller than Δ_{BCS} except for the recent one [2]. Our Δ is smaller than the Δ_{BCS} approximately by thirty percent, in agreement with Δ by the recent GFMC calculation [4], but disagree with the one by the AFDMC calculation [3].

Figure 2 presents the temperature-density phase diagram constructed from T_c and T^* in the thermodynamical and continuum limits. The figure illustrates thermodynamical properties of low-density neutron matter. For example, at a fixed density k_F , as the temperature goes down from the normal phase, the pairing is gradually enhanced, forming the pseudo-gap phase around and below T^* . As the temperature goes down further, the pairing gets stronger and eventually forms a long-range ordering at T_c , thereby generating the second-order phase transition to the superfluid phase. Note that the transition from the normal phase to the pseudo-gap phase is smooth, and the definition of T^* is somewhat subjective.

In conclusion, we report a determinantal quantum Monte Carlo lattice calculation of low-density neutron matter using the pionless, leading- and next-to-leading-order NN EFT potential. The 1S_0 pairing gap, the critical temperature of the normal-to-superfluid phase transition, and the pairing temperature scale are determined as a function of the neutron matter density. The pairing gap is found to be

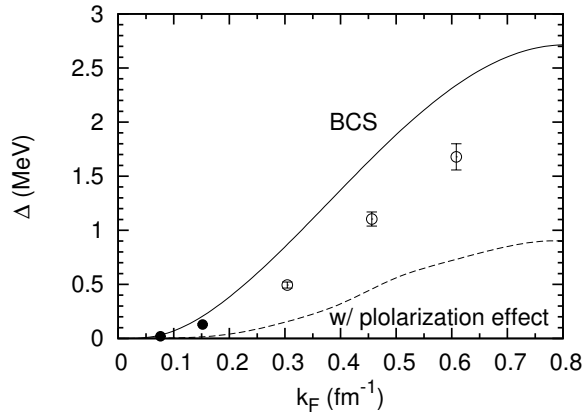


Figure 1. The 1S_0 pairing gap at $T = 0$, Δ , as a function of the Fermi momentum k_F representing the neutron density. The leading- and next-to-leading-order results in the thermodynamical and continuum limits are shown by solid and open circles, respectively, with statistical uncertainties. The solid curve is Δ_{BCS} of Ref. [14], while the dashed curve is a random-phase approximation of Ref. [15].

smaller than the BCS result approximately by thirty percent. The temperature-density phase diagram is presented for the density of $(10^{-4} - 10^{-1})\rho_0$. Though not elaborated here, the physics of neutron matter in this density region is clearly identified as a BCS-BEC crossover, in this work.

For the future work, we would like to improve following points related to the lattice size: 1) Our largest lattice size is $N_s = 10^3$, but the use of larger lattices is desirable to ensure a more reliable extrapolation to the thermodynamical limit. For such a large lattice size, the hybrid Monte Carlo method, commonly used in lattice QCD calculations, should require less computation time than the current determinantal method. 2) A closer examination of the continuum limit is needed, especially on its dependence of the lattice size so as to obtain the more accurate final results. This point may be important for T_c and T^* , which have a somewhat stronger lattice-filling dependence than Δ [6].

We thank U. van Kolck for his continuing support on our project and for clarifying various issues on EFT, H.-M. Müller for the use of his code with modification, and K.-F. Liu and T. Onogi for their instructive comments on lattice calculations. This work is supported by the U.S. DOE (Grant No. DE-FG02-87ER40347) at CSUN. The lattice calculations were carried out on Seaborg, Bassi, and Franklin at NERSC, U.S. DOE (Contract No. DE-AC03-76SF00098,) and at Titech Grid and TSUBAME, Tokyo Institute of Technology, Japan. We thank R. McKeown for his generous hospitality at Kellogg Rad. Lab., Caltech, where the major part of this work have been carried out over the last several years.

References

- [1] D. J. Dean and M. Hjorth-Jensen, *Rev. Mod. Phys.* **75** (2003) 607.
- [2] L. G. Cao, U. Lombardo, and P. Schuck, *Phys. Rev. C* **74** (2006) 064301.

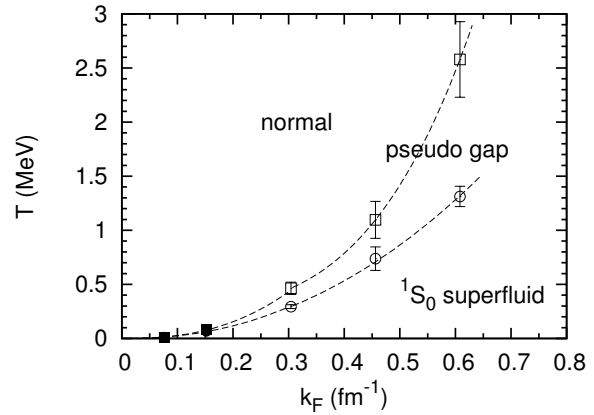


Figure 2. The 1S_0 temperature-density phase diagram of low-density neutron matter constructed from the critical temperature T_c and the pairing temperature scale T^* . The leading- and next-to-leading-order T_c and T^* in the thermodynamical and continuum limits are shown by solid and open symbols, respectively, with statistical uncertainties. The dotted curves are drawn by interpolation.

- [3] S. Gandolfi, A. Y. Illarionov, S. Fantoni, F. Pederiva and K. E. Schmidt, arXiv:0805.2513 [nucl-th] (2008).
- [4] A. Gezerlis and J. Carlson, *Phys. Rev. C* **77** (2008) 032801.
- [5] H.-M. Müller, S. E. Koonin, R. Seki, and U. van Kolck, *Phys. Rev. C* **61** (2000) 044320.
- [6] T. Abe and R. Seki, arXiv:0708.2523 [nucl-th] (2007).
- [7] D. Lee, arXiv:0804.3501 [nucl-th] (2008).
- [8] I. Stetcu, B. R. Barrett and U. van Kolck, *Phys. Lett. B* **653** (2007) 358.
- [9] T. Otsuka, T. Suzuki, and Y. Akaishi *AIP Conf. Proc.* **1011** (2008) 153.
- [10] A. Schwenk and J. D. Holt, *AIP Conf. Proc.* **1011** (2008) 159.
- [11] R. Seki and U. van Kolck, *Phys. Rev. C* **73** (2006) 044006.
- [12] T. Abe, R. Seki, and A. N. Kocharian, *Phys. Rev. C* **70** (2004) 014315 [Erratum-ibid. *C* **71** (2005) 059902].
- [13] T. Abe and R. Seki, arXiv:0708.2524 [nucl-th] (2007).
- [14] Ø. Elgarøy, L. Engvik, M. Hjorth-Jensen, and E. Osnes, *Nucl. Phys. A* **604** (1996) 466.
- [15] J. Wambach, T. L. Ainsworth, and D. Pines, *Nucl. Phys. A* **555** (1993) 218.

Other Activities

The Sixth CNS International Summer School (CISS07)

T. Kawabata, S. Kubono, S. Michimasa, T. Otsuka^a, H. Sakai^a, S. Shimoura, and T. Suzuki^b

Center for Nuclear Study, Graduate School of Science, University of Tokyo

^a*Department of Physics, Graduate School of Science, University of Tokyo*

^b*Department of Physics, Nihon University*

The 6th CNS International Summer School (CISS07) was held at the Wako branch of the Center for Nuclear Study (CNS), the University of Tokyo, in the period of August 28–September 1, 2007.

This summer school is the sixth one in the series which aimed at providing graduate students and Post Docs with basic knowledge and perspectives of nuclear physics. Topics of this year were “Green’s function method”, “High-energy RI-beam experiment”, “Nuclear astrophysics”, “Proton elastic scattering”, and “Di-neutron correlation”. Short lectures on “Quark-gluon plasma” and “RIKEN RI beam factory” were also presented.

The list of lecturers and the title of lectures are shown below.

W. H. Dickhoff (Washington University, USA)

“Comprehensive treatment of correlations at different energy scales in nuclei using Green’s functions”

T. Aumann (GSI, Darmstadt, Germany)

“Experiments with high-energy radioactive beams”

R. Hix (Oak Ridge National Laboratory, USA)

“An introduction to nuclear astrophysics”

H. Sakaguchi (Miyazaki University)

“Proton elastic scattering at intermediate energies and nuclear densities”

T. Suzuki (Nihon University and CNS)

“Weak and electromagnetic interactions in nuclei”

M. Matsuo (Niigata University)

“Di-neutron correlation and collective excitation in neutron-rich nuclei”

T. Hirano (University of Tokyo)

“Toward understanding of Quark-Gluon Plasma in relativistic heavy ion collisions”

T. Kubo (RIKEN)

“Overview of BigRIPS in-flight separator”

This year, 82 participants attended from 6 countries. Among them, 17 attendances were from Asian countries, China, Korea, Vietnam, Uzbekistan, and Bangladesh. Domestic participants were from 11 universities and 3 institutes over the country.

The lectures were given from 10:00 in the morning to 18:00 in the evening. The advanced lectures of the Green’s function method for theorists were given by Prof. W. H. Dickhoff after the normal lectures on Thursday and Friday. Student and Post Doc sessions were held in the school on Tuesday and Wednesday. 18 talks and 15 posters were presented by graduate students and Post Docs. Attendances also communicated each other in the free discussion time between the lectures and in the welcome and farewell parties with a relaxed atmosphere. All information concerning the summer school is open for access at the following URL:

<http://www.cns.s.u-tokyo.ac.jp/summerschool/>

Organizers thank all participants and all members of the CNS who supported the summer school. They are also grateful to RIKEN for their supports in the preparation of the school. This school was supported in part by the International Exchange Program of Graduate School of Science, the University of Tokyo, Japan-U.S. Theory Institute for Physics with Exotic Nuclei (JUSTIPEN) program, International Research Network for Exotic Femto Systems (EFES), and ICHOR project.

Laboratory Exercise for Undergraduate Students

T. Kawabata^a, K. Yako^b, S. Hayakawa^a, K. Miki^b, H. Sakai^b, and S. Shimoura^a

^aCenter for Nuclear Study, Graduate School of Science, University of Tokyo

^bDepartment of Physics, University of Tokyo, Tokyo

Nuclear scattering experiments were performed as a laboratory exercise for undergraduate students of the University of Tokyo. This program was aiming at providing undergraduate students with an opportunity to learn how to study the world of $< 10^{-14}$ m by using an ion beam from an accelerator. In 2007, 32 students joined this program.

The four beam times were scheduled in the second semester for juniors, and 8 students participated in each beam time. The experiment was performed at the RIKEN accelerator research facility (RARF) using a 26-MeV alpha beam accelerated by the AVF cyclotron. The alpha beam extracted from the AVF cyclotron was transported to the CRIB beam line in the E7 experimental room. In each beam time, the students were divided into two groups and took one of the following two subjects;

1. Measurement of gamma rays emitted in the cascade decay of the rotational bands in ^{154}Gd and ^{184}Os .
2. Measurement of elastic scattering of α particles from ^{197}Au .

A snapshot of students during a beam time is shown in Fig. 1.

Before the experiment, the students learned the basic handling of the semiconductor detectors and electronic circuits at the Hongo campus, and attended a radiation safety lecture at RIKEN. They also joined a tour to the RI beam facility, which was under construction at RIKEN.

In the measurement of the rotational bands, excited states in ^{154}Gd and ^{184}Os nuclei were populated by the $^{152}\text{Sm}(\alpha, 2n)$ and $^{182}\text{W}(\alpha, 2n)$ reactions, respectively. The gamma rays emitted from the cascade decay of the rotational bands were measured by a high purity germanium detector located 50 cm away from the target. The energies of the gamma rays were recorded by a multi-channel analyzer (MCA) system. The gain and the efficiency of the detector system had been calibrated with standard gamma-ray



Figure 1. Snapshot of students during a beam time.

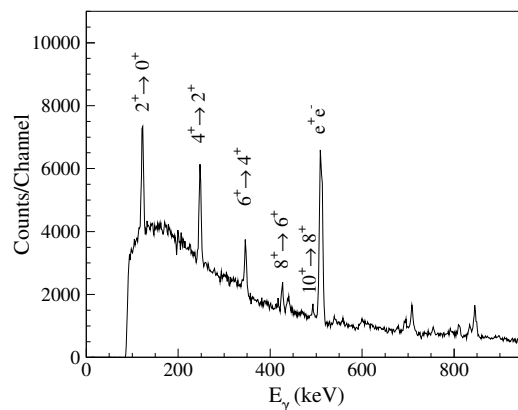


Figure 2. Typical spectrum of the gamma rays from the cascade decay of the rotational band in ^{154}Gd .

sources of ^{22}Na , ^{60}Co , ^{133}Ba , and ^{137}Cs . The typical spectrum of the gamma rays from the cascade decay of the rotational band in ^{154}Gd is shown in Fig. 2. The gamma rays from the $10^+ \rightarrow 8^+$ decay were successfully measured. Based on the energies of the gamma rays, the moment of inertia and the deformation parameters of the excited states were discussed by using a classical rigid rotor model and a irrotational fluid model. The students found that the reality lies between the two extreme models. The initial population among the levels in the rotational band was also discussed by taking the effect of internal conversion into account.

In the $\alpha + ^{197}\text{Au}$ measurement, α particles scattered from the Au target with a thickness of 1.42 mg/cm^2 were detected by a silicon PIN-diode located 11 cm away from the target. A plastic collimator with a diameter of 6 mm was attached on the silicon detector. The energy spectrum of the scattered α particles was recorded by the MCA system. The beam was stopped by a Faraday cup in the scattering chamber. The cross section for the alpha elastic scattering was measured in the angular range of $\theta_{\text{lab}} = 25\text{--}150^\circ$. The measured cross section was compared with the calculated cross section for the Rutherford scattering. The cross section was also analyzed by the potential-model calculation, and the radius of the gold nucleus was discussed. Some students obtained the radius of ~ 10 fm by using a classical model where the trajectory of the α particle in the nuclear potential is obtained by the Runge-Kutta method. Others tried to understand the scattering process by calculating the angular distribution by the distorted wave Born approximation with a Coulomb wave function and a realistic nuclear potential.

We believe this program is very impressive for the students. It was the first time for most of the students to use large experimental equipments. They learned basic things

about the experimental nuclear physics and how to extract physics from the data.

The authors would like to thank Dr. Y. Uwamino, Prof. Y. Sakurai, and the RARF cyclotron crew for their helpful effort in the present program.

Appendices

**Symposium, Workshop, Seminar, PAC and
External Review**

CNS Reports

Publication List

Talks and Presentations

Personnel

Workshop, Seminar, and PAC

A. Workshop

1. The International Workshop on "Direct reactions with Exotic Beams" (DREB2007) was held in Wako campus of RIKEN, on May 30-June 2, 2007. DREB2007 was the fifth International Workshop in a series of workshops initialized by researchers from MSU, Florida, Saclay and Orsay. DREB2007 intends to discuss the extraction of nuclear structure and astrophysical information from direct reactions with exotic beams as well as the understanding of reaction mechanisms. It also included the latest theoretical and experimental topics on varieties of reaction studies. DREB2007 was hosted by Faculty of Science at Kyushu University, RIKEN Nishina Center for Accelerator-Based Science and Center for Nuclear Study (CNS) at the University of Tokyo.
2. The third Japanese-German workshop on nuclear structure and astrophysics
September 29 - October 2, 2007, Frauenwoerth im Chiemsee, Germany
This was the third joint workshop between German and Japanese nuclear physicists. About 60 people joined including 19 Japanese participants. This workshop was organized by K. Langanke (GSI), P. Ring (Munich), T. Otsuka (Tokyo).
3. The first FIDIPRO-JSPS meeting on energy density functionals on nuclei
October 25-27, 2007, Jyväskylä, Finland.
This was a workshop to discuss the development of the density functional theory to calculate the wide mass range of nuclear systems. Also, this workshop was a good opportunity to celebrate the new theory group in Jyväskylä.
4. Correlations in Nuclei: From Di-nucleons to Clusters
November 26-29, 2007, Institute for Nuclear Theory, Washington University, USA.
This was a small workshop to discuss the many-body correlation in nuclear systems. The main issue was to include such correlations in the so called ab initio calculations. There were only 13 talks and much time was used for the discussions. The workshop was organized by B.R. Barrett (Arizona) and T. Otsuka (Tokyo).
5. The International Symposium on Origin of Matter and Evolution of Galaxies 2007: From Dawn of Universe to the Formation of Solar System,
Sapporo, Japan, December 4 – 7, 2007
This is the 10th international symposium of nuclear astrophysics, which started in 1988 by INS (predecessor of CNS) together with RIKEN.
It was hosted this time by seven institutions; Hokkaido University, Center for Nuclear Study, University of Tokyo (CNS), National Astronomical Observatory (NAO), RIKEN, Department of Astronomy (University of Tokyo), RCNP (Osaka), and KEK. The symposium was participated by 123 researchers, including 26 people from outside of Japan. Special emphasis was placed this time on evolution of first stars and nuclear astrophysics with RI beams. The symposium proceedings was published in a book of AIP conferences series (No. 1016).
Organizing committee was comprised of M.Y. Fujimoto (Hokkaido, Chair), S. Kubono (CNS, Tokyo, Co-chair), T. Kajino (NAOJ, Co-chair), K. Kato (Hokkaido, Co-chair), W. Aoki (NAOJ), T. Suda (RIKEN), H. Miyatake (KEK), T. Nozawa (Hokkaido), K. Ishikawa (Hokkaido), T. Suda (Hokkaido, scientific secretary), T. Motobayashi (RIKEN), T. Kishimoto (RCNP), K. Nomoto (Tokyo), S. Watanabe (Hokkaido), A. Ohnishi (Hokkaido), T. Nozawa (Hokkaido)
6. The 2nd LACM-EFES-JUSTIPEN Workshop
January 23-25, 2008, Oak Ridge National Laboratory, USA
The purpose of the present meeting was to bring together scientists (theorists and experimentalists) with interests in physics of radioactive nuclei, large amplitude collective motion, and theoretical approaches. One emphasis of the meeting was on topics related to future collaborations between US and Japanese groups (under JUSTIPEN). JUSTIPEN is the DOE project in USA to send nuclear physicists to Japan to promote the nuclear theory collaborations. About 70 scientists (20 were from Japan) have participated in. This workshop was organized by Hisashi Horiuchi (RCNP), Tetsuro Ishii (JAEA), Yoshiko Kanada-En'yo (YITP), Hiroari Miyatake (KEK), Tohru Motobayashi (RIKEN), Takashi Nakatsukasa (RIKEN), Takaharu Otsuka (CNS/Tokyo), Hideyuki Sakai (Tokyo), Tomohiro Uesaka (CNS), David Dean (Oak Ridge), Witek Nazarewicz (Oak Ridge), Thomas Papenbrock (Oak Ridge, Lead Organizer) Nicolas Schunck (Oak Ridge), Mario Stoitsov (Oak Ridge), Sherry Lamb (Oak Ridge, Secretary).

7. Future Prospects for Spectroscopy and Direct Reactions 2008
February 26-28, 2008, Michigan State University, USA.

The purpose of the workshop was to initiate and develop physics cases with upcoming heavy-ion spectrometers (for instance SHARAQ) in the field of structure of exotic nuclei and related problems. This workshop was organized by Alex Brown, Alexandra Gade, Thomas Glasmacher, Tohru Motobayashi, Tomohiro Uesaka, Taka Otsuka, Yutaka Utsuno, Remco Zegers, and Shari Conroy (secretary).

B. CNS Seminar

1. "Study of Single-particle structure in ^{23}F ",
S. Michimasa (CNS, University of Tokyo) May 25th, 2007.
2. "The Trojan Horse method and its application"
Silvio Cherubini (University of Catania and INFN-LNS) Nov. 28th, 2007.

C. Program Advisory Committee for Nuclear-Physics Experiments at RI Beam Factory

1. The 2nd NP-PAC meeting
Date: September 12–13, 2007
Place: Conference room, 2F RIBF building

Four experimental proposals for CRIB were examined in the 2nd NP-PAC meeting.

2. The 3rd NP-PAC meeting
Date: February 18–19, 2008
Place: Okochi Hall, RIKEN

Four experimental proposals for CRIB were examined in the 3rd NP-PAC meeting.

D. CNS Advisory Committee

The 7th CNS AC meeting
Date: February 21, 2008.
Place: Nishina Memorial Hall, RIKEN

A CNS advisory committee meeting was held on February 21, 2008, to receive oral presentations of research activities and future plans of the Center.

The Committee members:

Prof. Kichiji Hatanaka (Chair, RCNP Osaka University)
Prof. Hideto En'yo (RIKEN Nishina Center)
Prof. Kazuhiro Yabana (University of Tsukuba)
Prof. Atsuko Odahara (Osaka University)
Prof. Ikuko Hamamoto (Lund University)
Prof. Wolfgang Mittig (GANIL)

The Committee evaluated (i) scientific and educational activities of the research groups of CNS in fiscal year 2007, and (ii) research and education plans of each group from the fiscal year 2008.

CNS Reports

- #70** “Onset of J/ψ Melting in Quark-Gluon Fluid at RHIC”,
T. Gunji, H. Hamagaki, T. Hatsuda, and T. Hirano, February 2008.
- #71** “Lifetime of the Isomeric 0_2^+ State in ^{12}Be ”,
S. Shimoura, S. Ota, K. Demichi, N. Aoi, H. Baba, Z. Elekes, T. Fukuchi, T. Gomi, K. Hasegawa, E. Ideguchi, M. Ishihara, N. Iwasa, H. Iwasaki, S. Kanno, S. Kubono, K. Kurita, M. Kurokawa, Y.U. Matsuyama, S. Michimasa, K. Miller, T. Minemura, T. Motobayashi, T. Murakami, M. Notani, A. Odahara, A. Saito, H. Sakurai, E. Takeshita, S. Takeuchi, M. Tamaki, T. Teranishi, K. Yamada, Y. Yanagisawa, I. Hamamoto, April. 2007.
- #72** “Production of Direct Photons and Neutral Pions in Relativistic Au+Au Collisions”,
Tadaaki Isobe, July 2007.
- #73** “ J/ψ Production in High Energy Heavy Ion Collisions at RHIC”,
Taku Gunji, July 2007.
- #74** “Measurement of Single Electrons from Semileptonic Decays of Heavy Quarks in Au+Au Collisions at 200 A GeV”,
Fukutaro Kajihara, July 2007.
- #75** “Measurement of J/ψ Yield in d+Au Collisions at $\sqrt{s_{NN}} = 200$ GeV”,
Soichiro Kametani, July 2007.
- #76** “CNS Annual Report 2006”,
edited by T. Gunji, July. 2007.
- #77** “Development of a Cryogenic Gas Target System for Intense Radioisotope Beam Production at CRIB”,
H. Yamaguchi, Y. Wakabayashi, G. Amadio, S. Hayakawa, H. Fujikawa, S. Kubono, J.J. He, A. Kim, and D.N. Binh,
March 2008.

Publication List

A. Original Papers

1. Y. Satou, T. Nakamura, N. Fukuda, T. Sugimoto, Y. Kondo, N. Matsui, Y. Hashimoto, T. Nakabayashi, T. Okumura, M. Shinohara, T. Motobayashi, Y. Yanagisawa, N. Aoi, S. Takeuchi, T. Gomi, Y. Togano, S. Kawai, H. Sakurai, H.J. Ong, T.K. Onishi, S. Shimoura, M. Tamaki, T. Kobayashi, H. Otsu, Y. Matsuda, N. Endo, M. Kitayama, M. Ishihara, “Unbound excited states in $^{19,17}\text{C}$ ”, *Phys. Lett. B* **660** (2008) 320-325
2. I. Hamamoto and S. Shimoura: “Properties of ^{12}Be and ^{11}Be in terms of single-particle motion in deformed potential”, *J. Phys. G* **34** (2007) 2715–2725
3. T. Sugimoto, T. Nakamura, Y. Kondo, N. Aoi, H. Baba, D. Bazin, N. Fukuda, T. Gomi, H. Hasegawa, N. Imai, M. Ishihara, T. Kobayashi, T. Kubo, M. Miura, T. Motobayashi, H. Otsu, A. Saito, H. Sakurai, S. Shimoura, A.M. Vinodkumar, K. Watanabe, Y.X. Watanabe, T. Yakushiji, Y. Yanagisawa, K. Yoneda: “The first 2^+ state of ^{14}Be ”, *Phys. Lett. B* **654** (2007) 160–164
4. S. Shimoura, S. Ota, K. Demichi, N. Aoi, H. Baba, Z. Elekes, T. Fukuchi, T. Gomi, K. Hasegawa, E. Ideguchi, M. Ishihara, N. Iwasa, H. Iwasaki, S. Kanno, S. Kubono, K. Kurita, M. Kurokawa, Y.U. Matsuyama, S. Michimasa, K. Miller, T. Minemura, T. Motobayashi, T. Murakami, M. Notani, A. Odahara, A. Saito, H. Sakurai, E. Takeshita, S. Takeuchi, M. Tamaki, T. Teranishi, K. Yamada, Y. Yanagisawa, I. Hamamoto: “Lifetime of the isomeric 0^+ state in ^{12}Be ”, *Phys. Lett. B* **654** (2007) 87–91
5. T. Shizuma, T. Ishii, H. Makii, T. Hayakawa, S. Shigematsu, M. Matsuda, E. Ideguchi, Y. Zheng, M. Liu, T. Morikawa: “Evidence for a $K^\pi = 1/2^+$ isomer in neutron-rich ^{185}Ta ”, *Eur. Phys. J. A* **34** (2007) 1-4
6. M. Sandzelius, B. Hadinia, B. Cederwall, K. Andgren, E. Ganioglu, I.G. Darby, M.R. Dimmock, S. Eeckhaudt, T. Grahn, P.T. Greenlees, E. Ideguchi, P.M. Jones, D.T. Joss, R. Julin, S. Juutinen, A. Khaplanov, M. Leino, L. Nelson, M. Niikura, M. Nyman, R.D. Page, J. Pakarinen, E.S. Paul, M. Petri, P. Rahkila, J. Saren, C. Scholey, J. Sorri, J. Uusitalo, R. Wadsworth, R. Wyss: “Identification of Excited States in the $T_z=1$ Nucleus ^{110}Xe : Evidence for Enhanced Collectivity near the $N=Z=50$ Double Shell Closure”, *Phys. Rev. Lett.* **99** 022501 (2007) (4 pages)
7. C.J. Chiara, M. Devlin, E. Ideguchi, D.R. LaFosse, F. Lerma, W. Reviol, S.K. Ryu, D.G. Sarantites, O.L. Pechenaya, C. Baktash, A. Galindo-Uribarri, M.P. Carpenter, R.V.F. Janssens, T. Lauritsen, C.J. Lister, P. Reiter, D. Seweryniak, P. Fallon, A. Gorgen, A.O. Macchiavelli, D. Rudolph, G. Stoitcheva, and W.E. Ormand: “Probing sd-fp cross-shell interactions via terminating configurations in $^{42,43}\text{Sc}$ ” *Phys. Rev. C* **75** (2007) 054305 (18 pages); Correction: *Phys. Rev. C* **75** (2007) 059904
8. K. Morita, K. Morimoto, D. Kaji, T. Akiyama, S. Goto, H. Haba, E. Ideguchi, K. Katori, H. Koura, H. Kikunaga, H. Kudo, T. Ohnishi, A. Ozawa, N. Sato, T. Suda, K. Sueki, F. Tokanai, T. Yamaguchi, A. Yoneda, A. Yoshida: “Observation of Second Decay Chain from $^{278}113$ ”, *J. Phys. Soc. Jpn.* **76** (2007) 045001 (2 pages)
9. K. Morita, K. Morimoto, D. Kaji, T. Akiyama, S. Goto, H. Haba, E. Ideguchi, K. Katori, H. Koura, H. Kudo, T. Ohnishi, A. Ozawa, T. Suda, K. Sueki, F. Tokanai, T. Yamaguchi, A. Yoneda, A. Yoshida: “Experiment on Synthesis of an Isotope $^{277}112$ by $^{208}\text{Pb} + ^{70}\text{Zn}$ Reaction”, *J. Phys. Soc. Jpn.* **76** (2007) 043201 (5 pages)
10. J. Gibelin, D. Beaumel, T. Motobayashi, N. Aoi, H. Baba, Y. Blumenfeld, Zs. Dombradi, Z. Elekes, S. Fortier, N. Frascaria, N. Fukuda, T. Gomi, K. Ishikawa, Y. Kondo, T. Kubo, V. Lima, T. Nakamura, A. Saito, Y. Satou, E. Takeshita, S. Takeuchi, T. Teranishi, Y. Togano, A. M. Vinodkumar, Y. Yanagisawa, K. Yoshida: “Measurement of the $B(E2, 0_1^+ \rightarrow 2_1^+)$ in the $N=16$ nucleus ^{26}Ne ”, *Phys. Rev. C* **75** (2007) 057306.
11. T. Teranishi, S. Kubono, H. Yamaguchi, J.J. He, A. Saito, H. Fujikawa, G. Amadio, M. Niikura, S. Shimoura, Y. Wakabayashi, S. Nishimura, M. Nishimura, J.Y. Moon, C.S. Lee, A. Odahara, D. Sohler, L.H. Khiem, Z.H. Li, G.Lian and W.P. Liu: “Single-particle resonance levels in ^{14}O examined by $^{13}\text{N}+p$ elastic resonance scattering” *Phys. Lett. B* **650** (2007) 129-134.
12. J. J. He, S. Kubono, T. Teranishi, M. Notani, H. Baba, S. Nishimura, J.Y. Moon, M. Nishimura, H. Iwasaki, Y. Yanagisawa, N. Hokoiva, M. Kibe, J.H. Lee, S. Kato, Y. Gono, and C.S. Lee: “Investigation of Structure in ^{23}Al via Resonant Proton Scattering of $^{22}\text{Mg}+p$ and the $^{22}\text{Mg}(p,g)^{23}\text{Al}$ Astrophysical Reaction Rate”, *Phys. Rev. C* **76** (2007) 055802

13. Y.K. Kwon, C.S. Lee and S. Kubono: “Elastic Scattering of 120-MeV Alpha Particles by ^{28}Si ”, Jour. Korean Phys. Soc., 51 (2007) 1635 - 1639
14. J. J. He, S. Kubono, T. Teranishi, M. Notani, H. Baba, S. Nishimura, J. Y. Moon, M. Nishimura, S. Michimasa, H. Iwasaki, Y. Yanagisawa, N. Hokoïwa, M. Kibe, J. H. Lee, S. Kato, Y. Gono, and C.S. Lee: “A Study of the Proton Resonant Property in ^{22}Mg by Elastic Scattering of $^{21}\text{Na}+p$ and Its Astrophysical Implication in the $^{18}\text{Ne}(\alpha,p)^{21}\text{Na}$ Reaction Rate”, Eur. Phys. J. A. (2008) in press
15. H. Yamaguchi, Y. Wakabayashi, G. Amadio, S. Hayakawa, H. Fujikawa, S. Kubono, J. J. He, A. Kim, and D. N. Binh: “Development of a cryogenic gas target system for intense radioisotope beam production at CRIB”, Nucl. Instr. Meth. A. (2008) in press.
16. S. Terashima, H. Sakaguchi, H. Takeda, T. Ishikawa, M. Itoh, T. Kawabata, T. Murakami, M. Uchida, Y. Yasuda, M. Yosoi, J. Zenihiro, H. P. Yoshida, T. Noro, T. Ishida, S. Asaji, T. Yonemura, “Proton elastic scattering from tin isotopes at 295 MeV and systematic change of neutron density distributions”, Phys. Rev. C **77** (2008) 024317.
17. R. G. T. Zegers, E. F. Brown, H. Akimune, Sam M. Austin, A. M. van den Berg, B. A. Brown, D. A. Chamulak, Y. Fujita, M. Fujiwara, S. Galés, M. N. Harakeh, H. Hashimoto, R. Hayami, G. W. Hitt, M. Itoh, T. Kawabata, K. Kawase, M. Kinoshita, K. Nakanishi, S. Nakayama, S. Okumura, Y. Shimbara, M. Uchida, H. Ueno, T. Yamagata, M. Yosoi, “Gamow-Teller strength for the analog transitions to the first $T = 1/2$, $J = 3/2$ states in ^{13}C and ^{13}N and the implications for type Ia supernovae”, Phys. Rev. C **77** (2008) 024307.
18. F. Sakuma, J. Chiba, H. En’yo, H. Hamagaki, K. Ozawa, et al.; “Nuclear-Matter Modification of Decay Widths in the $\phi \rightarrow e^+e^-$ and $\phi \rightarrow K^+K^-$ Channels”, Phys. Rev. Lett. **98** (2007) 152302.
19. A. Adare, S. Afanasiev, C. Aidala, T. Gunji, H. Hamagaki, T. Isobe, F. Kajihara, S. Kametani, N. Kurihara, S.X. Oda, K. Ozawa, T. Sakaguchi, et al.; “Scaling Properties of Azimuthal Anisotropy in Au+Au and Cu+Cu Collisions at $\sqrt{s_{NN}} = 200$ GeV”, Phys. Rev. Lett. **98** (2007) 162301.
20. A. Adare, S. Afanasiev, C. Aidala, T. Gunji, H. Hamagaki, T. Isobe, F. Kajihara, S. Kametani, N. Kurihara, S.X. Oda, K. Ozawa, T. Sakaguchi, et al.; “Energy Loss and Flow of Heavy Quarks in Au+Au Collisions at $\sqrt{s_{NN}} = 200$ GeV”, Phys. Rev. Lett. **98** (2007) 172301.
21. S.S Adler, S. Afanasiev, C. Aidala, H. Hamagaki, M. Inuzuka, F. Kajihara, S. Kametani, T. Kawabata, T. Matsumoto, K. Oyama, K. Ozawa, T. Sakaguchi, et al. “Centrality Dependence of π^0 and η Production at Large Transverse Momentum in $\sqrt{s_{NN}} = 200$ GeV d+Au Collisions”, Phys. Rev. Lett. **98** (2007) 172302.
22. S.S. Adler, S. Afanasiev, C. Aidala, H. Hamagaki, M. Inuzuka, F. Kajihara, S. Kametani, T. Kawabata, T. Matsumoto, K. Oyama, K. Ozawa, T. Sakaguchi, et al.; “Production of omega mesons at large transverse momenta in p+p and d+Au collisions at $\sqrt{s_{NN}} = 200$ GeV”, Phys. Rev. C **75** (2007) 051902(R).
23. A. Adare, S. Afanasiev, C. Aidala, T. Gunji, H. Hamagaki, T. Isobe, F. Kajihara, S. Kametani, N. Kurihara, K. Ozawa, T. Sakaguchi, et al: “Correlated production of p and \bar{p} in Au+Au collisions at $\sqrt{s_{NN}} = 200$ GeV”, Phys. Lett. B **649** (2007) 359-369.
24. A. Adare, S.S Adler, S. Afanasiev, T. Gunji, H. Hamagaki, M. Inuzuka, T. Isobe, F. Kajihara, S. Kametani, T. Kawabata, N. Kurihara, T. Matsumoto, S.X. Oda, K. Oyama, K. Ozawa, T. Sakaguchi, et al.; “System size and energy dependence of jet-induced hadron pair correlation shapes in Cu+Cu and Au+Au collisions at $\sqrt{s_{NN}} = 200$ and 62.4 GeV”, Phys. Rev. Lett. **98** (2007) 232302.
25. A. Adare, S. Afanasiev, C. Aidala, T. Gunji, H. Hamagaki, T. Isobe, F. Kajihara, S. Kametani, N. Kurihara, S.X. Oda, K. Ozawa, et al.; “ J/ψ Production versus Transverse Momentum and Rapidity in p+p Collisions at $\sqrt{s} = 200$ GeV”, Phys. Rev. Lett. **98** (2007) 232002.
26. A. Adare, S. Afanasiev, C. Aidala, T. Gunji, H. Hamagaki, T. Isobe, F. Kajihara, S. Kametani, N. Kurihara, S.X. Oda, K. Ozawa, T. Sakaguchi, et al.; “ J/ψ production versus centrality, transverse momentum, and rapidity in Au + Au collisions at $\sqrt{s_{NN}} = 200$ GeV”, Phys. Rev. Lett. **98** (2007) 232301.
27. S. Afanasiev, C. Aidala, T. Gunji, H. Hamagaki, T. Isobe, F. Kajihara, S. Kametani, N. Kurihara, K. Ozawa, T. Sakaguchi, et al.; “Elliptic Flow for ϕ Mesons and (Anti)deuterons in Au+Au Collisions at $\sqrt{s_{NN}} = 200$ GeV”, Phys. Rev. Lett. **99** (2007) 052301.

28. S.S. Adler, S. Afanasiev, C. Aidala, H. Hamagaki, S. Kametani, T. Matsumoto, K. Oyama, K. Ozawa, T. Sakaguchi, et al.; “Measurement of density correlations in pseudorapidity via charged particle multiplicity fluctuations in Au plus Au collisions at $\sqrt{s_{NN}} = 200$ GeV”, Phys. Rev. C **76** (2007) 034903.
29. A. Adare, S. Afanasiev, T. Gunji, H. Hamagaki, I. Isobe, F. Kajihara, S. Kametani, N. Kurihara, S.X. Oda, K. Ozawa, et al.; “Inclusive cross section and double helicity asymmetry for π^0 production in p+p collisions at $\sqrt{s} = 200$ GeV : Implications for the polarized gluon distribution in the proton”, Phys. Rev. D **76** (2007) 051106(R).
30. S.S. Adler, S. Afanasiev, C. Aidala, H. Hamagaki, S. Kametani, T. Matsumoto, K. Oyama, K. Ozawa, T. Sakaguchi, et al.; “Detailed study of high-p(T) neutral pion suppression and azimuthal anisotropy in Au plus Au collisions at $\sqrt{s} = 200$ GeV”, Phys. Rev. C **76** (2007) 034904.
31. T. Gunji, H. Hamagami, T. Hatsuda, T. Hirano; “Onset of J/ψ Melting in Quark-Gluon Fluid at RHIC”, Phys. Rev. C **76** (2007) 051901.
32. S.S. Adler, S. Afanasiev, H. Hamagaki, S. Kametani, T. Matsumoto, K. Oyama, K. Ozawa, T. Sakaguchi, et al.; “Measurement of single muons at forward rapidity in p+p collisions at $\sqrt{s} = 200$ GeV and implications for charm production”, Phys. Rev. D **76** (2007) 092002.
33. A. Adare, S. Afanasiev, C. Aidala, T. Gunji, H. Hamagaki, T. Isobe, F. Kajihara, S. Kametani, N. Kurihara, S.X. Oda, K. Ozawa, et al.; “Transverse momentum and centrality dependence of dihadron correlations in Au+Au collisions at $\sqrt{s_{NN}} = 200$ GeV: Jet-quenching and the response of partonic matter”, Phys. Rev. C **77** (2008) 011901.
34. S.S. Adler, S. Afanasiev, C. Aidala, H. Hamagaki, M. Inuzuka, F. Kajihara, S. Kametani, T. Kawabata, T. Matsumoto, K. Oyama, T. Sakaguchi, et al.; “Centrality dependence of charged hadron production in deuteron-gold and nucleon-gold collisions at $\sqrt{s} = 200$ GeV”, Phys. Rev. C **77** (2008) 014905.
35. A. Adare, S.S. Adler, S. Afanasiev, T. Gunji, H. Hamagaki, M. Inuzuka, T. Isobe, F. Kajihara, S. Kametani, T. Kawabata, N. Kurihara, T. Matsumoto, S.X. Oda, K. Oyama, K. Ozawa, et al.; “Cold nuclear matter effects on J/ψ production as constrained by deuteron-gold measurements at $\sqrt{s_{NN}} = 200$ GeV”, Phys. Rev. C **77** (2008) 024912.

B. Proceedings

1. Z. Elekes, Zs. Dombrádi, N. Aoi, H. Baba, S. Bishop, K. Demichi, Zs. Fülöp, J. Gibelin, T. Gomi, H. Hasegawa, Y. Hashimoto, N. Imai, M. Ishihara, N. Iwasa, H. Iwasaki, G. Kalinka, S. Kanno, S. Kawai, T. Kishida, Y. Kondo, A.A. Korshennikov, T. Kubo, K. Kurita, M. Kurokawa, N. Matsui, Y. Matsuyama, S. Michimasa, T. Minemura, T. Motobayashi, T. Nakamura, T. Nakao, E.Yu. Nikolskii, M. Notani, T.K. Ohnishi, T. Okumura, H.J. Ong, S. Ota, A. Ozawa, A. Perera, A. Saito, H.K. Sakai, H. Sakurai, Y. Satou, S. Shimoura, D. Sohler, T. Sumikama, D. Suzuki, M. Suzuki, H. Takeda, E. Takeshita, S. Takeuchi, M. Tamaki, Y. Togano, K. Yamada, Y. Yanagisawa, K. Yoneda, “The study of shell closures in light neutron-rich nuclei”, Proc. of Nuclear Physics in Astrophysics III, DRESDEN, GERMANY, 26–31 MARCH 2007, J. Phys. G **35** (2008) 014038 (7 pages).
2. Z. Elekes, Zs. Dombrádi, A. Saito, N. Aoi, H. Baba, K. Demichi, Zs. Fülöp, J. Gibelin, T. Gomi, H. Hasegawa, N. Imai, M. Ishihara, H. Iwasaki, S. Kanno, S. Kawai, T. Kishida, T. Kubo, K. Kurita, Y. Matsuyama, S. Michimasa, T. Minemura, T. Motobayashi, M. Notani, T.K. Ohnishi, H.J. Ong, S. Ota, A. Ozawa, H.K. Sakai, H. Sakurai, S. Shimoura, E. Takeshita, S. Takeuchi, M. Tamaki, Y. Togano, K. Yamada, Y. Yanagisawa, K. Yoneda, “Study of N=20 shell gap with $^1\text{H}(^{28}\text{Ne}, ^{27,28}\text{Ne})$ reactions” Proc. of 7th International Conference on Radioactive Nuclear Beams (RNB7), Jul. 3–7, 2006, Cortina d’Ampezzo, Italy, Eur. Phys. J. Special Topics **150** (2007) 99–102.
3. S. Shimoura: “High Resolution Magnetic Spectrometer SHARAQ in RIBF”, Proc. Int. Symposium on Exotic Nuclei (EXON2006), ed. Yu. E. Penionzhkevich and E.A. Cherepanov, Khanty-Mansiysk, Russia, 17-22 July 2006, AIP Conf. Proc. **912** (2007) 406–411.
4. H. Baba, S. Shimoura, T. Minemura, Y.U. Matsuyama, A. Saito, H. Ryuto, N. Aoi, T. Gomi, Y. Higurashi, K. Ieki, N. Imai, N. Iwasa, H. Iwasaki, S. Kanno, S. Kubono, M. Kunibu, S. Michimasa, T. Motobayashi, T. Nakamura, H. Sakurai, M. Serata, E. Takeshita, S. Takeuchi, T. Teranishi, K. Ue, K. Yamada, Y. Yanagisawa: “Isoscalar compressional strengths in ^{14}O ”, Proc. of the 2nd International Conference on Collective Motion in Nuclei under Extreme Conditions (COMEX2), Jul. 20–23, 2006, Sankt Goar, Germany, Nucl. Phys. A **788** (2007) 188c–193c.

5. S. Michimasa, S. Shimoura, H. Iwasaki, M. Tamaki, S. Ota, N. Aoi, H. Baba, N. Iwasa, S. Kanno, S. Kubono, K. Kurita, N. Kurokawa, T. Minemura, T. Motobayashi, M. Notani, H.J. Ong, A. Saito, H. Sakurai, E. Takeshita, S. Takeuchi, Y. Yanagisawa, A. Yoshida: “Proton Shell Structure in Neutron-rich ^{23}F ”, Proc. of the Ninth International Conference on Nucleus-Nucleus Collisions - (NN2006), Nucl. Phys. A **787** (2007) 569c–574c.
6. J. Gibelin, D. Beaumel, T. Motobayashi, N. Aoi, H. Baba, Y. Blumenfeld, Z. Elekes, S. Fortier, N. Frascaria, N. Fukuda, T. Gomi, K. Ishikawa, Y. Kondo, T. Kubo, V. Lima, T. Nakamura, A. Saito, Y. Satou, E. Takeshita, S. Takeuchi, T. Teranishi, Y. Togano, A. M. Vinodkumar, Y. Yanagisawa, K. Yoshida: “Search for low lying dipole strength in the neutron rich nucleus ^{26}Ne ”, Nucl. Phys. A **788** (2007) 153c.
7. “Proton resonance scattering on ^7Be ”, H. Yamaguchi, A. Saito, J.J. He, Y. Wakabayashi, G. Amadio, H. Fujikawa, S. Kubono, L.H. Khim, Y.K. Kwon, M. Niikura, T. Teranishi, S. Nishimura, Y. Togano, N. Iwasa and K. Inafuku, Proceedings of the International Symposium on Nuclear Astrophysics “Nuclei in the Cosmos - IX”, CERN, Geneva, June 25-30, 2006, Proceedings of Science, PoS(NIC-IX)049, (2007).
8. K. Shimada, D. Nagae, K. Asahi, T. Arai, M. Takemura, T. Inoue, K. Takase, S. Kagami, N. Hatakeyama, Y. Kobayashi, H. Ueno, A. Yoshimi, D. Kameda, T. Nagatomo, T. Sugimoto, S. Kubono, H. Yamaguchi, Y. Wakabayashi, G. Amadio, S. Hayakawa, J. Murata, and H. Kawamura: “Production of polarized radioactive beams via the inverse-kinematics reactions and their applications”, AIP Conf. Proc. **915** (2007) 857–860.
9. T. Uesaka, T. Wakui, S. Sakaguchi, T. Kawahara, H. Sakai, “Polarized proton target for RI beam experiments”, Eur. Phys. J. Special Topics **150** (2007) 71–74.
10. J. Lajoie for the PHENIX Collaboration; “PHENIX highlights I: propagation of partons in a coloured medium”, Proc. of The 19th International Conference on Ultra-Relativistic Nucleus-Nucleus Collisions (Quark Matter 2007), Shanghai, China, Nov. 14 – 20, 2006, (editors) Ma Y-G, Wang E-K, Cai X, Huang H-Z, Wang X-N, and Zhu Z-Y, J. Phys. G **34** (2007) S191 – S198.
11. C. Zhang (for the PHENIX Collaboration); “Studying the medium modification of jets via high- p_T hadron angular correlations”, Proc. of The 19th International Conference on Ultra-Relativistic Nucleus-Nucleus Collisions (Quark Matter 2007), Shanghai, China, Nov. 14 – 20, 2006, (editors) Ma Y-G, Wang E-K, Cai X, Huang H-Z, Wang X-N, and Zhu Z-Y, J. Phys. G **34** (2007) S671 – S674.
12. A. Sickles (for the PHENIX Collaboration); “Identified particle jet correlations from PHENIX”, Proc. of The 19th International Conference on Ultra-Relativistic Nucleus-Nucleus Collisions (Quark Matter 2007), Shanghai, China, Nov. 14 – 20, 2006, (editors) Ma Y-G, Wang E-K, Cai X, Huang H-Z, Wang X-N, and Zhu Z-Y, J. Phys. G **34** (2007) S685 – S688.
13. A.M. Glenn (for the PHENIX Collaboration); “PHENIX results for J/ψ transverse momentum and rapidity dependence in Au+Au and Cu+Cu collisions”, Proc. of The 19th International Conference on Ultra-Relativistic Nucleus-Nucleus Collisions (Quark Matter 2007), Shanghai, China, Nov. 14 – 20, 2006, (editors) Ma Y-G, Wang E-K, Cai X, Huang H-Z, Wang X-N, and Zhu Z-Y, J. Phys. G **34** (2007) S737 – S740.
14. T. Gunji (for the PHENIX Collaboration); “Centrality dependence of J/ψ production in Au + Au and Cu + Cu collisions by the PHENIX experiment at RHIC”, Proc. of The 19th International Conference on Ultra-Relativistic Nucleus-Nucleus Collisions (Quark Matter 2007), Shanghai, China, Nov. 14 – 20, 2006, (editors) Ma Y-G, Wang E-K, Cai X, Huang H-Z, Wang X-N, and Zhu Z-Y, J. Phys. G **34** (2007) S749 – S752.
15. S. Sakai (for the PHENIX Collaboration); “Elliptic flow of electrons from heavy flavour decay by PHENIX”, Proc. of The 19th International Conference on Ultra-Relativistic Nucleus-Nucleus Collisions (Quark Matter 2007), Shanghai, China, Nov. 14 – 20, 2006, (editors) Ma Y-G, Wang E-K, Cai X, Huang H-Z, Wang X-N, and Zhu Z-Y, J. Phys. G **34** (2007) S753 – S756.
16. F. Kajihara (for the PHENIX Collaboration); “Heavy Quark Measurement by Single Electrons in the PHENIX Experiment”, Proc. of The 19th International Conference on Ultra-Relativistic Nucleus-Nucleus Collisions (Quark Matter 2007), Shanghai, China, Nov. 14 – 20, 2006, (editors) Ma Y-G, Wang E-K, Cai X, Huang H-Z, Wang X-N, and Zhu Z-Y, J. Phys. G **34** (2007) S763 – 768.
17. A. Bickley (for the PHENIX Collaboration); “Heavy quarkonia production in p+p collisions from the PHENIX experiment”, Proc. of The 19th International Conference on Ultra-Relativistic Nucleus-Nucleus Collisions (Quark Matter 2007), Shanghai, China, Nov. 14 – 20, 2006, (editors) Ma Y-G, Wang E-K, Cai X, Huang H-Z, Wang X-N, and Zhu Z-Y, J. Phys. G **34** (2007) S779 – S782.

18. V.S. Pantuev (for the PHENIX Collaboration); “PHENIX measurements of reaction plane dependence of high- p_T photons and pions”, Proc. of The 19th International Conference on Ultra-Relativistic Nucleus-Nucleus Collisions (Quark Matter 2007), Shanghai, China, Nov. 14 – 20, 2006, (editors) Ma Y-G, Wang E-K, Cai X, Huang H-Z, Wang X-N, and Zhu Z-Y, J. Phys. G **34** (2007) S805 – S808.
19. J. Jin (for the PHENIX Collaboration); “PHENIX measurement of high- p_T hadron-hadron and photon-hadron azimuthal correlations”, Proc. of The 19th International Conference on Ultra-Relativistic Nucleus-Nucleus Collisions (Quark Matter 2007), Shanghai, China, Nov. 14 – 20, 2006, (editors) Ma Y-G, Wang E-K, Cai X, Huang H-Z, Wang X-N, and Zhu Z-Y, J. Phys. G **34** (2007) S813 – S816.
20. D. Peressounko (for the PHENIX Collaboration); “Direct photons at low p_T measured in PHENIX”, Proc. of The 19th International Conference on Ultra-Relativistic Nucleus-Nucleus Collisions (Quark Matter 2007), Shanghai, China, Nov. 14 – 20, 2006, (editors) Ma Y-G, Wang E-K, Cai X, Huang H-Z, Wang X-N, and Zhu Z-Y, J. Phys. G **34** (2007) S869 – S872.
21. T. Chujo (for the PHENIX Collaboration); “Excitation function of baryon anomaly and freeze-out properties at RHIC-PHENIX”, Proc. of The 19th International Conference on Ultra-Relativistic Nucleus-Nucleus Collisions (Quark Matter 2007), Shanghai, China, Nov. 14 – 20, 2006, (editors) Ma Y-G, Wang E-K, Cai X, Huang H-Z, Wang X-N, and Zhu Z-Y, J. Phys. G **34** (2007) S893 – S896.
22. J.T. Mitchell (for the PHENIX Collaboration); “Scaling properties of fluctuation and correlation results from PHENIX”, Proc. of The 19th International Conference on Ultra-Relativistic Nucleus-Nucleus Collisions (Quark Matter 2007), Shanghai, China, Nov. 14 – 20, 2006, (editors) Ma Y-G, Wang E-K, Cai X, Huang H-Z, Wang X-N, and Zhu Z-Y, J. Phys. G **34** (2007) S911 – S914.
23. Yu Riabov (for the PHENIX Collaboration); “Measurements of leptonic and hadronic decays of ω – and ϕ – mesons at RHIC by PHENIX”, Proc. of The 19th International Conference on Ultra-Relativistic Nucleus-Nucleus Collisions (Quark Matter 2007), Shanghai, China, Nov. 14 – 20, 2006, (editors) Ma Y-G, Wang E-K, Cai X, Huang H-Z, Wang X-N, and Zhu Z-Y, J. Phys. G **34** (2007) S925 – S928.
24. B. Sahlmueller (for the PHENIX Collaboration); “Diagnosing energy loss: PHENIX results on high- p_T hadron spectra”, Proc. of The 19th International Conference on Ultra-Relativistic Nucleus-Nucleus Collisions (Quark Matter 2007), Shanghai, China, Nov. 14 – 20, 2006, (editors) Ma Y-G, Wang E-K, Cai X, Huang H-Z, Wang X-N, and Zhu Z-Y, J. Phys. G **34** (2007) S969 – S973.
25. M. Konno (for the PHENIX Collaboration); “High- p_T identified hadron production in Au+Au and Cu+Cu collisions at RHIC-PHENIX”, Proc. of The 19th International Conference on Ultra-Relativistic Nucleus-Nucleus Collisions (Quark Matter 2007), Shanghai, China, Nov. 14 – 20, 2006, (editors) Ma Y-G, Wang E-K, Cai X, Huang H-Z, Wang X-N, and Zhu Z-Y, J. Phys. G **34** (2007) S975 – S978.
26. T. Isobe (for the PHENIX Collaboration); “Systematic study of high- p_T direct photon production with the PHENIX experiment at RHIC”, Proc. of The 19th International Conference on Ultra-Relativistic Nucleus-Nucleus Collisions (Quark Matter 2007), Shanghai, China, Nov. 14 – 20, 2006, (editors) Ma Y-G, Wang E-K, Cai X, Huang H-Z, Wang X-N, and Zhu Z-Y, J. Phys. G **34** (2007) S1015 – 1018.
27. S. Campbell (for the PHENIX Collaboration); “Dielectron continuum measurements in $\sqrt{s_{NN}} = 200$ GeV Au+Au and Cu+Cu collisions at PHENIX”, Proc. of The 19th International Conference on Ultra-Relativistic Nucleus-Nucleus Collisions (Quark Matter 2007), Shanghai, China, Nov. 14 – 20, 2006, (editors) Ma Y-G, Wang E-K, Cai X, Huang H-Z, Wang X-N, and Zhu Z-Y, J. Phys. G **34** (2007) S1055 – S1058.
28. M. Naruki, H. En’yo, H. Hamagaki, K. Ozawa, et al. (KEK-PS E325 Collaboration); “Medium modification of vector mesons observed in 12 GeV p+A reaction”, Proc. of The 19th International Conference on Ultra-Relativistic Nucleus-Nucleus Collisions (Quark Matter 2007), Shanghai, China, Nov. 14 – 20, 2006, (editors) Ma Y-G, Wang E-K, Cai X, Huang H-Z, Wang X-N, and Zhu Z-Y, J. Phys. G **34** (2007) S1059 – S1063.
29. A. Taranenko (for the PHENIX Collaboration); “PHENIX studies of the scaling properties of elliptic flow at RHIC”, Proc. of The 19th International Conference on Ultra-Relativistic Nucleus-Nucleus Collisions (Quark Matter 2007), Shanghai, China, Nov. 14 – 20, 2006, (editors) Ma Y-G, Wang E-K, Cai X, Huang H-Z, Wang X-N, and Zhu Z-Y, J. Phys. G **34** (2007) S1069 – S1072.

30. T. Isobe (for the PHENIX Collaboration); “Direct Photon Production in Au+Au Collisions at RHIC-PHENIX Experiment”, Proc. of the 2nd International Conference on Hard and Electromagnetic Probes of High-Energy Nuclear Collisions, Asilomar, Pacific Grove, California, 9-16 June 2006 Nucl. Phys. A **783** (2007) 569 – 572.
31. Y.L. Yamaguchi, H. Hamagaki, T. Gunji, S.X. Oda, Y. Aramaki, S. Sano and T. Tamagawa: “Development and Performance Evaluation of Thick-GEM”, Proc. of 2007 IEEE Nuclear Science Symposium and Medical Imaging Conference, Oct. 27–Nov. 3, 2007, Honolulu, Hawaii, USA, IEEE Conference Record 4645 – 4648 (2007).
32. T. Suzuki, S. Chiba, T. Yoshida, T. Kajino and T. Otsuka: “Advances in Shell Model Calculations and Neutrino-Nucleus Reactions”, Progress in Particle and Nuclear Physics **59** (Proc. Suppl.) (2007) 486–493.

C. Theses

1. A. Yoshida: “Study of High-spin States in ^{107}Cd ”, Master Thesis, Kyoto University, March 2007
2. S. Kametani: “Measurement of J/ψ Yield in d+Au Collisions at $\sqrt{s_{NN}} = 200$ GeV”, Doctor Thesis, University of Tokyo, July 2007.
3. T. Isobe: “Production of Direct Photons and Neutral Pions in Relativistic Au+Au Collisions”, Doctor Thesis, University of Tokyo, July 2007.
4. S. Oda: “Production of Charmonia in Cu+Cu and $p+p$ Collisions at $\sqrt{s_{NN}} = 200$ GeV”, Doctor Thesis, University of Tokyo, March 2008.
5. S. Sano: “Development of a Readout Circuit for 2D-Imaging using Gas Electron Multiplier (GEM)”, Master Thesis, University of Tokyo, March 2008

Talks and Presentations

A. Conferences

1. S. Shimoura: “Cluster Structure and Reaction in Neutron-Rich Nuclei”, RIKEN Workshop on Structure and Reaction Dynamics of Highly Excited Molecular Resonances in Light Neutron Rich Nuclei, March 19, 2008, RIKEN, Wako, Saitama, Japan.
2. S. Michimasa: “Focal Plane Detector for SHARAQ”, RIBF Detector Workshop 08, Mar. 17 – 18, 2008, RIKEN, Saitama, Japan.
3. S. Shimoura (Oral) “Gamma-ray spectroscopy using direct reactions” Future Prospects for Spectroscopy and Direct Reactions 2008, Feb. 26–28, 2008, National Superconducting Cyclotron Laboratory, Michigan State University, Michigan, USA
4. S. Michimasa: “Focal plane and beamline detectors of SHARAQ”, TORIJIN-EFES- FJNSP LIA Joint Workshop on Next Generation Detector System for Nuclear Physics with RI beams, Feb. 14 – 15, 2008, GANIL, France.
5. E. Ideguchi “Status of CNS GRAPE and γ -ray spectroscopy community in Japan” The 2nd LACM-EFES-JUSTIPEN Workshop, Jan. 23–25, 2008, Oak Ridge National Laboratory, Tennessee, USA.
6. M. Niikura, E. Ideguchi, N. Aoi, H. Baba, T. Fukuchi, Y. Ichikawa, H. Iwasaki, T. Kubo, M. Kurokawa, M. Liu, S. Michimasa, T. Ohnishi, T.K. Onishi, S. Ota, S. Shimoura, H. Suzuki, D. Suzuki, Y. Wakabayashi, K. Yoshida and Y. Zheng “Study of High-Spin States in 49-51Ti” The 2nd LACM-EFES-JUSTIPEN Workshop, Jan. 23–25, 2008, Oak Ridge National Laboratory, Tennessee, USA.
7. E. Ideguchi: “Study of high-spin states in $A\sim 30$ -50, 110 region using low-energy beam”, 4th workshop on nuclear spectroscopy study using stopped or slow RI beam, Dec. 20–21, 2007, CYRIC Tohoku University, Japan.
8. S. Michimasa: “Status of SHARAQ”, MUST2-RIBF Collaboration Workshop, Nov. 19 –20, 2007, RIKEN, Saitama, Japan.
9. E. Ideguchi: “Search for superdeformed states in $A\sim 110$ region”, 28th CYRIC workshop, Nov. 19–20, 2007, CYRIC Tohoku University, Japan
10. S. Shimoura (invited): “Direct reactions of Borromean nuclei”, International Symposium on New Facet of Three Nucleon Force –50 years of Fujita-Miyazawa Three Nucleon Force– (FM50), Oct. 29–31, 2007, University of Tokyo, Tokyo, Japan.
11. S. Shimoura (invited): “Scientific Opportunities of GRETINA at RIBF in RIKEN”, GRETINA Working Group Workshop, Oct. 14–15, 2007, Richmond, USA.
12. S. Michimasa: “Direct reactions and exotic nuclei”, 3rd Japanese-German EFES(JSPS)-DFG/GSI workshop on Nuclear Structure and Astrophysics, Sept. 29 – Oct. 2, 2007, Frauenwörth im Chiemsee, Germany.
13. A. Saito, S. Shimoura, T. Minemura, Y.U. Matsuyama, H. Baba, N. Aoi, T. Gomi, Y. Higurashi, K. Ieki, N. Imai, N. Iwasa, H. Iwasaki, S. Kanno, S. Kubono, M. Kunibu, S. Michimasa, T. Motobayashi, T. Nakamura, H. Ryuto, H. Sakurai, M. Serata, E. Takeshita, S. Takeuchi, T. Teranishi, K. Ue, K. Yamada, Y. Yanagisawa: “The ${}^6\text{He}+{}^6\text{He}$ and $\alpha+{}^8\text{He}$ cluster states in ${}^{12}\text{Be}$ studied via α -inelastic scattering”, Clusters Conference (Cluster '07), Sep. 3–7, 2007, Holiday Inn, Stratford upon Avon, UK.
14. S. Shimoura (invited): “Light neutron-rich nuclei studied by α -induced reactions”, International Symposium on Physics of Unstable Nuclei (ISPUN07), July 3–7, Hoi An, Vietnam.
15. S. Shimoura (invited): “SHARAQ spectrometer and GRAPE”, 15th International Conference on Electromagnetic Isotope Separators and Techniques Related to their Applications (EMIS2007), June 24–29, 2007, Deauville, France.
16. T. Kawabata, G. P. A. Berg, T. Kubo, H. Sakai, S. Shimoura, T. Uesaka (poster): “High Resolution Beam Line for the SHARAQ Spectrometer”, 15th International Conference on Electromagnetic Isotope Separators and Techniques Related to their Applications (EMIS2007), June 24–29, 2007, Deauville, France.

17. T. Uesaka, S. Shimoura, H. Sakai, T. Kawabata, A. Saito, K. Nakanishi, Y. Sasamoto, S. Michimasa, S. Kubono, E. Ideguchi, H. Yamaguchi, T. Kubo, G.P.A. Berg (poster): “Current Status of the SHARAQ Spectrometer”, 15th International Conference on Electromagnetic Isotope Separators and Techniques Related to their Applications (EMIS2007), June 24–29, 2007, Deauville, France.
18. E. Ideguchi, D.G. Sarantites, W. Reviol, C.J. Chiara, M. Devlin, D.R. LaFosse, F. Lerma, S.K. Ryu, J.N. Wilson, M.P. Carpenter, R.V.F. Janssens, T. Lauritsen, C.J. Lister, P. Reiter, D. Seweryniak, C. Baktash, A. Galindo-Uribarri, D. Rudolph, A. Axelsson, M. Weiszflog, P. Fallon, A. Gørgen, A.O. Macchiavelli, H. Madokoro, M. Oi (Oral): “High-spin negative-parity states in ^{40}Ca ”, International Workshop on Nuclear Structure: New Pictures in the Extended Isospin Space (NS07), June 11–14, 2007, Kyoto, Japan.
19. M. Niikura, E. Ideguchi, N. Aoi, H. Baba, T. Fukuchi, Y. Ichikawa, H. Iwasaki, T. Kubo, M. Kurokawa, M. Liu, S. Michimasa, T. Ohnishi, T.K. Onishi, S. Ota, S. Shimoura, H. Suzuki, D. Suzuki, Y. Wakabayashi, K. Yoshida, Y. Zheng (poster): “Study of high-spin states in $^{49-51}\text{Ti}$ by the secondary fusion reaction”, International Workshop on Nuclear Structure: New Pictures in the Extended Isospin Space (NS07), June 11–14, 2007, Kyoto, Japan.
20. S. Shimoura, S. Ota, H. Iwasaki, M. Kurokawa, S. Michimasa, S. Kubono, T. Teranishi, M. Notani, M. Tamaki, T. Murakami, N. Iwasa, T. Motobayashi, Y. Yanagisawa, T. Minemura, S. Takeuchi, T. Gomi, K. Yamada, A. Saito, H. Baba, Y.U. Matsuyama, S. Kanno, E. Takeshita, H. Demichi, K. Hasegawa, K. Kurita, H. Sakurai, N. Aoi, E. Ideguchi, A. Odahara, T. Fukuchi, K. Miller, Z. Elekes, M. Ishihara: “Lifetime of the low-lying isomeric 0^+ state in ^{12}Be ”, International Nuclear Physics Conference (INPC2007), June 3 – 8, 2007, Tokyo, Japan.
21. H. Baba, S. Shimoura, T. Minemura, Y.U. Matsuyama, A. Saito, H. Ryuto, N. Aoi, T. Gomi, Y. Higurashi, K. Ieki, N. Imai, N. Iwasa, H. Iwasaki, S. Kanno, S. Kubono, M. Kunibu, S. Michimasa, T. Motobayashi, T. Nakamura, H. sakurai, M. Serate, E. Takeshita, S. Takeuchi, T. Teraishi, K. Ue, K. Yamada, Y. Yanagisawa (poster): “Measurement of isoscalar monopole and dipole strengths in ^{14}O ”, International Nuclear Physics Conference (INPC2007), June 3 – 8, 2007, Tokyo, Japan.
22. E. Ideguchi, B. Cederwall, E. Ganioglu, B. Hadinia, K. Lagergren, T. Bäck, A. Johnson, R. Wyss, S. Eeckhaudt, T. Grahn, P. Greenlees, R. Julin, S. Juutinen, H. Kettunen, M. Leino, A.-P. Leppanen, P. Nieminen, M. Nyman, J. Pakarinen, P. Rakhila, C. Scholey, J. Uusitalo, D. T. Joss, E. S. Paul, D. R. Wiseman, R. Wadsworth (poster): “Onset of well-deformed structure in ^{107}In ”, International Nuclear Physics Conference (INPC2007), June 3 – 8, 2007, Tokyo, Japan.
23. S. Michimasa et al. (poster): “Proton inelastic scattering study on the very neutron-rich nuclei located in the sd-pf region”, International Nuclear Physics Conference (INPC2007), June 3 – 8, 2007, Tokyo, Japan.
24. M. Niikura, E. Ideguchi, N. Aoi, H. Baba, T. Fukuchi, Y. Ichikawa, H. Iwasaki, T. Kubo, M. Kurokawa, M. Liu, S. Michimasa, T. Ohnishi, T.K. Onishi, S. Ota, S. Shimoura, H. Suzuki, D. Suzuki, Y. Wakabayashi, K. Yoshida, Y. Zheng (poster): “Study of High-spin States in $^{49-51}\text{Ti}$ by the Secondary Fusion Reaction”, International Nuclear Physics Conference (INPC2007), June 3 – 8, 2007, Tokyo, Japan.
25. S. Ota, S. Shimoura, H. Iwasaki, M. Kurokawa, S. Michimasa, S. Kubono, T. Teranishi, M. Notani, M. Tamaki, T. Murakami, N. Iwasa, T. Motobayashi, Y. Yanagisawa, T. Minemura, S. Takeuchi, T. Gomi, K. Yamada, A. Saito, H. Baba, Y.U. Matsuyama, S. Kanno, E. Takeshita, H. Demichi, K. Hasegawa, K. Kurita, H. Sakurai, N. Aoi, E. Ideguchi, A. Odahara, T. Fukuchi, K. Miller, Z. Elekes, M. Ishihara (poster): “Proton Intruder State in ^{13}B via Proton Transfer Reaction on ^{12}Be ”, International Nuclear Physics Conference (INPC2007), June 3 – 8, 2007, Tokyo, Japan.
26. A. Saito, S. Shimoura, T. Minemura, Y.U. Matsuyama, H. Baba, N. Aoi, T. Gomi, Y. Higurashi, K. Ieki, N. Imai, N. Iwasa, H. Iwasaki, S. Kanno, S. Kubono, M. Kunibu, S. Michimasa, T. Motobayashi, T. Nakamura, H. Ryuto, H. Sakurai, M. Serata, E. Takeshita, S. Takeuchi, T. Teranishi, K. Ue, K. Yamada, Y. Yanagisawa (poster): “Exotic cluster states in ^{12}Be via alpha-inelastic scattering”, International Nuclear Physics Conference (INPC2007), June 3 – 8, 2007, Tokyo, Japan.
27. S. Shimoura et al. (poster): “Segmented germanium detector array GRAPE for high resolution in-beam gamma-ray spectroscopy with RI beams”, International Nuclear Physics Conference (INPC2007), June 3 – 8, 2007, Tokyo, Japan.
28. T. Uesaka, S. Shimoura, H. Sakai, T. Kawabata, A. Saito, K. Nakanishi, Y. Sasamoto, S. Michimasa, S. Kubono, E. Ideguchi, H. Yamaguchi, T. Kubo, G.P.A. Berg (poster): “High Resolution SHARAQ Spectrometer”, International Nuclear Physics Conference (INPC2007), June 3 – 8, 2007, Tokyo, Japan.

29. H. Baba, S. Shimoura, T. Minemura, Y.U. Matsuyama, A. Saito, H. Ryuto, N. Aoi, T. Gomi, Y. Higurashi, K. Ieki, N. Imai, N. Iwasa, H. Iwasaki, S. Kanno, S. Kubono, M. Kunibu, S. Michimasa, T. Motobayashi, T. Nakamura, H. Sakurai, M. Serate, E. Takeshita, S. Takeuchi, T. Teraishi, K. Ue, K. Yamada, Y. Yanagisawa “Isoscalar excitations in ^{14}O ” Direct Reaction with Exotic Beams (DREB2007) May 30 – June 2, 2007, RIKEN, Japan
30. S. Ota, S. Shimoura, N. Aoi, E. Takeshita, S. Takeuchi, H. Suzuki, H. Baba, T. Fukuchi, T. Fukui, Y. Hashimoto, E. Ideguchi, K. Ieki, N. Iwasa, H. Iwasaki, S. Kanno, Y. Kondo, T. Nakabayashi, T. Nakamura, M. Niikura, D. Suzuki, M.K. Suzuki, M. Tamaki, K. Tanaka, Y. Togano, Y. Wakabayashi, K. Yamada: “High Resolution Gamma-ray Spectroscopy of Neutron-rich Nuclei around $N = 20$ with Liquid Helium Target”, Direct Reaction with Exotic Beams (DREB2007), May 30 – June 2, 2007, RIKEN, Japan.
31. A. Saito, S. Shimoura, T. Minemura, Y.U. Matsuyama, H. Baba, N. Aoi, T. Gomi, Y. Higurashi, K. Ieki, N. Imai, N. Iwasa, H. Iwasaki, S. Kanno, S. Kubono, M. Kunibu, S. Michimasa, T. Motobayashi, T. Nakamura, H. Ryuto, H. Sakurai, M. Serata, E. Takeshita, S. Takeuchi, T. Teranishi, K. Ue, K. Yamada, Y. Yanagisawa: “ $^4\text{He}+^8\text{He}$ cluster state in ^{12}Be via alpha-inelastic scattering”, Direct Reaction with Exotic Beams (DREB2007), May 30 – June 2, 2007, RIKEN, Japan.
32. T. Uesaka, S. Shimoura, H. Sakai, T. Kawabata, A. Saito, K. Nakanishi, Y. Sasamoto, S. Michimasa, S. Kubono, E. Ideguchi, H. Yamaguchi, T. Kubo, G.P.A. Berg: “Future experiments with the SHARAQ spectrometer”, Direct Reaction with Exotic Beams (DREB2007), May 30 – June 2, 2007, RIKEN, Japan.
33. H. Yamaguchi, Y. Wakabayashi, G. Amadio, S. Hayakawa, H. Fujikawa, S. Kubono, T. Teranishi, J.J. He, A. Saito, S. Nishimura, Y. Togano, Y.K. Kwon, A. Kim, M. Niikura, N. Iwasa, S. Inafuku, L.H. Khiem, and D.N. Binh (Oral), “Nuclear astrophysics studies using low-energy ^7Be beams at CRIB”, International Nuclear Physics Conference 2007 (INPC07), June 3–8, 2007, Tokyo Internatinal Forum, Tokyo, Japan.
 H. Yamaguchi, S. Kubono, Y. Wakabayashi, S. Hayakawa, Y. Kurihara, D. N. Binh, N. Yamazaki S. Watanabe and Y. Oshiro (Oral): “Development status on Low-energy Radioisotope Beam Production at CRIB”, Stopped slow RI beam Fourth workshop of nuclear spectroscopy study using stopped or slow RI beam, December 20–21, 2007, Tohoku Unibersity, Sendai, Japan.
34. H. Yamaguchi, Y. Wakabayashi, S. Hayakawa, G. Amadio, S. Kubono, H. Fujikawa, A. Saito, J.J. He, T. Teranishi, Y.K. Kwon, Y. Togano, N. Iwasa, K. Inafuku, A. Kim, M. Niikura, D.N. Binh, and L.H. Khiem (Oral): “Nuclear structure of 8B studied by proton resonance scatterings on 7Be ”, The 10th Int. Symp. on Origin of Matter and Evolution of Galaxies - From the Dawn of Universe to the Formation of Solar System -, December 4–7, Hokkaido University, Sapporo, Japan
35. H. Yamaguchi, S. Kubono, Y. Wakabayashi, S. Hayakawa, Y. Kurihara, D. N. Binh, N. Yamazaki S. Watanabe and Y. Oshiro (Oral): “Recent Developments on Low-energy Radioisotope Beam Production at CNS-CRIB”, Workshop on “r-process nucleosynthesis and Quantum Beam” March 13–14, Tsukuba University, Tsukuba, Japan.
36. K. Shimada, D. Nagae, K. Asahi, T. Inoue, K. Takase, S. Kagami, N. Hatakeyama, Y. Kobayashi, H. Ueno, A. Yoshimi, D. Kameda, T. Nagatomo, T. Sugimoto, S. Kubono, H. Yamaguchi, Y. Wakabayashi, G. Amadio, S. Hayakawa, J. Murata, and H. Kawamura (Oral): “Production of spin-polarized ^{17}N beam using inverse-kinematics low-energy transfer reaction”, XIV International Conference on Hyperfine Interactions (HFI 2007) & XVIII International Symposium on Nuclear Quadrupole Interactions (NQI 2007), Aug. 6–10, 2007. Foz do Iguaçu, Brazil.
37. K. Shimada, D. Nagae, K. Asahi, T. Arai, M. Takemura, T. Inoue, K. Takase, S. Kagami, N. Hatakeyama, Y. Kobayashi, H. Ueno, A. Yoshimi, D. Kameda, T. Nagatomo, T. Sugimoto, S. Kubono, H. Yamaguchi, Y. Wakabayashi, G. Amadio, S. Hayakawa, J. Murata, and H. Kawamura (Oral): “Production of low-energy spin-polarized ^{17}N beam with CRIB”, XVth International Conference on Electromagnetic Isotope Separators and Techniques Related to their Applications (EMIS2007), Jun. 25–29, 2007. Deauville, France.
38. K. Shimada, D. Nagae, K. Asahi, T. Arai, M. Takemura, T. Inoue, K. Takase, S. Kagami, N. Hatakeyama, Y. Kobayashi, H. Ueno, A. Yoshimi, D. Kameda, T. Nagatomo, T. Sugimoto, S. Kubono, H. Yamaguchi, Y. Wakabayashi, G. Amadio, S. Hayakawa, J. Murata, and H. Kawamura (Poster): “First production of spin-polarized radioactive nuclear beam with CRIB”, International Nuclear Physics Conference (INPC2007), Jun. 4–8, 2007. Tokyo, Japan.

39. T. Uesaka (Oral), “Spin Asymmetry Measurement at RIBF”, The 2nd LACM-EFES-JUSTIPEN Workshop, Jan. 23–25, 2008, Oak Ridge National Laboratory, Tennessee, USA.
40. T. Uesaka, S. Shimoura, H. Sakai, S. Michimasa, T. Kawabata, A. Saito, K. Nakanishi, Y. Sasamoto, T. Kubo, Y. Yanagisawa, G.P.A. Berg (Oral), “The SHARAQ spectrometer”, TORIJIN-EFES-FJNSP LIA Joint Workshop on Next Generation Detector System for Nuclear Physics with RI beams, Feb. 14–15, 2008, GANIL, Caen, France.
41. T. Uesaka (Oral), “Experimental Determination of Spin-orbit splitting via spin asymmetry measurement at SHARAQ”, Future Prospects for Spectroscopy and Direct Reactions 2008, Feb. 26–28, 2008, National Superconducting Cyclotron Laboratory, Michigan State University, Michigan, USA
42. T. Uesaka (Oral), “Requirements of detectors for SHARAQ”, RIBF Detector workshop 08, Mar. 17–18, RIKEN, Saitama, Japan
43. T. Uesaka (Oral): “Spin-orbit splitting in unstable nuclei and three-nucleon forces”, Workshop on Few-body Physics in Atomic Nuclei, March 8-9, 2008, Kyushu University, Fukuoka, Japan.
44. T. Kawabata, Y. Sasamoto, M. Fujiwara, H. Hashimoto, K. Hatanaka, K. Itoh, M. Itoh, K. Kawase, Y. Maeda, H. Matsubara, K. Nakanishi, S. Sakaguchi, Y. Shimizu, K. Suda, Y. Tameshige, A. Tamii, M. Uchida, T. Uesaka, H. P. Yoshida (Oral): “Alpha inelastic scattering and cluster structures in ^{11}B and ^{13}C ”, RIKEN Workshop on Structure and Reaction Dynamics of Highly Excited Molecular Resonances in Light Neutron Rich Nuclei, March 19, 2008, RIKEN, Wako, Saitama, Japan.
45. T. Kawabata, Y. Sasamoto, M. Fujiwara, H. Hashimoto, K. Hatanaka, K. Itoh, M. Itoh, K. Kawase, Y. Maeda, H. Matsubara, K. Nakanishi, S. Sakaguchi, Y. Shimizu, K. Suda, Y. Tameshige, A. Tamii, M. Uchida, T. Uesaka, H. P. Yoshida (Oral): “Alpha inelastic scattering and cluster structures in ^{11}B ”, Workshop on Few-body Physics in Atomic Nuclei, March 8-9, 2008, Kyushu University, Fukuoka, Japan.
46. Y. Sasamoto, T. Kawabata, T. Uesaka, K. Suda, Y. Maeda, S. Sakaguchi, K. Itoh, K. Hatanaka, M. Fujiwara, A. Tamii, Y. Shimizu, K. Nakanishi, K. Kawase, H. Hashimoto, Y. Tameshige, H. Mathubara, M. Itoh, H.P. Yoshida and M. Uchida ” Cluster states in ^{13}C ”, Workshop on Few-body Physics in Atomic Nuclei, March 8-9, 2008, Kyushu University, Fukuoka, Japan.
47. Y. Sasamoto, T. Kawabata, T. Uesaka, K. Suda, Y. Maeda, S. Sakaguchi, K. Itoh, K. Hatanaka, M. Fujiwara, A. Tamii, Y. Shimizu, K. Nakanishi, K. Kawase, H. Hashimoto, Y. Tameshige, H. Mathubara, M. Itoh, H.P. Yoshida and M. Uchida ” Cluster states in ^{13}C ”, RIKEN Workshop on Structure and Reaction Dynamics of Highly Excited Molecular Resonances in Light Neutron Rich Nuclei, March 19, 2008, RIKEN, Wako, Saitama, Japan.
48. S. Sakaguchi, T. Uesaka, T. Kawabata, Y. Shimizu, Y. Sasamoto, T. Kawahara, T. Wakui, K. Itoh, N. Aoi, K. Sekiguchi, Y. Kondo, Y. Ichikawa, T. Nakao, H. Kuboki, M. Sasano, S. Noji, H. Sakai, T. Shimamura, Y. Nakayama, T. Nakamura, M. Itoh “Analyzing power in p - ^8He elastic scattering”, Workshop on Few-body Physics in Atomic Nuclei, March 8-9, 2008, Kyushu University, Fukuoka, Japan.
49. F. Kajihara (Oral); “Measurement of Single Electrons from Semileptonic Decays of Charm/Bottom Quarks in the RHIC-PHENIX experiment”, Heavy Ion Cafe (workshop on high-energy heavy-ion collisions), April 7, 2007, University of Tokyo, Tokyo, Japan.
50. S.X. Oda (Oral Presentation); “ J/ψ production in Au+Au and Cu+Cu collisions at PHENIX”, International Nuclear Physics Conference (INPC2007), June 3 – 8, 2007, Tokyo, Japan,
51. F. Kajihara (Oral Presentation); “Heavy Quark Measurements by Weak-Decayed Electrons at RHIC-PHENIX”, International Nuclear Physics Conference (INPC2007), June 3 – 8, 2007, Tokyo, Japan,
52. T. Gunji (Oral Presentation); “Onset of J/ψ Melting in QGP Fluid at RHIC”, International Nuclear Physics Conference (INPC2007), June 3 – 8, 2007, Tokyo, Japan,
53. H. Hamagaki (Oral Presentation); “Recent results on Electromagnetic Measurements at RHIC”, Heavy Ion Meeting 2007-10 on Physics with PHENIX and ALICE, Oct. 19 – 20, 2007, International Convention Center Jeju & TRAVELLERS Hotel, Jeju, Korea.
54. Y.L. Yamaguchi (oral), H. Hamagaki, T. Gunji, S.X. Oda, Y. Aramaki, S. Sano, T. Tamagawa; “Development and Performance Evaluation of Thick-GEM”, 2007 Nuclear Science Symposium and Medical Imaging Conference (IEEE) Oct. 27 – Nov.3, 2007, Honolulu, Hawaii, USA.

55. S.X. Oda (Oral presentation); “Measurement of charmonia at RHIC-PHENIX”, RCNP Workshop on QGP Phenomenology in Heavy Ion Collisions – from SPS, RHIC to LHC –, Oct. 29 – 30, 2007, RCNP, Osaka University, Osaka, Japan.
56. Y. Morino (Oral presentation); “Measurement of Heavy Quark production at RHIC-PHENIX”, RCNP Workshop on QGP Phenomenology in Heavy Ion Collisions – from SPS, RHIC to LHC –, Oct. 29 – 30, 2007, RCNP, Osaka University, Osaka, Japan.
57. Y.L. Yamaguchi, H. Hamagaki, T. Gunji, S.X. Oda, Y. Aramaki, S. Sano and T. Tamagawa (Oral): “Development and Performance Evaluation of Thick-GEM”, 2007 IEEE Nuclear Science Symposium and Medical Imaging Conference, Oct. 27 – Nov. 3, 2007, Honolulu, Hawaii, USA.
58. T. Gunji, H. Hamagaki, T. Hatsuda, T. Hirano, Y. Akamatsu (Oral): “Onset of J/ψ Melting in Quark-Gluon Fluid at RHIC”, 20th International Conference on Ultra-Relativistic Nucleus Nucleus Collisions (Quark Matter 2008), Feb. 4 – 10, 2008, Jaipur, Rajasthan, India.
59. Y. Morino for the PHENIX collaboration (Oral): “Measurement of charm and bottom production in pp collisions at $\sqrt{s} = 200$ GeV at RHIC-PHENIX”, 20th International Conference on Ultra-Relativistic Nucleus Nucleus Collisions (Quark Matter 2008), Feb. 4 – 10, 2008, Jaipur, Rajasthan, India.
60. S.X. Oda for the PHENIX Collaboration (Oral); “ J/ψ production in Cu+Cu and Au+Au collisions at RHIC-PHENIX”, 20th International Conference on Ultra-Relativistic Nucleus Nucleus Collisions (Quark Matter 2008), Feb. 4 – 10, 2008, Jaipur, Rajasthan, India.
61. Y.L. Yamaguchi for the PHENIX collaboration (Poster); “Measurement of direct photon via internal conversion in $\sqrt{s} = 200$ GeV p+p collisions at RHIC-PHENIX”, 20th International Conference on Ultra-Relativistic Nucleus Nucleus Collisions (Quark Matter 2008), Feb. 4 – 10, 2008, Jaipur, Rajasthan, India.
62. Y. Aramaki for the PHENIX Collaboration (Poster); “Neutral pion production with respect to reaction plane in Au+Au collisions at RHIC-PHENIX”, 20th International Conference on Ultra-Relativistic Nucleus-Nucleus Collisions (Quark Matter 2008), Feb4 – 10, 2008, Jaipur, Rajasthan, India
63. Y.L. Yamaguchi for the PHENIX collaboration (Invited); “Di-electron Continuum at PHENIX”, 43th Rencontres de Moriond, Mar. 8–15, 2008, La Thuile, Aosta, Italy.
64. T. Suzuki, S. Chiba, T. Yoshida, K. Higashiyama, M. Honma, T. Kajino, T. Otsuka (Oral): “Neutrino-nucleus reactions based on recent advances in shell-model calculations”, International Nuclear Physics Conference INPC2007, Jun. 3–8, 2007, Tokyo International Forum, Japan.
65. T. Suzuki, T. Otsuka (Oral): “Magnetic properties of light neutron-rich nuclei and shell evolution”, International Symposium on Physics of Unstable Nuclei (ISPUN07), Jul. 3–7, 2007, Hoi An, Vietnam.
66. T. Suzuki, S. Chiba, M. Honma, K. Higashiyama, T. Yoshida, H. Umeda, K. Nomoto, T. Kajino, T. Otsuka (Oral): “Spin-Dependent Transitions in Nuclei and Neutrino-Nucleus Reactions”, 2nd International Conference on Frontiers in Nuclear Structure, Astrophysics and Reactions (FINUSTAR2), Sept. 10–14, 2007, Aghios Nikolaos, Greece
67. T. Suzuki (Invited): “Neutrinonucleus reactions and nucleosynthesis”, 3rd Japanese-German EFES(JSPS)-DFG/GSI Workshop on Nuclear Structure and Astrophysics, Sep. 29–Oct. 6, 2007, Frauenwoerth im Chiemsee, Germany.
68. T. Suzuki (Invited): “Spin structure of stable and unstable nuclei and neutrino-induced reactions”, ECT* Workshop on Exotic Modes of Excitations: from Nuclear Structure to Astrophysics, Oct. 8–12, 2003, ECT, Trento, Italy.
69. T. Suzuki (Invited): “Neutrinonucleus Reactions and Nucleosynthesis”, 10th International Symposium on Origin of Matter and Evolution of Galaxies (OMEG07), Dec. 4–7, 2007, Sapporo, Japan.
70. T. Abe and R. Seki (Oral): “Thermal properties of neutron matter by lattice calculation with NN effective field theory at the next-to-leading order”, KEK Workshop on Nuclear-Hadron Physics: Cross-sectoral Workshop, Nov. 19–21, 2007, KEK, Tsukuba, Japan.
71. T. Abe and R. Seki (Oral): “Thermal properties of neutron matter by lattice calculation with NN effective field theory at the next-to-leading order”, RCNP Workshop on Toward a Unified View of Many-body Problem for Nucleons and Mesons, Dec. 14–15, 2004, RCNP, Osaka, Japan.

B. JPS Meetings

1. S. Michimasa, Y. Yanagisawa, K. Inafuku, N. Aoi, Z. Elekes, Zs. Fülöp, Y. Ichikawa, N. Iwasa, K. Kurita, M. Kurokawa, T. Machida, T. Motobayashi, T. Nakamura, T. Nakabayashi, M. Notani, H. J. Ong, T. K. Onishi, H. Otsu, H. Sakurai, M. Shinohara, T. Sumikama, S. Takeuchi, K. Tanaka, Y. Togano, K. Yamada, M. Yamaguchi and K. Yoneda: “Gamma-ray spectroscopy of neutron-rich magnesium isotopes by using proton inelastic scattering”, JPS Spring Meeting, March 23–26, Kinki University, Osaka, Japan
2. H. Baba, Y. Watanabe, Y. Kawasaki, Y. Takizawa, T. Hamada, S. Ebisuzaki, M. Uesaka, T. Motobayashi, H. Sato, K. Hirota, H. Shimizu, M. Sato, T. Fukuchi, S. Shimoura, S. Ota: “Development of ubiquitous detector – try of applying autonomy to detector”, JPS Spring Meeting, March 23–26, Kinki University, Osaka, Japan
3. E. Ideguchi, M. Liu, T. Morikawa, Y. Toh, M. Koizumi, M. Oshima, A. Kimura, K. Furutaka, Y. Hatsukawa, B. Cederwall, Y. Zheng, H. Kusakari, M. Sugawara, S. Mitarai: “Study of high-spin states in $A \sim 30$ region via $^{18}\text{O}+^{24}\text{Mg}$ reaction”, JPS Fall Meeting, September 21–24, Hokkaido University, Hokkaido, Japan
4. T. Kawabata, G.P.A. Berg, T. Kubo, H. Sakai, S. Shimoura, T. Uesaka: “High resolution beam line for the SHARAQ spectrometer”, JPS Fall Meeting, September 21–24, Hokkaido University, Hokkaido, Japan
5. T. Uesaka, S. Shimoura, H. Sakai, T. Kawabata, A. Saito, K. Nakanishi, Y. Sasamoto, S. Michimasa, S. Kubono, E. Ideguchi, H. Yamaguchi, T. Kubo, G.P.A. Berg: “Current Status of the SHARAQ Spectrometer III”, JPS Fall Meeting, September 21–24, Hokkaido University, Hokkaido, Japan
6. K. Nakanishi, T. Uesaka, T. Kubo, A. Saito, H. Sakai, Y. Sasamoto, S. Shimoura, S. Michimasa, N. Yamazaki, R. Yoshino (Oral): “Magnetic field measurement for the superconducting doublet quadrupole magnet in the SHARAQ spectrometer”, at the JPS Fall meeting, Sep. 21–24, 2007, Hokkaido University, Sapporo, Japan.
7. T. Gunji, H. Hamagaki, T. Hatsuda, T. Hirano: “Onset of J/ψ melting in quark-gluon fluid at RHIC”, JPS Fall Meeting, Sep. 20 – 24, 2007, Hokkaido University, Hokkaido, Japan
8. S.X. Oda (for the PHENIX collaboration): “Measurement of charmonia at mid-rapidity at RHIC-PHENIX”, JPS Fall Meeting, Sep. 20 – 24, 2007, Hokkaido University, Hokkaido, Japan
9. Y. Morino (for the PHENIX collaboration): “Study of charm/bottom ratio in non-photonic electron via electron-hadron correlation in p+p collisions at $\sqrt{s} = 200$ GeV”, JPS Fall Meeting, Sep. 20 – 24, 2007, Hokkaido University, Hokkaido, Japan
10. Y.L. Yamaguchi (for the PHENIX collaboration): “Direct photon measurement via internal conversion in $\sqrt{s} = 200$ GeV p+p collisions at RHIC-PHENIX”, JPS Fall Meeting, Sep. 20 – 24, 2007, Hokkaido University, Hokkaido, Japan
11. Y. Aramaki (for the PHENIX collaboration): “Measurement of neutral pion in $\sqrt{s_{NN}} = 200$ GeV Cu+Cu collisions at RHIC-PHENIX”, JPS Fall Meeting, Sep. 20 – 24, 2007, Hokkaido University, Hokkaido, Japan
12. S. Sano, H. Hamagaki, Y. Tanaka, T. Fusayasu, K. Kiyoyama: “Development of LSI for 2D Imaging using GEM”, JPS Fall Meeting, Sep. 20 – 24, 2007, Hokkaido University, Hokkaido, Japan
13. Y.L. Yamaguchi for the PHENIX collaboration: “Study of low pT direct photon production in p+p and Au+Au collisions at RHIC-PHENIX”, JPS Annual meeting, Mar. 22–26, 2008, Kinki University, Osaka, Japan.
14. Y. Aramaki for the PHENIX Collaboration: “Reaction plane dependence of π^0 yields in Au+Au collisions at RHIC-PHENIX”, JPS Annual Meeting, Mar. 22 – 26, 2008, Kinki University, Osaka, Japan
15. S. Sano, H. Hamagaki, Y. Tanaka, T. Fusayasu, and F. Kajihara: “Performance test of a readout LSI for an imaging using GEM”, JPS Annual Meeting, Mar. 22 – 26, 2008, Kinki University, Osaka, Japan
16. A. Takahara for the ALICE-TRD Collaboration: “Study of the electron identification capability of the ALICE Transition Radiation Detector”, JPS Annual Meeting, Mar. 22 – 26, 2008, Kinki University, Osaka, Japan
17. T. Suzuki (Oral): “Tensor force in shell-model calculations”, at the JPS Spring meeting, Mar. 22–26, 2008, Kinki University, Osaka, Japan.

18. T. Abe. and R. Seki (Oral): “Lattice calculation of thermal properties of neutron matter with NN effective field theory at the next-to-leading order”, at the JPS Spring Meeting, Mar. 22–26, 2008, Kinki University, Osaka, Japan.

C. Lectures

1. T. Suzuki: Lecture on Weak and Electromagnetic Interactions in Nuclei, The 6th CNS International Summer School (CISS07), Aug. 28–Sept. 1, 2007, CNS, Wako, Japan.

D. Seminars

1. Y. Sasamoto, “Cluster states in ^{13}C ” Feb. 6 2008, special seminar at Gesellschaft fuer Schwerionenforschung (GSI), Darmstadt, Germany
2. T. Abe: “Lattice calculation of thermal properties of neutron matter with NN effective field theory”, Jan 21, 2008, COE Cross-sectoral Seminar for Young Researchers at Nagoya University, Aichi, Japan.
3. T. Abe: “Lattice calculation of thermal properties of neutron matter with NN effective field theory”, Jan 22, 2008, E,Q,H Lab Combinational Seminar at Nagoya University, Aichi, Japan.

Personnel

Director

OTSUKA, Takaharu

*Professor, Department of Physics,
Graduate School of Science*

Scientific Staff

1. Heavy-Ion Collisions

SHIMOURA, Susumu

Professor

UESAKA, Tomohiro

Associate Professor

IDEGUCHI, Eiji

Lecturer

IWASAKI, Hironori

Research Associate

KAWABATA, Takahiro

Research Associate

MICHIMASA, Shin'ichiro

Research Associate

2. Nuclear Structure in Extreme States

KUBONO, Shigeru

Professor

HAMAGAKI, Hideki

Associate Professor

YAMAGUCHI, Hidetoshi

Research Associate

GUNJI, Taku

Research Associate

Guest Professors

SUZUKI, Toshio

Nihon University

MITSUMOTO, Toshinori

Sumitomo Heavy Industries, Ltd.

Technical Staff

OHSIRO, Yukimitsu

YAMAZAKI, Norio

Technical Assistants

WATANABE, Shin-ichi

YAMAHA, Shoichi

YOSHINO, Ryo

KUREI, Hiroshi (November 2007 ~)

NAGATA, Takeshi (~ July 2007)

NINOMIYA, Hideaki (November 2007 ~)

Post Doctoral Associates

KAJIHARA, Fukutaro

SHIMIZU, Yohei

LIU, Minlang (~ April 2007)

OTA, Shinsuke

NAKANISHI, Kosuke

FUJII, Shinichiro (~ June 2007)

ABE, Takashi (November 2007 ~)

ZHENG, Yong (~ April 2007)

WAKABAYASHI, Yasuo

Graduate Students

ISOBE, Tadaaki (~ July 2007)

ODA, Susumu

SAKAGUCHI, Satoshi

YAMAGUCHI, Yorito

SANO, Satoshi

TAKAHARA, Akihisa

NIIKURA, Megumi

MORINO, Yuhei

SASAMOTO, Yoshiko

ARAMAKI, Youki

HAYAKAWA, Seiya

KURIHARA, Yuzo

Administration Staff

HIRANO, Midori

YAMAMOTO, Ikuko

FUJIWARA, Yuko

KISHI, Yukino

ITAGAKI, Toshiko

ENDO, Takako

Committees

Council

YAMAMOTO, Masayuki (chair)	<i>Dean, Graduate School of Science</i>
SAKAI, Hideyuki	<i>Department of Physics, Graduate School of Science</i>
YAMAGATA, Toshio	<i>Department of Earth and Planetary Science</i>
UCHIDA, Shinichii	<i>Department of Physics, Graduate School of Science</i>
OTSUKA, Takaharu	<i>Department of Physics, Graduate School of Science</i>
Hayano, Ryugo	<i>Department of Physics, Graduate School of Science</i>
KUBONO, Shigeru	<i>Center for Nuclear Study, Graduate School of Science</i>
SHIMOURA, Susumu	<i>Center for Nuclear Study, Graduate School of Science</i>
NAGAMIYA, Shoji	<i>J-PARC Project Office, High Energy Accelerator Research Organization</i>

Steering Committee

OTSUKA, Takaharu	<i>Department of Physics, Graduate School of Science</i>
SHIMOURA, Susumu	<i>Center for Nuclear Study, Graduate School of Science</i>
KUBONO, Shigeru	<i>Center for Nuclear Study, Graduate School of Science</i>
HAMAGAKI, Hideki	<i>Center for Nuclear Study, Graduate School of Science</i>
SAKAI, Hideyuki	<i>Department of Physics, Graduate School of Science</i>
AIHARA, Hiroaki	<i>Department of Physics, Graduate School of Science</i>
HAYANO, Ryugo	<i>Department of Physics, Graduate School of Science</i>
HAMAGUCHI, Hiroo	<i>Department of Chemistry, Graduate School of Science</i>
KOBAYASHI, Tomio	<i>International Center for Elementary Particle Physics</i>
YAMAZAKI, Yasunori	<i>Institute of Physics, Graduate School of Arts and Sciences</i>
MADARAME, Haruki	<i>Department of Nuclear Engineering and Management</i>

Program Advisory Committee

HATANAKA, Kichiji (chair)	<i>Research Center for Nuclear Physics, Osaka University</i>
EN'YO, Hideto	<i>The Institute of Physical and Chemical Research, Nishina Center</i>
YABANA, Kazuhiro	<i>University of Tsukuba</i>
ODAHARA, Atsuko	<i>Osaka University</i>
HAMAMOTO, Ikuko	<i>University of Lund, Sweden</i>
MITTING, Wolfgang	<i>Grand Accelérateur National D'Ions Lourds</i>

